UNIVERSITÀ DEGLI STUDI DI TRIESTE

XXXII CICLO DEL DOTTORATO DI RICERCA IN NANOTECNOLOGIE

Study of the Interactions among Functional Gold Nanoparticles for Controlled Self-Assembly

Settore scientifico-disciplinare: **CHIM/06 – CHIMICA ORGANICA**

DOTTORANDO
PAOLO RONCHESE

COORDINATORE
PROF. LUCIA PASQUATO

SUPERVISORE DI TESI
PROF. LUCIA PASQUATO

TUTORE
PROF. PAOLO PENGO

ANNO ACCADEMICO 2018/2019

occorre diffidare del quasi-uguale (...), del praticamente identico, del pressapoco, dell'oppure, di tutti i surrogati e di tutti i rappezzi. Le differenze possono essere piccole, ma portare a conseguenze radicalmente diverse, come gli aghi degli scambi; il mestiere del chimico consiste in buona parte nel guardarsi da queste differenze, nel conoscerle da vicino, nel prevederne gli effetti. Non solo il mestiere del chimico.

Primo Levi, *Il Sistema Periodico*

Abstract

Along the recent years, gold nanoparticles (Au NPs) have been one of the most investigated species within Nanotechnology, thanks to the peculiar properties that these hybrid organic-inorganic materials exhibit. Undoubtedly, the exploitation of their properties as well as their tunable character have made these nanosystems promising candidates for a lead role in a wide range of applications, spanning many fields of science, such as medicine, electronics, catalysis and sensing. Furthermore, the use of Au NPs as building-blocks for the production new materials is an emerging branch in the study of these systems, aiming at taking advantage of the controlled selfassembly of conveniently functionalized Au NPs. However, this strategy can be possible only if a certain degree of control is achieved in the bottom-up preparation of Au NPs, concerning both the size of the core and the layer of ligands that protect the core itself, so that obtaining batches of Au NPs with homogeneous chemical behaviour and regulating their interactions among themselves and with the environment. The first condition is easily attainable by controlling the size distribution by means of *ad hoc* devised synthetic conditions, whereas the latter can be reached by employing mixtures of ligands, giving rise to specific organizations of the monolayer surrounding the core, or by introducing functional ligands responsible for the interactions among the NPs at precise sites within the ligands shell.

The context in which this work of thesis has been carried out is related to the pursuit of the adequate conditions for the achievement of a control self-assembly of Au NPs. For the purpose, the interactions among functional Au NPs have been studied both in organic and in aqueous environment. In the first case, a preliminary screening of synthetic procedures for the preparation of Au NPs protected by dodecanethiolates with narrow size distribution has been performed, followed by several attempts of controlled functionalization of the so-prepared Au NPs with terpyridine-terminating ligands, which were the responsible for the interactions among the NPs in organic media, triggered by metal ions coordination. The outcomes from the self-assembly process have been analysed by means of UV-Visible Spectroscopy and Transmission Electron Microscope (TEM), evidencing indeed the formation of large aggregates without precise order in the cases where large amount of terpyridine-terminating ligands were employed for the functionalization of the Au NPs.

Concerning the study of the interactions in aqueous environment, water-soluble mixed-monolayer (MM) Au NPs protected by blends of fluorinated and hydrogenated ligands were taken into account. The interesting feature of these NPs was related to the fact that there are some evidences that the arrangement of the fluorinated domains on the gold surface resembled a tetrahedral organization, as suggested by Small Angle Neutron Scattering Spettroscopy measurements, making them suitable substrates for the formation of superstructures with defined geometry. These NPs were made interact with MM Au NPs possessing fluorinated domains or tails so to exploit fluorophilic interactions for producing the superstructures. Cryo-TEM and High-Resolution TEM were employed for studying the results from the self-assembly of these MM Au NPs.

Finally, Matrix-Assisted Laser Desorption/Ionization Time-Of-Flight Mass Spectrometry (MALDI-TOF MS) experiments on batches of MM Au NPs protected by mixture of fluorinated and hydrogenated amphiphilic thiolates were performed in order to exploit the potentialities

and the points of strength of the technique for characterizing mixed monolayers, grafted onto the surface of Au NPs, containing fluorinated species, in terms of both composition and morphology. The outcomes highlighted the criticality of the approach in analysing fluorinated Au NPs, which underwent desorption of ligands from the gold surface, instead of the expected desorption of gold-ligand complexes during MALDI-TOF MS experiments, hampering their proper characterization.

Riassunto

Nel corso degli anni, le nanoparticelle d'oro hanno rivestito uno dei ruoli più importanti nel campo delle nanotecnologie grazie alle proprietà uniche che questi materiali ibridi organico-inorganici dimostrano. L'utilizzo delle loro proprietà, insieme alla possibilità di modificare le loro caratteristiche in fase di sintesi, hanno indubbiamente reso questi nanosistemi dei candidati promettenti per un ruolo da protagonisti in un'ampia gamma di applicazioni, interessando molti settori della scienza, quali la medicina, l'elettronica, la catalisi e la sensoristica. Inoltre, l'impiego delle nanoparticelle d'oro come punto di partenza per la realizzazione di nuovi materiali è un ramo emergente nello studio di questi sistemi, con l'intenzione di sfruttare l'autoassemblaggio controllato di nanoparticelle d'oro opportunamente funzionalizzate. Ad onor del vero, questa strategia è possibile solamente se viene raggiunto un determinato livello di controllo nella preparazione *bottom-up* delle nanoparticelle, in riferimento sia alle dimensioni del nucleo metallico che allo strato di leganti organici che proteggono il nucleo stesso, così da ottenere, da un lato, lotti di nanoparticelle con il medesimo comportamento chimico, dall'altro regolare le loro interazioni reciproche e con l'ambiente circostante. La prima condizione è facilmente raggiungibile attraverso il controllo della distribuzione delle dimensioni dei nuclei metallici mediante condizioni sintetiche adeguatamente messe a punto, mentre la seconda può essere ottenuta tramite l'utilizzo di miscele di leganti, dando luogo ad organizzazioni specifiche dei leganti stessi nel monostrato che circonda il nucleo, oppure introducendo in siti specifici del monostrato dei leganti recanti all'estremità gruppi funzionali, responsabili delle interazioni tra le nanoparticelle.

Il contesto in cui questo lavoro di tesi è stato realizzato è correlato alla ricerca di condizioni opportune per il raggiungimento di un autoassemblaggio controllato di nanoparticelle d'oro. Per tale scopo, le interazioni tra nanoparticelle funzionalizzate sono state studiate sia in ambiente organico che in ambiente acquoso. Nel primo caso, è stato condotto un vaglio preliminare delle procedure per la preparazione di nanoparticelle d'oro protette da dodecantiolati caratterizzate da ridotta distribuzione delle dimensioni, seguito da un certo numero di tentativi per la funzionalizzazione controllata delle nanoparticelle mediante leganti terminanti con unità di terpiridina, responsabili delle interazioni delle nanoparticelle in ambiente organico innescate dall'aggiunta di ioni metallici. I risultati ottenuti dal processo di autoassemblaggio sono stati analizzati mediante spettroscopia UV-Visibile e microscopio elettronico a trasmissione, mettendo in luce la formazione di aggregati estesi senza ordine preciso nei casi in cui una considerevole quantità di leganti recanti le unità di terpiridina è stata impiegata per la funzionalizzazione delle nanoparticelle.

Lo studio delle interazioni in ambiente acquoso ha visto protagoniste nanoparticelle d'oro solubili in acqua protette da un monostrato misto formato da miscele di leganti fluorurati e idrogenati. La caratteristica interessante di queste nanoparticelle consiste nella particolare disposizione dei domini fluorurati sulla superficie del nucleo d'oro; infatti, vi sono alcune analisi eseguite mediante spettroscopia SANS in merito a tale disposizione che evidenziano un'organizzazione tetraedrica dei domini fluorurati. Questa particolare caratteristica rende tali nanoparticelle dei substrati adatti per la formazione di sovrastrutture dalla geometria definita. Conseguentemente, sono stati condotti studi sulle interazioni di tali nanoparticelle con nanoparticelle dal mono-

strato misto recante domini o code fluorurati, in modo tale da sfruttare interazioni fluorofiliche per produrre le sovrastrutture. I risultati sono stati quindi analizzati mediante microscopia crioelettronica a trasmissione e microscopia elettronica a trasmissione ad alta risoluzione.
Infine, la tecnica di spettrometria di massa che sfrutta il desorbimento/ionizzazione laser assistito da matrice accoppiato ad un analizzatore a tempo di volo è stata impiegata per l'analisi di campioni di nanoparticelle d'oro dal monostrato misto composto da miscele di tiolati anfifilici idrogenati e fluorurati, con il fine di trarre vantaggio delle potenzialità e dei punti di forza della tecnica per la caratterizzazione di monostrati misti ancorati alla superficie di nanoparticelle contenenti specie fluorurate, sia in termini di composizione che di morfologia. I risultati hanno evidenziato gli aspetti più critici della tecnica nell'analisi di nanoparticelle fluorurate, i cui leganti vanno incontro a desorbimento dalla superficie di oro anziché desorbire come complessi oro-leganti, ostacolando la caratterizzazione del monostrato stesso.

Contents

Abbreviations

1D	One-dimensional
2D	Two-dimensional
3D	Three-dimensional
AFM	Atomic Force Microscope
Ar	Argon
Au	Gold
Au NPs	Gold Nanoparticles
C8	Octanethiolate
C12	Dodecanethiolate
C16	Hexadecanethiolate
d	Doublet
DCM	Dichloromethane
EtOH	Ethanol
F6	3,3,4,4,5,5,6,6,7,7,8,8,8-Tridecafluoro-1-octanethiolate
F8	2,2,3,3,4,4,5,5,6,6,7,7,8,8,9,9,9-Heptadecafluoro-1-nonanethiolate
Fe	Iron
g	Grams
h	Hours
HR	High Resolution
Hz	Hertz
i-PrOH	Isopropanol
J	Coupling Constant
m	multiplet
MALDI-TOF MS	Matrix-Assisted Laser Desorption/Ionization-Time Of Flight Mass Spectroscopy
M	Molar
MDDS	Mercaptododecylsulphonate
MeOH	Methanol
mg	Milligrams
min	Minutes
mL	Milliliters
MS	Mass Spectroscopy
OLAM	Oleylamine
nm	Nanometer
NMR	Nuclear Magnetic Resonance
NPs	Nanoparticles
PEG	Polyethilene glycol
ppm	Parts per million
q	Quartet
RT	Room Temperature
rpm	Revolutions per minute

s	Singlet
SPB	Surface Plasmon Band
STM	Scanning Tunnelling Microscopy
t	triplet
TEG	Triethylenglycol Monomethyl Ether
TEM	Transmission Electron Microscope
Terpy	Terpyridine
TFE	Trifluoroethanol
TGA	Thermogravimetric Analysis
THF	Tetrahydrofuran
TLC	Thin-Layer Chromatography
TOAB	Tetraoctylammonium Bromide
UV-Vis	Ultraviolet-Visible
V	Volt
δ	Chemical Shift
λ	Wavelength
σ	Standard Deviation
σ^*	Variation Coefficient

Part I

Introduction

CHAPTER 1

Introduction

During the years, gold nanoparticles (Au NPs) have been one of the major topic of Nanotechnology thanks to their unique properties, which contributed to the growth of the ensemble of their possible applications, assuming a relevant role not only among researchers but also into society. The resonance gained by the studies concerning AuNPs is indeed mainly due to their possible applications in several scientific disciplines. The versatility of Au NPs is due to their hybrid inorganic-organic nature that implies the presence of a gold core, whose size and shape can be tuned according to the intended application, surrounded by an organic monolayer.
The extraordinary characteristics of the core involve the reduced dimensions, providing the NPs with unique optical and electronic properties[1] for quantum confinement effects and a high surface to volume ratio, representing the most interesting property for catalytic applications.[2]
On the other hand, the monolayer has the double role of protecting the cores from mutual aggregation and modulating the interactions of the NPs themselves with the environment. In fact, this outer shell is indeed the part of the NPs that communicates with the environment: therefore, it is the major responsible for the behaviour of the NPs in solution, affecting the solubility, wettability, ability to self-assemble and to recognize specific target species. Furthermore, the stability of the whole system strongly depends not only on the monolayer but also on the inorganic-organic interface bridging the gold core and the monolayer. This interface is formed by the chemical bonds between the gold atoms, representing the inorganic part, and the organic molecules acting as capping agents. The ligands coating the gold core can be thiols, phosphines or amines. As a matter of fact, the considerably high dissociation energy of the gold-sulphur bond, equal to 184 kJ/mol,[3] made the thiolates-capped Au NPs the most investigated and prepared type of Au NPs among the family of Au NPs.
The monolayer can then be composed of ligands of the same type or ligands of different chemical nature, forming mixed monolayers whose properties will be further discussed in this chapter. The employment of mixed monolayers grafted onto Au NPs can eventually be used for giving rise to particular morphologies of the monolayer: each of these morphologies provides the monolayer with specific properties. Moreover, the strategy of forming mixed monolayer Au NPs can be exploited for the engineering of *ad hoc* prepared Au NPs acting as building blocks for the production of newer, cheaper and more performing materials, expanding the

already wide range of applications the Au NPs possess.
The coating ligands forming the monolayer can also bear functional moieties at their ends, which can be taken in advantage for all those applications that require specific interactions with other species or among the NPs themselves, *e.g.* self-assembly purposes, molecular recognition, drug delivery or selective targeting.
Figure 1.1 displays a graphical representation of a gold nanoparticle, evidencing their anatomy.

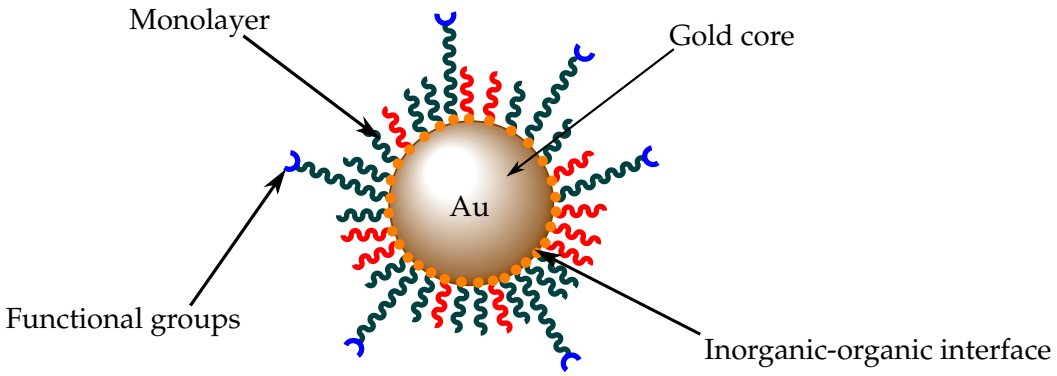

Figure 1.1: Schematic representation of a gold nanoparticle.

The ease in preparation of Au NPs combined with the possibility of tuning the behaviour of these systems by a convenient functionalization of the ligand shell made these systems an appealing tool for countless different applications, spanning over a considerable number of fields, embracing chemistry,[4] physics, biology[5] and medicine[6]. Nevertheless, the success in implementing a certain application through the exploitation of a property of interest is intertwined with a careful and precise process that involves preparation, characterization and eventually functionalization of the NPs in order to take advantage of their potential at best. Therefore, in dealing with these powerful nanosystems a specific know-how is essential. Most of the applications involving Au NPs are based on the interactions that these systems are able to establish with environment or among themselves. One of the most important is indeed the possibility of using the NPs as building blocks for the preparation of new materials based on superstructures of Au NPs, arisen from a self-assembly process.

1 Self-assembly of Au NPs

The versatility of Au NPs is not only due to their behaviour as single entities but also to the properties that they gain as larger aggregates. Indeed, the process of self-assembly can be induced satisfying some conditions. One of these conditions is the possibility to use of ligands able to give rise to weak interactions among NPs or the presence of proper functional groups in the outer shell of the monolayer, able to form connections triggered by the introduction in the environment of peculiar chemical species or by external stimuli, such as temperature, pH or ionic strength. Another focal point is the capability of producing Au NPs whose monolayer presents binding center in precise positions. This is one of the most challenging aspects of this field of Nanotechnology. Indeed, the building up of aggregates of NPs opens the door up to the realization of new materials whose properties can eventually be exploited in order to replace

expensive or less available materials. Furthermore, some properties arising as a consequence of the self-assembly of Au NPs could be exploited for applications in sensing or optoelectronic. Even though the ensemble of possible applications of self-assembled NPs is considerably wide,[7,8] the most investigated ones are related to chemical[9] and biochemical sensing,[10] involving Surface Enhanced Raman Scattering phenomenon,[11] fluorescence emission-based imaging of infectious agents and cancer cells,[12] near-Infrared fluorescence sensing of harmful compounds,[13] and detection of metal ions in low concentrations through self-assembled structures functionalized with metal-chelating ligands.[14]In future, superstructures composed of NPs could as well be employed for biomedical applications, exploiting the capability of metal NPs of absorbing radiation in the visible and near-Infrared spectral regions;[15] indeed, assembles of NPs are able to release the absorbed radiation in form of heat to the surrounding medium through non-radiative energy transfer.[16] By taking advantage of this phenomenon, it could then be possible to implement therapeutic devices for treating infections or killing cancer cells, thanks to the ability of producing localised heat. The properties of self-assembled NPs could also be combined, leading to the development of new strategies in the so-called theranostics,[17] an emerging field of science that couples therapeutic and diagnostic purposes of nanodevices. Eventually, self-assembled structures of NPs are currently promising candidates also for catalytic applications, with a particular interest in photoswitchable catalysts[18] arising from light-induced self-assembly of NPs capped with catalytic ligands: the aggregation of these NPs implies a decrease of surface area and a consequent modulation of the catalytic activity. The use of mixtures of NPs protected by catalytic ligands, which responds to different light wavelengths, may be exploited for selective synthesis of a desired compound.

The concept of self-assembly related to Au NPs is rather broad, however an initial distinction on the dimensionality of the aggregates produced can be outlined, as represented in Figure 1.2. In fact, the rise of the self-assembly can lead to linear aggregates extending in one dimension (1D) or networks of NPs growing in two (2D) or three dimensions (3D). The strategies followed to form these superstructures of higher hierarchical order can be divided in two main approaches:[19] the first one involves a template on which NPs initially stick and then eventually aggregate one another; the latter is a template-free approach, involving physical techniques, *e.g.* Electron Beam Lithography[20], or chemical synthesis, involving for instance linker molecules.[21,22]

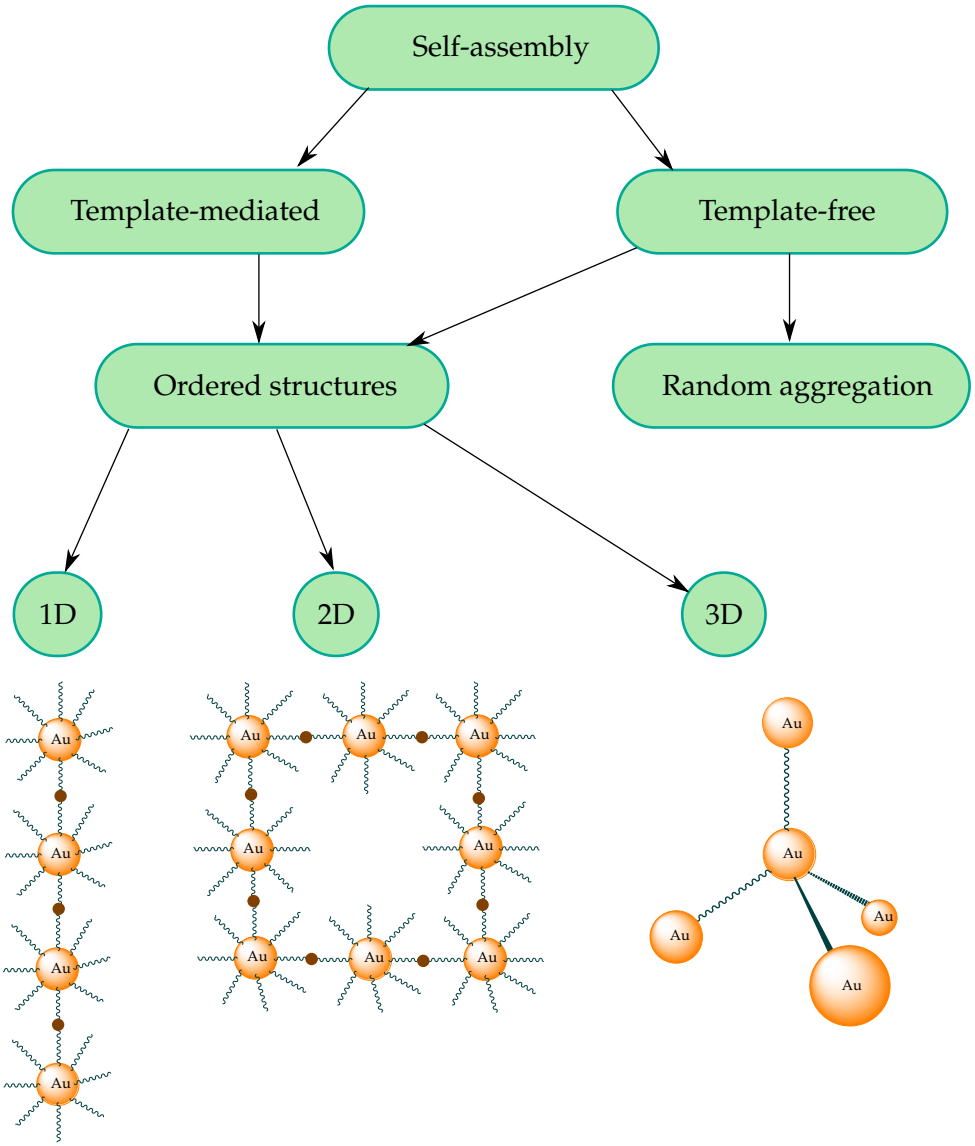

Figure 1.2: Possible strategies for the achievement of self-assembled superstructures of Au NPs.

The next sections present some representative examples of strategies developed aiming at producing superstructures of Au NPs. Examples involving both methods are presented, in order to outline the strength and the limitations of template-assisted and template-free approaches.

1.1 Examples of template-mediated self-assembly of Au NPs in one dimension

In literature, many different kinds of template have been employed for the achievement of linear arrays of Au NPs, as for instance polymers,[23] self-assembling of molecules[24] or peptide fibrils.[25] One illustrative example concerning the synthesis of linear aggregates of Au NPs by means of a template is represented by the work by Fitzmaurice and co-workers[26] where the templating agents employed are carbon nanotubes (CNs). In this study, a dispersion in chloroform of Au NPs possessing a size of 6±1 nm and protected by TOAB was mixed with CNs. The Au NPs stuck to the CNs thanks to hydrophobic interactions between the chains of TOAB and the surface of the CNs. Moreover, the separation between one NPs and another was guaranteed by the TOAB adsorbed on the NPs themselves. Polycristalline nanowires of a length up

to 10 μm were then obtained as results of a heat treatment performed in air at a temperature of 300°C for 120 seconds. After 30 seconds from the beginning of the treatment, the NPs started to melt and joined together. After the heating was carried on for 120 seconds, it was possible to achieve uninterrupted nanowires. Figure 1.3 displays an example of the outcomes of the overall procedure.

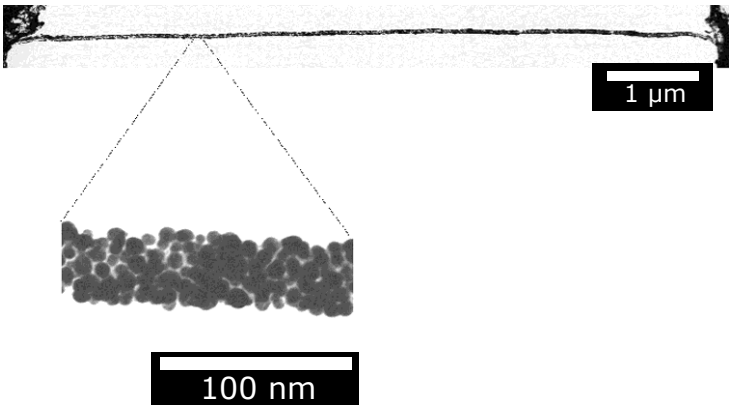

Figure 1.3: Result of the self-assembly of Au NPs using CNs as templating agents.[26] Adapted with permission from reference [26]. Copyright © 2007 John Wiley and Sons.

Nevertheless, the main drawback of this method is that the high-regularity of the structures obtained is very sensitive to the temperature at which the treatment is performed and its duration, since if the heating lasts too long, less regular polycristalline structures are achieved. Furthermore, the whole process is obviously not reversible.

1.2 Examples of template-free self assembly of Au NPs in one dimensions

In the *template-free* approach the chemical synthesis in solution is widely exploited in order to achieve 1D arrays of Au NPs. Moreover, the junctions between the NPs can be reached by means of disparate species, such as ssDNA[27], peptides[28] or ligands covalently bound one another[22], connecting the NPs at which are covalently bound as well. Related to the preparation of linear arrays, a study performed by Liz-Marzàn and co-workers[27] focuses on the use of Polymerase Chain Reaction (PCR) in order to connect Au NPs functionalized with primers of DNA. A scheme exposing the strategy employed is reported in Figure 1.4, together with TEM images of the outcomes from the procedure of self-assembly.

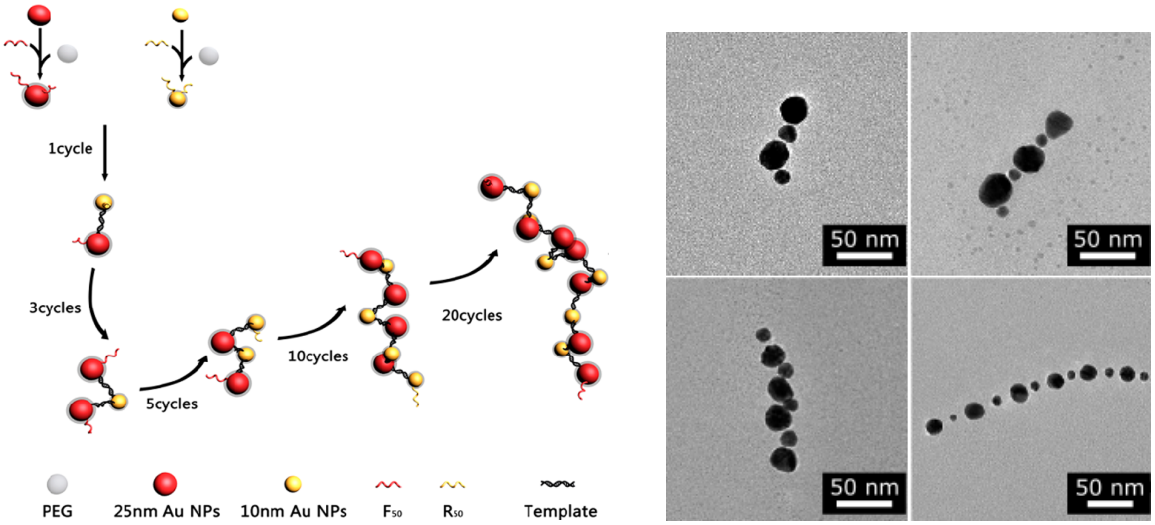

Figure 1.4: On the left, a scheme of the procedure of self-assembly of Au NPs exploiting PCR. On the rigth, TEM images of the linear arrays of Au NPs prepared by Liz-Marzàn and co-workers.[27] Adapted with permission from reference [27]. Copyright © 2013 The American Chemical Society.

In particular, the Au NPs employed in the study had different dimensions: one group of smaller Au NPs characterized by having a core diameter of 10 nm and functionalized with specific primers and another group of bigger Au NPs with a core diameter of 25 nm and bearing a different type of primer. Indeed, the authors established that the average number of primers on each NPs was 2.3. Then, the NPs were stabilized with thiolated polyethylene glycol and made undergo to PCR. According to the number of cycles of the PCR, the length of the aggregates changed: higher numbers of cycles resulted in longer chains.
This is a very interesting procedure that allows the realization of ordered linear arrays of Au NPs with well-defined periodicity miparted by the different dimensions of the particles employed. However, a critical point is the fact that a total control of the number of primers on each NP is rather difficult, therefore the risk of obtaining chaotic aggregates is quite high.
A milestone in approaching the linear self-assembly of Au NPs is represented by the study of Stellacci and coworkers[22] related to divalent Au NPs. The NPs involved were covered by a mixed monolayer composed of 1-nonanethiolates and 4-methylbenzenethiolates in 2:1 molar ratio, giving phase segregation on the surface of the NPs. The functional groups interacting with the linker molecules in forming the bonds were introduced at the poles of Au NPs after a rapid place-exchange reaction. Indeed, the striped NPs were dissolved in a solution of 11-mercaptoundecanoic acid and then stirred for 30 minutes, after which the reaction was rapidly quenched. The reason why the poles are preferred in the exchange has to be ascribed to the types of ligands forming the monolayer: in fact, the thiols were chosen in such a way that the resulting monolayer possessed stripe-like domains because of phase segregation. In this situation, the ligands at the poles experience more conformational freedom since they are less packed and constrained than the others, therefore they are the first involved in a place-exchange reaction.[29] Finally, by activating the carboxylic groups and then introducing in the environment the linker molecules, 1,6-hexamethylenediamine, amide bonds were formed and connected the NPs one another, producing linear arrays on Au NPs linked by covalent bonds. The TEM images reveal the absence of branched aggregates, proving that the functionaliza-

tion has involved only the ligands at the poles. A graphical representation of the strategy is reported in Figure 1.5, as well as a TEM image of the linear superstructures formed.

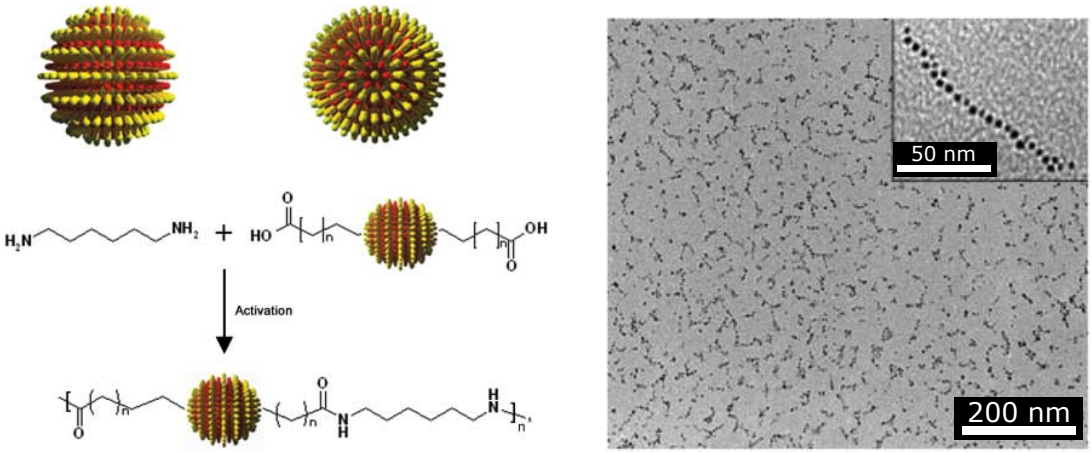

Figure 1.5: On the left,Strategy employed by Stellacci and co-workers for the preparation of linear arrays of MM Au NPs. On the rigth, TEM image displaying the results of the self-assembly obtained by fast place exchange reaction on MM Au NPs and subsequent formation of covalent bonds.[22] Adapted with permission from reference [22]. Copyright © 2007 The American Association for the Advancement of Science.

The point of strength of this work lies in the implementation of a method that allows the divalent functionalization of Au NPs and their connection in arrays triggered by introducing the adequate specie in the environment. Nevertheless, in this case the self-assembly is not reversible, since the cleavage of an amide bond is not trivial; moreover, the strategy of introducing the ligands at the poles in order to realize nanowires of Au NPs strictly depends on the arrangement of the ligands forming the monolayer, together with a careful control of reaction conditions, that have to be refined in order to increase the number of divalent NPs. Eventually, another drawback is due to the fact that this approach does not allow to precisely determine the number of carboxylic groups per NP.

1.3 Two-dimensional self-assembled structures of Au NPs

The template-free strategies that allow the formation of two-dimensional superlattices from self-assembly of Au NPs involve the use of linker agents of different nature.[30] The common point for all the types of linker agent relies on a precise and rationale engineering of capped NPs: indeed, the sites of interaction among NPs must lay on the same plane in order to assure the two-dimensional extension of the superlattices.

The employment of ligand molecules as linker agents has been widely investigated during the years: the approaches for the self-assembly of Au NPs in two-dimensional superstructures involved the exploiting of ligand interdigitation[31,32] based on van der Waals forces, the use of linking molecules with precise geometry[33] or bearing head groups able to give rise to several kinds of interaction, such as hydrogen bonding[34], electrostatic forces[35], π-π stacking[36] or metal ion complexation.[37] The major limitation of this approach is due to the fact that the inter-particle distances cannot exceed the length of the linking molecules: therefore, it is not possible to achieve well-ordered two-dimensional superstructures of NPs whose inter-particle distances

are on large regimes. This drawback can be overcome by making use of polymers, which can be either directly grafted on the surface of the NPs through a cross-linking reaction,[38,39] producing polymeric shells, or introduced *via* place-exchange reaction, as a result of the displacement of weakly chemisorbed species.[23,40] Moreover, the mechanical properties of the polymers exploited are such that the superstructures produced can easily withstand swelling or high temperatures.
The template-mediated approaches to the preparation of two-dimensional self-assembled structures of Au NPs generally rely on the use of DNA scaffolds exhibiting precise geometry[41,42] as substrates for the assembly of Au NPs, which are conveniently functionalized with complementary single strands of DNA. The overall self-assembly is governed by the process of base coupling between the single-strands on the surface of NPs and those composing the templating agent; this latter process can also be reverted by increasing the temperature, restoring the initial conditions of free NPs. Other examples of templates for two-dimensional superstructures of Au NPs include micelles[43] and nanosheets assembled from diamide molecules,[24] where the interactions responsible for the self-assembly of Au NPs are van der Waals forces among the chains of the ligands capping the NPs and the walls of the templates.

1.4 Three-dimensional self-assembled structures of Au NPs

As previously stated, Au NPs can self-assemble also in networks that extend in the three dimensions. Although the realization of these nanosystems requires a lower degree of control over the position of the interacting sites with respect to that of the mono-dimensional ones which requires the presence of only two interacting center on each NP in opposed positions, the risk of obtaining chaotic aggregates with no possible applications is still present, especially if the number of interacting centers is too high. From the first studies by the groups of Mirkin and Alivisatos concerning preliminary attempts of self-assembling Au NPs taking advantage of weak interactions between ssDNA[44,45], the strategy has been developed and more and more refined, leading to the achievement of 3D aggregates by means of many expedients, as for example ssDNA coupling,[46,47] dithiols[48] and metal ions complexation.[49–52]

1.4.1 Example of DNA-template-mediated self-assembly of Au NPs in three dimensions

An exemplary study involving the employment of templates for producing three-dimensional superstructures of Au NPs is the one performed by Tagawa and co-workers[47] where, by exploiting a DNA tetrahedral scaffold, ordered lattices of Au NPs were produced. Each vertex of the template was able to bind one Au NP thanks to free ssDNAs; moreover, ssDNAs were present also in the inner part of the tetrahedron, differing from those at the vertices though. Therefore, using two kinds of Au NPs, one functionalized with ssDNAs complementary to those at the vertices and one with ssDNAs complementary to those in the inner part of the scaffolds, the authors were able to produce superstructures exhibiting a diamond-like lattice. On the other hand, employing Au NPs bearing ssDNAs complementary only with those at the vertices, FCC lattices are produced. Therefore, according to the type of Au NPs employed in the process, supercrystals with different hierarchical order could be attained. Figure 1.6 summarizes the approach behind the preparation of these NPs-based lattices.

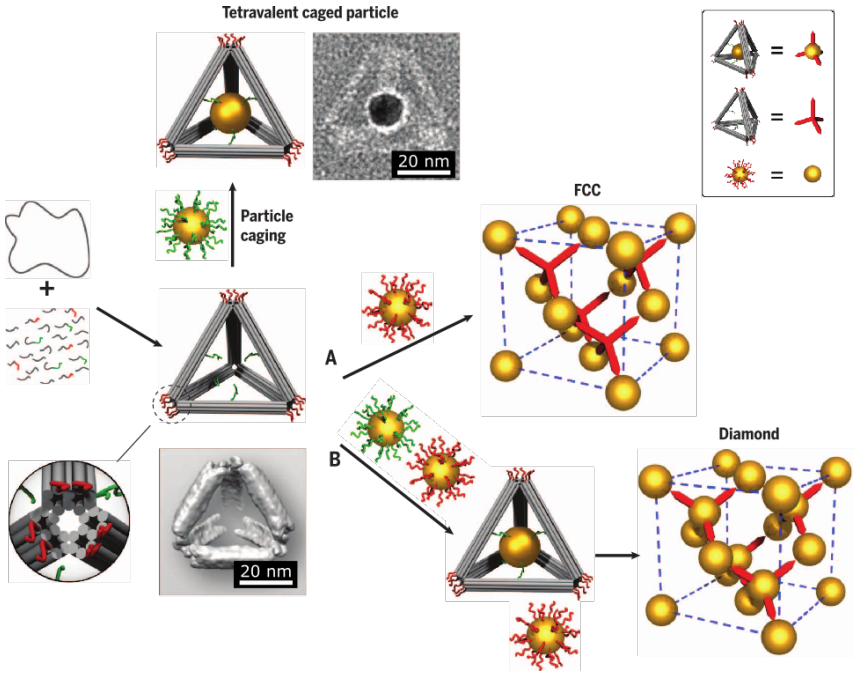

Figure 1.6: Schematic representation of the strategy employed by Tagawa and co-workers.[47] Adapted with permission from reference [47]. Copyright © 2016 The American Association for the Advancement of Science.

This strategy is without doubt very intriguing allowing in principle the realization of superstructures with many applications, even though further experiments are needed to test the stability of the self-assembled species so-produced. Only then, these structures could be exploited for the building up of new materials with tunable properties according to the organization of the NPs composing the systems. Furthermore, complex templates that require *ad hoc* syntheses are needed.

1.4.2 Examples of template-free self-assembly of Au NPs in three dimensions by metal ions complexation

The strategy of employing metal ions complexation to achieve self-assembling of Au NPs makes the whole process versatile since, most of the times, it is possible to reverse the self-assembly simply by adding to the solution a stronger complexation agent which breaks the complexes up, sequestering the metal ions. Moreover, most of the complexation agents are able to coordinate several kinds of metal ions, giving rise to complexes with octahedral, tetrahedral or square-planar geometries. The resulting organization of the NPs within the self-assembled structures may lead to tunable properties according to the type of ion employed in forming the complexes. As a matter of fact, the usefulness and the possibility of exploitation of the aggregates produced is related to the proper functionalization of the monolayer. Indeed, by conveniently selecting the agent responsible for the formation of the complexes and by introducing ligands bearing this agent at specific sites in the monolayer, it is possible to achieve controlled self-assembly of Au NPs, producing therefore ordered structures whose geometry can be indeed tuned by changing the metal ion. One representative work employing metal ions complexation as base for the self-assembly of Au NPs is the one by R. W. Murray and

coworkers[49] using Au NPs of 3.1 nm protected with tiopronin. This type of NPs was able to self-assemble in presence of Cu(II) ions. The approach exploited in the work is depicted in Figure 1.7

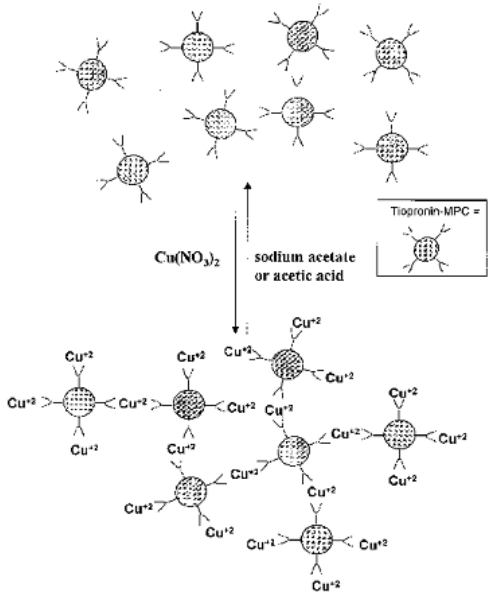

Figure 1.7: Process of self-assembly of Au NPs protected by tiopronin by means of Cu(II) ions.[49] Adapted with permission from reference [49]. Copyright © 2000 The American Chemical Society.

The exploitation of the chemical properties of tiopronin made the overall process strongly dependent on the pH of the solution, as well as the concentration of Cu(II). Indeed, at higher values of pH, the carboxylic groups of tiopronin are deprotonated, requiring lower concentrations of Cu(II) ions in order to form the complexes. Therefore, the aggregates could be broken by lowering the pH, protonating the carboxylate groups, making the process reversible. Moreover, this study showed how the aggregates could be disrupted by adding a number of moles of sodium acetate equivalent to the moles of Cu(II) ions necessary to form the aggregates. The aggregates could be also broken by the addition of few drops of concentrated acetic acid. The possibility of reversing the process by acting on various parameters certainly makes the approach versatile and suitable for different applications, *e.g.* in sensing techniques; on the other hand, the use of tiopronin for bigger Au NPs can be critical because of the presence of the methyl group in α position with respect to the sulphur atom, producing a less packed and then less stable monolayer.

Linear aggregates can be produced also by exploiting the intrinsic anisotropy of Au nanorods (NRs). Indeed, thanks to their elongated form, Au NRs can be easily functionalized at their lateral cups corresponding to the Au(111) face, where the packing of their protecting agent CTAB is looser. Chan and coworkers[53] took advantage of this aspect and implemented a strategy that allows the achievement of linear arrays of Au NRs by metal ions complexation. Indeed, in this study the Au NRs were connected one another through ligands bearing a terpyridine unit. Fe(II) ions were complexed before introducing the ligands at the lateral facet of the Au NRs. Once the solution of ligands already complexed was added to that of Au NRs, the mixture was sonicated for 10 minutes and left rest at 25 °C for two days, producing a violet precipitate,

isolated by centrifugation and removing of the supernatant. The TEM images evidenced the formation of the arrays of Au NRs, as reported in Figure 1.8.

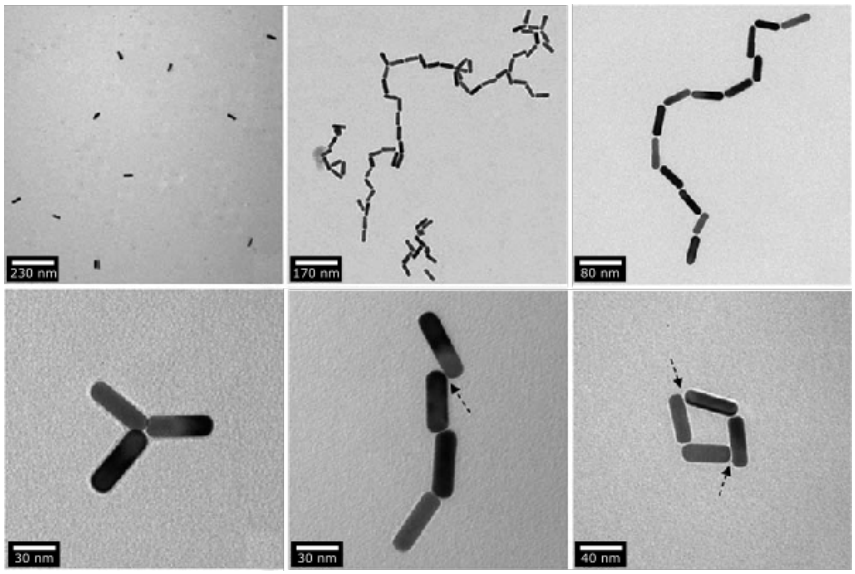

Figure 1.8: Aggregates of Au NRs produced by metal ion complexation.[53] Adapted with permission from reference [53]. Copyright © 2010 John Wiley and Sons.

The authors tested the reversibility of the self-assembling process taking advantage of the instability of terpyridine-based complexes of Fe(II) in basic conditions; therefore, the addition of a 1mM solution of NaOH dissolved the aggregates previously formed, restoring the situation of free Au NRs in solution. Nevertheless, the major drawback of this procedure relies on the fact that the extension of its application to spherical NPs could be cumbersome, since their intrinsic isotropy hampers the possibility of precisely controlling their functionalization as in the case of Au NRs.

For the purpose of self-assembly of Au NPs by means of metal ions complexation, terpyridine is widely used because of its ability of producing stable complexes with a considerable number of cations. Indeed, the thermodynamic constants for formation of complexes with $[M(terpy)_2]^{2+}$] stoichiometry are considerably high, as reported in Table 1.1, proving that the process of formation is extremely favoured even at low concentrations of metal ion and complexing agent.

Table 1.1: Formation constants for complexes with $[M(terpy)_2]^{2+}$ stoichiometry involving most common M^{2+} metal ions, measured in water[54] or acetonitrile.[55]

Metal ion	Formation constant	Solvent
Fe^{2+}	$10^{20.9}$	water
Co^{2+}	$10^{18.3}$	water
Ni^{2+}	$10^{21.8}$	water
Zn^{2+}	$10^{14.3}$	acetonitrile
Mg^{2+}	$10^{11.8}$	acetonitrile

As a matter of fact, by changing the nature of the metal ion, the properties of the aggregates

vary accordingly. Related to this latter aspect, a study by Rotello and co-workers[51] focuses the attention on different aggregates of Au NPs achieved via terpyridine complexation with Fe(II), Zn(II), Ag(I) and Cu(I) ions. Three groups of Au NPs have been employed in this work: they differ one from the others for the length of the chain of the alkane thiols which cover the gold core. Pentanethiol has been used to synthesize the first group of NPs, then the other two groups have been prepared from the first by making use of large excesses respectively of octanethiol and undecanethiol in place-exchange reactions. The three groups of Au NPs have been then functionalized by introducing into the monolayer alkane thiols bearing a terpyridine units as ending group. Figure 1.9 reports the process of functionalization of Au NPs with terpyridine-terminating ligands.

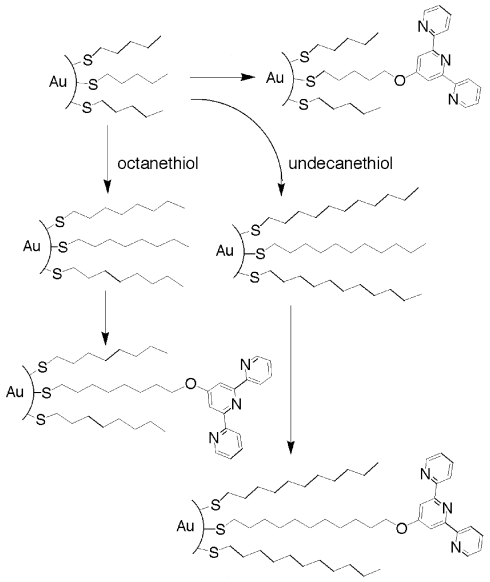

Figure 1.9: Functional Au NPs prepared in the work of Rotello and co-workers.[51] Adapted with permission from reference [51]. Copyright © 2002 The American Chemical Society.

Once again, the functionalization of the Au NPs has been carried out through place-exchange reaction and NMR tests evidenced that the molar ratio between alkanethiolates and terpyridine-terminating ligands was 3 to 1. Thereupon, tests on different cations were performed in order to establish how the properties of the produced aggregates could be affected by the nature of the metal ion. Figure 1.10 displays two sets of results achieved by using Fe(II) ions, on the left, and Ag(I) ions, on the right. The employment of Fe(II) gives rise to stable hexacoordinated complexes with two terperydine molecules in mild conditions. At low concentrations of Fe(II), no aggregates were observed and this is probably due to the quite high solubility of the Au NPs aggregates at that value of concentration. More concentrated solutions of Fe(II) in MeOH added to solutions of Au NPs in $CHCl_3$ led to microscopic aggregates. On the other hand, the aggregates produced by Ag(I) ions complexation formed from weaker interactions; therefore, the self-assembly could be reverted by the addition of a large excess of free terpyridine, restoring the initial conditions.

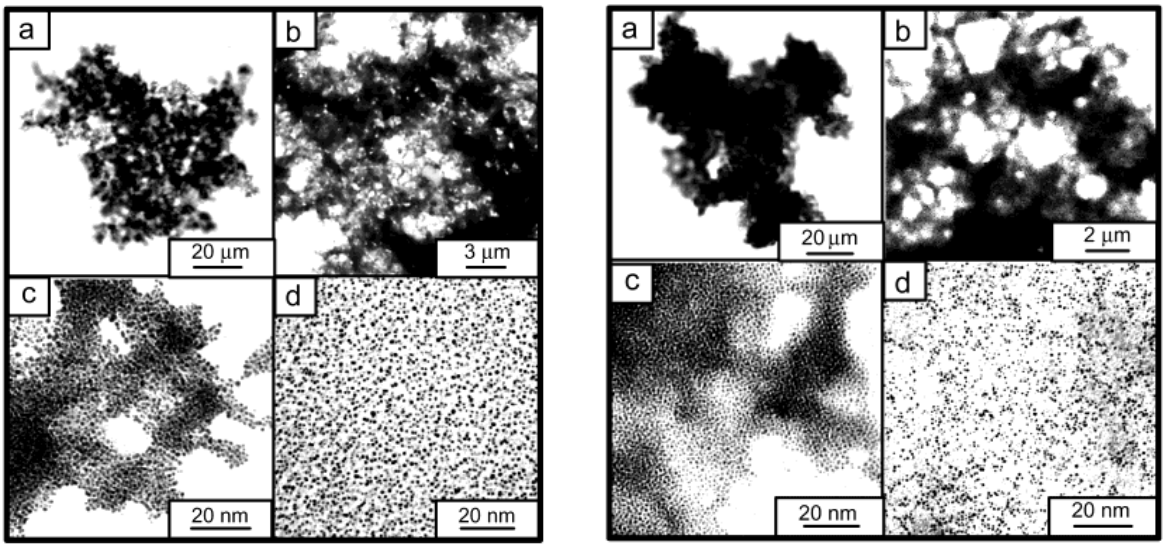

Figure 1.10: On the left: phase contrast micrograph (a) and TEM images (b,c) of a sample of Au NPs functionalized with ligands bearing terpyridine units at their ends after the addition of Fe(II) ions in the environment. TEM image (d) of the same batch of Au NPs before the functionalization with terpyridine-terminating ligands after the addition of Fe(II) in the environment. On the right: phase contrast micrograph (a) and TEM images (b,c) of a sample of Au NPs functionalized with ligands bearing terpyridine units at their ends after the addition of Ag(I) ions in the environment. TEM image (d) of the result of the addition of an excess of free terpyrdine terminating ligands to a solution containing aggregates of Au NPs produced consequently to Ag(I) complexation by means of terpyridine.[51] Adapted with permission from reference [51]. Copyright © 2002 The American Chemical Society.

More studies were carried out, involving Zn(II) and Cu(I) ions as well. The outcomes outlined a possible competition between thermodynamic self-assembly and kinetic self-assembly; indeed, the aggregates achieved by means of Fe(II) and Zn(II) were the product of a strong coordination of the cations by terpyridine molecules, whereas those obtained through Cu(I) and Ag(I) complexation resulted from a weaker coordination. Therefore, the first arose more rapidly which implicated a higher amount of voids; the latter instead formed more slowly and so they presented an higher degree of packing, thanks to a thermodynamically regulated process. All the aggregates had in common the fact that they were insoluble in many organic solvents, such as DMF, MeOH, CH_3CN, acetone and ethyl acetate, except those obtained by means of Ag(I) which are partially soluble in DMF. Finally, SAXS analysis of the aggregates provides values of distance between Au NPs that agree with the length of the thiolate chains.

2 Mixed-Monolayer Au NPs as a possible starting point for controlled self-assembly

One of the most fascinating features of Au NPs is the possibility to conveniently functionalize the monolayer according to the purpose for which the NPs will be employed. Moreover, the engineering of the monolayer is crucial also for the building up of new materials rising from the self-assembly of the NPs themselves. As a matter of fact, this latter aspect is tightly connected with the concept of controlled self-assembly. Indeed, since the monolayer constitutes the outer part of a NP involved in interactions with the surrounding, the control over these interactions

could be achieved only through a control over the morphology of the monolayer itself. Consequently, all the ensemble of interactions among NPs and other species, *e.g.* molecules of solvent, cells, viruses, templating agents, other NPs, are directly related to the way how the ligands arrange themselves surrounding the gold core and then what morphology the monolayer acquires. Therefore, understanding what is the morphology of a precise batch of Au NPs and what conditions have led to that particular outcome is a step forward for understanding both the mutual behaviour of the NPs themselves and how to tune the interactions with the surroundings.
Controlling the arrangement of the ligands within the monolayer is a crucial point for the achievement of a certain degree of control over the whole self-assembly process. In fact, as already said, the self-assembly of Au NPs acquires a certain resonance in producing new materials that will be involved in new applications only if the properties acquired as a result from the self-assembly can be deeply understood and the behaviour of the superstructures predicted in advance. This condition is possible when the superstructures resulting from process have a defined geometry that allows a proper characterization of the systems. Random aggregates are challenging to characterize and they hardly have exploitable properties for useful applications. Obviously, a precise control of the morphology involving a deep control over the position of each ligand within the monolayer is extremely difficult to obtain; however, by making use of binary blends of immiscible ligands differing for their chemical nature, it is possible to take advantage of the phase segregation occurring during the formation of the monolayer. As a matter of fact, the shape of the domains arising for this phase segregation depends on many parameters, such as the molar ratio of the ligands composing the blends, the size of the gold core, the degree of mixing and the difference between the chain lengths, which affects the interactions among the ligands themselves, involving the overall energy balance that regulates the formation of the monolayer. By tuning these conditions, NPs protected by a monolayer characterized by peculiar organization of the ligands can be reached, *e.g.* random, Janus or stripe-like.[56,57] These morphologies differ indeed one another for the arrangement of the ligands covering the NPs: random monolayers do not exhibit a precise order in the arrangement of the ligands around the gold core, whereas the monolayer of Janus NPs is divided in two domains. Eventually, stripe-like domains can be seen as sequential alternating stripes of ligands. Figure 1.11 represents the three different types of morphology that a mixed monolayer may assume.

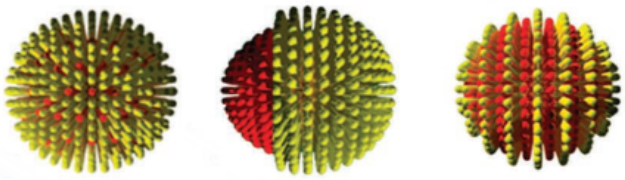

Figure 1.11: From left to right: random, Janus and stripe-like morphologies.[58] Adapted with permission from reference [58]. Copyright © 2012 Springer Nature.

One important aspect related to the morphology of the monolayer is strictly connected to the arising of peculiar properties, as for instance the solubility of the NPs only in specific solvents, the arising of certain interactions with different species[56] or the behaviour of the ligands grafted

onto the cores during place exchange reactions[22,29]. The exploitation of this latter feature may represent the key for introducing functional ligands at precise sites of the monolayer, achieving a certain degree of control over the number and the spatial organization of the interaction point, eventually leading to the production of adequate substrates for controlled self-assembly of Au NPs.

2.1 Theoretical investigation on the formation of mixed monolayer grafted onto gold surfaces

The early theoretical studies on mixed-monolayer Au NPs helped to pinpoint the effect of chain length and core dimensions on the overall arrangement of binary mixtures of ligands on the surface of Au NPs. In particular, Glotzer and co-workers[59] performed atomistic and mesoscale calculations in order to provide an attempt of explanation regarding the results achieved in a previous work[56] concerning the formation of stripe-like domains in the monolayer of Au NPs, synthesized using binary blends of chemically different thiols and the subsequent analyses by means of Scanning Tunneling Microscopy.[57] The theoretical investigation on stripe-like domains allowed the achievement of some important information concerning the factors that implicates the arising of that peculiar morphology. Indeed, stripe-like domains arise when immiscible thiols are employed and the loss in van der Waals (vdW) interactions due to the contact among chains of different chemical nature is balanced by the entropic gain resulting from a difference in chain lengths that involves more conformational freedom for longer thiols with respect to the shorter ones. As a matter of fact, if this gain in entropy is not adequate, the organization of the thiols on the surface of the Au NPs resembles the so-called Janus morphology. Nevertheless, this tendency towards bulk phase separation driven by free energy minimization is somehow modified by an increasing of the conformational entropy of the ligands tails achieved when longer or bulkier ligands are surrounded by shorter or less bulky ones. This latter condition provides a separation of the ligands in "microphases". In particular, the atomistic simulations that helped in drawing this explanation were performed adopting the Molecular Dynamics (MD) approach in the canonical ensemble keeping fixed the number of particles N and the volume in which the simulation has been carried out. The NPs simulated had a diameter of 7.0 nm and they were covered by different equimolar mixtures of thiolates. Starting from high temperature, the system was then cooled to the desired temperature and let evolve until no further changes in the structure were observed. The mesoscale simulations concerning the ligands bound to gold surface were performed once again in the canonic ensemble adopting the Dissipative Particle Dynamics (DPD) approach. The head groups (HS-) of the ligands were confined to the gold surface by employing some constrains ("Constrained Dynamics"). Eventually, starting from high temperature, during the simulation the system was cooled reaching the temperature at which the phase segregation occurred. Simulations involving mixtures of 1-butanethiol and 1-hexanethiol (C4:C6), 11-mercaptoundecanoic acid and 1-dodecanethiol (C11:C12) and finally 3-mercaptopropionic acid and 1-propanethiol (C3:C3) provided interesting results: indeed, stripe-like domains formed in those cases where there was a difference either in chain lengths (C4:C6 mixture) or in the tail groups (C11:C12 mixture). On the other hand, the simulations predicted that no stripe-like domains arising for

chains having the same length (C3:C3 mixture), despite the presence of a bulky tail group as the carboxylic group. The results of the simulations are reported in Figure 1.12, together with STM images of the experimental batches analysed.

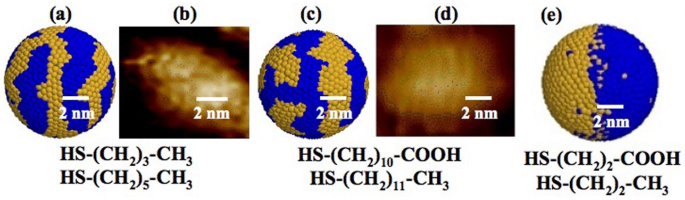

Figure 1.12: From left to right: results for C4:C6 mixture from atomistic simulations (a) and STM experiments (b). The tail end-groups are identical, but the lengths differ. Results for C11:C12 mixture from atomistic simulations (c) STM experiment (d). Here the tail end-groups differ in size but the tail lengths are nearly identical. Atomistic simulation (e) of C3:C3 mixture of equal length but with different tail end-groups.[59] Adapted with permission from reference [59]. Copyright © 2007 American Physical Society.

Figure 1.13 displays the ligands taken into account for modelling the MM Au NPs simulated.

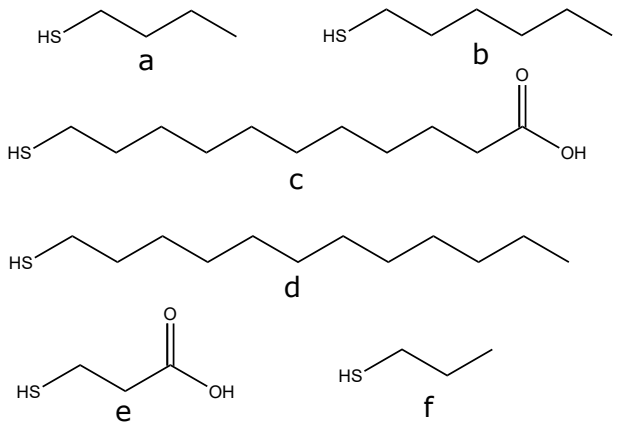

Figure 1.13: Ligands employed for modelling MM Au NPs in the theoretical study: 1-butanethiol (a), 1-hexanethiol (b), 11-mercaptoundecanoic acid (c), 1-dodecanethiol (d), 3-mercaptopropionic acid (e) and 1-propanethiol (f).[59]

A possible explanation of this behaviour can be ascribed to the fact that for sufficiently long ligands, the entropic gain is due to the formation of interfaces where the ligands possessing bulkier tail groups are close to ligands having less bulky tail groups. Therefore, the bulkier tails can benefit from more free volume and consequently this fact balances the energetic cost of forming new interfaces. In order to maintain the energetic balance, the whole system adopts the compromise of giving rise to stripe-shaped separated microphases.
The parameters which influence the formation of one morphology over the others can be then resumed in the difference in chain lengths, the hindrance of the tail groups and the curvature of the surface where ligands bind. The results of simulations pointed out that considering two kinds of ligand differing only for the chain lengths, the longer ligands tend to bind and cover the shorter ones, whereas if the two types of ligand have the same lengths, Janus NPs are formed, no matter which the degree of curvature of the surface is. Moreover, even though a type of ligand is characterized by carrying a bulkier tail group, no stripes are observed for short chains or if the hindrance is negligible. As a matter of fact, considering ligands with tail groups

providing the same hindrance, stripes are formed only if the difference in length is higher than three carbon atoms and this is a consequence of the fact that the more the chain is long, the more the conformational entropy increases. Eventually, the analysis of the morphology of the ligands with respect to the curvature of the surface showed that considering a binary mixture of ligands C4:C7, the more is the degree of curvature and the less is the entropic gain. The results of these simulations are displayed in Figure 1.14.

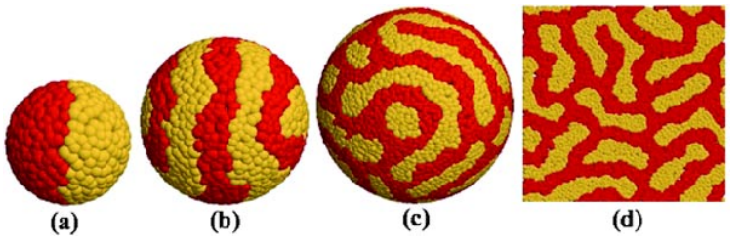

Figure 1.14: Equilibrium structures obtained by mesoscale simulations of binary mixture of thiolates of length ratio 4:7 on surfaces with varying degrees of curvature. Increasing sphere radius from (a) to (c), (d) corresponds to a sphere of infinite radius.[59] Adapted with permission from reference [59]. Copyright © 2007 American Physical Society.

Consequently, the monolayer of NPs of reduced dimensions, which are characterized by a high degree of curvature, adopts a Janus morphology since the size of the NPs is smaller compared to the length of the ligands, leading to the fact that the entropic gain arising from the formation of extra interfaces is not sufficient to produce stripe-like domains. On the other hand, bigger NPs present stripe-like domains into their monolayer. Furthermore, the stripes alignment is related to the curvature of the surface as well: indeed, for flat surface or big NPs, the stripes are not aligned whereas by reducing the dimensions of the spheres, a progressive alignment is observed.
As previously stated, this latter study was one of the first theoretical analyses of the arrangement of the binary mixture of immiscible ligands surrounding NPs of spherical shape. Although its theoretical character, it turned out to be essential for the comprehension of how changing some specific conditions in the preparation of MM Au NPs can affect the morphology of the monolayer.

2.2 Experimental studies on mixed monolayer Au NPs

Several works followed the theoretical study reported in the previous section, meant to characterize MM Au NPs with experimental techniques. In particular, STM[60] and NMR[58] investigations of MM Au NPs were carried out, providing further information concerning the formation of specific monolayer morphologies. Generally, a STM study of the morphology of the monolayer is rather complex because of the specific conditions for sample preparation and handling during the measurements that the STM technique implicates, *e.g.* the NPs have to be fixed to a substrate and the acquisition time of the measurements is generally longer than the variations of molecular conformation of the ligands on the gold surface, producing differences in STM images taken very close in time; moreover, some of these conformational changes can be ascribed to the interaction between the tip of the instrument and the ligand tails. Nevertheless,

HR-STM studies of Mixed Monolayer Protected Au NPs (MMP Au NPs) were carried out[60] on three different types of Au NPs covered respectively by mixture of 11-mercapto-1-undecanol and 4-mercapto-1-butanol (NP1), 1-octanethiol and 3-mercaptopropionic acid (NP2) and finally 1-octanethiol (NP3). Figure 1.15 displays the chemical structures of these ligands.

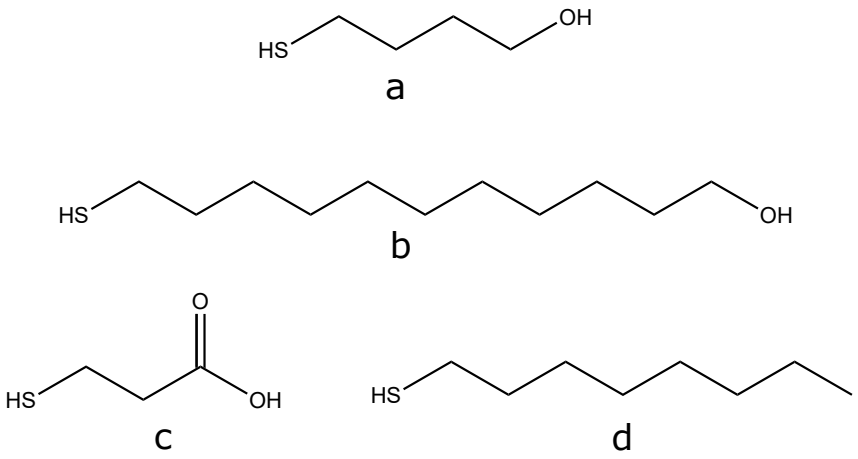

Figure 1.15: Ligands employed for preparing the NPs studied by means of STM: 4-mercapto-1-butanol (a), 11-mercapto-1-undecanol (b), 3-mercaptopropionic acid (c) and 1-octanethiol (d).[60]

All the three different types of NPs had the same core size of 5.0 nm. In this study, for each kind of Au NPs two different STM pictures were taken at very short interval of time, analysed and then treated in order to obtain the difference with the aim of enhancing the variations between the two. The analysis of NP1 clearly pointed out that the difference between the two STM images provides a third image that is almost featureless. As a matter of fact, being 11-mercapto-1-undecanol (C11ol) longer than 4-mercapto-1-butanol(C4ol), the movement of the terminal OH group of the C11ol chains can somehow disturb the imaging of the shorter C4ol ligands, appearing as sort of shadows in the STM images. The same behaviour can be found considering the results concerning NP2: also in this case, the difference between two STM images shows a picture where no evident features can be pointed out and the overall roughness is lower. For this kind of MM Au NPs, the stripes on their surface can have variable thickness and point defects can be enhanced in some regions of the monolayer. Figures 1.16 and 1.17 display a STM image of the two types of MM Au NPs, together with a second image where the OH terminating groups have been highlighted by violet and red dots.

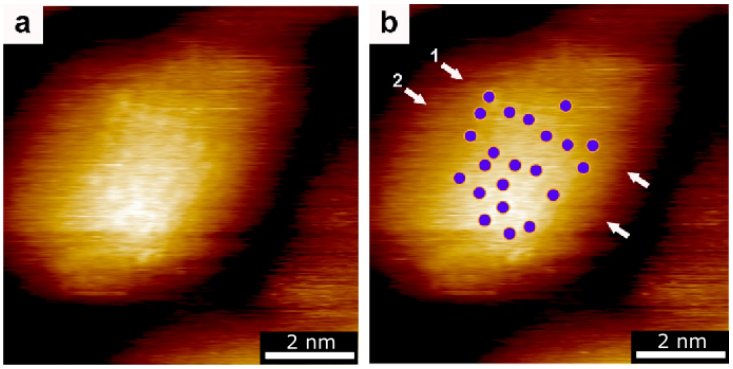

Figure 1.16: On the left: HR-STM image of MM Au NPs identified as NP1. On the right: the same HR-STM image where violet dots and arrows were drawn to highlighted the terminating OH group of 11-mercapto-1-undecanol and their arrangement.[60] Adapted with permission from reference [60]. Copyright © 2013 American Chemical Society.

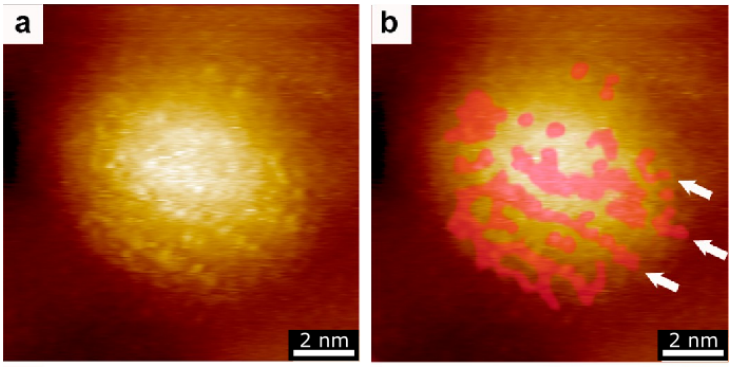

Figure 1.17: On the left: HR-STM image of MM Au NPs identified as NP2. On the right: the same HR-STM image where red dots and arrows were drawn to highlighted the terminating OH group of 11-mercapto-1-undecanol and their arrangement.[60] Adapted with permission from reference [60]. Copyright © 2013 American Chemical Society.

Eventually, the analysis of NP3 did not give pictures showing a well-defined alignment of the dots, proving that the arrangement of the thiolates was random, as displayed in Figure 1.18.

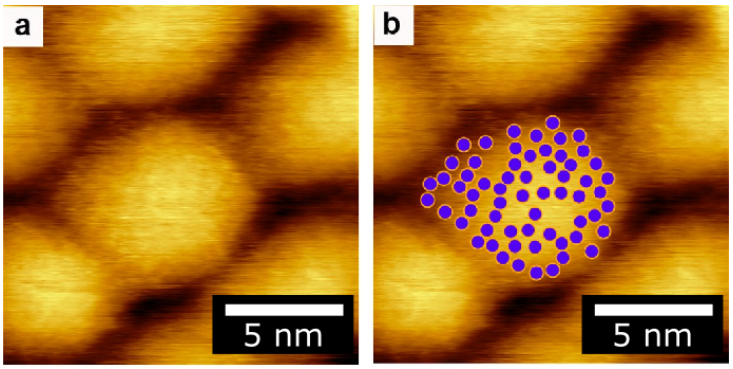

Figure 1.18: On the left: HR-STM image of MM Au NPs identified as NP3. On the right: the same HR-STM image where violet dots were drawn to highlighted the arrangement of the ligands of the surface of the gold core. No particular arrangement of the ligands can be pointed out.[60] Adapted with permission from reference [60]. Copyright © 2013 American Chemical Society.

NMR studies of the morphology of MMP Au NPs were performed as well.[58,61] In particular, in order to carry out a clear and helpful study, it is necessary to employ combinations of ligands able to generate well-separated NMR peaks, as the chemical shifts due to different chemical surroundings can induce observable shifts. A NMR study[58] of MM Au NPs by Stellacci and co-workers took into account two different binary mixtures of ligands: diphenylthiol (DPT) mixed with 3,7-dimethyloctanethiol (DMOT), and DPT mixed with dodecanethiol (DDT). Figure 1.19 reports the ligands used to prepare the MM Au NPs involved in the study.

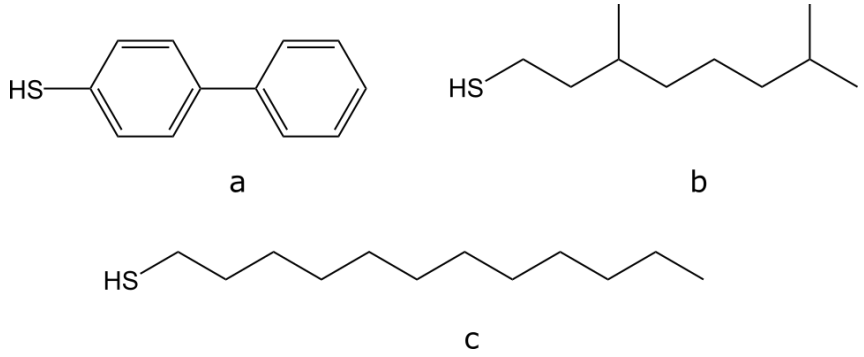

Figure 1.19: Ligands used to prepare the MM Au NPs studied by means of NMR spectroscopy by the group of Stellacci: diphenylthiol, DPT (a); 3,7-dimethyloctanethiol, DMOT (b); dodecanethiol, DDT (c).[58]

The use of DPT is justified for the fact that aryl protons are upfielded for the arising of the currents of proximal aryl rings. Then, the chemical shifts of the protons of this kind of thiol are well-separated with respect to the others, guaranteeing the goodness of the analysis. As a matter of fact, NMR signals of NPs are not only determined by the chemical structure of the ligands but are also affected by the presence of the surrounding ligands. Then, changes of the chemical shift are related to variations of the surroundings. The assumptions made for the interpretation of the results are related to the dependence of the chemical shift of the protons of the ligands forming the monolayer with respect to the composition of the monolayer. Indeed, for random mixtures of thiolates on the gold surface the average composition of the shell of First Nearest Neighbours (FNN) for each molecule coincides with the whole composition of the ligands shell. Therefore, the trend of the chemical shift linearly decreases with the increasing of the molar ratio of one thiol (χ_A) with respect to the other. For Janus NPs, only the ligands at the interface have a mixed composition of FNN whereas the others are surrounded by homoligands. For these latter NPs, the trend of the chemical shift is $\frac{1}{\chi_A}$. Finally, for patchy NPs the relationship between chemical shift and composition is more complex as consequence of the fact that the shape of the patches themselves changes with the composition of the monolayer. The resulting trend is then described by a sigmoid and it is strictly related to the evolution of the shape of the domains. Two-dimensional NMR experiments were also employed in the study[58] by Stellacci and co-workers, taking advantage of the Nuclear Överhauser Effect (NOE) which is due to dipole-dipole interactions between nuclear spins conveniently spatially close, within a distance below 0.4 nm. These interactions are responsible of cross-peaks visible in a NOESY spectrum. In particular, since the intensity of the cross-peaks is inversely proportional to the distance of the nuclei, this technique can be then exploited to estimate the distance between the nuclei themselves. Indeed, the presence in the NOESY spectra of Au NPs of cross-peaks can

prove the fact that the distance between different ligands is below 0.4 nm. Therefore, for Au NPs covered by a monolayer characterized by random mixtures of ligands, strong cross-peaks are expected since each ligand of one kind is in the FNN shell of the other kind. Similarly, also for patchy NPs, NOESY spectra should exhibit strong cross-peaks. On the other hand, for Janus NPs, since only the ligands at the interface are in the FNN shell of the other kind of ligands, no strong cross-peaks are expected. Figure 1.20 displays the predicted chemical shifts trends and the NOE spectra of MM Au NPs with different morphologies.

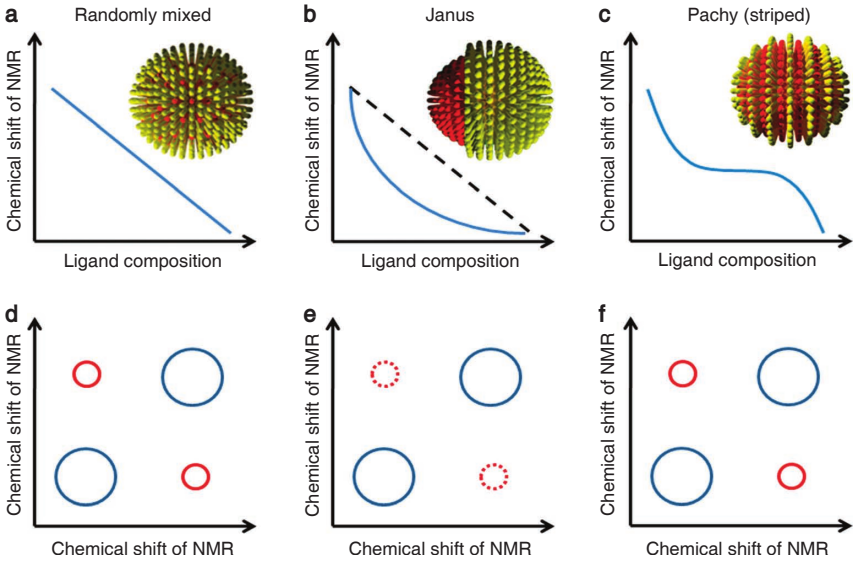

Figure 1.20: Predicted chemical shift trends with composition of the monolayer and NOE spectra for MM Au NPs with different morphologies.[58] Adapted with permission from reference [58]. Copyright © 2012 Springer Nature.

The ^{1}H-NMR spectra of the MM Au NPs covered by mixture of DPT and DMOT showed that the peak moved towards lower chemical shifts by increasing the amount of DPT in the monolayer, proving the linear decreasing trend. Moreover, the NOESY spectra showed strong cross-peaks. Then, the authors claimed that this kind of NPs was covered by a random mixture of DPT and DMOT. The NPs synthesized employing a mixture of DPT and DDT had two different sizes: one group had an average core size of 2 nm, whereas the other had a core size in between 4 and 5 nm. For the first group, ^{1}H-NMR spectra revealed that the peaks of the aryl protons were roughly in the same region when the composition of the monolayer was rich in DPT or DPT and DDT were almost in the same ratio, whereas they moved towards higher chemical shifts if the monolayer was rich in DDT. This trend can be related to the fact that the morphology of the monolayer of these NPs was Janus. Furthermore, the NOESY spectra did not present strong cross-peaks, evidencing that the number of ligands of different type close one another was rather low. For the NPs having a diameter in between 4 and 5 nm, instead, the interpretation of the ^{1}H$-$NMR and the NOESY spectra suggested the formation of stripes in the monolayer of the NPs. Indeed, the peaks ascribed to the aryl protons were in the same positions for intermediate molar ratio of ligands or in case of higher amount of DDT, whereas they moved towards lower chemical shifts if the monolayer was richer in DPT. This would mean that phase segregation occurred and Janus NPs were obtained. However, the NOESY

spectra showed strong cross-peaks due to a considerable number of ligands at the interface. By combining these information, a reasonable explanation lies in the fact that stripe-like domains characterized the morphology of the monolayer of this type of NPs. The outcomes of the overall NMR analysis of the MM Au NPs presented is summarized in Figure 1.21.

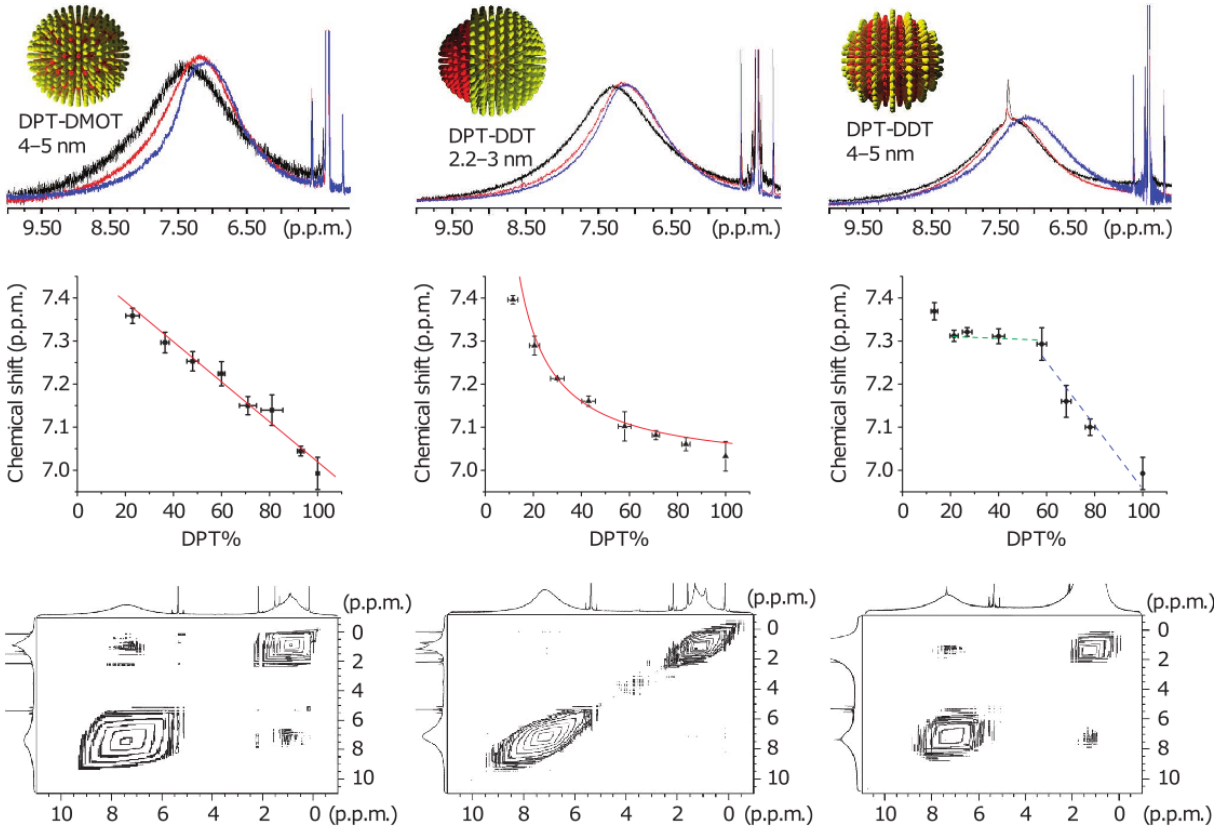

Figure 1.21: Outcomes from 1D and 2D NMR analysis of MM Au NPs protected by DPT, DMOT and DDT.[58]. Adapted with permission from reference [58]. Copyright © 2012 Springer Nature.

2.3 Studies on hydrogenated and fluorinated mixed monolayer Au NPs

Recent studies[61–64] have been published concerning the use of binary blends of fluorinated and hydrogenated thiols in order to achieve a certain control of the morphology of the monolayer of Au NPs, tuning specific conditions related to the length of the ligands, the size of the gold core and the molar ratios of the thiols. The reason behind the use of fluorinated species is due to the easiness in giving rise to phase segregation phenomena between fluorinated ligands and the hydrogenated counterparts, leading to different morphologies once tuned the synthetic conditions. Moreover, fluorinated species are able to interact among themselves thanks to fluorophilic interactions.[65–68] Even though many synthetic conditions must be taken into account, the fluorophilic/fluorophobic interactions can therefore represent an adequate strategy for controlling the formation of domains whit a precise morphology in the monolayer and the arising of self-assembled superstructures of MM Au NPs. Consequently, ordered superstructures may be produced by taking advantage of mixed-monolayer Au NPs characterized by the presence of regularly patterned fluorinated domains within the monolayer. The spatial arrangement of

these domains may then address the orientation and the dimensionality of the superstructures formed. For instance, dimers could be produced by using Janus mixed-monolayer Au NPs or linear chains may arise by employing mixed-monolayer Au NPs presenting two fluorinated poles.

The properties of MM Au NPs vary accordingly to the morphology of the monolayer, not only in terms of solubility, but also of wettability, the possibility of interactions with biological membranes, the ability of self-assembly and catalytic activity as well. During the years, the relationship between the final composition of the monolayer and the initial reaction mixture employed for prepared hydrogenated and fluorinated MM Au NPs has been investigated in depth, outlining considerable deviations from linearity. In particular, in the study[64] of Şologan and co-workers, the analysis of the relationship between final composition of the monolayer and the synthetic conditions exploited was carried out on several types of Au NPs: Au NPs covered by ligands with different chain lengths (NP-C12/F6 and NP-C16/F6, C12: dodecanethiol, C16: hexadecanethiol, F6: 1H,1H,2H,2H-perfluorooctanethiol), comparable chain lengths (NP-C12/F10 and NP-C8/F6, F10: 1H,1H,2H,2H-perfluorododecanethiol, C8: octanethiol) and with branches (NP-HbrC12/F6, HbrC12:3-methyldodecane-1-thiol). A schematic representation of these samples is given in Figure 1.22.

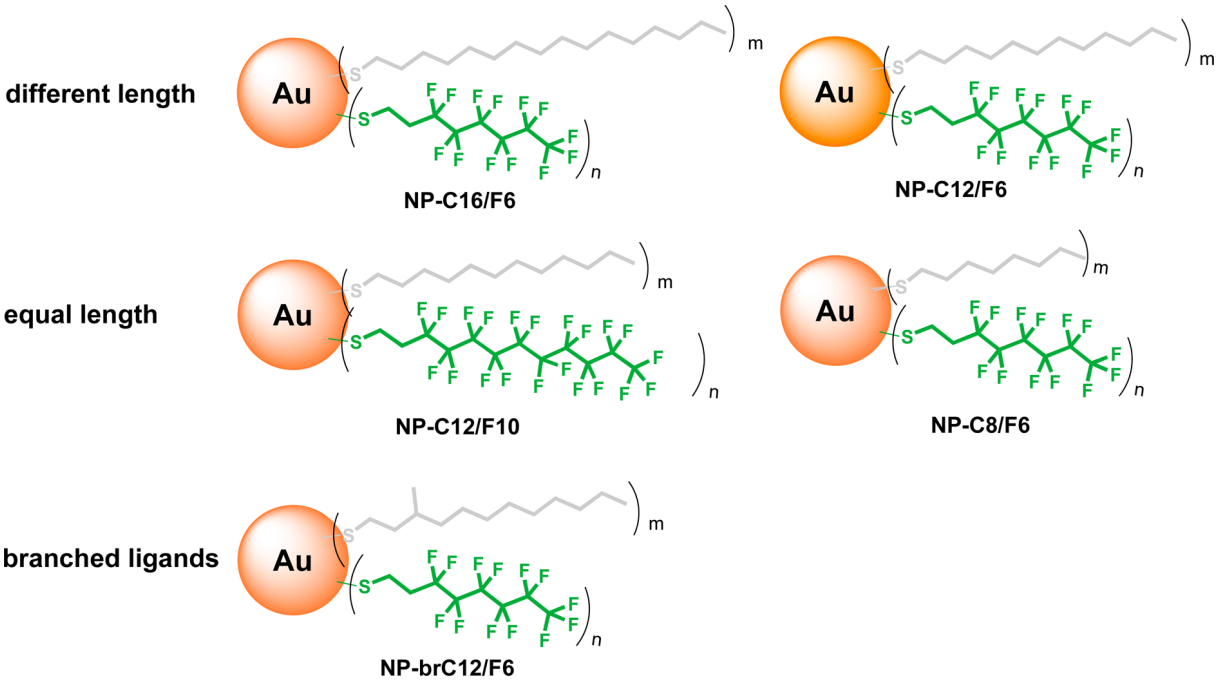

Figure 1.22: Batches of hydrogenated and fluorinated MM Au NPs analysed in the study of the relationship between the final composition of the monolayer and the initial reaction mixture[64] and in the NMR investigation concerning composition and morphology of the monolayer.[61] Adapted with permission from reference [61]. Copyright © 2016 American Chemical Society.

The analysis focused on how the difference in chain length and chain structure modifies the composition and consequently the morphology of the monolayer. Nevertheless, according to the difference in chain length between the incoming fluorinated thiols and the hydrogenated ones already bound the gold surface, the introduction of the fluorinated compounds can be promoted or not, keeping in mind that also the molar fraction of fluorinated thiols in the so-

lution where place-exchange takes place has to be taken into account. The composition of the monolayer of the so-formed Au NPs was determined by means of ^{1}H-NMR spectroscopy by decomposing a small amount of the desired NPs in presence of excess iodine and analysing the resulting mixture of disulfides. The ratio between the two thiolates composing the monolayer was therefore achieved by integrating the areas of the signals of the methylene group in α position with respect to the sulphur atom. Thereupon, the final composition of the monolayer was related to the composition of the initial reaction mixture. The results observed are reported in Figure 1.23.

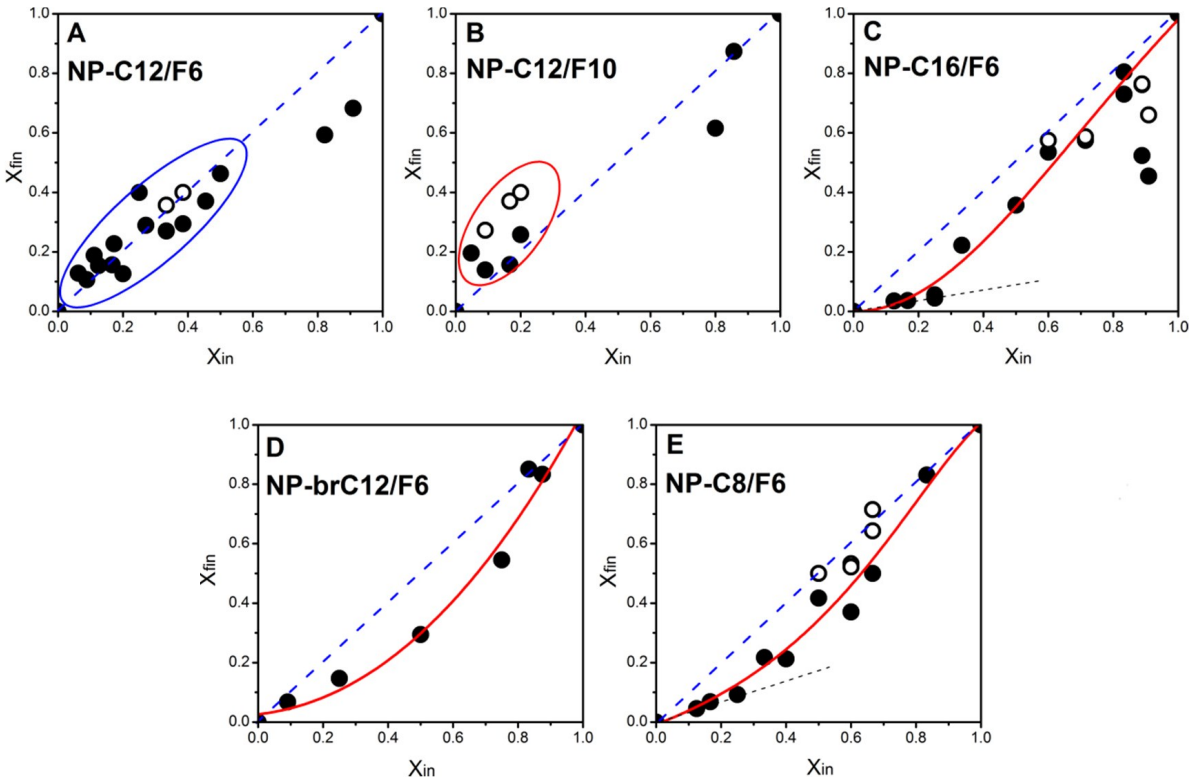

Figure 1.23: Results obtained from the analyses on the study of the relationship between the final composition of the monolayer and the initial reaction mixture. X_{in} and X_{fin} refer to the molar fraction of the fluorinated ligand respectively in the reaction mixture and in the monolayer.[64]. Adapted from reference [64] with permission of The Royal Society of Chemistry.

For NP-C12/F6 and NP-C12/F10 the introduction of fluorinated ligands is favoured even at lower fractions in the reaction mixture, exhibiting a sort of linear correspondence between initial and final compositions, with slight deviations only for higher fractions of fluorinated component. By elongating the hydrogenated chain, the introduction of fluorinated ligands in the C16 monolayer becomes unfavoured at low fractions up to a certain threshold; once passed it, fluorinated thiols enter more easily into the monolayer. Au NPs covered by branched thiols (NP-HbrC12/F6) are characterized by possessing a poorly organised monolayer and therefore the inserting of fluorinated thiols is unfavourable at every composition of the initial mixture. Eventually, for NP-C8/F6 an intermediate behaviour was pointed out where the introduction is not favourable at lower concentrations but it becomes favoured at higher concentrations. All these results are very important, since they prove that it is quite impossible to precisely establish the composition of the monolayer simply relying on the initial composition of the reaction

mixture. However, it is possible to point out that when the monolayer is characterized by a certain difference between the chain lengths and the amount of fluorinated component is low, the resulting interactions among fluorinated chains seldom happen together with the arise of H/F interfaces which are indeed unfavoured because they involve a decrease in vdW interactions among hydrogenated chains. Only when the molar fraction of fluorinated ligands reaches a considerable value, the number of fluorinated interactions grows and a remarkable entropic gain is achieved; consequently the formation of fluorinated domains is promoted, producing different interfaces H/F in the monolayer. Moreover, if no difference in chain lengths is observed, the loss of interactions among hydrogenated chains and the increase of those among fluorinated ones are two unfavourable contributes to the formation of many H/F interfaces, considering also the fact that there is no effective entropic gain due to conformational freedom. Then, this situation leads to the arising of small islands of fluorinated thiolates which enlarge and become more packed in order to minimize the H/F interactions.
The study also showed how the use of fluorinated thiols affects the size of the Au NPs themselves. Bulkier ligands involved in the Brust-Schiffrin procedure promote smaller NPs; since fluorinated chains possess a cross-sectional area larger than that of hydrogenated ones, the more is the amount of fluorinated thiols in the initial reaction mixture, the smaller should be the size of NPs produced. The TEM analysis of the Au NPs obtained by means of direct synthesis exhibits that, by increasing the molar fraction of fluorinated thiols of the reaction mixture, the size of the gold core decreases, being consistent with the bulky nature of fluorinated chains. The trends of the average diameter of the MM Au NPs involved in the study with respect to the molar fraction of fluorinated ligands are reported in Figure 1.24.

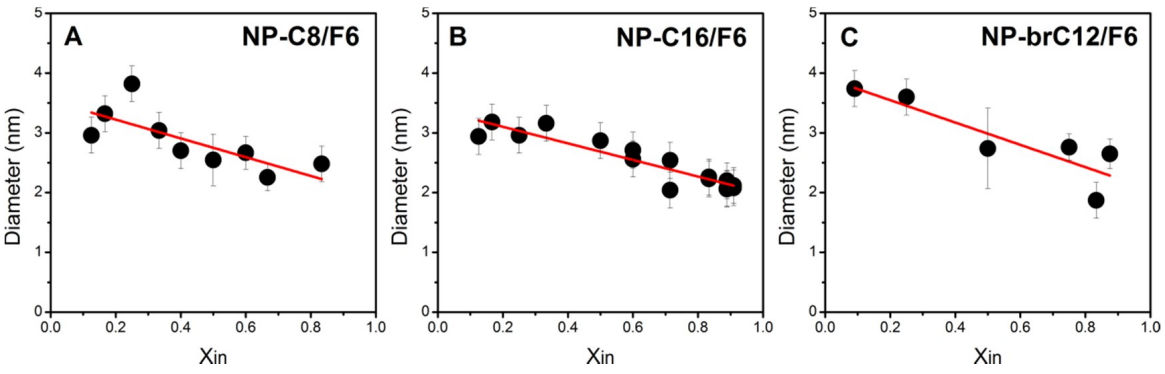

Figure 1.24: Trends of the average diameter of the MM Au NPs involved in the study with respect to the molar fraction of fluorinated ligands in the reaction mixture.[64] Adapted from reference [64] with permission of The Royal Society of Chemistry.

Finally, also the relationship between the solubility of the NPs and the composition of the monolayer was investigated and the outcomes from the analyses displayed a common trend related to the solvents employed: when the amount of fluorinated component is low, all NPs are soluble in chloroform and methylene chloride; at intermediate fractions, the NPs turn out to be soluble in hexane; at high percentage of fluorinated ligands, they are soluble in hexafluorobenzene. Once again, these results proved how the composition of the monolayer provides specific properties to the MM Au NPs themselves.
As a matter of fact, the ensemble of experimental techniques exploitable for a direct char-

acterization of the morphology of mixed monolayers containing fluorinated species is rather restricted, therefore the approaches need to be combined with computational multiscale simulations able to provide models whose analysis helps to understand the behaviour and the arrangement of the thiolates on the gold surface. This is the path followed in a recent study[61] by the group where the work concerning this thesis has been performed. Indeed, a combined experimental and computational investigation was carried out on the previously presented types of NPs (Figure 1.22), considering a range of core size in between 2 and 4 nm. Focusing on the difference in chain lengths of the thiolates composing the monolayer, the steric hindrance and the ratio between the two different types of ligand, the experiments provided results that pointed out different morphologies of monolayer of the NPs. In particular, 1D ^{19}F-NMR and 2D Heteronuclear Overhauser Effect Spectroscopy (HOESY) experiments were performed in order to explore the trend of the chemical shifts with respect to the chemical composition of the monolayer itself. Moreover, a combination of atomistic and coarse-grained calculations was adopted with the aim of achieving a model for each kind of NPs that could help to interpret the outcomes from NMR studies. The MM Au NPs were examined also with standard techniques such as UV-Vis spectroscopy, TEM, TGA and ^{1}H-NMR with the intent of gaining information related to the chemical composition of the monolayer and the size of the gold core. For what concerns the ^{19}F-NMR experiments, since the solubility differs according to the amount of fluorinated component of the monolayer, as previously discussed, the NPs soluble in $CHCl_3$ were dissolved in $CDCl_3$, whereas the others were dissolved in a mixture of $CDCl_3$ and C_6F_6. As a matter of fact, the characteristic peaks due to the terminal group CF_3 and the CF_2 group proximal to the terminal CF_3 move as the composition of the solvent changes. Therefore, all the chemical shifts were corrected. The computational complementary analysis was performed adopting a combined approach where the atomistic results achieved by means of MD were used as input for mesoscale calculations in the DPD method, allowing longer simulation times and consequently describing in a more proper way self-assembling phenomena. Also the solvents in their correct ratio ($CHCl_3$ and C_6F_6) were considered in the calculations. Eventually, the shape of simulated cores was icosahedral, providing more reliability to the results. Very important outcomes were achieved from both the experimental part and the computational predictions. For NP-brC12/F6, the branched structure of the hydrogenated thiolates did not allow an ordered crystalline arrangement on the surface of the gold core: the ligands did not tend to form packed domains and preferred to remain isolated. This produced a random organization of the monolayer, no matter which were the compositions of the monolayer and the sizes of the core. In the case of NPs covered by thiolates whose chain lengths are comparable, two different behaviours were observed: the morphology of the monolayer of NP-C12/F10 was Janus type; indeed, the ligands formed two distinct domains. On the other hand, the ligands of NP-C8/F6 did not separate in two defined domains but at low concentration of fluorinated component they tended to stay isolated, giving rise to a random organization, whereas by increasing the amount of fluorinated ligands, the monolayer was characterized by the presence of irregular patches. The authors provided a possible explanation for this behaviour: being the F6 chain quite short, the strength of the fluorophilic interactions is lower than that interesting the F10 chains and consequently the formation of fluorinated domains is less favoured.

Moreover, the organization of the thiolates can be disturbed by the fact that the absence of strong fluorophilic interactions is responsible for not counterbalancing the difference in hindrance between the hydrogenated and the fluorinated chains. Finally, when the difference in chain lengths is remarkable (NP-C16/F6 and NP-C12/F6), the ligands arranged themselves in domains with striped form, even at lower concentrations of fluorinated component. This is due to the considerable entropic gain arising from the difference in chain lengths. Indeed, the entity of this gain is so significant that it balances the loss in vdW interactions between hydrogenated chains produced by the formation of H/F interfaces. HOESY NMR experiments were performed as well. The HOESY spectra of the NPs which possessed a monolayer randomly organized or striped presented intense cross-peaks between CF_2 groups of the fluorinated ligands and CH_2 groups of the hydrogenated ones: these results are actually consistent to the formation of a consistent number of H/F interfaces due to the various domains present on the monolayer. However, the HOESY spectrum of NPs which were expected to possess Janus morphology (NP-C12/F10) presented strong cross-peaks between the two groups as well. Since the number of ligands at the interface of a Janus monolayer is rather small, the intensity of the cross-peaks should be reduced. A possible explanation for this phenomenon is that, being both types of chains quite long, the high number of CF_2 groups determined a considerable amount of interactions, producing therefore strong cross-peaks clearly visible in HOESY spectra.

CHAPTER 2

Synthesis and Characterization of Gold Nanoparticles

1 Introduction

This second chapter is meant to briefly present the approaches for the synthesis of Au NPs protected by solely one type of ligand, defined therefore homoligands NPs, and Au NPs protected by mixtures of ligands, whose monolayer is consequently mixed due to the fact that the chemical nature of the composing ligands is different. Countless procedures have been proposed along the years, moved by the pursuit of controlling several structural properties of the metal core such as sizes, shapes and size distribution as well. The need of achieving a so high degree of control is motivated on one hand by the demanding need to employ these nanotools as building blocks for new materials; on the other, the development of efficient characterization techniques for studying their behaviour in order to completely exploit their properties for tailoring the numerous potential applications of these systems. According to what type of properties are desired the most, either physical or chemical procedures are taken into account for the preparation of metal-based NPs: indeed, these nanosystems can be produced by a "top-down" approach, which implies the formation of NPs by making use of physical agents able to etch the bulk material, followed by the rearrangement of gold atoms in Au NPs, or by means of a "bottom-up" approach, which involves the formation of Au NPs starting from chemical precursors. Within the possibilities of production that the first method offers, different strategies and pathways for the preparation of NPs have been proposed along the years, taking advantage of several techniques, such as laser ablation[69], electrophoretric deposition[70], sputtering[71] or UV radiation[72]. The latter,chemical, method instead is more focused on the procedures that allow the assembly of metal atoms in supramolecular entities and their coating with species that prevent the so-formed NPs from the aggregation. As a matter of fact, this approach is the one that was followed for preparing the batches of Au NPs studied within this work of thesis. However, concerning Au NPs, the chemical syntheses that have been developed in recent years are countless and an in-depth description of all of them goes beyond the goal of this chapter. Therefore, the first part of the chapter itself will provide few details on the procedures that were

employed for preparing the batches Au NPs presented in the next part of this thesis, pointing out their major strengths and the weaknesses. A short historical background precedes the section, giving information of the birth of the synthesis and the study of Au colloids and Au NPs. The second part of the chapter is devoted to the description of some techniques for the characterization of Au NPs. Being hybrid organic-inorganic materials, Au NPs can be characterized exploiting a wide range of techniques, thanks to the different behaviour of the core with respect to the ligands in responding to a certain stimulus, *e.g.* a radiation, arising from the application of a characterization technique. Therefore, a proper analysis of a batch of Au NPs involves the NPs as whole supramolecular object, taking into account both the properties of the core, such as dimension and shape, and those of the monolayer, which can be related to its chemical composition and the arrangement of the ligands on the gold surface. The step of characterization of Au NPs is undoubtedly essential for an effective exploitation of the properties that can be consequently modulated for many possible applications. However, the process of characterization is sometimes rather challenging and time consuming, due to the need of investigating a consistent number of samples with different characteristics for achieving a deep degree of knowledge about a specific behaviour. Moreover, most of the times the outcomes from several characterization techniques must be combined, in order to gather more complete and exhaustive information on the system itself. Different methodologies have been implemented and improved during the years, allowing to get a clearer insight into the properties of Au NPs and MM Au NPs, namely: microscopies techniques[73,74], nuclear magnetic resonance studies,[75] mass spectrometry investigation on the organization of the ligands within the monolayer[76] and the place exchange process[77], theoretical calculations and modelling.[59] The number of characterization techniques and their developments has grown exponentially over the years and, similarly to the synthetic procedures, the complete enumeration and description of them goes beyond the purposes of this chapter. The second part of the chapter will therefore cite some of the major techniques for the characterization of the metallic core and the monolayer, focusing on the ones that were mostly used during this thesis work.

2 Synthesis of homoligand Au NPs

The scientific interest for Au NPs rooted in the second part of nineteenth century when Michael Faraday proposed in 1857 the first synthesis *tout court* of colloidal gold, mixing an aqueous solution of $NaAuCl_4$ with a solution of white phosphorous, used as reducing agent, in carbon disulphide.[78] Since then onwards, the interest on colloidal gold started to grow among the scientists and the study of its properties became one of the major topics of discussion that lasts up to nowadays. Richard Adolf Zsigmondy was then awarded the nobel prize in chemistry in 1926 for its study on heterogeneous nature of colloidal solutions. In 1951, Turkevich *et al.* proposed the synthesis of gold colloids capped with citrate molecules:[79] the method is one of the simplest and most used approaches for the preparation of gold colloids of 20 nm in diameter. The synthesis was then improved by Frens in 1970, when he reported a procedure for tuning the dimensions of the colloids by varying the ratio between gold and citrate.[80] The first report on gold colloids stabilized by thiolates was published in 1993 by Giersig and Mulvaney[81] and, subsequently, Brust *et al.* proposed the first synthesis[82] of Au NPs protected by dodecanethi-

olates in 1994, which has become over the years one of the most widely used synthesis of Au NPs of small dimensions within 1 and 3 nm. This latter method will be treated further in details in the next section.

2.1 Brust-Schiffrin Procedure

One of the most widely used methodologies for the synthesis of Au NPs having moderate dimensions is the Brust-Schiffrin procedure.[82] It has gained a lot of resonance along the years thanks to its efficiency and simplicity. It consists in a two-phase water/toluene synthesis in which $AuCl_4^-$ is reduced by means of $NaBH_4$ in presence of an alkanethiol, leading to the growth of the gold clusters together with the adhesion of the thiols on the gold core in order to form the monolayer. As a matter of fact, a two-phase system is needed to guarantee the simultaneity of these two processes and therefore the synthesis involves the employment of tetraoctylammonium bromide (TOAB) as phase-transfer agent which transfers the $AuCl_4^-$ anion from the aqueous to the organic phase. Then, once the phases have been separated, the mixture is vigorously stirred and the solution of thiols is added. The authors claimed that addition of thiols leads to a preliminary reduction of Au(III) ions to Au(I), forming gold-thiol polymers. The final reduction of Au(I) to Au(0) is carried out by the addition of an aqueous solution of $NaBH_4$. A simple scheme of the reaction is reported in Figure 2.1.

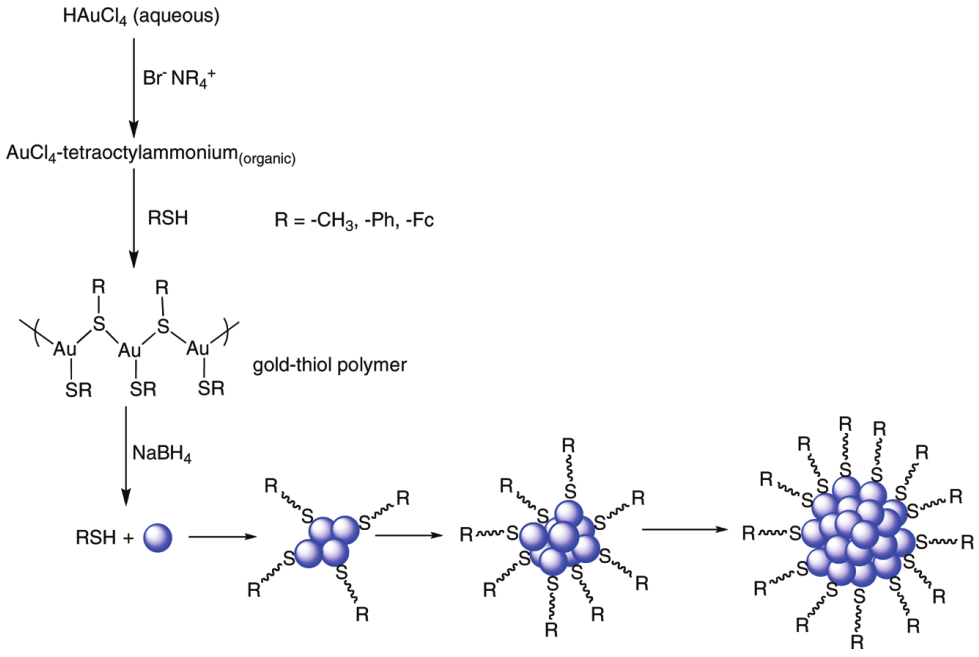

Figure 2.1: Scheme of the procedure proposed by Brust *et al.*[83] Adapted with permission from reference [83]. Copyright © 2009 American Chemical Society.

Further studies[84] by Goulet and Lennox on the mechanism involved in the synthesis evidenced instead that the Au(I) species formed upon addition of thiols are mainly Au(I) dihalogenide complexes, being the formation of Au(I) thiolate polymers only noticeable in media containing a considerable amount of water. Figure 2.2 displays the revisited mechanism of the Brust-Schiffrin procedure for the synthesis of Au NPs.

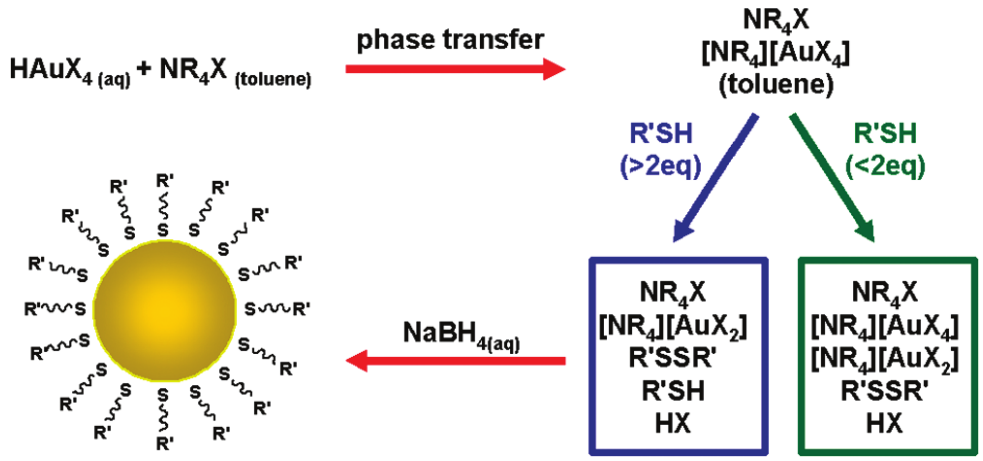

Figure 2.2: Scheme of the procedure[84] proposed by Goulet and Lennox, resulting from further studies on the two-phase synthesis of Au NPs proposed by Brust et al., 1994. Adapted with permission from reference [84]. Copyright © 2010 American Chemical Society.

The whole procedure is rather fast and efficient, it assures a high yield and the stability of these NPs is excellent, both in solution and in the solid state. HR-TEM images of the NPs synthesized by this method display that the diameters are between 1 and 3 nm with a maximum in the distribution of the sizes around 2.0-2.5 nm. Although a certain form of control can be bestowed to the method by tuning the reaction conditions, *e.g.* the thiol/gold ratio, as well as the temperature or the rapidity in adding the reducing solution, this procedure hardly allows the achievement of NPs possessing a size over the 3 nm. Moreover, narrow size distributions are quite difficult to obtain for larger NPs. This latter critical aspect is related to the fact that the employment of strong reducing agents, such as $NaBH_4$, does not assure an adequate balance between nucleation of new gold cores and growth of the already existing ones. The rapid reduction of Au(I) precursors implies indeed the production of a considerable number of sites of aggregation, strongly moving the equilibrium towards the nucleation process. Therefore, during the synthesis, most of the gold in the environment undergoes nucleation and it is involved in forming new cores, rather than contributing to the growth of the one previously formed. At the end, the batch is composed by part of the cores that grew and part that did not, altering the size distribution. The narrowing of size distribution is however possible, and it can be achieved by *post*-synthesis heat treatment of the solid NPs produced according to Brust-Schiffrin procedure in presence of TOAB, which was firstly proposed by the group of Miyake,[85] or by the employment of mild reducing agents, assuring a balance between nucleation and growth of the cores.[86,87]

2.2 Control over dimensions and size distribution

As previously discussed, the synthesis of Au NPs according to the Brust-Schiffrin procedure does not allow to prepare batches of Au NPs protected by alkanethiolates with narrow size distribution. The main reason behind this drawback is related to the use of a strong reducing agent such as $NaBH_4$.

2.2.1 *Post*-synthesis heat treatment

The method[85] proposed by the group of Miyake consists in a heat treatment performed on Au NPs produced *via* the Burst-Schiffrin synthesis. The particularity of this treatment is related to the fact that it is possible to reach a certain control of the dimensions of the NPs by carefully selecting the conditions at which the treatment is carried out. In their study, Miyake and coworkers used Au NPs protected by alkanethiolates with an average size of 1.5 ± 0.2 nm and subjected these materials to several heat treatments at different temperatures ranging between 150 °C and 250 °C. Starting from room temperature, this latter parameter is progressively increased with a rate of 2 °C·min^{-1}. The size evolution of the NPs upon heat treatment is observed only in presence of TOAB. Indeed, it seems that TOAB melting at the temperatures at which the heat treatment is performed, acts as a solvent for the NPs. The results for the different treatments display how higher temperature values produce NPs with larger core dimensions. In particular, the treatments performed at 150 °C,190 °C and 230°C produced NPs having respectively a size of 3.4 ± 0.3 nm, 5.4 ± 0.7 nm and 6.8 ± 0.5 nm. Obviously, also the period of time during which the NPs are maintained at the final temperature is a factor that can affect the size of the NPs after the treatment.
The major drawback of the approach is related to the difficulty in reproducing the outcomes obtained, since neither clear indications nor rules exist addressing defined conditions for the achievement of batches with a given average core dimension. Moreover, few limitations affect the method since problems may arise by carrying out heat treatment at a temperature close to the boiling point of the ligands that coat the cores: the consequence could result in desorption of ligands from the Au cores, leading to aggregation of the NPs.

2.2.2 Synthesis proposed by Zheng *et al.*

This procedure was proposed by Stucky and coworkers[86] and it is different from the one proposed by Brust and Schiffrin since it involves the use of a single organic phase together with the employment of amino-borane complexes as reducing agents. The precursors have to be soluble in organic solvent: for this reason, $AuPPh_3Cl$; this compound is readily available from commercial sources or is employed and it can be obtained from the reaction of $HAuCl_4 \cdot nH_2O$ with PPh_3 in ethanol. The whole synthesis is performed in air mixing the metal salts and the ligands in an organic solvent. Afterwards, the amino-borane complex is added under stirring. As a matter of fact, the reducing strength of the amino-borane complexes is lower with respect to $NaBH_4$, consequently, the reduction is slowed, establishing a balance between nucleation and growth of the NPs, which leads to a certain degree of control over the sizes of the cores. Indeed, employing a stronger reducing agent causes the Au(III) to be reduced more rapidly, giving rise to smaller NPs. Nevertheless, the more the reduction is slowed, the more is the time needed to complete the reaction. It is possible to easily deal with this inconvenient by increasing the concentration of the reducing agents and the temperature at which the reaction is performed, speeding the whole process up. In fact, performing this kind of synthesis at low temperatures in short periods of time results in a broad size distribution, whereas if the temperature is rather high and the period of time is conveniently long, smaller NPs grow until reaching bigger dimensions. Moreover, also the solvent plays an important role: the employ-

ment of polar solvents produces stable small NPs; on the other hand, bigger NPs are achieved through the use of non-polar solvents. The study by Stucky and coworkers proves that by employing strong ligands the formation of monodisperse NPs is facilitated as compared to weaker ligands as amines or phosphines. As a matter of fact, bigger NPs can be seen as thermodynamically metastable states stabilized by long chains of alkyl thiols.
Within this approach, there are several factors that affect the size of the gold cores: the solvent employed, the chemical nature of the thiols and the temperature turned out to be really important for the outcome of the synthesis. Obviously, the more the temperature is increased, the faster the reaction is carried out. Rising up the temperature is also exploited in order to obtain a higher homogeneity of the reaction solution, improving the outcomes in terms of dispersion. The dimensions of the NPs and consequently the dispersion can be substantially affected by the interactions arising between the chains of the ligands bound to the gold surface. For instance, the employment of ligands bearing groups that repelled themselves, *e.g.* charged groups, will promote the formation of smaller NPs in order to increase the distance among the chains forming the monolayer. On the other hand, thiols capable to favourably interact thanks to van der Waals forces will allow the formation of larger NPs, whose monolayer is more packed. Eventually, the choice of the solvent can represent the most straightforward tunable parameter in order to vary the size of the gold core. Different studies[88,89] have pointed out that the employment of polar solvents promotes the formation of NPs having reduced dimensions whereas using non-polar solvents leads to higher dimensions. One possible explanation for this behaviour has to be ascribed to the interactions of different nature arising among the thiols and the molecules of solvent. Indeed, considering alkanethiols, *e.g* dodecanethiols, protic polar solvents, such as ethanol, seem to promote strong hydrogen bond between the hydroxyl group of the solvent and the thiolic group which facilitates the formation of the Au(I)-SR bond and therefore the surrounding of the incipient nanoclusters (NCs) by the thiols. *Vice versa*, aprotic non-polar solvents give rise to hydrophobic effects with the alkyl chain of the thiols, leading to a higher degree of desorption of the thiolates from the surface of the NCs and promoting their growth. A schematic representation of the concept is given in Figure 2.3.

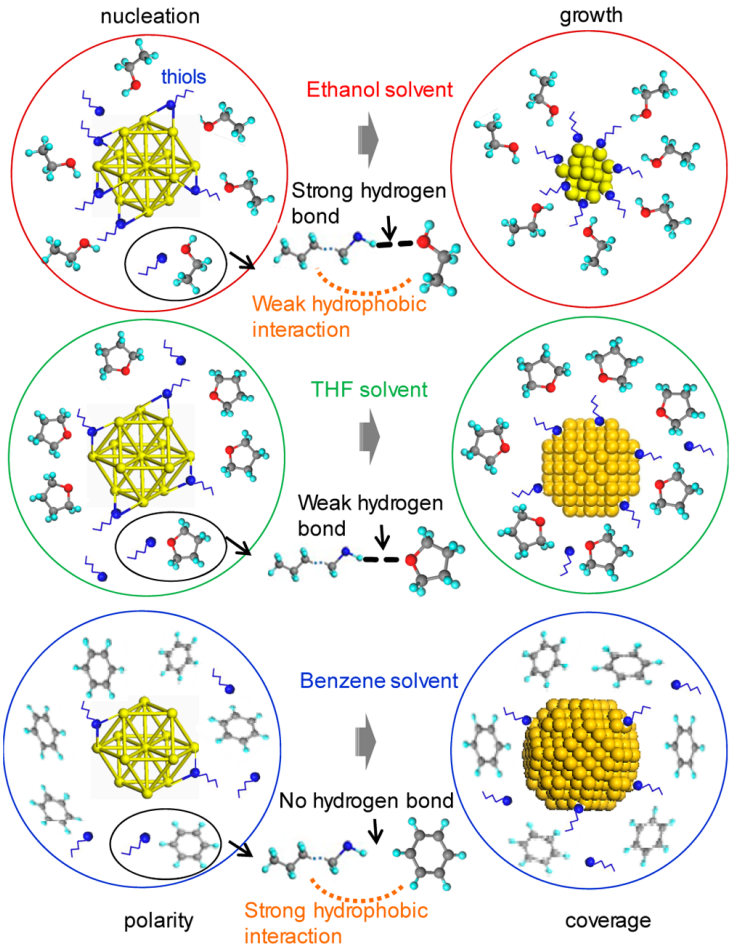

Figure 2.3: Interactions arising among ligands and solvent molecules during the synthesis of Au NPs according to Zheng *et al.*[89] Adapted with permission from reference [89]. Copyright © 2014 American Chemical Society.

2.2.3 Synthesis proposed by Peng *et al.*

The approach has been proposed by Peng and coworkers,[87] which involves the use of $HAuCl_4 \cdot 3H_2O$ as gold precursor and oleylamine (OLAM) as both capping ligand and phase transfer agent. Indeed, the synthesis is carried out in aliphatic or aromatic non-polar solvents, such as hexane, tetraline, 1-octadecene or benzene, therefore a transfer agent is necessary to bring the gold precursor in the organic phase. The reducing agent is *tert*butyl-aminoborane complex whose reducing strength is mild, as already described, allowing the control over NPs core dimensions. This latter property can be easily tuned according to the temperature at which the reaction is carried out, producing NPs of reduced cores sizes at high temperature, whereas low temperatures give rise to NPs exhibiting bigger core sizes. Furthermore, the choice of the solvent is another key aspect for achieving narrow size distribution and stabilizing the NPs.[90] Long linear aliphatic solvents are able to intercalate among the molecules of oleylamine (OLAM) bound to the gold atoms, leading to supporting interactions for the stability of the overall monolayer and decreasing the desorption of ligands from the core. On the other hand, the use of bulky aromatic or alicyclic solvents brings to the formation of a looser monolayer, less stable and more subjected to desorbing phenomena. Figure 2.4 displays the effects of different solvents on the packing of the monolayer.

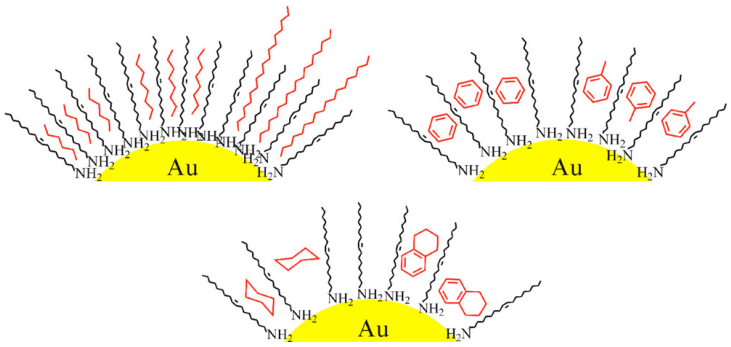

Figure 2.4: Effects of the different solvents on the packing of the monolayer of Au NPs coated with oleylamine.[90] Adapted with permission from reference [90]. Copyright © 2013 Elsevier.

This synthesis has been widely employed for the production of Au NPs with relatively low size distribution, although with minor changes.[90–92] The key feature of this synthesis is indeed the possibility of obtaining monodisperse batches of Au NPs protected by OLAM which can then either be subsequently used as substrates for producing seeds for catalysis[92] or be involved in place exchange reaction, coating the gold cores with the desired ligands. This latter approach generally aims at introducing in the monolayer ligands which are able to form more stable interactions[93] both with gold atoms of the core, *i.e.* thiols, and among themselves. With reference to the latter point, a high number of favourable VdW interactions is possible when the monolayer contains alkanethiolates while this is not possible in the case of OLAM because of the steric hindrance due to its *cis* conformation. Thiolates-coated Au NPs can therefore be produced by taking advantage of the weaker Au-N bonds whose lability allows to obtain a complete substitution of ligands after a place exchange reaction, involving species which are able to form stronger bonds with Au atoms, such as indeed thiols.
Although the procedure is simple and it provides satisfying results in terms of size distribution, the reduced strength of the bonds between gold and nitrogen respect to gold-sulfur bond represents the most critical point of the protocol. As a matter of fact, if the NPs produced are used as seeds for subsequent growth for catalytic purposes, then the weakness of the bonds among oleylamine and gold atoms facilitates the process, which requires the removal of ligands for exploiting the catalytic properties of bare nanometric gold. However, if the NPs produced must undergo functionalization or monolayer engineering, then the overall instability may lead to problems concerning the aggregation of the cores or their decomposition.

3 Synthesis of Mixed Monolayer Au NPs

The mixed monolayer (MM) Au NPs can be produced according to one of the two procedures herein described: the first one is the direct synthesis, in which the MM Au NPs are prepared starting from the precursors mixed with blends of thiols; the latter is the place exchange reaction that implies that the NPs have been previously prepared and characterized to estimate the average number of ligands per NP, so that having an idea of the necessary amount of exchanging ligands. Both are carried out in solution and both require subsequent purification of the NPs before their characterization.

3.1 Direct Synthesis

The direct synthesis approach involves the reduction of gold precursor in the presence of a mixture of ligands that will eventually coat the surface of the gold core. This method allows obtaining mixed monolayer Au NPs without any further treatment; however the ligands used for the synthesis must be compatible with the reductive conditions, stable during the reaction and easily available in large amount. The control over the final composition of the monolayer is not always easy to achieve, since competition among thiols grafting the gold atoms may arise during the formation of the gold cores. Moreover, place exchange reaction could take place during the growth of the cores themselves.

3.2 Place Exchange Reaction

During a place exchange reaction, or ligand exchange reaction, the thiolate forming the monolayer is displaced by a new ligand. This method is commonly used when the second ligand it is not compatible with the conditions for a direct synthesis or it is very expensive either in terms of cost or time devolved for its synthesis. The control over the composition of the monolayer is higher than that obtained after a direct synthesis, especially if the place exchange reaction is carried out for a period of time sufficiently long, allowing the system to reach the equilibrium.
During a place exchange reaction, or ligand exchange reaction, the thiolate forming the monolayer is displaced by a new ligand. This method is commonly used when the second ligand it is not compatible with the conditions for a direct synthesis or it is very expensive either in terms of cost or time devolved for its synthesis. The control over the composition of the monolayer is higher than that obtained after a direct synthesis, especially if the place exchange reaction is carried out for a period of time sufficiently long, allowing the system to reach the equilibrium.
The group of Royce W. Murray deeply investigated[94] the process of place exchange reaction on Au NPs, claiming that the overall mechanism is based on an associative process where the incoming ligand gets through the monolayer undergoing place-exchange and leading to the exit of the displaced ligand as thiol. The reaction rate depends on the molar ratio between entering thiols and thiolates bound to the gold atoms, as well as the structural characteristics of the chains of the ligands, such as their relative length and the steric hindrance associated both to the chains themselves and to any terminating functional group that may be present.[95]
The early studies[96] on the subject pointed out that some sites on the surface of gold core are the first to be involved in the exchange: this is the case of vertexes, edges or defects of the gold core where the monolayer presents discontinuities. On the other hand, the higher degree of packing of the monolayer on regions like terraces or facets of the core implies more difficulties in exchanging ligands. For this reason the rate of exchange on NPs is initially rapid because the first ligands involved in the place exchange are those on the edges and vertex; subsequently, the ligands on the more packed region of the monolayer starts to be involved in the exchange. The more the chains of the ligands are long, the more packed is the monolayer and consequently the rate of the reaction of place exchange is lower. This phenomenon is due to the fact that a higher number of interactions among the ligands composing the monolayer arise, providing more stability to the overall system and implying a denser layer of ligands that hinder the incoming of other ligands.

This apparent preference for certain sites of the core during the initial period of time of the place exchange reaction can be exploited for the functionalization of particular sites on the surface of the gold core. Indeed, since the involving of ligands bound to gold atoms at the vertexes or on the edges of the core is the first that takes place, carrying out the place exchange reaction for short periods of time could help in achieving the insertion of ligands in precise sites of the monolayer. The approach of fast place exchange reaction[22] is however affected by a considerably high number of variables that must be considered, such as temperature, concentration of the species involved, solvent, length of the entering ligands and obviously time. Consequently, although being a potentially powerful approach for the controlled functionalization of Au NPs, fast place exchange reaction could lead to totally unexpected outcomes without a proper tuning of the reaction conditions, which requires a methodical approach. Unfortunately, the fact that is hardly possible to find general conditions suitable for every type of Au NPs worsens the situation, making the overall process extremely challenging and time demanding. One possible strategy to smooth the complexity of the approach is attempting to reduce the size distribution of the Au cores, obtaining NPs with similar chemical behaviour within the same batch. As a matter of fact, the intrinsic statistic nature of these systems cannot be totally avoided; however, the more the sizes of the cores are similar one another, the higher the number of NPs with equal stoichiometry will be, allowing to reach a higher degree of control in the process of place exchange reaction.

4 Charachterization of Au NPs

The characterization of Au NPs is a fundamental step in the study of these nanosystems and their possible applications. Indeed, an in-depth characterization allows gathering all the necessary information for exploiting the properties of the NPs *in toto*. The emerging potential applications of these nanosystems will eventually be possible only if a careful investigation on their properties and behaviour is carried out. As an example, the possibility of actualising size-dependent applications concerning cellular uptakes[97,98] and biodistribution is strongly affected by the size and shape of the gold core, and requires a complete structural and morphological study of the NPs. The same considerations apply to catalytic processes[99] involving Au NPs of reduced dimensions: complete structural characterization of the NPs is mandatory to properly guide the design of systems in which the surface to volume ratio is such to exploit at maximum the catalytic activity of surface atoms. On the other hand, applications based on the interactions of Au NPs and MM Au NPs with the surroundings depend on the composition of the monolayer and its morphology; consequently, only an adequate characterization of the monolayer opens the door to the tailoring of the procedures for the engineering of the mutual arrangement of the ligands within the monolayer itself. Addressing the task of characterizing systems whose nature is intrinsically statistic is challenging, since the answers achieved from the investigation of the properties of a single batch are indeed mediated over the NPs composing the batch itself. Undoubtedly, the characterization process becomes smoother and the outcomes obtained are more intelligible if the batch of Au NPs studied exhibits narrow size distribution; indeed, a narrowly dispersed batch is composed of NPs that possess similar properties and behaviour which may be more predictable.

4.1 Characterization of the metal core

4.1.1 Transmission Electron Microscope

The dimensional and morphological characterization of the core is mainly performed by means of microscopy techniques such as transmission electron microscopy (TEM) and its developed variant High-Resolution TEM. Carrying out an analysis on part of the NPs that composed a given batch, these techniques allow to measure with precision the diameter of the NPs and then establish the average core diameter for the batch, together with the standard deviation related to the average size of the gold core, so that estimating the size distribution that characterizes the batch. Moreover, HR-TEM allows also the visualization of the atomic layers within a single core: with this technique is then possible to measure interlayer distances, gathering information on how the gold atoms are arranged. Figure 5.24 displays a HR-TEM image of a Au NP coated with a layer of Pd.[100] The typical fringes outlining the atomic layers are clearly appreciable.

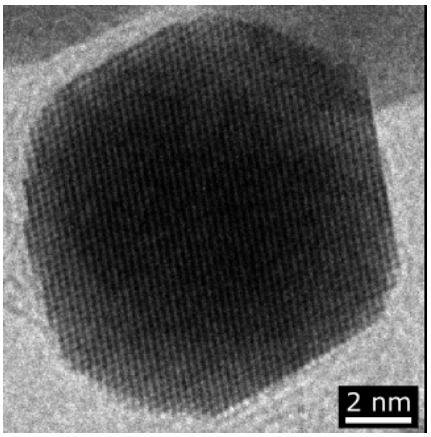

Figure 2.5: HR-TEM image of a Au NP coated with a layer of Pd. Note the fringes outlining the atomic layers.[100] Adapted with permission from reference [100]. Copyright © 2010 American Chemical Society.

4.1.2 X-ray Diffraction

X-ray Diffraction (XRD) is another powerful technique that can be exploited for analysing the structure of the metal core. The work[101] of Jadzinsky *et al.* pioneered the study of the structure of the core of Au clusters and spread light to the organization of self-assembled monolayers on 3D surfaces, such as Au NPs. The outstanding achievement of a crystal structure of Au_{102} cluster protected by *para*-mercaptobenzoic acid by means of XRD highlighted the presence of the so-called staple motifs involving the presences of RS-Au-SR moieties on the the outer part of the core, where a gold adatom is between two thiolates. Moreover, the crystal structure evidenced also the fact that the morphology of the metallic core resembles to a Mark decahedron. Although being an incredibly useful technique, XRD is affected by the fact that it can be applied only on crystalline materials; in the case of $Au_{102}(SR)_{44}$, the authors were able to prepare crystalline clusters thanks to *inter* and *intra* clusters forces, such as hydrogen bonds and π-π stacking, that arose due to the chemical properties of the particular ligand employed as cap-

ping agent. However, in the case of Au NPs, obtaining crystalline substrates to analyse with diffraction techniques is very challenging and not always possible.

4.1.3 UV-Visible Spectroscopy

UV-Visible (UV-Vis) Spectroscopy is a straightforward technique that can be used to estimate the average dimension of the cores within a batch of Au NPs, besides the investigation of the optical features of the NPs. As already reported in literature,[102] the gold core is the main contribution to light absorption by Au NPs. Indeed, by means of this type of spectroscopy it is possible to achieve a preliminary analysis concerning the size of the gold core. Obviously, the kind of information that can be collected from an UV-Vis spectrum is far from possessing the precision of a TEM analysis, since their absorption is not very sensitive to the changes in core size; however, UV-Vis measurements are usually quite fast and they do not require sophisticated sample preparations. As a matter of fact, the first outcomes from a UV-Vis analysis of Au NPs can be employed as a tool for establishing whether the overall core dimensions are over a certain value or not. Indeed, if the gold cores possess an adequate size, the electrons at the gold surface are involved in a physical phenomenon called Surface Plasmon Resonance due to the oscillation of these superficial electrons induced by absorption of photons, possessing an energy between the visible and the infra-red portions of the electromagnetic radiation. The effect of this collective oscillation on a UV-Vis spectrum is the arising of the so-called Surface Plasmon Band (SPB), whose maximum intensity can be generally visualized in the range of wavelengths between 510 and 520 nm. In the case of Au NPs, this phenomenon takes place if the dimensions of the gold cores are over 3 nm, otherwise, no SPB is observed. In Figure 2.6, several UV-Vis spectra[103] of Au NPs characterized by different average dimensions are reported; in the picture, it is also possible to appreciate the shift of the maximum of absorption of the SPB with respect to the core size.

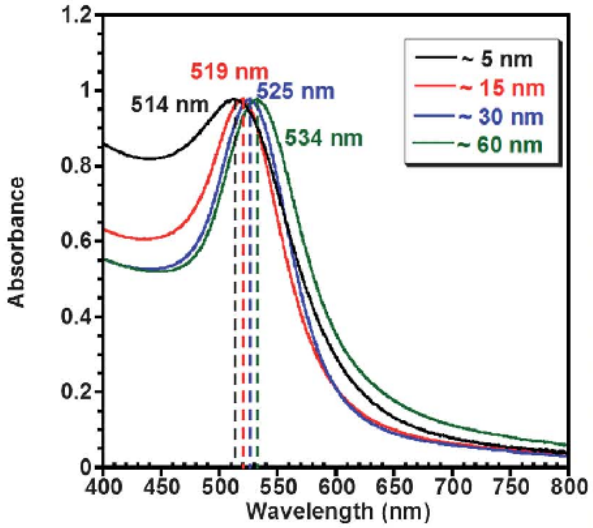

Figure 2.6: UV-Vis spectra of Au NPs of different dimensions.[103] The values of wavelength reported refer to the absorption maxima of the surface plasmon band, which vary with respect to the average core size. Adapted with permission from reference [103]. Copyright © 2013 Royal Society of Chemistry.

4.1.4 X-ray Photoemission Spectroscopy

X-ray Photoemission Spectroscopy (XPS) can be used to establish the oxidation state of the surface atoms composing the gold core. Indeed, in the already cited work[82] of Brust *et al.*, the authors claimed that XPS spectra recorded on the Au NPs prepared evidenced the presence of the typical $4\,f_{7/2}$ and $4\,f_{5/2}$ doublet whose binding energy were 83.8 eV and 87.5 eV respectively. Figure 2.7 displays the cited XPS spectrum. The binding energy values are characteristic for metallic gold; moreover, the absence of a band at 84.9 eV proved that the majority of the gold atoms composing the cores were in Au(0) oxidation state. The authors performed an elemental analysis on the NPs as well, pointing out that one third of the overall gold atoms were superficial atoms bound to thiols, exhibiting metallic character.

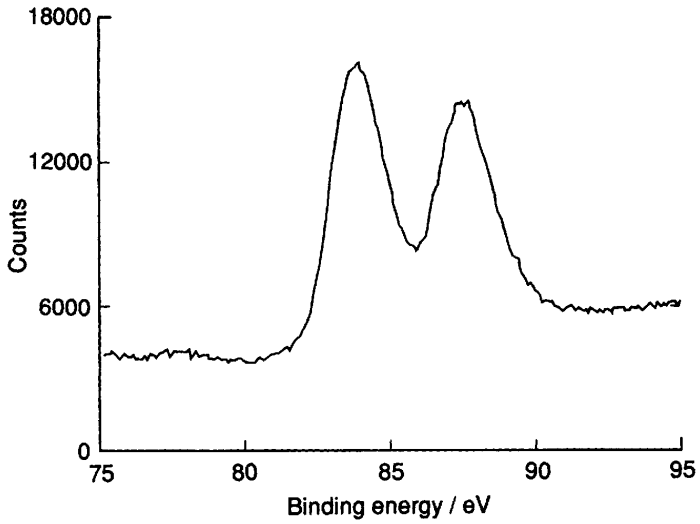

Figure 2.7: XPS spectrum of Au NPs prepared in the work[82] of Brust *et al.* Adapted with permission from reference [82]. Copyright © 2010 Royal Society of Chemistry.

4.2 Characterization of the monolayer

The characterization of the monolayer is probably the most challenging part of the analyses aimed at assessing the properties of Au NPs. Indeed, according to the protocol and the ligands employed for the preparation of the NPs, the layer of capping agents surrounding the core can reach high levels of complexity when blend of immiscible ligands are employed, due to their mutual arrangement on the surface of the gold core. The characterization techniques concerning the monolayer can be further divided in three main groups, according to the classification proposed in the account[104] of Ong *et al.*, which are microscopy techniques, spectroscopy techniques and simulations. Figure 2.8 reports a sketch that illustrates the principal techniques belonging to the three categories.

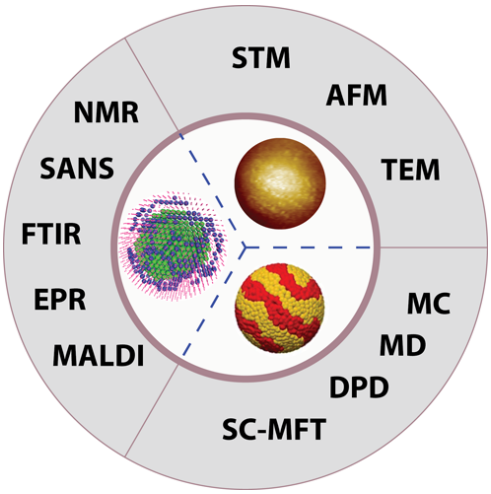

Figure 2.8: Principal techniques employed for the characterization of homoligand and mixed monolayers on Au NPs.[104] Adapted with permission from reference [104]. Copyright © 2017 American Chemical Society.

All of them have their strength and their limitations: microscopies allow a direct visualization of the monolayer and its morphology, however the analysis is limited only on a reduced part of the whole batch and the process of sample preparation is challenging, time consuming and sometimes it implies a *trial-and-error* approach. On the other hand, spectroscopy techniques provide answers that involve the whole batch of NPs; however, the answers are obviously averaged over the behaviour of every single NP. Therefore, if the sample studied is affected by a broad size distribution, difficulties in the interpretation of the outcomes may arise. Eventually, simulations are powerful and precise, but the methods need to be validate and the results provided must be inevitably compared with the experimental ones; furthermore, the programs used for the modelling of the monolayer are limited by the performance of the existing hardware.
The following sections will briefly describe some of the major techniques for characterizing the monolayers in terms of both composition and morphology.

4.2.1 Microscopy techniques

The study of mixed monolayers by means of microscopy techniques is indeed biased by the fact that the ligands domains usually possess reduced dimensions, limiting the number of

techniques applicable to the purpose. Up to now, scanning probe microscopies, such as Scanning Tunneling Microscopy (STM) and Atomic Force Microscopy (AFM), are the most suitable techniques for this type of analysis. **Scanning Tunneling Microscopy** uses as a feedback the tunneling current between a sharp metallic tip and a substrate. Several studies[56,57,60,74,105,106] using this technique have been carried out by the group of F. Stellacci on mixed monolayers, as discussed in Chapter 1. In those studies, the authors were able to point out the organization of the ligands on the surfaces of Au NPs by analysing the arrangement of the features visible in the STM images produced by the conductivity and height difference of the molecular component of the ligand shell. Figure 2.9 reports an example of two STM images[56] of the same NP where it is possible to perceive the arrangement of the ligands in ordered alternating stripes.

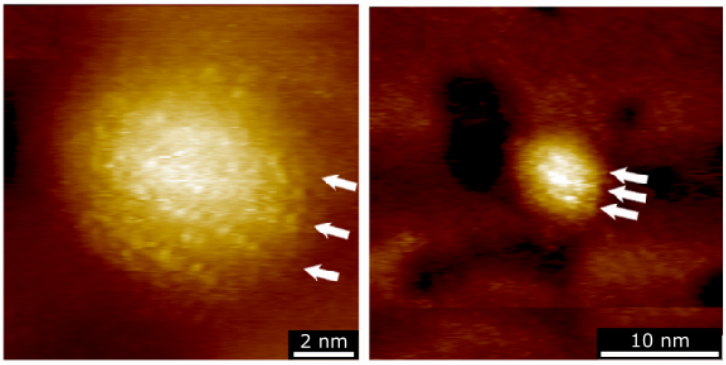

Figure 2.9: Two STM images of the same MM Au NP acquired at different magnifications.[104] The white arrows point the direction of the stripe-like features visible on the surface of the monolayer. Adapted with permission from reference [104]. Copyright © 2017 American Chemical Society.

The technique requires absolutely clean samples, since any residual free ligand can spoil the quality of the images due to contamination of the tip and mislead their interpretation. Moreover, in the case of NPs, these must be anchored to a substrate, which is usually a 2D SAM of shorter thiolates acting as filler agents and long alkyl dithiolates on Au(111) surface on mica substrate. The anchoring step is crucial because any movement of the NPs can affect the quality of the images obtained. Furthermore, the images recorded by STM can be affected by feedback loop artefacts that could be generated by an improper setting of the imaging setup. This problem can be circumvented by acquiring the same image at several tip velocities and scanning the area at different angles. However, this procedure increases the complexity in the interpretation of the images because of ligands domains could be characterized by local defects and differences in thickness. Therefore, Biscarini *et al.*, developed a method[106] that extracts the correlation length from STM images employing the Power Spectral Density (PSD) which represents the contribution of different length scales displayed in the frequency domain of the image. The approach allows then extracting the spacing between the ridges in the domains that characterize the monolayer. Figure 2.10 displays a typical PSD curve obtained from the analysis of a STM image representing striped NPs.

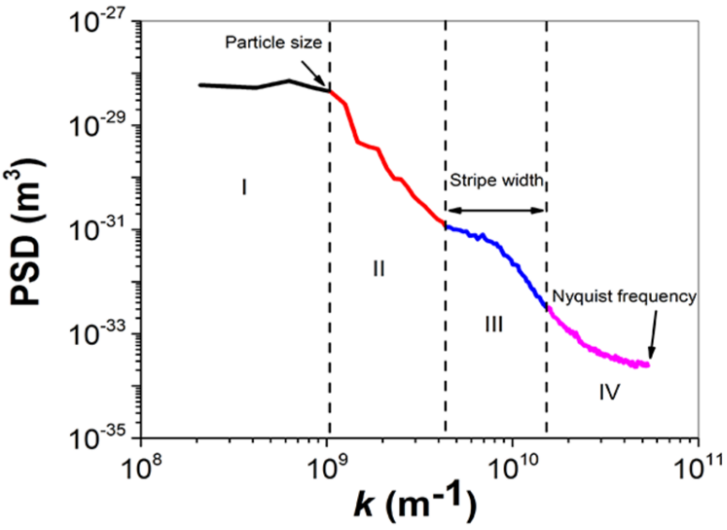

Figure 2.10: PSD curve of an STM image representing NPs with stripe-like domains. Four different regions of the curve are highlighted which represent the four segments that can be outlined in typical a PSD curve of an STM image of gold NP: the region indicated with I is a plateau at low frequency that stops at the frequency from which the particle size can be estimated, the one indicated with II is a decay that is related to the particle curvature and the characteristic noise of the microscope, the region outlined as III corresponds to a broad shoulder or peak at high frequency that contains the length scale of the features on the surface of the Au NP, and finally the region IV is a flat part that ends at the Nyquist frequency which indicates length scales that lack content in the image.[104,106] Adapted with permission from reference [104]. Copyright © 2017 American Chemical Society.

The characteristic features of the PSD curve relies on the properties of the Au NPs analysed, such as size of the NPs and the distribution of the stripe-like domains. Thanks to its quantitative nature, the PSD curve can be employed for comparison between samples of different NPs, referring to the spatial frequencies of the shoulder located in the region III of the previous figure: a higher spatial frequency of the shoulder is correlated to a reduced average size of the features on the surface of the NP.

Atomic Force Microscope is another scanning probe technique that can be employed for gathering information on the morphology of the ligands shell grafted onto NPs in liquid by measuring the contact angles between the solid/liquid interfaces working on small-amplitude mode, that probes amplitudes inferior to 2 nm, allowing to analyse the molecular domains on the surface of the NPs whose extensions are generally inferior than 2 nm. The studies[107] carried out were able to resolve the structure of MM Au NPs by focusing on the dependency of the working of adhesion of the solid/liquid interface on the average surface composition.

Scanning Electron Microscopy and Transmission Electron Microscopy are two techniques that are not suitable to the study of the organization of the monolayer due to low contrast of the ligand molecules which are not visible under the electron beam in standard operative conditions. However, by finely tuning the conditions for sample preparation, as the substrate where the NPs are deposited or the acceleration voltage at which the instrument works, and employing an aberration-corrected TEM[108] or exploiting staining techniques[109] is possible to perceive the presence of the ligands layer around the gold core. Cryo-TEM[110] is an emerging microscopy technique that can be employed for an indirect study of the organization of the monolayer. The main difference with conventional TEM is due to the fact that cryo-TEM allows

the imaging of the NPs in solution, by freezing the specimen and observing the sample under the electron beam. Obviously, the major limitation of the technique is the need of working with water soluble samples, feature that is not always possible in the case of Au NPs, especially those coated with non-polar ligands. Initially, cryo-TEM was mainly employed for the study of the architectures of cells and biomolecules; in recent years, it started to be exploited also for the study of the interactions of Au NPs with biomolecules and viruses.[111,112] The analysis of MM Au NPs and the organization of the ligands shell can be pursuit by exploiting the interactions of MM Au NPs among themselves or with tailored probing agents: the arising of these interactions leads to the formation of superstructures whose building blocks are the NPs investigated. The geometry and spatial orientation of the so-formed superstructures may reflect the organization of the ligands within the monolayer and then it could be possible to indirectly reconstruct the monolayer morphology.

4.2.2 Spectroscopic techniques

Nuclear Magnetic Resonance Spectroscopy (NMR) has been widely used in the study of both the composition and the morphology of the monolayer and it has become one of the routinely employed techniques for the characterization of NPs. The reason is due to the possibility of checking the absence of free ligands in a sample of NPs. Indeed, in a proton NMR spectrum of Au NPs, the signals pertaining to the protons of the ligands bound to the gold core are severely broadened because of their proximity to the gold core. The broadening is more severe for the protons closer to the gold core, since they are more densely packed and solid-like, whereas the protons close to the outer part of the monolayer possess more freedom of motion.[113]. Therefore, taking advantage of this phenomenon, every sharp peak visible in a ^{1}H-NMR spectrum of Au NPs can be assigned to unbound species or traces of impurities or residual solvent. Figure 2.11 reports five ^{1}H-NMR spectra of samples of Au NPs protected by dodecanethiolates. The phenomenon of broadening increases with the increasing of the dimensions of the gold core; therefore, it can be useful for a preliminary assessment of the average dimensions of the NPs within a batch.

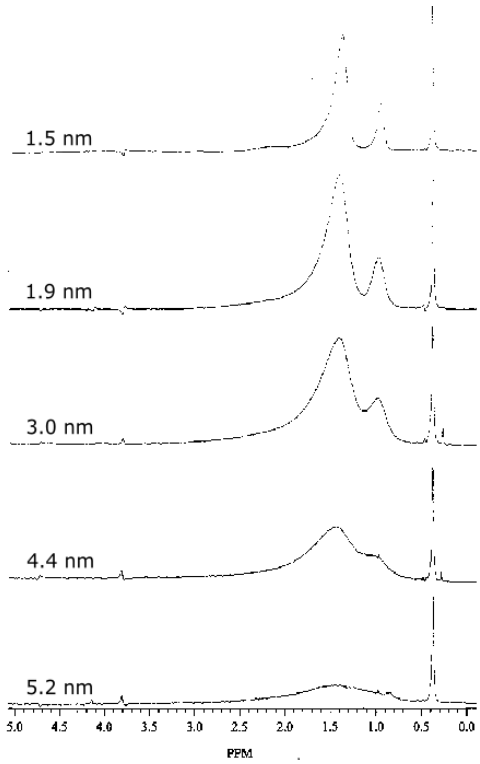

Figure 2.11: ^{1}H-NMR spectra of different batches of Au NPs protected by dodecanethiolates. Note the intensifying of the broadening of the spectra with the increase of the average core diamensions.[113] Adapted with permission from reference [113]. Copyright © 1998 American Chemical Society.

NMR spectroscopy can be employed for evaluating the ratio of ligands composing a mixed monolayer. Indeed, after the etching of the gold cores, the ligands previously bound to the gold atoms are freed; therefore, recording the ^{1}H-NMR spectrum of mixture of ligands resulting from the decomposition of the NPs and evaluating the integrals of the area of the peaks pertaining to characteristic protons of the ligands, it is possible to obtain the ratio between the ligands simply by evaluating the ratio between these integrals. In Chapter 1, it has been already presented that a combination of 1D and 2D NMR techniques can be exploited for a morphological study of the monolayer. In fact, several studies[58,61] outlined a dependence of the chemical shifts of the nuclei of the ligands forming the monolayer on the neighbouring ligand species. Therefore, by studying the dependence of the chemical shifts of a diagnostic peak with respect to the monolayer composition, it is possible to outline characteristic trends for specific monolayer morphologies. Moreover, 2D NMR Nuclear Overhauser Effect Spectroscopy (NOESY) and Heteronuclear Overhauser Effect Spectroscopy (HOESY) can be employed for a deeper analysis of the arrangement of ligands of different nature on the surface of the gold core. Indeed, these methods allows observing cross-correlation peaks when the nuclei involved are closely located in space, within a distance of 0.4 nm. Therefore, NOESY experiments on MM Au NPs evidence the presence of cross peaks due to the proximity of the nuclei belonging to different ligands; however, the intensity of the cross peaks is strictly correlated to the number of nuclei that are within the threshold distance of 0.4 nm. Therefore, the higher is the number of nuclei at the boundaries of the domains composing the monolayer, the more intense are the cross peaks. If the domains possess reduced dimensions or the ligands are randomly dis-

tributed on the surface of the gold core, the number of boundaries is high and consequently intense cross peaks are observable. On the other hand, if the domains are larger or complete phase segregation occurs between the ligands, the intensity of the cross peaks may be rather low. As a matter of fact, the absence of cross peaks can tell a situation in which total phase segregation is present on the monolayer from the others, where ligands can be randomly distributed or organized in small domains, giving rise to intense cross peaks. Even though this is a powerful approach, it is affected by the need of several analyses involving various samples of MM Au NPs, each of them exhibiting a precise composition of the monolayer for studying the trend of the chemical shifts and deeply understanding the system.

Matrix-Assisted Laser Desorption/Ionization Time of Flight Mass Spectrometry (MALDI-TOF MS) is one of the main techniques exploited for Au cluster characterization and place exchange of ligands.[77,114]This technique is also useful in Au NPs characterization concerning their mass[115] and the ratio of the ligands composing the mixed monolayer[116], determined using the matrix-free variant of the technique. The most interesting possibility that the technique offers is the investigation[117,118] of the morphology of mixed monolayers grafted onto Au NPs by the analysis of the intensities of the peaks related to the $Au_4L_{4-x}L'_x$ complexes, which are the most abundant species among the Au complexes formed after laser irradiation of a sample of Au NPs undergone MALDI-TOF MS experiments. In fact, according to the work[76] of Harkness *et al.*, the $Au_4L_{4-x}L'_x$ complexes could be directly desorbed from the gold surface or they could arise from the rearrangement of the staple motifs, involving their predominant presence in a MALDI-TOF mass spectrum of MM Au NPs. For a binary mixture of ligands, five different complexes with Au_4L_4 composition may be observable in a MALDI-TOF mass spectrum. Consequently, the distribution of the intensities of their peaks in the spectrum reflects the arrangement of the ligands within a mixed monolayer: the more the distribution deviates from a binomial distribution, the more phase segregation is present on the surface of the NPs. Figure 2.12 displays a scheme that illustrates very effectively the concept.

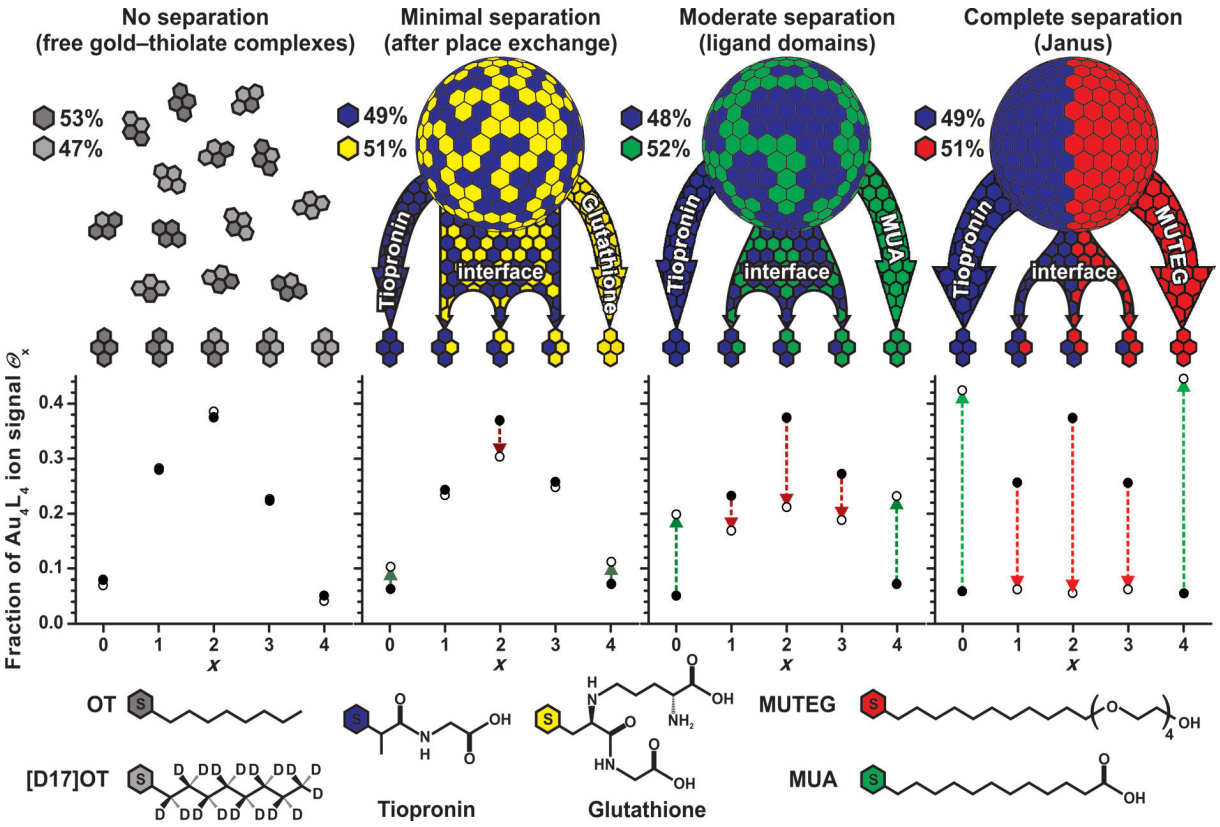

Figure 2.12: MALDI-TOF MS analysis of the distribution of $Au_4L_{4-x}L'_x$ complexes in batches of MM Au NPs protected by a binary mixture of ligands of different natures. The white dots correspond to the distribution of the intensities of the $Au_4L_{4-x}L'_x$ where x goes from 0 to 4, the black dots refer to binomial distribution. If the two distributions are similar, no phase segregation is present on the surface of the NPs and the ligands are randomly distributed on the gold surface; on the other hand, if the distribution of the intensities sensibly deviates from the binomial one, then total phase segregation occurred.[76] Adapted with permission from reference [76]. Copyright © 2011 John Wiley and Sons.

This approach is straightforward and rapid; moreover, the amount of specimen required is in the order of hundredth of milligrams. However, the optimal conditions for running MALDI-TOF MS experiments on Au NPs are not *a priori* established and the reliability of the results is affected by several variables, such as the type of matrix employed, the molar ratio between Au NPs and matrix and the nature of the ligands. Therefore, each type of MM Au NPs requires a preliminary screening of the conditions to employ before studying the distribution of the intensities pertaining to Au_4L_4 complexes and determining the morphology of the monolayer. Eventually, the desorption probability of the complexes composed of the different ligands forming the monolayer must be the same, otherwise the outcomes will be biased by an incorrect estimate of the ligands ratio and, consequently, the monolayer morphology, due to the predominant desorption of one type of ligand with respect to the other.

Small Angle Neutron Scattering (SANS) is another spectroscopic technique that can be used for a multicomponent core-shell study of Au NPs.[119]. Several studies[120–122] involving application of SANS on batches of Au NPs have been carried out, aiming at investigating the structure of the gold core and the thickness of the ligands shell. In recent years, SANS has been also exploited for the analysis of the organization of ligand domains within the monolayer.[123–125] This latter approach takes into account the contrast variation arising from the remarkable dif-

ference in neutron scattering contrast of hydrogen and deuterium and the consequent selective employment of hydrogenated and deuterated ligands coating the NPs in order to highlight the organic monolayer. Several conditions must be fulfilled for performing a SANS study on MM Au NPs: indeed, the NPs must be stable in concentrated solution without aggregation and they must be characterized by narrow size distributions, otherwise the data could be hardly intelligible; eventually, one of the two ligands must be deuterated in order to be distinguished, outlining its arrangement on the gold surface. The scattering patterns obtained from a SANS experiment are then fitted by means of computational programs, that allow a 3D reconstruction of the structure of the ligands shell. Among all computational approaches, the program MONSA turned out to be one of the most successful algorithms for achieving detailed 3D models of ligands shell structures making use of Monte Carlo methods.[124] Figure 2.13 displays an example of SANS analysis on MM Au NPs: three scattering patterns of three different batches of MM Au NPs are reported together with the computational reconstructions of the shells of ligands.

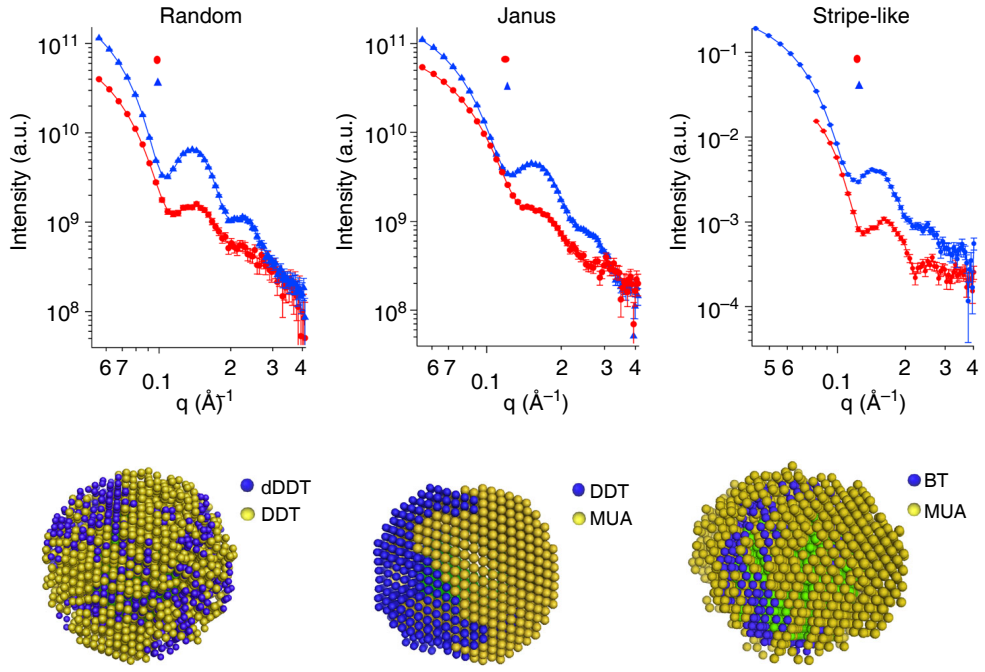

Figure 2.13: SANS data (top) and 3D models (bottom) of Au NPs coated with hydrogenated and deuterated ligands and exhibiting different morphologies.[124] Adapted with permission from reference [124]. Copyright © 2018 Springer Nature.

4.2.3 Simulations

The computational approaches played a key role in the analysis of the morphology of mixed monolayer since the early studies on the subject. The most exploited methods involved combinations of atomistic and mesoscale calculations. As discussed in Chapter 1, the seminal results presented in the work[59] of Singh *et al.*, pointed out that the formation of stripe-like domains is driven by the gain in conformational entropy arising from the creation of interfaces where bulkier and longer ligands are adjacent to shorter ones; consequently, the longer ligands benefit of additional free volume. The gain in conformational entropy counterbalances the energetic

cost for the formation of new interfaces. In later years, other computational studies on the topics have been performed, involving atomistic discrete Molecular Dynamics for investigating the presence of stripe-like domains on NPs surface[126] or Monte Carlo approaches for analysing the evolution of the morphology of different monolayers composed of binary mixtures of thiolates, achieving various degrees of phase segregation.[127]. Dissipative Particle Dynamics approaches have also been employed for gathering complementary information on monolayer morphologies of NPs protected by blends of fluorinated and hydrogenated ligands[61,63] previously studied with ESR and NMR techniques.

CHAPTER 3

Aim

The aim of the work carried out during the PhD concerned an investigation on non-covalent interactions among functional Au NPs and MM Au NPs in organic and aqueous media that may eventually lead to their controlled self-assembly. Once the viability of this approach has been established, the conditions that give rise to the interactions themselves will need to be precisely optimized in further studies.

At the outset, the strategy chosen for the test performed in organic media implied a screening of the common synthetic procedures for the preparation of narrowly dispersed batches of Au NPs protected by dodecanethiolates, in order to work with NPs exhibiting homogeneous chemical behaviour and similar chemical composition. This is the most important prerequisite for a subsequent controlled functionalization of the monolayer by means of place exchange reaction, performed by the precisely tuning of the amount of entering ligands. Subsequently, the idea was to performed fast place exchange reactions involving the narrowly dispersed Au NPs so that introducing within the monolayer a precise number of interacting sites.

Our route to the self-assembly of NPs in organic media was devised to merge and exploit the best features of two previously presented approaches, one[22] proposed by the group of F. Stellacci concerning the preparation of divalent Au NPs and the other reported[51] by the group of V. Rotello, exploiting metal ions coordination by terpyridine-terminating ligands. As presented in Chapter 1, the point of strength of the first method relies on exploiting of a fast place exchange reaction for functionalizing the Au NPs, leading to the formation of divalent Au NPs whose interacting sites were located in precise points within the monolayer. This latter aspect is important to bestow a certain organization to the superstructures that may form as a result of the self-assembly process. However, the approach developed by Stellacci and co-workesr lacked the possibility of precisely know the number of interacting ligands per NP and it was intrinsically irreversible, since it exploited the formation of covalent bonds to connect the NPs one another. The latter approach took into account the employment of terpyrdine-terminating ligands, introduced into the monolayer by means of place-exchange reaction, acting as moieties responsible for the self-assembly process among Au NPs. The self-assembly was indeed triggered by the addition of metal ions, leading to metal coordination by terpyridine molecules which eventually results in the formation of supramolecular aggregates of NPs. The interest-

ing features of the approach concerned the possibility of established the concentration of the complexes formed by means of UV-Visible spectroscopy and the employment of reversible interactions responsible for the self-assembly process. No control over the number of interacting sites was reached though, producing chaotic aggregates of NPs. Therefore, the estimation of the number of functional ligands per NPs would have been then accomplished by means of UV-Visible spectroscopy, obtaining the concentration on the complexes formed from UV-Vis titration.

The aim of the studies in aqueous environment was addressed towards the self-assembly of tetrahedral superstructures whose cores would have been composed of water soluble hydrogenated and fluorinated MM Au NPs previously prepared in the research group where this thesis work was carried out. The fascinating characteristic of these MM Au NPs relied on the peculiar organization of the fluorinated domains coating the gold cores. Indeed, the 3D reconstruction of the monolayer of those NPs achieved through fitting of the data gathered from SANS analyses presented the fluorinated ligands clustered together forming four domains pointing at the vertex of a tetrahedron. Considering these outcomes, the interest in further analyses on the morphology of the monolayer of these NPs merged with the idea to use the MM Au NPs themselves as starting materials for producing self-assembled superstructures. This strategy takes advantage of fluorophilic interactions arising in aqueous environment, and may achieve a degree of control over the self-assembly process that starts from the intrinsic morphology of the monolayer and does not rely on specific recognition moiety introduced in the NPs monolayer, as in the case of the studies carried out in organic media. The superstructures would then have been produced by self-assembly of the tetrahedral MM Au NPs with MM Au NPs of small diameter bearing fluorinated domains or tails able to interact thanks to the arising of fluorophilic interactions. The overall structures would then have been analysed by means of electron microscopy techniques, such as cryo-TEM and HR-TEM.

Eventually, within this work, MALDI-TOF MS experiments were performed on batches of MM Au NPs protected by hydrogenated and fluorinated ligands, aiming to test the adequacy of this technique for the characterization of mixed monolayers containing fluorinated species. Indeed, MALDI-TOF MS had been already[76] successfully used for the study of the morphology of mixed monolayers grafted on Au NPs; moreover, this type of analyses are fast and require very low amount of sample. On the other hand, the characterization of MM Au NPs containing fluorinated species is usually time consuming, needing several experiments and consequently a considerable amount of material. The employment of MALDI-TOF MS for elucidating the morphology of hydrogenated and fluorinated mixed monolayer could then represent a huge step ahead in the study of these systems.

Part II

Results and Discussion

CHAPTER 4

Synthesis and functionalization of Au NPs with narrow size distributions for their interactions in organic media

1 Introduction

This chapter presents the experiments carried out aiming at preparing the substrates for studying non-spontaneous interactions among functional Au NPs in organic media and exploiting them for setting the conditions for controlled self-assembly. As it will be described in the chapter, the forces behind the interacting process object of the study are here due to metal ions coordination by terpyridine terminating alkyl thiolates bound to the gold cores. The crucial point for their employment for controlled self-assembly purposes is the precise engineering of the ligand shell surrounding the core; indeed, the positions occupied within the monolayer by the ligands responsible for the interactions will eventually induce a specific arrangement of the superstructures created as a consequence of the self-assembly process. It is clear that if the interacting ligands are placed within the monolayer with no precise order, the randomness will be reflected in the outcomes from the self-assembly. This will consequently lead to chaotic superstructures whose properties are not well-defined and, for this reason, not easy to be exploited because not well understood, due to their lack in systematic behaviour.
With these premises, the first part of the following chapter describes numerous attempts carried out by making use of different synthetic procedures for the preparation of batches of Au NPs protected by dodecanethiolates with narrow size distribution, in order to produce Au NPs with similar chemical behaviour. Three different approaches[85–87] were tested and the results obtained are herein discussed in details. Then, the attention is addressed to preliminary experiments concerning controlled place exchange reactions on the so-prepared NPs, aiming at functionalizing the monolayer with terpyridine terminating alkyl thiolates at precise positions and triggering their interaction by addition of Fe(II) ions. The final part of the chapter eventually presents the TEM and UV-Vis results of the analysis of outcomes from the process of

self-assembly of the NPs obtained from place exchange reaction.

2 Synthesis of Au NPs protected by dodecanethiolates with narrow size distribution

The synthesis of batches of Au NPs exhibiting narrow size distributions is one of the main prerequisites for reaching a higher degree of control in the process of self-assembly among Au NPs. Indeed, the narrower is the size distribution, the more similar is the chemical behaviour of the NPs within the same batch. Therefore, the control over the functionalization of the monolayer at precise sites could be smoother for narrowly dispersed Au NPs.
One possible strategy for producing Au NPs characterized by narrow size distribution involves the employment of mild reducing agents during the synthesis of Au NPs, establishing an equilibrium between the process of nucleation of new cores and the growth of the already existing ones, contributing therefore to the formation of cores of similar dimensions. Another approach relies on the size evolution of NPs of reduced dimensions thanks to heat treatment. The temperature at which the treatment is performed allows controlling the evolution of the size of the NPs. Moreover, the employment of tetraoctyl ammonium bromide assures the homogeneous growth of the NPs, giving rise to batches characterized by narrow size distributions.

2.1 Synthesis performed using mild reducing agents

Several experiments have been carried out following two approaches for the preparation of Au NPs employing borane tert-butylamine complex as mild reducing agent. The reducing strength of this specie is lower than that of $NaBH_4$, which is widely used for the synthesis of Au NPs according to the protocol[82] published by Brust *et al.* in 1994. This characteristic should guarantee an adequate balance between nucleation and growth during the formation of the cores, so that improving the control over size distribution. As a matter of fact, the reducing strength is simply one of the factors that have to be taken into account for controlling size distribution: indeed, several conditions play an equal key role and the goodness of the outcomes can evenly depends on temperature, reaction time and solvent as well. Consequently, some of the reactions herein presented have been performed aiming at pinpoint the effects of changing some of these conditions, meaning to spread light on the contribution of these factors to the overall process. The first method[86] taken into account was the one proposed by Zheng *et al.* The authors claim that the strength of the approach lies indeed in the use of reducing agents able to slowly reduce metal cations, gaining control over the particles growth. The protocol implies that the reaction is carried out solely in organic phase, making use of several metal precursors for obtaining NPs composed of Pt, Ag or Au. Furthermore, according to the results therein reported, the authors were able to obtain metal NPs with size distributions lower than 10 %. For producing Au NPs, $AuPPh_3Cl$ was employed as gold precursor and dodecanethiolates as capping agents. The first experiments presented in the next section follow the same strategy reported in the original paper. Since the results obtained were not satisfying, few changes in the procedures were carried out, taking into account a work[128] by Goldmann *et al.* The batches

synthesised from the modified procedure were then characterized by narrow size distributions. Several experiments were therefore carried out to understand the effects of synthetic conditions such as temperature, Au/ligand molar ratio and solvent in which the synthesis was performed. Although providing satisfying results in terms of size distribution, the latter method is affected by a lack of control over the final composition of the NPs monolayer, due to contaminations of triphenylphosphine-based species. For this reason, another approach was considered, which is the second herein presented and it is the synthesis[87] proposed by Peng *et al.*, where $HAuCl_4 \cdot 3\,H_2O$ is used as gold precursor and oleylamine acts as both capping ligand and phase transfer, bringing the gold precursor in the organic phase. The reducing agent is once more *tert*-butilamine borane complex. This procedure was then considered as an alternative to the one published by the group of G.D Stucky aiming at overcoming the drawbacks that the latter presents, which are related to triphenylphosphine-based leftovers. However, the synthesis proposed by Peng and co-workers is meant to be exploited for preparing batches of Au NPs that will eventually be used as catalysts. Therefore, the ligands surrounding the gold cores possess the mere role of protecting them from aggregation until the final step, without paying attention to the engineering of the monolayer. In this case, instead, the NPs prepared with this method were intended to be used as substrates for further functionalization and self-assembly studies. Therefore, several place exchange reactions were carried out in order to displace oleylamine and replace it with dodecanethiolates, providing the NPs with more stability, allowing to be subsequently functionalized with the ligands of interest.

2.1.1 Strategy proposed by Zheng *et al.*

The first experiments were carried out by strictly following the condition for the synthesis of Au NPs in benzene reported in the work[86] published by the group of Galen D. Stucky. As described before, this procedure employs $AuPPhCl_3$ as gold precursor and dodecanethiols as capping ligands; the molar ratio between these two species is 1 to 2. Two attempts at different temperatures were performed, so that pinpointing whether the temperature had a strong effect on the outcomes of the process. As long as the temperature changes, also the time of the reaction can be accordingly modified, as at higher temperatures the reduction should run quicker. Figures 4.1 and 4.2 display a selected TEM image for each batch, together with the histograms resulting from the analysis of the dimensions of the gold core, conducted on the images recorded with the TEM. The black vertical line present in each histogram refers to the average diameter evaluated on the data collected from the analysis.

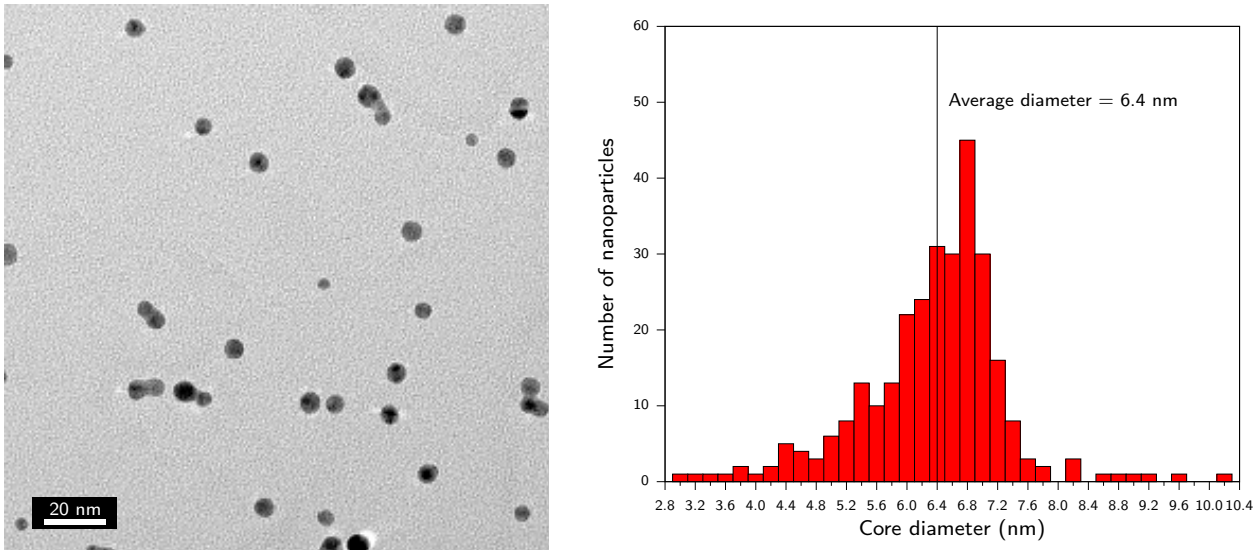

Figure 4.1: On the left, TEM image of a sample of Au NPs prepared in benzene at 55 °C. On the right, histogram displaying size distribution, obtained after the analysis of core sizes over 300 NPs.

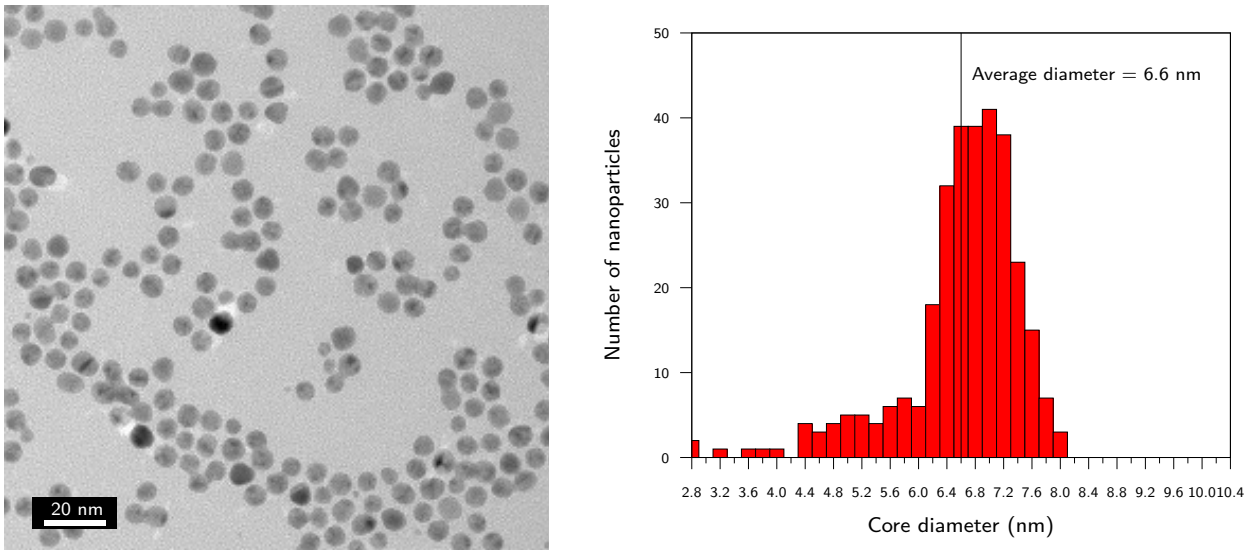

Figure 4.2: On the left, TEM image of a sample of Au NPs prepared in benzene at RT. On the right, histogram displaying size distribution, obtained after the analysis of core sizes over 300 NPs.

The results achieved by carefully replicating the synthetic conditions described by the authors of the already cited paper[86] sensibly deviate from those reported in the paper itself. Indeed, the size distribution of both batches is rather broad compared to the ones reported. The batch prepared at 55 °C is characterized by an average core diameter of 6.4 nm with a standard deviation of 1 nm, whereas the NPs composing the batch synthesised at RT have an average core diameter of 6.6 nm, with a standard deviation of 0.9 nm. The results presented in the paper, instead, clearly show that those procedures lead to batches of Au NPs with an average core diameter of 5.3 nm with a standard deviation of 0.4 nm at RT and 6.2 nm with a standard deviation of 0.3 nm at 55 °C. By evaluating the variation coefficients of the NPs obtained reproducing the synthesis with the conditions reported in the paper highlights remarkable differences respect to the literature data. Table 4.1 reports a direct comparison among the properties concerning

the dimensions of the NPs in the different batches, both the ones prepared during this work and those presented in the paper from the group of G.D. Stucky.

Table 4.1: Comparison between results obtained reproducing the protocol for the synthesis of Au NPs proposed by the group of G. D. Stucky and the ones indicated in the paper.

	Batch at RT	**Batch at 55 °C**	**Zheng *et al.*, RT**	**Zheng *et al.*, 55 °C**
Average diameter (nm)	6.6	6.4	5.3	6.2
Standard deviation	0.9	1	0.4	0.3
Variation coefficient	0.14	0.16	0.08	0.05

The initial results suggested that the approach was far from being useful for the purpose of obtaining batches of NPs with homogeneous chemical behaviour. Nevertheless, a further attempt was made by slightly changing few synthetic conditions. These changes turned out to be decisive for the achievement of monodisperse batches of NPs. The idea came from a work[128] of Goldmann *et al.*, where the authors employed the synthesis by G.D. Stucky and co-workers for preparing batches of Au NPs characterized by an average diameter of 5 nm, even though the overall approach was slightly different: the synthesis was carried out in toluene at 100 °C for 3 minutes, employing a molar ratio between Au and ligand equal 1 to 8. Eventually, the crucial change is related to the addition of the reducing agent. Indeed, Goldmann *et al.* added the *tert*butylammine- borane complex not as a solid, but dissolved in the same solvent in which the gold precursor and the ligands were previously dissolved. Consequently, the reducing solution was prepared, preheated before the addition at the same temperature of the solution containing the gold precursor and the ligands and quickly added to the latter solution. The TEM analysis of the outcomes of the so-modified procedure is reported in Figure 4.3.

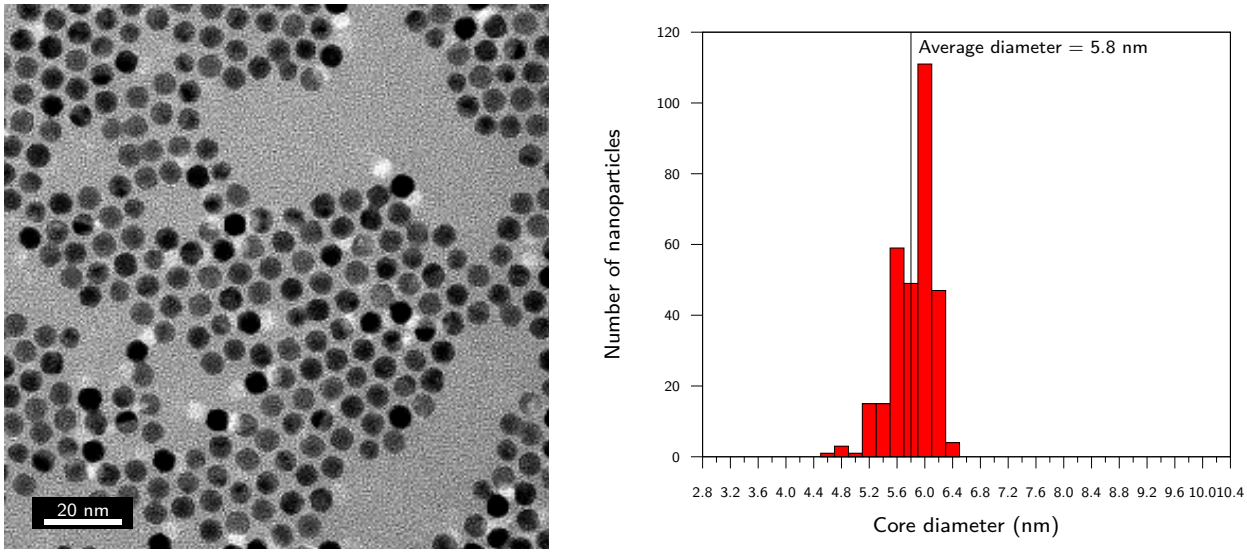

Figure 4.3: On the left, TEM image of a sample of Au NPs prepared in toluene at 100 °C. On the right, histogram displaying size distribution, obtained after the analysis of core sizes over 300 NPs.

As it can be seen from the histogram, the size distribution that characterized the batch of NPs prepared by applying the previously mentioned changes at the procedure is remarkably nar-

row. Indeed, the average core diameter is 5.8 nm and the standard deviation is only 0.3, which corresponds to a variation coefficient of 0.05. This result is obviously much closer than the previously reported ones to the claim of the paper by G.D. Stucky and co-workers, concerning the potentialities of the method for preparing batches of NPs with size distributions lower than 10 %. However, further variation to the protocol were progressively performed, meant to understand the effect of temperature, molar ratio between gold and ligands and solvent to the outcomes of the synthesis.

The first further modification concerned the molar ratio between gold and ligands. The reason behind this variation was due to the fact that the use of such a high molar excess of thiols with respect to gold could represent critical point when the ligands used for the synthesis are not commercially available and considerable synthetic efforts must be faced for their preparation. Aiming therefore at expanding the application of the procedure to those cases, two syntheses were performed by lowering the molar amount of ligands. The molar ratios between gold and ligands investigated were 1 to 4 and 1 to 2. Figures 4.4 and 4.4 exhibit the outcomes from the two preparation.

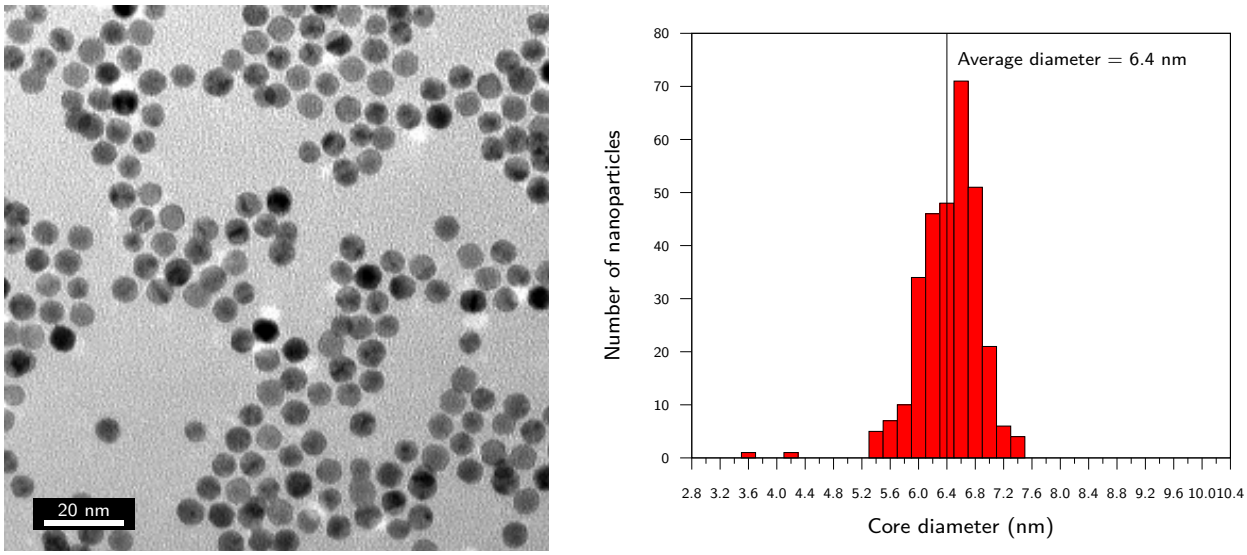

Figure 4.4: On the left, TEM image of a sample of Au NPs prepared in toluene at 100 °C with a molar ratio between gold and ligands of 1 to 4. On the right, histogram displaying size distribution, obtained after the analysis of core sizes over 300 NPs.

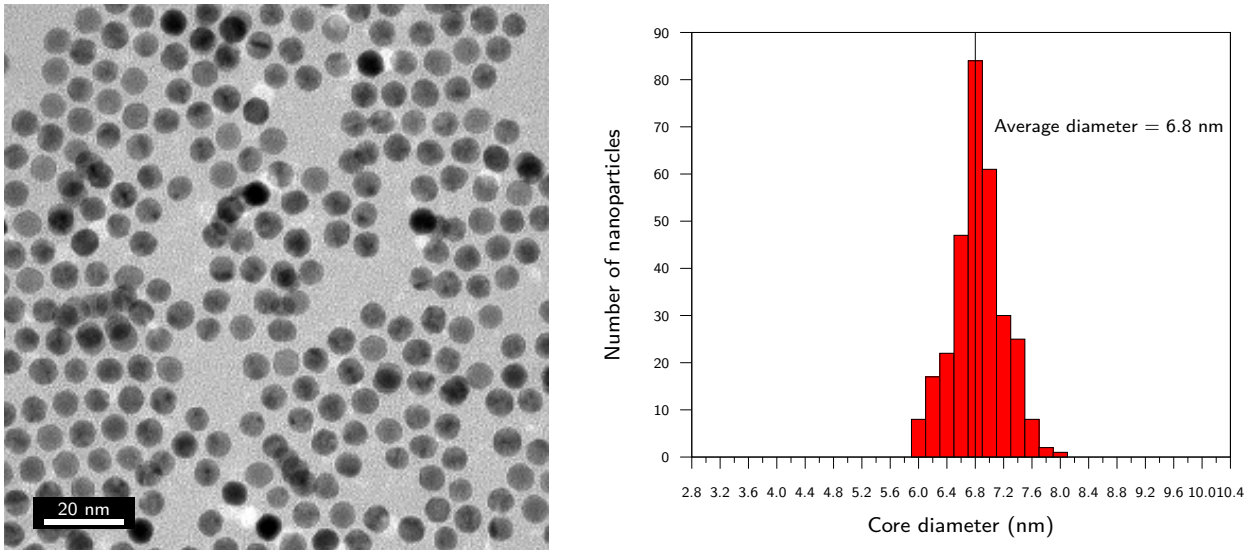

Figure 4.5: On the left, TEM image of a sample of Au NPs prepared in toluene at 100 °C with a molar ratio between gold and ligands of 1 to 2. On the right, histogram displaying size distribution, obtained after the analysis of core sizes over 300 NPs.

The effect of lowering the overall amount of ligand for the preparation of the NPs is immediately evident by considering the average diameters of both batches: the one prepared by employing a molar amount between gold and ligand of 1 to 4 is characterized by an average core diameter of 6.4 nm, while that produced using a molar amount of 1 to 2 possesses an average core diameter of 6.8 nm. Then, recalling the previously showed results of the batch prepared with a molar ratio of 1 to 8, it is clear that by decreasing the molar amount of ligands, bigger NPs can be produced. Table 4.2 collects the outcomes of the three experiments presented up to now, for an easier comparison.

Table 4.2: Comparison among the average core dimensions, standard deviation and variation coefficient of the batches prepared according Goldmann *et al.*, using 1 to 8, 1 to 4 and 1 to 2 molar ratio between gold and ligand.

	Molar ratio of 1:8	**Molar ratio of 1:4**	**Molar ratio of 1:2**
Average diameter (nm)	5.8	6.4	6.8
Standard deviation	0.3	0.4	0.4
Variation coefficient	0.05	0.06	0.06

The trend of the average core dimensions with respect to the Au/ligand molar ratio of these batches agrees with the seminal studies[113] on the topic, reported by the group of R. W. Murray. A lower molar amount of ligands implies a lower number of molecules of ligands covering the NPs during the early stages of the process of formation of gold cores. Consequently, the growth of the formed cores is promoted, since their degree of coverage is so that the merging among partially covered cores is not avoided.
Although the average dimension of the cores increases by decreasing the molar amount of ligands in the synthetic environment, the size distribution is not affected by this variation. By considering the histograms, in fact, the distribution of the sizes does not sensibly deviate from the average values. Furthermore, the variation coefficients of the syntheses carried out ex-

ploiting Au/ligand molar ratios of 1 to 4 and 1 to 2 increase only by 1%. These outcomes are encouraging, since the possibility of obtaining batches of Au NPs with narrow size distribution is preserved, even by varying the molar ratio between gold and ligands.
The next modifications to the procedure were meant to point out the effects of lowering the reaction temperature on the outcomes of the synthesis. Indeed, running the reaction at 100 °C is not generally applicable, since many organic solvents boil at considerably lower temperatures, at least at atmospheric pressure which is the pressure at which this type of synthesis is performed. Therefore, the synthesis in toluene was repeated using once again a gold/ligand molar amount of 1 to 8, but this time the reaction temperature was decreased at 65 °C and the reaction time was consequently increased, in order to compensate the slowing of the reaction rate due to the lowering in temperature. Figure 4.6 reports a TEM image of the product of the reaction, together with the relative histogram displaying the size distribution.

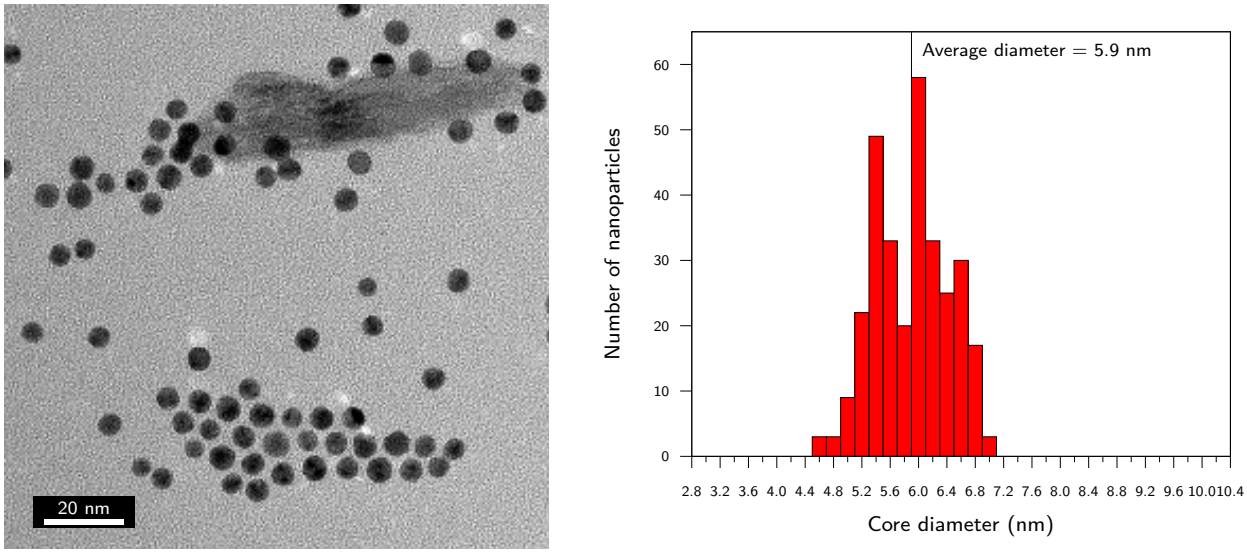

Figure 4.6: On the left, TEM image of a sample of Au NPs prepared in toluene at 65 °C. On the right, histogram displaying size distribution, obtained after the analysis of core sizes over 300 NPs.

The decrease in the reaction temperature did not significantly alter the average diameter of the NPs, since it moved from 5.8 nm to 5.9 nm. The size distribution is slightly broader though, since the standard deviation is 0.5 nm, while the standard deviation of the batch prepared at 100 °C is 0.3 nm; nevertheless, the variation coefficient is equal to 0.1, which could still be considered an acceptable value for this type of synthesis.
Once established that the decrease of reaction temperature and consequent increase of reaction time do not consistently alter the outcome of the synthesis, few more experiments were performed with the intention of understanding the role of the solvent in the overall process. Besides toluene, chloroform and tetrahydrofuran (THF) were employed. The reasons behind this choice lie in two works concerning the subject of tuning the core dimensions by changing the solvent for the reaction. The first one is a paper[88] by Song *et al.*, where the authors studied the outcomes from the same synthesis performed in benzene or chloroform and their mixtures. They outlined the fact that by increasing the polarity of the reaction media, the average dimensions of the NPs obtained decrease. The other article[89] taken into account describes the

work by Jiang *et al.*, where the authors pointed out that the use of polar solvents, able to form hydrogen bonds with thiols, favours the formation of NPs with lower average dimensions. The authors claim that this behaviour is due to the fact that the formation of hydrogen bonds weakens the bond between sulphur and hydrogen atom, facilitating therefore the formation of bonds between gold and sulphur. On the other hand, the employment of nonpolar solvent unable to induce the formation of hydrogen bonds leads to NPs of bigger dimensions. The authors justified this evidence by addressing the fact that in the case of alkyl thiols, the chains of the ligands form stronger hydrophobic interactions with the nonpolar molecules of solvent, implying desorption of ligands from the surface of the NPs.
Figures 4.7 and 4.8 display two TEM images and the histograms resulting from the analysis of the dimensions of the core of the experiments carried through respectively in THF and chloroform. The temperature at which the syntheses were performed was 65 °Cfor the case where THF was the solvent and the synthesis in chloroform was conducted at reflux. Since the outcomes of the experiment run in toluene at 65 °C and 36 minutes were satisfying, both reactions were performed in the same time.

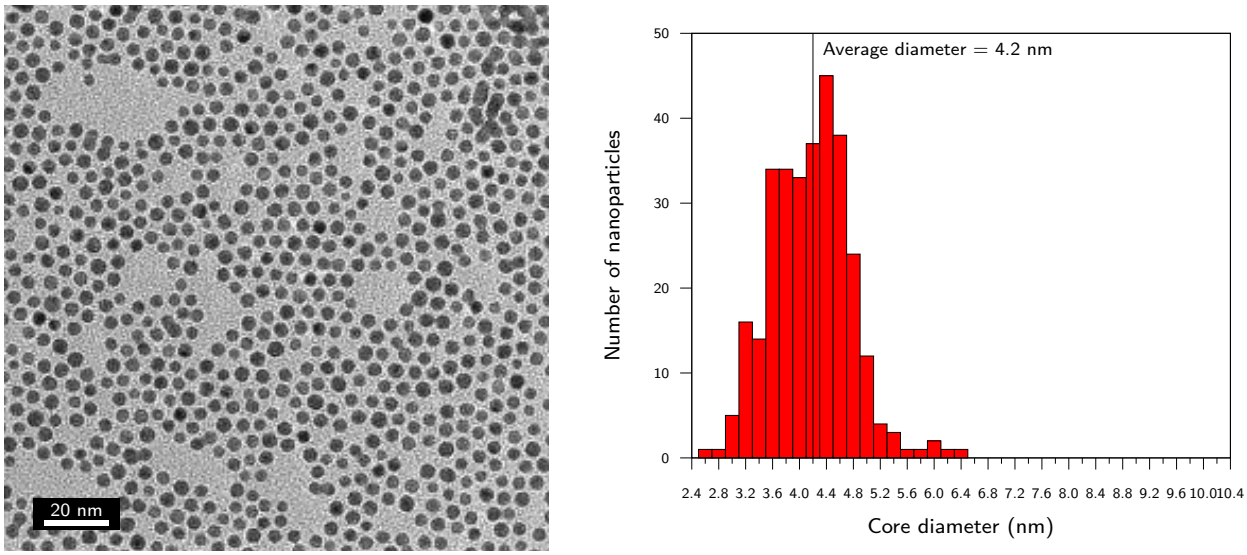

Figure 4.7: On the left, TEM image of a sample of Au NPs prepared in THF at 65 °C. On the right, histogram displaying size distribution, obtained after the analysis of core sizes over 300 NPs.

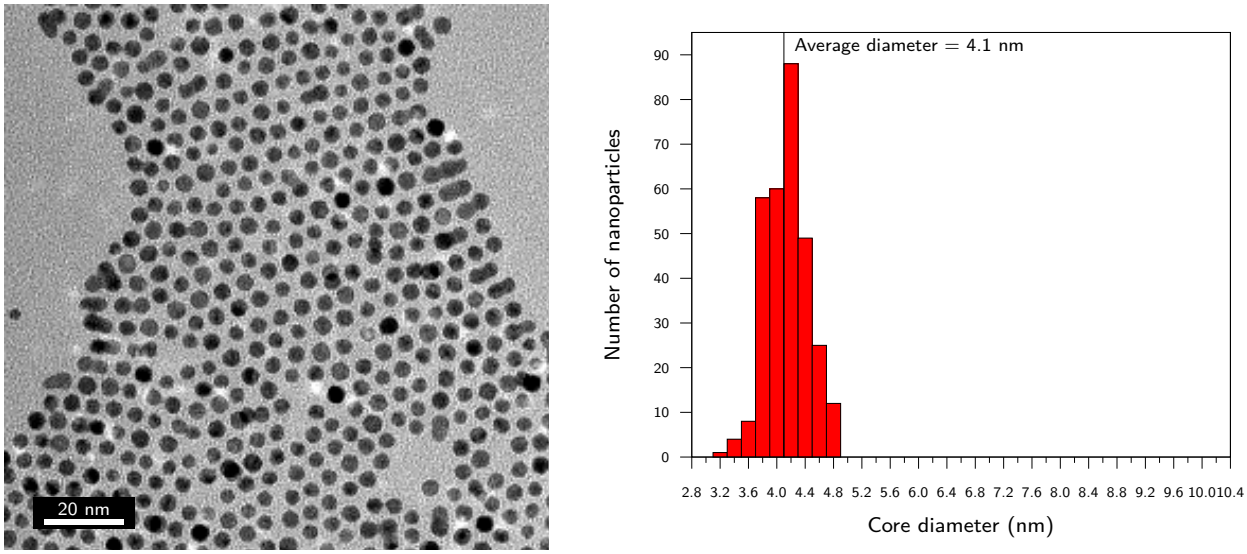

Figure 4.8: On the left, TEM image of a sample of Au NPs prepared in chloroform at reflux. On the right, histogram displaying size distribution, obtained after the analysis of core sizes over 300 NPs.

The outcomes from both syntheses reflect the considerations previously discussed. The average core diameters of both batches are very similar: in fact, the synthesis performed in THF resulted in NPs whose average diameter is 4.1 nm while that carried out in chloroform led to a batch of NPs with an average diameter of 4.2 nm. Good results related to size distribution were also obtained for what concerns the use of THF as solvent. Indeed, in that case the standard deviation is 0.3 nm with a variation coefficient of 0.07. The batch prepared in chloroform instead is characterized by a standard deviation of 0.6 nm, which corresponds to a variation coefficient of 0.14, which is the highest one within the batches prepared with this type of synthesis.
Table 4.3 collects and resumes the synthetic conditions for all the batches prepared following the procedure presented in this section and reported by the group of G.D. Stucky[86] and its variation reported by the group of D. Portehault.[128].

Table 4.3: Synthetic conditions followed for the synthesis of the batches of Au NPs presented so far.

Size properties (nm)	Solvent	Temperature (°C)	Time (min)	Au/thiol molar ratio
6.6 ± 0.9	benzene	55	60	1:2
6.4 ± 1.0	benzene	RT	240	1:2
5.8 ± 0.3	toluene	100	3	1:8
6.4 ± 0.4	toluene	100	3	1:4
6.8 ± 0.4	toluene	100	3	1:2
5.9 ± 0.5	toluene	65	36	1:8
4.2 ± 0.6	chloroform	reflux	36	1:2
4.1 ± 0.3	THF	65	36	1:2

The outcomes from the different experiments suggest that this approach is indeed a versatile method for preparing batches of Au NPs with narrow size distribution. Moreover, the tuning of the synthetic conditions allows modulating the dimensions of the gold cores. However, as a

matter of fact, the protocol lacks of being general, forcing to repeat the process of optimization whenever the type of ligand is changed. Furthermore, the method is also affected by two heavy drawbacks which will be treated in details in the next section: the first is related to the presence of leftovers of phosphine-based species within the monolayer of the synthesised NPs; the latter concerns an unexpected behaviour of the NPs produced through this protocol during place exchange reaction.

2.1.2 Drawbacks of the procedure proposed by Zheng *et al.*

As briefly mentioned in the previous section, the procedure published by Zheng et al. presents some drawbacks. Even though the preparation of batches of NPs with narrow size distribution is feasible once the optimal synthetic conditions have been pointed out through a careful screening process, the use of a triphenylphosphine-based gold complex instead of the classic tetrachloroauric acid as gold precursor turned out to be the cause for the presence of leftovers of phosphine-related species within the monolayer of the synthesised NPs. However, from the ^{1}H-NMR spectra of pristine NPs it is not possible to appreciate the presence of residues of phosphine-based species, because of their low concentration which leads to low intensities of the NMR peaks. This unfortunate situation combined with the phenomenon of peak broadening, due to the constrain of the ligands bound to the gold core and the size of the gold core itself, does not allow to get an insight on the amount of phosphine-based residual species. As an example, Figure 4.9 displays three NMR spectra of pristine NPs, prepared according to the synthesis of Zheng *et al.* in different solvents.

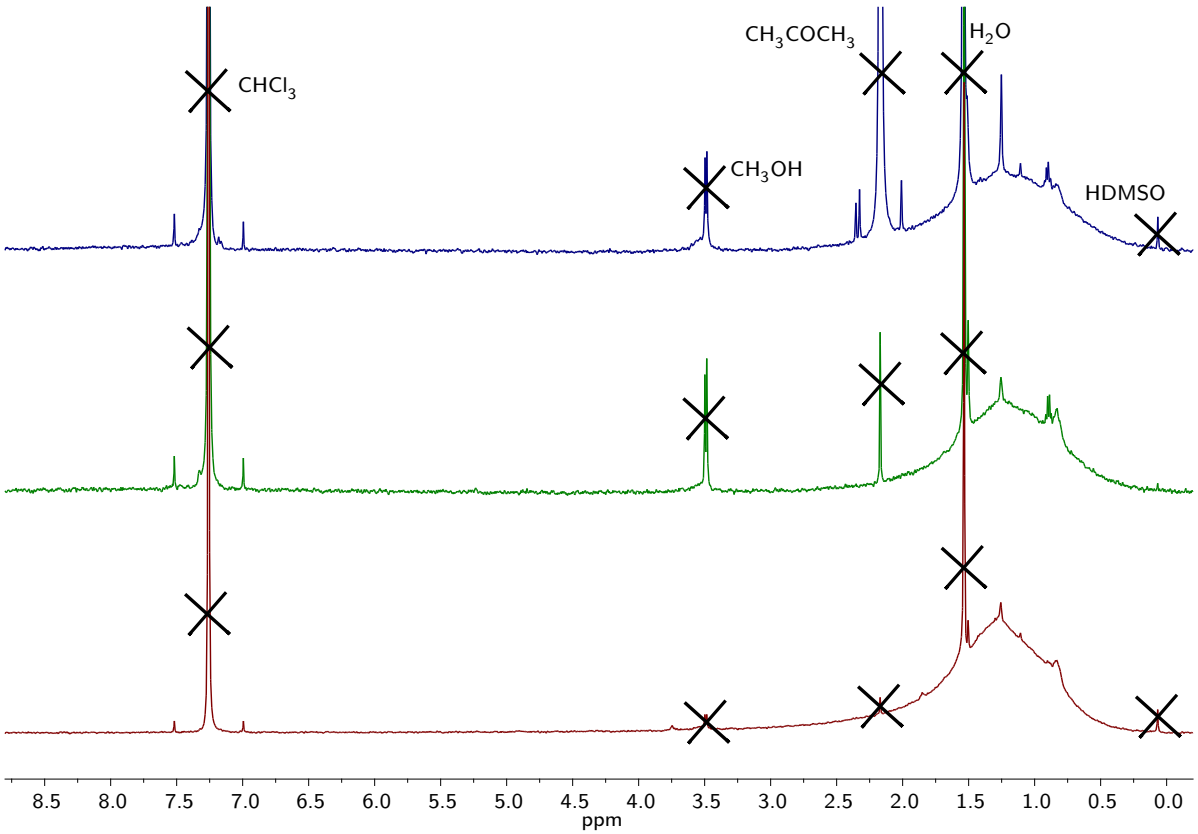

Figure 4.9: ^{1}H-NMR spectra (400 MHz, $CDCl_3$) of three batches of NPs prepared according to Zheng *et al.* The top spectrum pertains to Au NPs prepared in toluene, the middle one to those prepared in chloroform and the bottom one to those synthesised in THF.

As it can be seen from the spectra of pristine NPs, no peaks pertaining to triphenylphosphine-related species are visible. Nevertheless, the detection of these species has been possible by the analysis through ^{1}H-NMR of the product of the decomposition of a certain amount of NPs by means of an solution of iodine in $CHCl_3$. Figures 4.10 collects three ^{1}H-NMR spectra of the product resulting from the decomposition with iodine of the same three batches illustrated before, together with a ^{1}H-NMR spectrum of dodecanethiol and a ^{1}H-NMR spectrum of the gold precursor, $AuPPh_3Cl$.

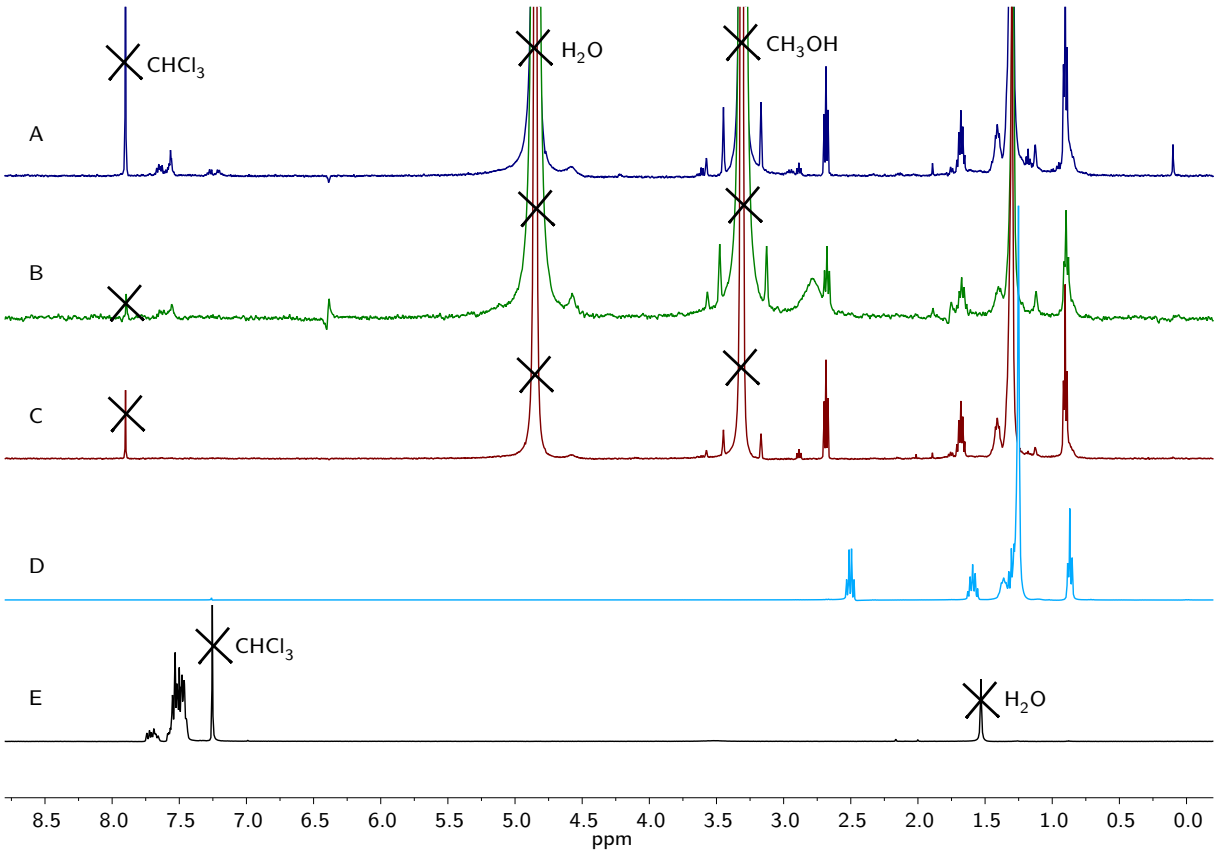

Figure 4.10: **A**: ^{1}H-NMR spectrum (400 MHz, CD_3OD) of the product of the decomposition of the batch of Au NPs synthesised according the procedure[86] of Zheng and co-workers in toluene. **B**: ^{1}H-NMR spectrum (400 MHz, CD_3OD) of the product of the decomposition of the batch of Au NPs synthesised according the procedure[86] of Zheng and co-workers in chloroform. **C**: ^{1}H-NMR spectrum (400 MHz, CD_3OD) of the product of the decomposition of the batch of Au NPs synthesised according the procedure[86] of Zheng and co-workers in THF. **D**: ^{1}H-NMR spectrum (400 MHz, $CDCl_3$) of dodecanethiol. **E**: ^{1}H-NMR spectrum (400 MHz, $CDCl_3$) of $AuPPh_3Cl$.

Once the decomposition is carried out, the signals of triphenylphosphine-related species are clearly visible in the aromatic region of the spectra for two of the three batches, within 7.7 and 7.5 ppm. The fact that the batch prepared in THF does not exhibit any peak related to triphenylphosphine-based species does not necessary imply their total absence. Indeed, the leftovers could be present as well, but in so low concentrations that they are not detectable by means of NMR.

The quantification of the triphenylphosphine-based leftovers was carried out by evaluating the integrals of the areas of the peaks pertaining to the aryl protons of triphenylphosphine-based species, visible in the low-field region of ^{1}H-NMR spectra of the decomposed Au NPs. Then, for each batch, the so-calculated value was compared to that achieved from the integration of the area of the peak pertaining to the α protons of the disulphides arising from the oxidation of dodecanethiolates by iodine, noticeable at 2.7 ppm in each ^{1}H-NMR spectrum reported in Figure 4.10. The ratio between the two kinds of capping ligands can be obtained by simply evaluating the ratio between the normalised integrals and, consequently, their percentage amount within the monolayer. Table 4.4 presents the ratio between triphenylphosphine-based leftovers and dodecanethiolates for the three batches of interest.

Table 4.4: Ratio between phosphorous-based species and sulphur-based ones in the final monolayer of NPs prepared in different solvent according to Zheng *et al.* and Goldmann *et al*, determined by means of $^{1H}-$NMR on the decomposed NPs mixtures.

Solvent for the synthesis	Average dimension (nm) and standard deviation	Ratio P/S	Percentage of PPh_3-based leftovers
Toluene	5.8 ± 0.3	0.19	16 %
Chloroform	4.2 ± 0.6	0.06	6 %
THF	4.1 ± 0.3	< 0.01	$< 1\%$

No changes in the amount of triphenylphosphine-based leftovers were outlined after repeated cycles of washings performed on pristine Au NPs, implying that these species are directly bound to the gold atoms forming the cores.

Focusing on the type of solvents used for the synthesis, the percentage amounts of triphenylphosphine-based species suggest a relationship between the polarity of the solvents and the amount of residues. Indeed, this amount decreases by increasing the polarity of the solvent. This trend agrees with what has been already mentioned concerning the use of a certain solvent rather than the others for tuning the size of the gold cores.[89] Since THF is able to form hydrogen bonds with thiols thanks to its oxygen atom, the formation of gold-sulphur is easier since the sulphur-hydrogen bond weakens. Therefore, a higher number of gold-sulphur bond will be present, whereas the gold-phosphorus ones will be less. In the case of toluene, instead, no hydrogen bonds are formed.

The presence of residual molecules of triphenylphosphine is obviously the major obstacle to a precise engineering of the monolayer. Indeed, when the desired product are Au NPs coated by thiols, not all the triphenyphosphine molecules are easily displaced from the surface of the cores, leading to binary monolayers. As a result, the behaviour of such systems cannot be predicted, therefore the outcomes could not exhibit the foreseen properties. Consequently, the control over the morphology of the monolayer and the related distribution of its composing ligands is jeopardized by adventitious contaminants. The employment of such systems cannot then fulfil the prerequisites for achieving a controlled self-assembly; for this reason, in the view of exploiting Au NPs with narrow size distribution for the implementation of methodologies for their controlled self-assembly, the degree of tolerance related to any kind of contamination is zero.

Considering the spatial organization of ligands composing the monolayer, the phenyl rings bound to the phosphorous atom of triphenylphosphine occupy the space describing a cone, whose vertex angle is 145° for triphenylphosphine[129], involving a sensibly high steric hindrance. Consequently, the degree of packing of a monolayer presenting a high amount of triphenylphosphine molecules will be inevitably lower than that of a monolayer presenting only linear aliphatic ligands such as dodecanethiolates. This can lead to an overall instability of the NPs, since the gold cores are less protected and therefore more susceptible of aggregation or etching by external agents. This fact could be the responsible for a process that resembles digestive ripening. This phenomenon occurred when the batches of NPs prepared through the procedure of G.D. Stucky and co-workers underwent place exchange reaction. Figure 4.11

displays two TEM images recorded after a place exchange reaction on Au NPs prepared in THF.

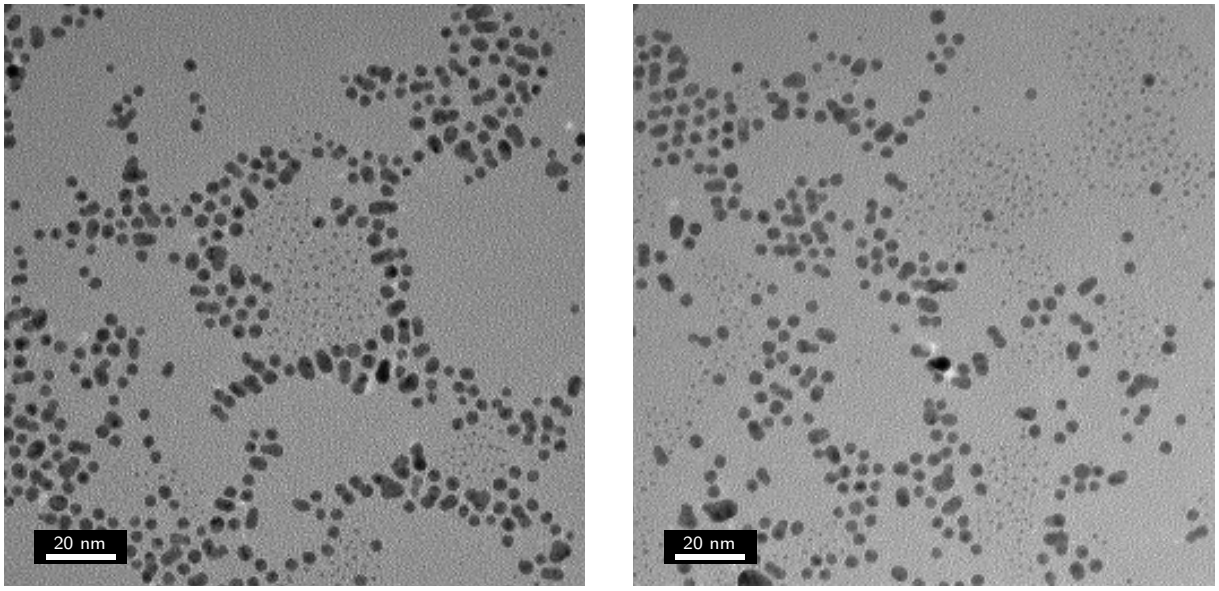

Figure 4.11: TEM images of a batch of Au NPs prepared according to Zheng *et al.* in THF and undergone place exchange reaction. Notice the NPs of reduced dimensions, formed after a process of digestive ripening.

Two populations are clearly visible in the images. One population composed of NPs having maintained the same core sizes of the NPs before the place exchange reaction, which are in between 3.5 nm and 4.5 nm. The other population is composed of NPs of smaller dimensions, which are in between 1 nm and 2 nm. Goldmann *et al.* have encountered a similar phenomenon after a place exchange reaction on a batch of Au NPs prepared with the same procedure in toluene.[128] As mentioned above, the authors claimed that this behaviour is similar to NPs undergone digestive ripening. The latter is a process where from NPs of given dimensions, smaller NPs form; it is the inverse process of Ostwald ripening, which is one of the main mechanisms of growth of NPs. Indeed, during an Ostwald ripening, gold atoms desorb from the cores of small particles and they are captured by bigger particles, which increase their sizes. Usually, both processes occurred at moderately high temperatures, since the considerable amount of energy required. As a matter of fact, the place exchange reactions that gave as results the formation of small NPs were all conducted at room temperature. Therefore, there are no clear indicators concerning the reason behind the arising of this phenomenon. One cause could probably lies in an intrinsic instability of the monolayer of NPs prepared the procedure by G.D. Stucky and co-workers. As briefly mentioned, the instability could be a consequence of the presence of triphenylphosphine-based leftovers in the monolayer of the NPs, resulting in a less packed and therefore unstable monolayer. The protection of the gold cores by the shell of ligands would consequently be less effective and the etching of part of the NPs composing the batch may occur, leading to formation of smaller NPs. Clearly, this unforeseen and unpredictable behaviour makes useless all the efforts for the achievement of batches of NPs with narrow size distribution.

2.1.3 Synthesis proposed by Peng *et al.*

The synthesis[87] proposed by Peng and co-workers involves the use of oleylamine as capping ligands and phase transfer agent for bringing gold into the organic phase. The reducing agent employed is *tert*-butylamminoborane complex which is the same mild reducing agent of the synthesis of Zheng *et al.* Once again, the smoother reducing strength of this specie is exploited for the achievement of batches of Au NPs of uniform size. As a matter of fact, this procedure was taken into account in order to overcome the drawbacks and difficulties exhibited by the synthesis reported by the group of G.D. Stucky, concerning the leftovers of triphenylphosphine-based species and the ambiguous behaviour during place exchange reactions. As previously mentioned, the main employment of this protocol is for the preparation of NPs used as materials for catalysis. Indeed, the catalytic potential of Au NPs is expressed only when bare gold is exposed or accessible; therefore, for applications in heterogeneous catalysis, ligands are no more necessary and they could be removed from the gold surface. If the bond between gold atoms and ligands is characterized by a relatively low binding energy, the process of removal of the capping agents is easier. Indeed, the bond between gold and nitrogen is weaker than a gold-sulphur bond. For this reason, oleylamine is widely exploited for the synthesis of NPs that are employed for catalytic purposes.
In the present research work, since the application of the NPs prepared by the method of Peng *et al.* would not have been catalysis, it was necessary to endow them with higher stability, so that making possible to work with NPs without experiencing aggregation induced by the desorption of ligands from the gold surface. For this purpose, the so-prepared NPs were made undergo place exchange reaction with dodecanethiols in order to wholly replace oleylamine with dodecanethiolates, able to form a more packed monolayer.
The first experiments were performed at different temperatures in order to confirm the claim of Peng and co-workers according to which, the temperature at which the synthesis is carried out affects the average cores diameter. The experiments were carried out in 1-octadecene, an aliphatic solvent whose long chain would help stabilized monolayers of NPs protected by oleylamine, thanks to van der Waals interactions, giving rise to NPs with narrow size distributions.[90] The monolayers composed of oleylamine present a long linear alkyl chain, giving rise to interactions with the molecules of solvent, stabilizing the forming particles.
Figures 4.12, 4.14 and 4.13 report three TEM images with relative histograms displaying size distributions of three batches of Au NPs protected by oleylamine, prepared in 1-octadecene at different temperatures, according the protocol of Peng *et al.*

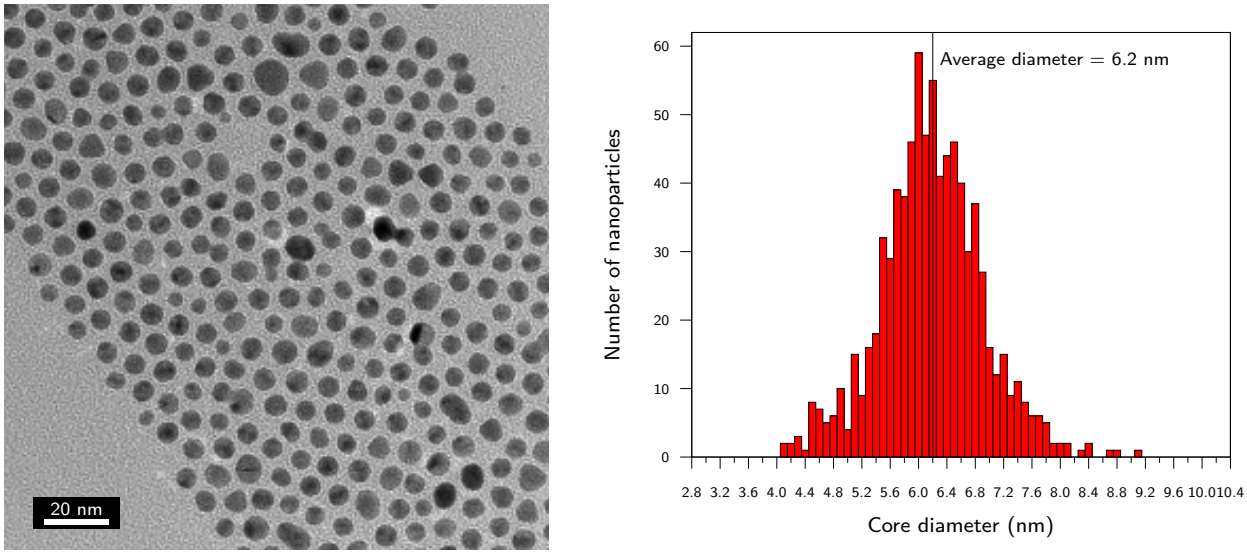

Figure 4.12: On the left, TEM image of a batch of Au NPs protected by oleylamine, prepared in 1-octadecene at 15 °C. On the right, histogram displaying size distribution, obtained after the analysis of core sizes over 1000 NPs.

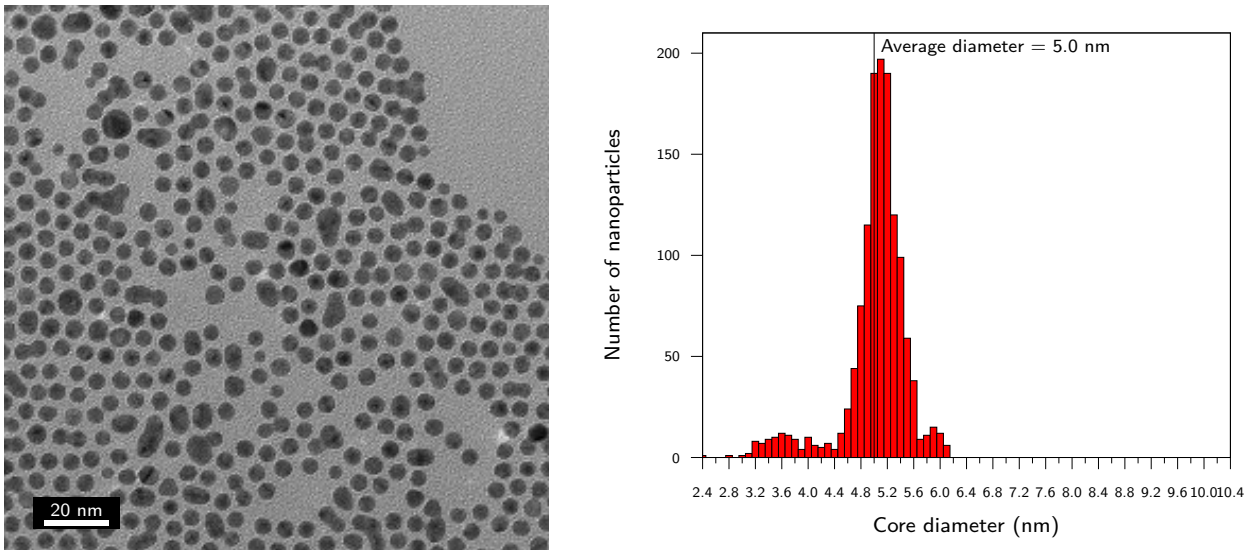

Figure 4.13: On the left, TEM image of a batch of Au NPs protected by oleylamine, prepared in 1-octadecene at 25 °C. On the right, histogram displaying size distribution, obtained after the analysis of core sizes over 1000 NPs.

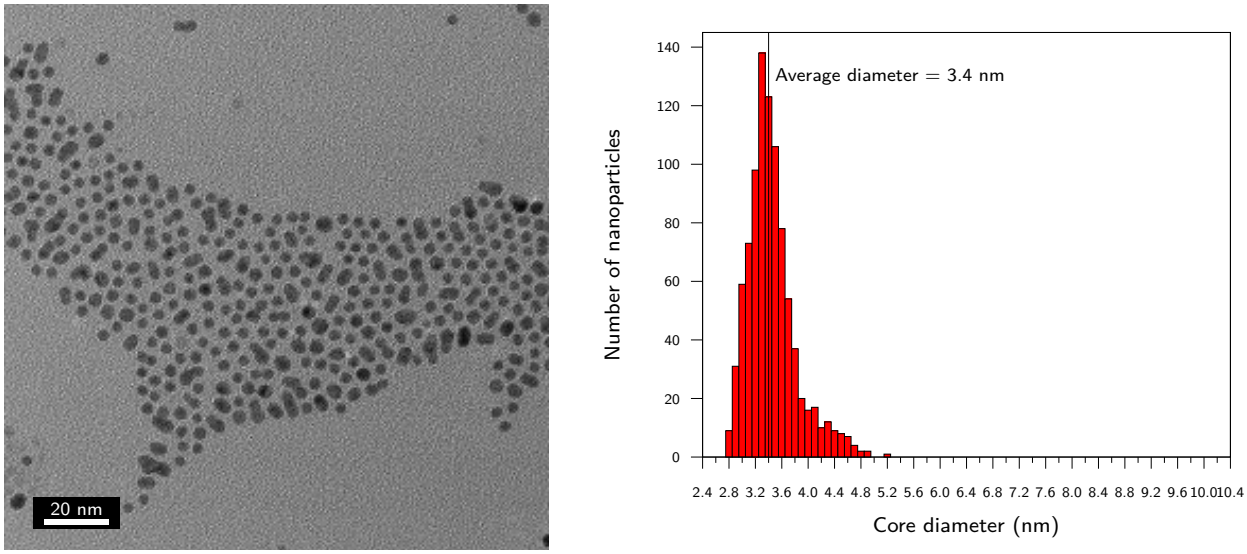

Figure 4.14: On the left, TEM image of a batch of Au NPs protected by oleylamine, prepared in 1-octadecene at 32 °C. On the right, histogram displaying size distribution, obtained after the analysis of core sizes over 1000 NPs.

As the histrograms display, the size distribution of these batches is rather narrow. Table 4.5 collects the properties related to the dimensions of the gold cores of three samples, together with the temperature at which they were prepared.

Table 4.5: Properties of oleylamine-capped Au NPs prepared in 1-octadecene at different temperatures.

Average core dimension (nm)	Standard deviation	Variation coefficient	Temperature (°C)
6.2	0.7	0.11	15
5.0	0.5	0.10	25
3.4	0.4	0.12	32

The results obtained confirmed the relationship between the average core dimensions and the temperature at which the synthesis is performed. In fact, by increasing the temperature the average core size decreases. This evidence agrees with the outcomes[87] reported Peng and co-workers. The reason behind this behaviour is due to the fact that an increment of the temperature of the reaction mixture involves an increase in the reduction rate; therefore, the nucleation of new center is faster than the growth of the already existing ones. This should also lead to a broadening of the size distribution, since the growth starts to become less and less homogeneous with the increase of the temperature. As a matter of fact, for the three batches here presented, the increase of the temperature does not involve huge broadening of size distributions, even though the variation coefficient of the batch synthesised at 32 °C is slightly higher than the others.

Further experiments were performed in hexane, so that pointing out whether the solvent had a strong effect on the outcomes of the synthesis affecting size distribution. The reactions were performed at 25 °C and the results are displayed in Figures 4.15 and 4.16. By comparing the size distribution of the two batches obtained using the exact same conditions, it is possible to perceive a consistent degree of reproducibility characterizing the approach.

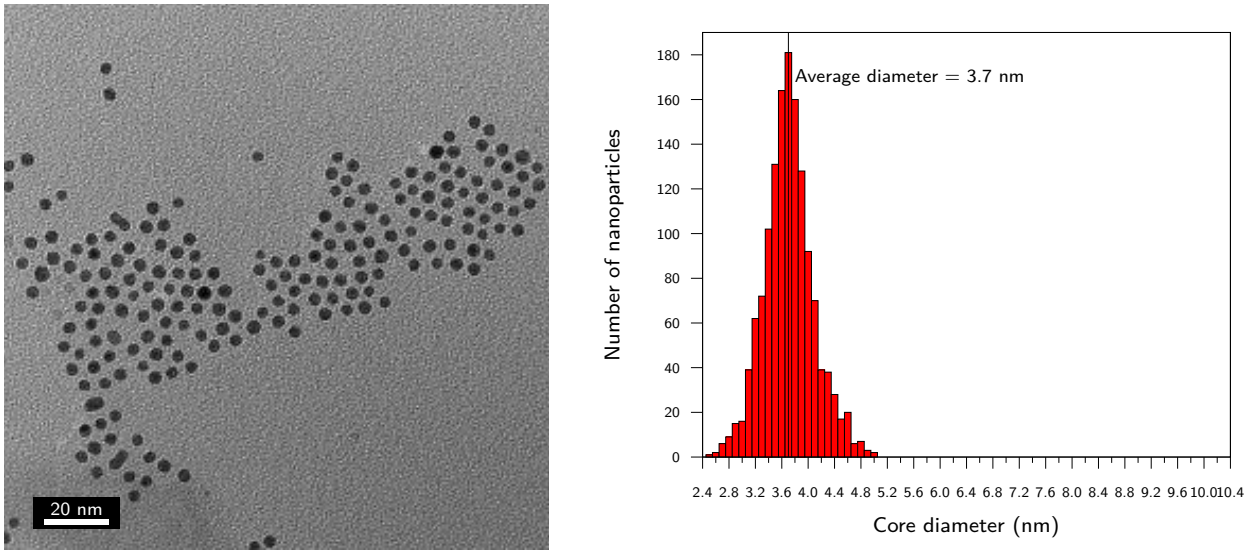

Figure 4.15: On the left, TEM image of a first batch of Au NPs protected by oleylamine, prepared in hexane at 25 °C. On the right, histogram displaying size distribution, obtained after the analysis of core sizes over 1000 NPs.

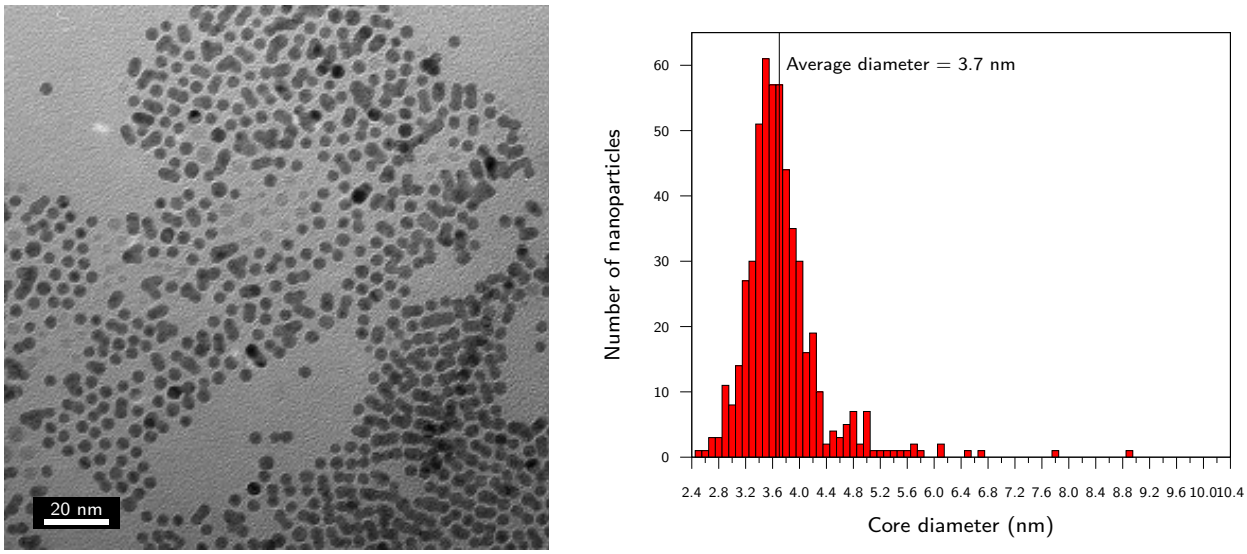

Figure 4.16: On the left, TEM image of a second batch of Au NPs protected by oleylamine, prepared in hexane at 25 °C. On the right, histogram displaying size distribution, obtained after the analysis of core sizes over 1000 NPs. The size distribution of this batch is comparable to the one of the batch presented in Figure 4.15.

By comparing the products of the reaction performed in hexane at 25 °C with the ones obtained by performing the reaction in 1-octadecene at the same temperature, a slight decrease of average core diameter can be appreciated. Indeed, the synthesis in 1-octadecene allowed to obtain a batch of Au NPs characterized by an average core diameter of 5.0 nm, whereas the one in hexane led to batches of Au NPs possessing an average core diameter of 3.7 nm. The use of hexane as solvent for the synthesis does not significantly alter the size distribution though, since the standard deviation for the average diameter of the first batch here presented is characterized by a standard deviation of 0.4 nm, with a variation coefficient of 0.11, while for the latter the standard distribution is slightly higher, having a value of 0.6 nm, with a variation coefficient of 0.16. One of the reasons behind this subtle broadening of size distribution could be related

to the use of hexane instead of 1-octadecene. Indeed, since the length of the chain of hexane is considerably lower than that of 1-octadecene, the number of van der Waals interactions that stabilize the monolayer composed of oleylamine is lower. Consequently, the NPs are less stable and ripening phenomena can occur during the course of the reaction.

2.1.4 Place exchange reaction on NPs protected by oleylamine

Different experiments of place exchange reaction were carried out involving the previously presented Au NPs covered by oleylamine and synthesised following the procedure of Peng and co-workers. Indeed, the aim was to completely replace oleylamine in favour of dodecanethiolates, so that providing the NPs with major stability over time. The main cause of the lower stability is indeed the strength of the Au-N bond, whose lability could easily bring to the detachment of ligands from the gold surface. Indeed, the dissociation energy for the gold-nitrogen bond is reported to be about 33 kJ/mol[130]. Nevertheless, this lability can be exploited to performed a quite straightforward place exchange reaction employing ligands able to more strongly bind to gold atoms, aiming at wholly replacing amines from the gold surface. Dodecanethiolates are in fact able to stabilized the gold cores in a more efficient way thanks to the stronger gold-sulphur bond, whose dissociation energy is reported to be 184 kJ/mol[3], and their linear chains which are involved by mutual van der Waals interactions, contributing to a highly packed monolayer. As a matter of fact, oleylamine chains are capable of giving rise to van der Waals interactions as well; however, the structure of oleylamine is characterized by a carbon-carbon double bond involving the ninth and tenth carbon atoms of the chain. Furthermore, the conformation of the double bond is *cis*, which implies a consistent steric hindrance, contributing to lower degree of packing of the monolayer with respect to linear alkyl ligands. Indeed, even though the oleylamine chains interact through van der Waals forces, they arrange themselves farther apart from one another on the gold surface, leading to a looser monolayer due to the fact that the stacking among the chains is not ordered. Figure 4.17 reports the structures of dodecanethiol and oleylamine, for comparison.

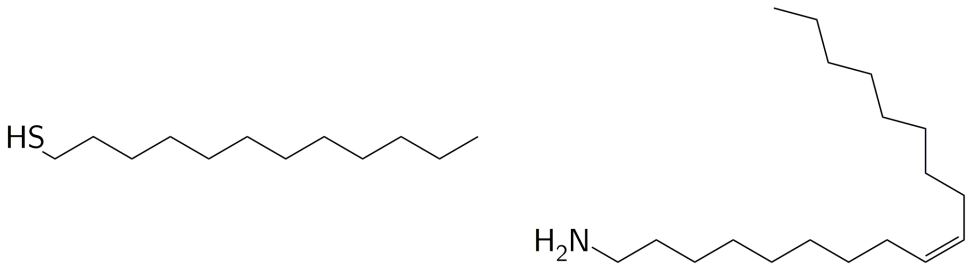

Figure 4.17: Chemical structures of dodecanethiol and oleylamine. Notice the higher steric hindrance of oleylamine aliphatic chain.

The place exchange reactions were performed according to the procedure reported in a paper[131] by Kluenker *et al.* whit slight modifications: the experimental details for the procedure are reported in Part III. A high molar excess of thiol was employed in order to assure the complete displacement of oleylamine from the gold surface. Figure 4.18 reports the TEM analysis of

the outcomes of a place exchange reaction performed on the batch of Au NPs protected by oleylamine presented in Figure 4.14, whose average core diameter is 3.4 nm.

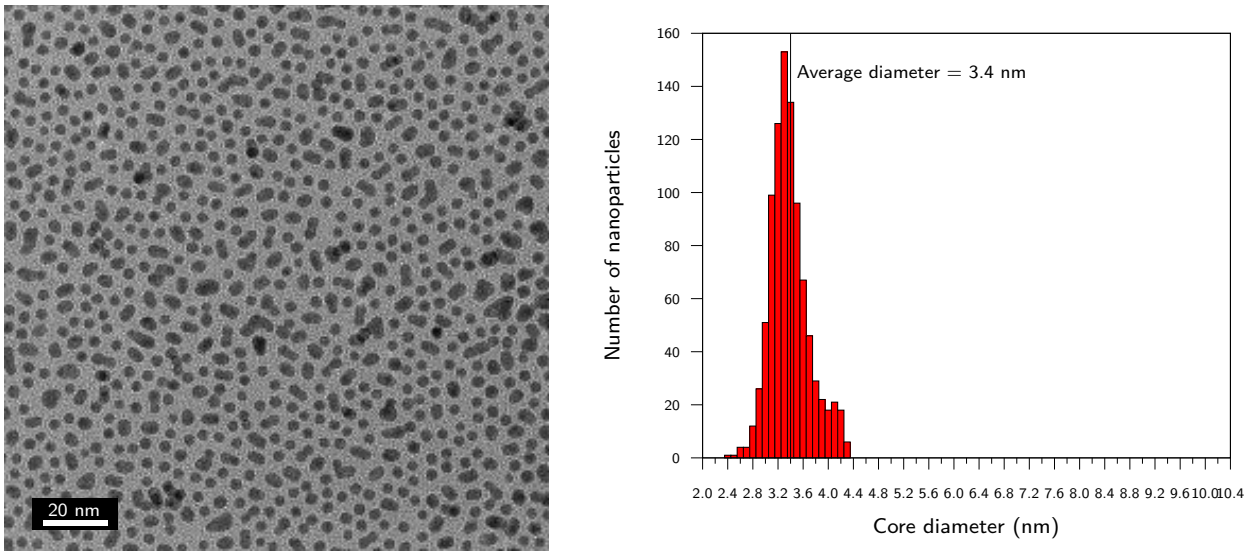

Figure 4.18: On the left, TEM image of a batch of Au NPs protected by oleylamine undergone place exchange reaction with dodecanethiols. On the right, histogram displaying size distribution, obtained after the analysis of core sizes over 1000 NPs.

The TEM analysis provided encouraging results concerning the average core diameter and relative size distribution of the NPs after the place exchange reaction. Indeed, neither changes in average core dimension nor size distribution can be pointed out, suggesting that the considerably high amount of dodecanethiol does not alter the structure of the gold core. The average core size remained unaltered, with a value of 3.4 nm; the standard deviation associated with it is 0.3 nm, resulting in a variation coefficient equal to 0.09. The so-produced NPs appeared to be stable in solution or as dry solid. Indeed, they can be easily brought to dryness and subsequently redispersed in apolar solvent (hexane, toluene) or moderately polar ones (chloroform, methylene chloride).
At the end of the place exchange reaction, the NPs were precipitated and washed several times with EtOH. The ^{1}H-NMR spectrum of the purified NPs is reported in Figure 4.19, identified as A. The figure displays the ^{1}H-NMR spectra of the result of the decomposition with iodine of a small portion of the Au NPs produced by means of place exchange reaction (B), oleylamine (C) and dodecanethiol (D) as well.

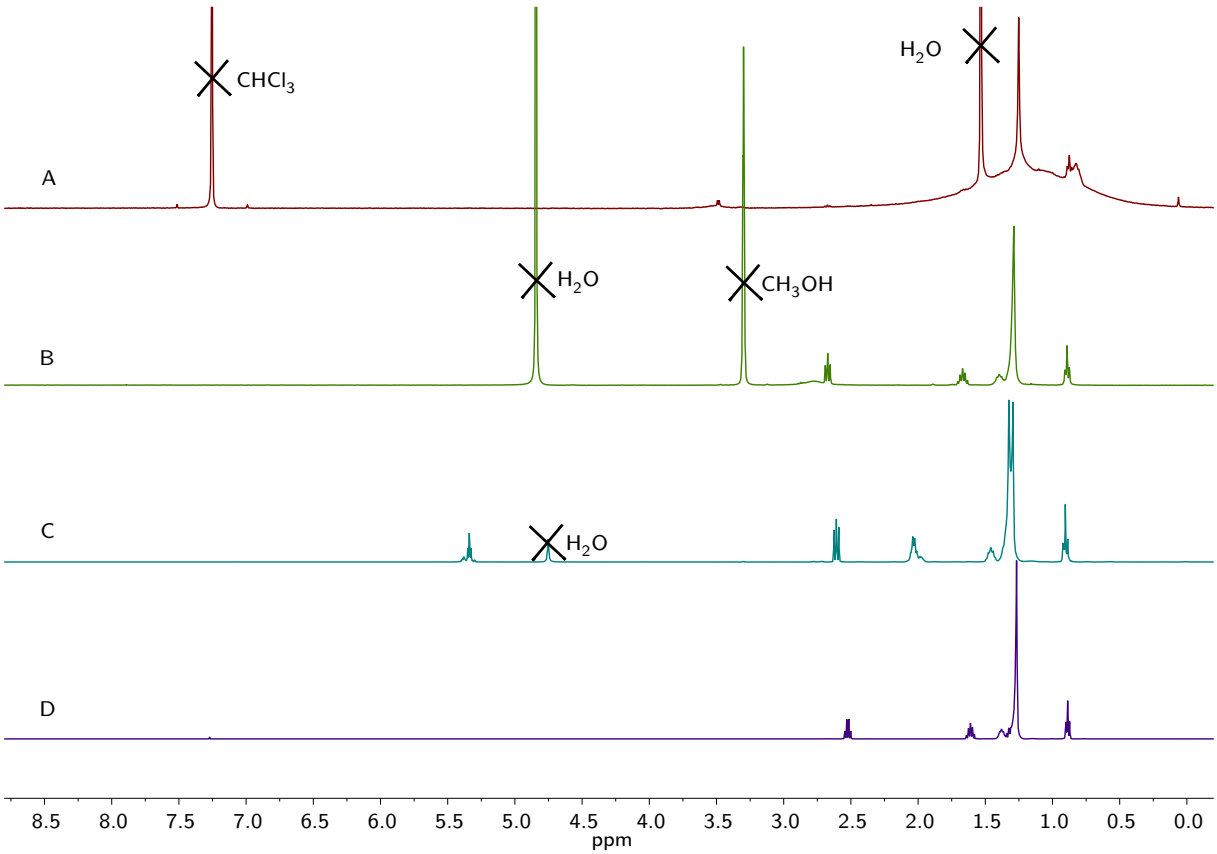

Figure 4.19: **A**: ^{1}H-NMR spectrum (400 MHz, $CDCl_3$) of Au NPs protected by dodecanethiolates, resulting from place exchange reaction on Au NPs covered by oleylamine. **B**: ^{1}H-NMR spectrum (400 MHz, CD_3OD) of the decomposed Au NPs produced by place exchange reaction. **C**: ^{1}H-NMR spectrum (400 MHz, CD_3OD) of oleylamine. **D**: ^{1}H-NMR spectrum (400 MHz, $CDCl_3$) of dodecanethiol.

The presence of the peak at 5.3 ppm, resulting from the resonance of the olefinic protons of oleylamine, is diagnostic for outlining any unwanted residue. No sharp peaks pertaining to free thiols nor free oleylamine can be highlighted in the ^{1}H-NMR spectrum of the Au NPs prepared through place exchange reaction, meaning that the washing procedure was effective. The ^{1}H-NMR analysis on the product obtained after the decomposition does not exhibit any trace of residual oleylamine, meaning that the whole amount of oleylamine coating the gold cores was replaced by DDT.

As a matter of fact, not all the batches underwent to place exchange reaction with dodecanethiol provided satisfying results. In fact, some of the batches decomposed during the place exchange reaction and some others were once again affected by the same phenomenon previously described, resembling digestive ripening. Figure 4.20 displays a TEM image of a batch of Au NPs coated with oleylamine underwent place exchange reaction: besides original sized NPs, NPs of inferior dimensions are clearly visible. In this case, the arising of the NPs of smaller core size could be ascribed to the looseness of oleylamine-composed monolayer. This feature, together with the low energy for the dissociation of gold-nitrogen bond, estimated to be 33 kJ/mol,[130] could lead to a higher probability of desorption of gold atoms from the surface of larger NPs and their rearrangement, giving rise to NPs of reduced dimensions.

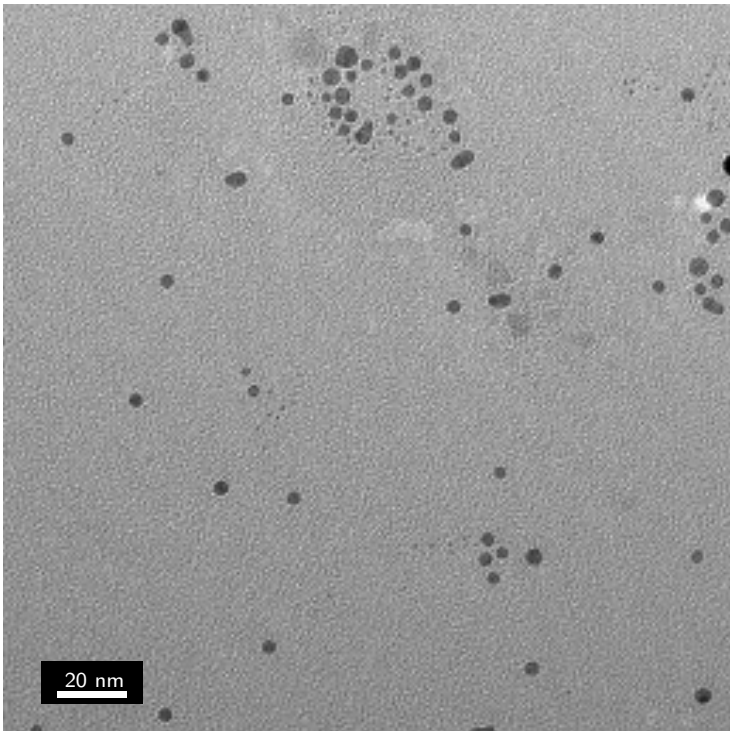

Figure 4.20: TEM image of a batch of Au NPs protected by oleylamine undergone place exchange reaction with dodecanethiols. Note the presence of NPs of reduced dimensions, resulting from digestive ripening.

The unpredictable behaviour of this type of NPs did not allow their use for further functionalization and experiments for tuning the conditions for controlled self-assembly. Indeed, the overall process of functionalization and subsequent triggering of mutual interactions among NPs requires a careful tuning of the reaction conditions and precise monolayer functionalization at specific positions for each NP. As a consequence, unforeseen behaviour during place exchange reactions would lead to total lack of control during functionalization. For this reason, even though the synthesis of Peng and co-workers does provide satisfying results in terms of size distribution and possibility of tailoring the dimensional properties of NPs, the intrinsic stability of NPs protected by olyelamine is a heavy drawbacks that prevent them to be employed as substrates for engineering of precisely functionalized NPs.

2.2 Synthesis *via* heat treatment

As stated before, the *post*-synthesis heat treatment is a method[85] proposed by the group of M. Miyake, which allows the growth of gold cores through controlled gradient of heating at a given interval of time. As a result, NPs of reduce dimensions, around 1.5 nm, synthesised following the Brust-Schiffrin procedure[82] can be employed as starting materials for preparing batches of NPs with tunable dimensions depending on the temperature at which the heat treatment is performed. Furthermore, the presence of tetraoctylammonium bromide tuned out to be essential for the success of the protocol. The importance of its role has to be ascribed to the fact that it melts at the temperatures at which the heat treatment is carried out, that are usually within 150 °C and 250 °C, acting as solvent for NPs. The higher is the temperature at which the NPs are heat-treated, the bigger are the average core dimension of the resulting NPs.

However, bigger NPs with an average core diameter of around 10 nm can be obtained only at very high temperature, such as 250 °C. Consequently, it is necessary that the starting NPs are coated with ligands whose boiling points are higher than these temperatures, otherwise NPs will aggregate, with no possibility of redissolving them.
This procedure was therefore employed for the preparation of batches of Au NPs protected by dodecanethiolates, aiming at controlling the size growth for the achievement of moderately disperse NPs. Undoubtedly, it is not possible to tune the size of the cores as the previously described procedures do, since the only tunable parameter is the temperature of the heat treatment. Moreover, it is hardly possible to reach very narrow size distributions, since the process of growth is not mediated by agent assuring the homogeneous growth of each core. However, the procedure does not involved any other type of ligands beside thiols, therefore no contaminations from other species are possible. The latter is actually one of the major drawbacks of the previously explained protocols, which rely on other ligands besides thiols for achieving batches of NPs with narrow size distributions. Furthermore, the capping with thiols assures a high stability of NPs, feature that should avoid inconvenient phenomena such as digestive ripening.
Figure 4.21 reports a TEM image of a batch of NPs obtained through the method proposed by Miyake and co-workers and the histogram displaying the size distribution. The NPs were heat-treated in air, starting from a temperature of 25 °C and reaching a temperature of 154 °C, at which they were maintained for 30 minutes. The resulting NPs were characterized by an average core diameter of 4.2 nm; the standard deviation associated to the size distribution is 0.8 nm. The variation coefficient is 0.19.
The overall method was repeated a second time to test the reproducibility of the approach. For this purpose, a new batch of Au NPs coated by dodecanethiols was prepared and heat-treated at the exact same conditions of the previous time. The outcomes of the second experiment were slightly different from those of the first treatment. In fact, the average core diameter after the heat treatment is 4.5 nm, with a standard deviation of 1.0 nm, resulting in a variation coefficient of 0.22.
Although the conditions employed were exactly the same, the size distribution of the second heat treated batch is slightly broader, evidencing a certain criticality on reproducibility of the approach. However, the batches of NPs obtained from this protocol were used for subsequent functionalization with terpyridine-terminating thiols for the reasons previously exposed concerning the prevention from adventitious contaminations from other kinds of ligands and intrinsic lack of stability of the monolayer due to loose packing and weaker bounds among capping ligands and gold atoms.

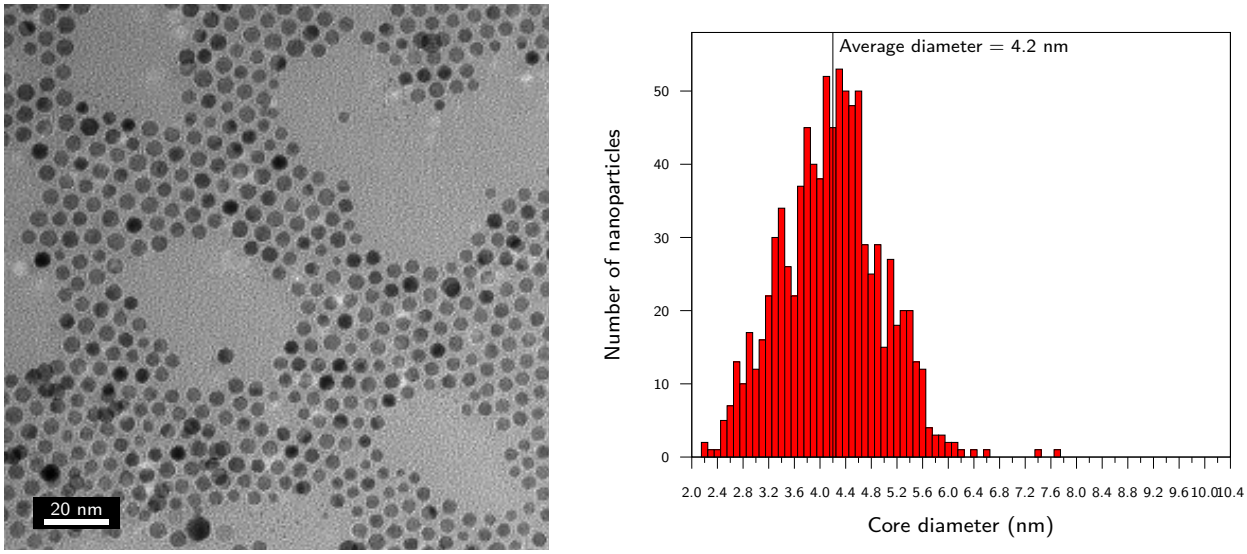

Figure 4.21: On the left, TEM image of the first batch of Au NPs protected by dodecanethiolates, obtained as a result of heat treatment at 154 °C. On the right, histogram displaying size distribution, obtained from the analysis of core sizes over 1000 NPs.

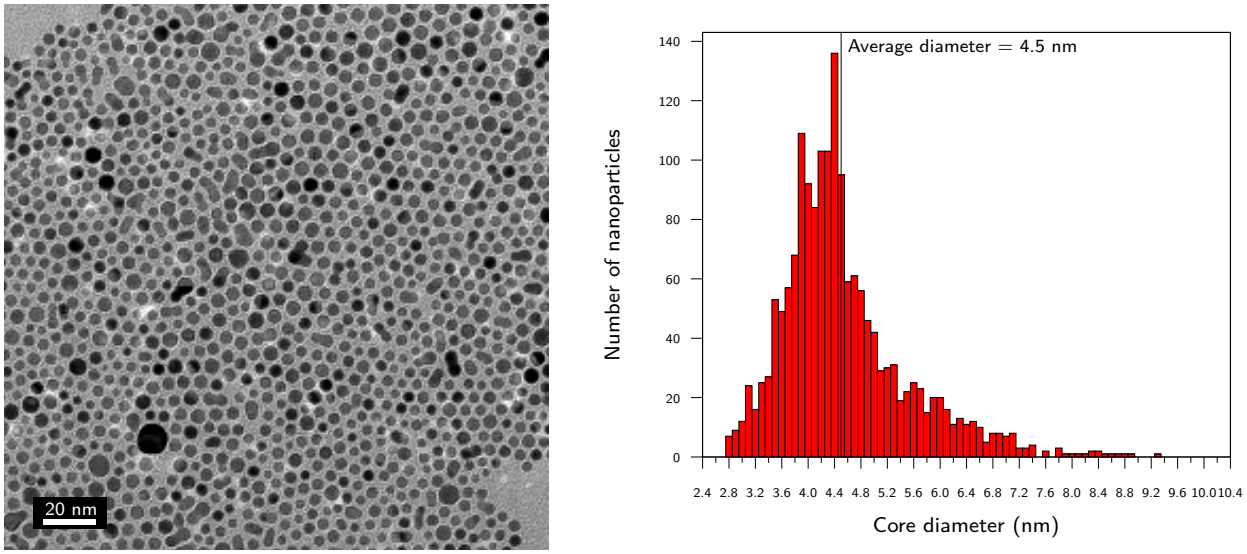

Figure 4.22: On the left, TEM image of the second batch of Au NPs protected by dodecanethiolates, resulting from heat treatment at 154 °C. On the right, histogram displaying size distribution, obtained from the analysis of core sizes over 1000 NPs. Note the broader size distribution affecting this batch, compared to that presented in Figure 4.21.

3 Functionalization of Au NPs coated with dodecanethiolates for controlled self-assembly

The engineering of functional Au NPs for conducing a preliminary study of their interactions in organic media was performed taking advantage of the NPs prepared by the procedure[85] proposed by Miyake and co-workers, for the reasons previously exposed. The approach involved the place exchange reaction with a synthesised terpyridine-terminating thiol. The functional group at the end of this latter specie is able to coordinate several metal ions[54] and the result of

the coordination of two molecules of terpyridine with a metal center is a complex with octahedral geometry. Moreover, the whole process can be reverted by adding a stronger complexation agent which subtracts the metal ion from the center of the complex and it restores the initial condition of terpyrdine molecules free in solution. This feature could be indeed transferred to the functional NPs, so that achieving a system which would be able to cyclic pass from one configuration and to the other thanks to external stimuli. Figure 4.23 displays the process of formation of octahedral complexes by terpyridine units, together with the reversing process of disrupting the complexes.

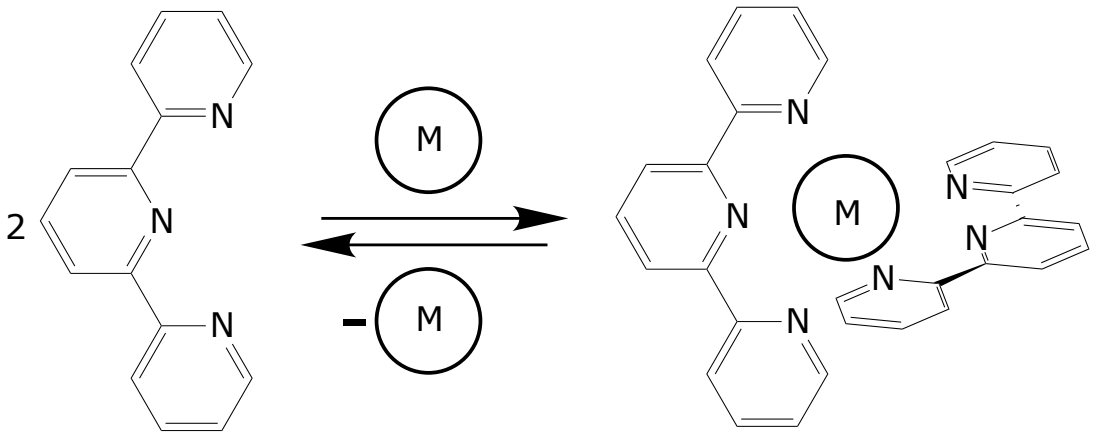

Figure 4.23: Equilibrium reaction between the metal complex and two molecules of terpyridine and free metal ion.

The insertion of the terpyridine-terminating ligands in the monolayer of the NPs was performed by means of a rapid place exchange reaction so that limiting the number of ligands entered in the monolayer and therefore reaching a certain degree of control over the functionalization of the NPs. This was undoubtedly the fundamental prerequisite, since the interest was addressed towards the achievement of ordered superstructures of NPs. However, the process is far from being trivial and requires large sets of experiments meant to set up the best conditions for controlling the number of interacting points within the monolayer. What have been done here is performing preliminary trials in order to understand if the strategy chosen is feasible and compatible with the characterization techniques. Inserting a limited number of interacting points for each NP is challenging for two main reasons: the first one is related to the not homogeneous chemical behaviour of the NPs because of moderately broad size distribution, leading to a not uniform functionalization of the NPs; the second one is due to the very low concentration of functional groups attached to each NP within a batch. If the adverse effect of the first can be somehow limited by working with batches of NPs with narrow size distribution, the latter cannot be overcome so easily, since every characterization technique has its own limit of detection. As a matter of fact, working with a consistent amount of material is the obvious method to avoid this situation. Nevertheless, the scale-up of the procedure can only be carried out once the optimal conditions for the functionalization have been pinpointed and a solid protocol built up, risking otherwise considerable loss of starting materials.
The experiments herein discussed have been then performed with a view of progressively changing the conditions for the process of functionalization through place exchange reaction according to the results obtained. As presented in Chapter 1, the conditions followed for the

place exchange reaction were those outlined in a paper[132] from the group of F. Stellacci, where the authors prepared divalent Au NPs by carrying out a place exchange reaction for 15 minutes so that inserting a limited number of functional groups for each NP. The authors claimed that, using NPs with protecting monolayer displaying a stripe-like morphology, the rapid place exchange reaction allows to functionalized the monolayer only at the poles, because in those positions the shell of ligands is less packed and consequently the ligands are the first involved in the place exchange reaction, given the reduced steric hindrance.[29] Consequently, the same strategy was employed for the functionalization of Au NPs with terpyrdine-terminating thiolates and a scheme of the procedure of place exchange reaction is reporeted in Figure 4.24.

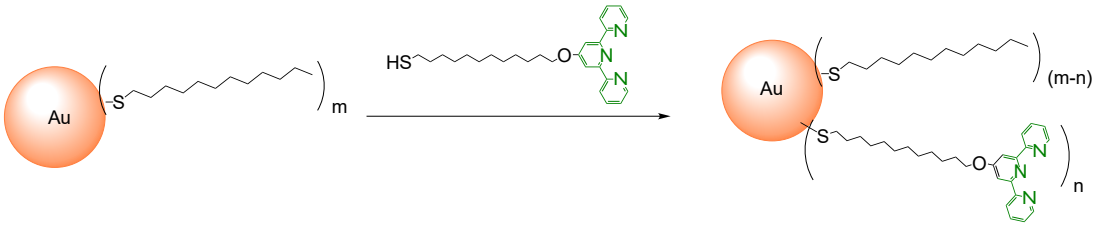

Figure 4.24: Place exchange reaction of Au NPs protected by dodecanethiolates for insertion of terpyridine-terminating thiols.

The interactions among the so-prepared functional Au NPs functionalized with the terpyridine-terminating thiols in chloroform were therefore triggered by the addition of a solution containing Fe(II) ions, obtained by dissolving $Fe(BF_4)_2$ in a 3:1 mixture of chloroform and methanol. This type of salt was chosen because of the ability of terpyridine of forming strong complexes with Fe(II) ions[54], giving characteristic absorptions in the UV-Visible region. The outcomes from the metal ions complexation were then studied by means of TEM. As a matter of fact, the analysis of the process of self-assembly by means of conventional TEM could be misleading, since many artefacts can arise due to the fact that NPs are driven closer one to the others because of solvent evaporation. However, it can be used for preliminary studies focused on outlining any differences from the images collected before and after the addition of the agent triggering the aggregation, which in this case are Fe(II) ions. In some cases, UV titrations were also performed in order to estimate the number of interacting points inserted within the monolayer of Au NPs. The titrations were carried out by progressively adding defined amount of Fe(II) and recording the UV-Vis spectrum after each addition. The attention was then focused on the feature at 319 nm, which is one of the characteristic features of $[Fe(terpy)_2]^{2+}$ complex.

3.1 Analysis of the results from the interactions the terpyridine-functionalized Au NPs triggered by Fe(II) ions

The first experiment was performed on 6 mg of 4.2 nm Au NPs, synthesised through the Brust-Schiffrin procedure[82] and then heat-treated according to the protocol of Miyake and coworkers[85], whose TEM analysis has been presented in Figure 4.21. A 15 mg/mL solution in DCM was treated with terpy-terminating thiol in 400 molar excess with respect to the moles of NPs. The place exchange reaction was carried out for 15 minutes and then stopped by evaporating the solvent and adding EtOH. Repeated washings on the solid were carried out in order

to be sure to remove all the unbound species. Figure 4.25 displays two TEM images of the batch, one before the place exchange reaction, on the left, and the other recorded after the place exchange reaction but before adding Fe(II) ions to the environment, on the right. No sensible variations in average core dimensions can be outlined, evidencing a certain stability of the NPs themselves towards the conditions at which the place exchange was performed, without leading to phenomena ascribable to any ripening.

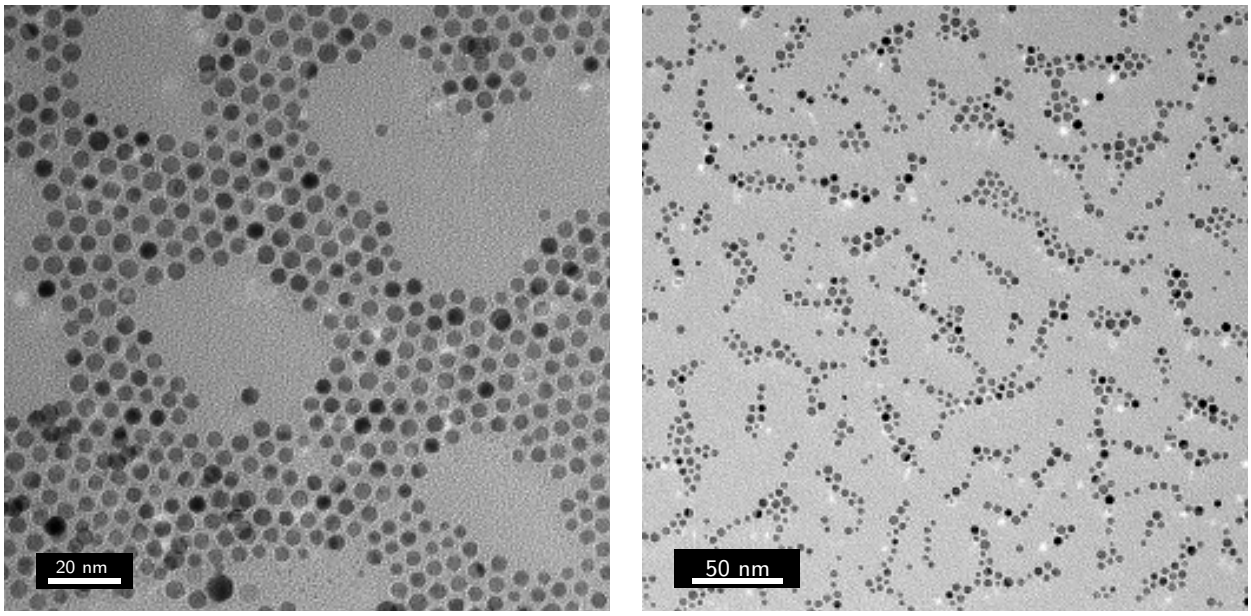

Figure 4.25: On the left, a TEM image of the batch of Au NPs before the place exchange reaction with terpy-terminating thiol. On the right, a TEM image of the same batch after the place exchange reaction. No sensible variations in core dimensions are appreciable.

Once the place exchange was completed, an experiment for testing the capability of mutual interactions among the so-achieved functional NPs was performed by adding 15 μL of a $2.5 \cdot 10^{-3}$ M solution of $Fe(BF_4)_2$ in a 3:1 mixture of chloroform and methanol to a 10^{-7} M solution of functional NPs in chloroform. The outcomes from the test were analysed by means of TEM. Figure 4.26 collects four TEM images displaying the results after the addition of Fe(II) ions to the solution containing the functional NPs. All the images reports the formation of large aggregates as a consequence of the addition of Fe(II) ions, suggesting the actual interactions among functional NPs. Indeed, the NPs are brought to interact thanks to the formation of metal complexes composed of two terpyridine units surrounding a metallic center. The aggregates appear dense and constituted by a consistent number of NPs. As a matter of fact, neither a precise geometry nor a certain periodicity in the arrangement of the NPs could be highlighted, whereas only random aggregates with no intrinsic order were found. Therefore, the conditions employed for the functionalization by means of place exchange reaction were not adequate to bestow a precise degree of order in the organization of the monolayer of the NPs used as substrates for the process of self-assembly triggered by metal ions coordination.

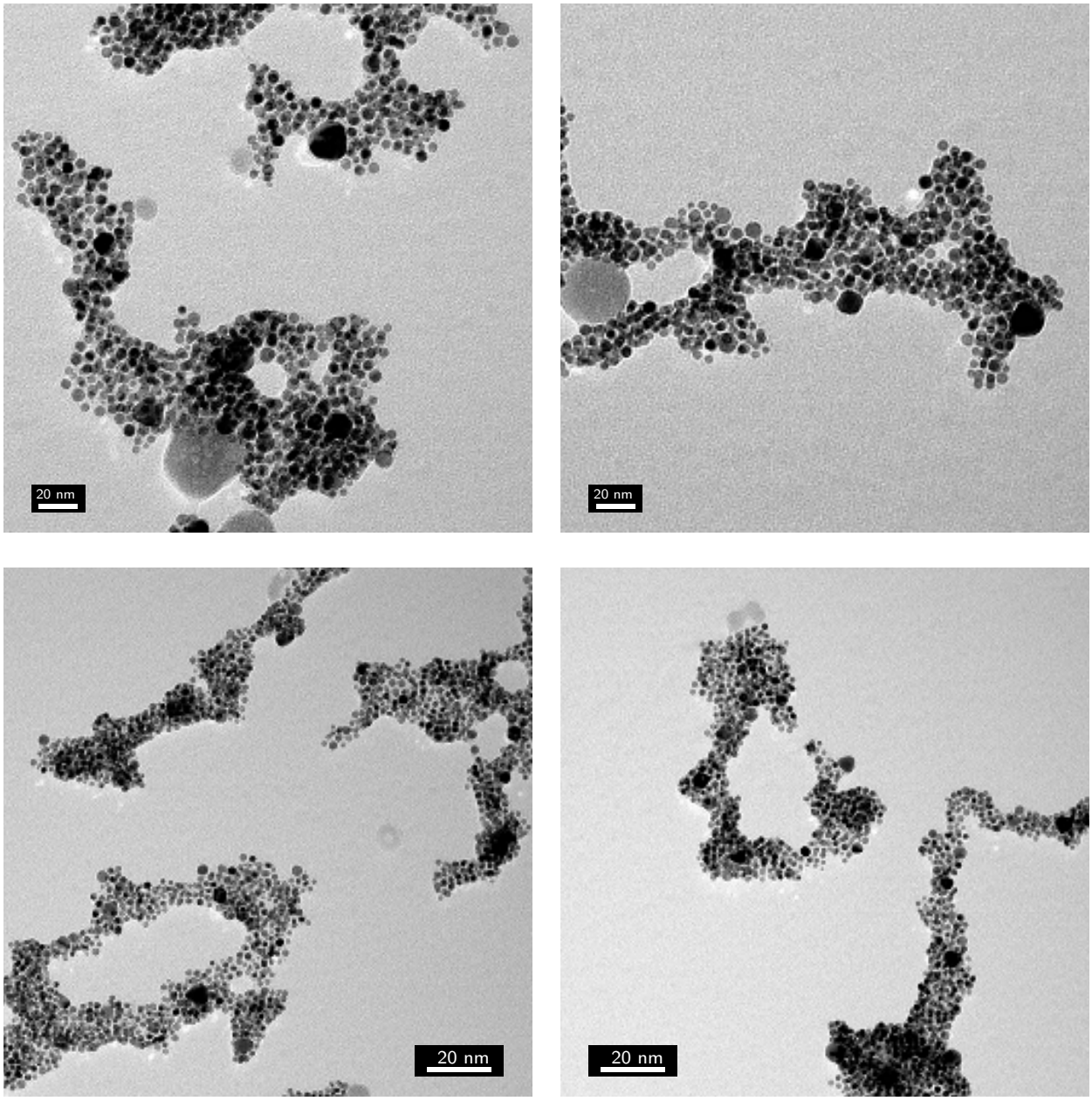

Figure 4.26: TEM images of the outcomes from the experiment carried out by triggering the interactions among Au NPs functionalized by terpyridine-terminating thiolates through the addition of an excess of $Fe(BF_4)_2$.

Further investigations were performed so that getting an insight on the average number of interacting sites within the monolayer of each NP. For this purpose, an UV-Visible titration was carried out on 1 mL of a10^{-7} M solution of terpyridine-functionalised NPs dissolved in chloroform. Six subsequent additions of aliquots of 2.5 μL of a $2.5 \cdot 10^{-3}$ M solution of $Fe(BF_4)_2$ prepared in a 3:1 mixture of chloroform and methanol were made. After each addition, a UV-Vis spectrum was recorded, focusing the attention on the arising of the characteristic features of $[Fe(terpy)_2]^{2+}$ complex. All the spectra recorded are reported in Figure 4.27, which also presents an inset of the UV-Visible region within 380 and 300 nm. In the inset of the figure is clearly noticeable an absorption peak at λ = 319 nm, ascribable to the$[Fe(terpy)_2]^{2+}$ complex. Consequently, the value of the absorbtion a that wavelength were reported as a function of the concentration of Fe(II) added, in order to point out the minimum concentration of metal ions

necessary to coordinate all the terpyridine molecules contained in the sample analysed. This latter graph is depicted in Figure 4.28.

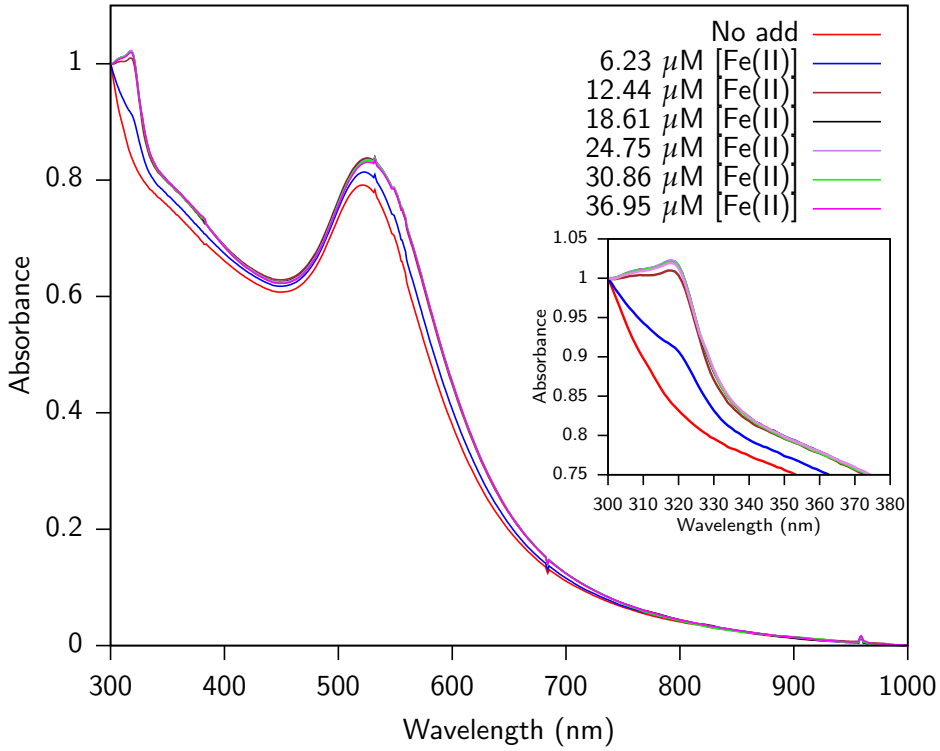

Figure 4.27: UV-Visible spectra recorded during the titration of 1 mL of a10^{-7} M solution of terpyridine-functionalised NPs dissolved in chloroform with six aliquots of 2.5 μL of a $2.5 \cdot 10^{-3}$ M solution of $Fe(BF_4)_2$ in a 3:1 mixture of chloroform and methanol. The inset focuses on the region of the UV-Visible spectrum within 380 and 300 nm where a characteristic feature of $[Fe(terpy)_2]^{2+}$ complex appeared.

One Fe(II) ion is coordinated by two molecules of terpyrdine according to the following reaction:

$$Fe^{2+} + 2terpy \rightarrow [Fe(terpy)_2]^{2+} \tag{4.1}$$

Therefore, the stoichiometry of the reaction describing the process of complex formation states that one moles of Fe(II) is able to coordinates two moles of terpyridine. By referring then to the graph reported in Figure 4.28, taking into account the minimum concentration of Fe(II) which titrates the terpyridine molecules within the batch analysed, it is possible to roughly estimate the number of terpyridine molecules simply by evaluating the ratio between the concentration of terpyridine, obtained from the titration by doubling the concentration of Fe(II), and the concentration of NPs themselves. The titration curves suggests that the minimum Fe(II) concentration for titrating all the terpyrdine molecules contained in the batch is 18.6 μM. In fact, at that concentration of Fe(II) ions, the value of absorbance of the feature at 319 nm reaches a plateau, meaning that the concentration of $[Fe(terpy)_2]^{2+}$ complex does not increase further. Consequently, as stated before, since the complex is composed of two molecules of terpyridine and one Fe(II) ion, the concentration of terpyridine units within the batch is obtained by doubling the concentration of Fe(II) at the equivalence point. Consequently, the concentration of terpyridine in solution is 37.2 μM; by considering this value and dividing it by the concentra-

tion of NPs in solution, it is possible to get the ratio between terpyridine units and NPs, which is equal to 372, meaning that each NPs bears 372 molecules of terpyridine. Taking into account a paper[113] published by the group of R. W. Murray, the theoretical number of ligands for a NP characterized by a diameter of 4.2 nm is 369, with a standard deviation of 138. It is clear that the degree of substitution of dodecanethiolates by terpyridine-terminating thiols is undoubtedly high, due to an almost total replacement of ligands, representing a situation surely far from being controlled. It is also compatible with the outcomes observed at TEM, evidencing large aggregates composed of a huge amount of interacting NPs.

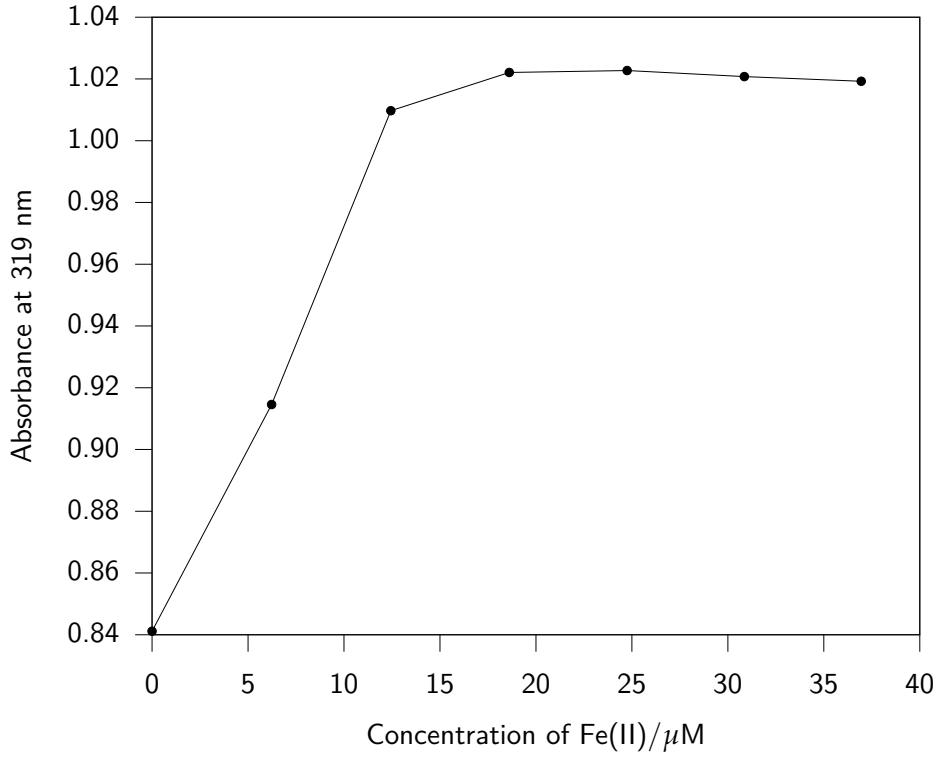

Figure 4.28: Titration curve obtained by reporting the trend of the value of absorbance of the feature at 319 nm pertaining to the $[FE(terpy)_2]^{2+}$ complex as a function of the concentration of Fe(II) ions in solution.

A second place exchange reaction was performed on another aliquot of the same batch involved in the previous experiment. In this case, the experiment was performed on 3 mg of Au NPs protected by dodecanethiolates and all the conditions remained the same except for the molar amount of terpyridine-teriminated thiol, which was ten times lower, corresponding to 40 molar excess of it with respect to Au NPs. Figure 4.29 displays a TEM image of the NPs after the place exchange reaction, whereas the situation before the reaction has been already presented in Figures 4.21 and 4.25.

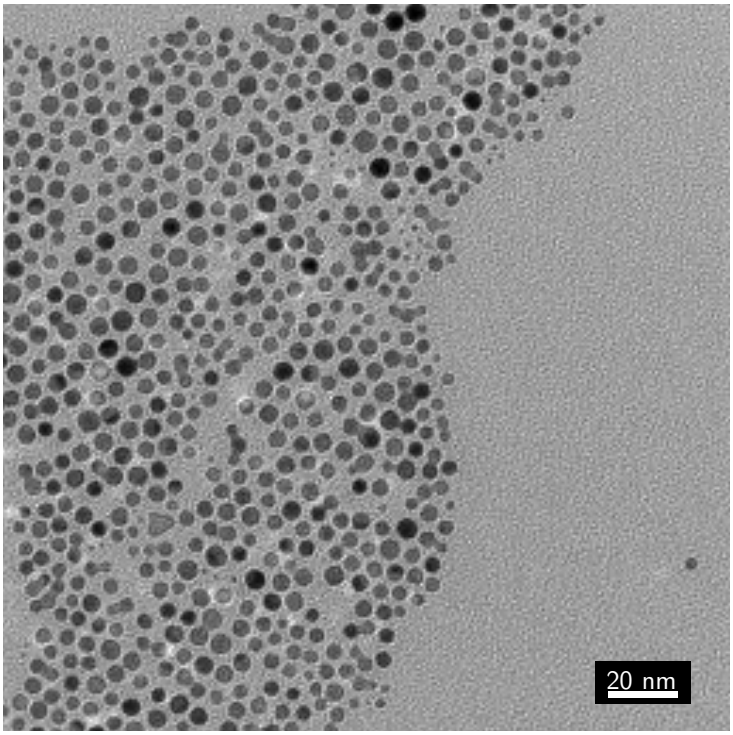

Figure 4.29: TEM image of the batch of functional NPs after the place exchange reaction with a molar ratio between entering ligands and NPs of 40:1, before the addition of Fe(II) ions.

The triggering of the interactions among the so-prepared functional NPs was once again carried out by adding a 15 μL of a $2.5 \cdot 10^{-3}$ M solution of $Fe(BF_4)_2$ dissolved in a 3:1 mixture of chloroform and methanol. The results obtained were analysed at TEM, whose response is resumed in the four images presented in Figure 4.30. This time, the aggregates formed are still randomly organized, lacking of a defined geometry. However, their spatial extension is smaller compared to the aggregates depicted in Figure 4.26. This aspect could be due to a lower degree of substitution of dodecanethiolates by terpyridine-terminating ligands, justified by the lower molar amount of entering ligand employed in the place exchange reaction. Unfortunately, this batch of functional NPs was affected by an intrinsic instability that prevented the study by means of UV-Vis spectroscopy for the estimation of the number of interacting sites for NPs. In fact, the NPs decomposed before running the UV-Vis experiments. Consequently, no further analyses on this batch were possible. However, the TEM outcomes indirectly suggested an uncontrolled functionalization of Au NPs, leading indeed to no ordered superstructures.

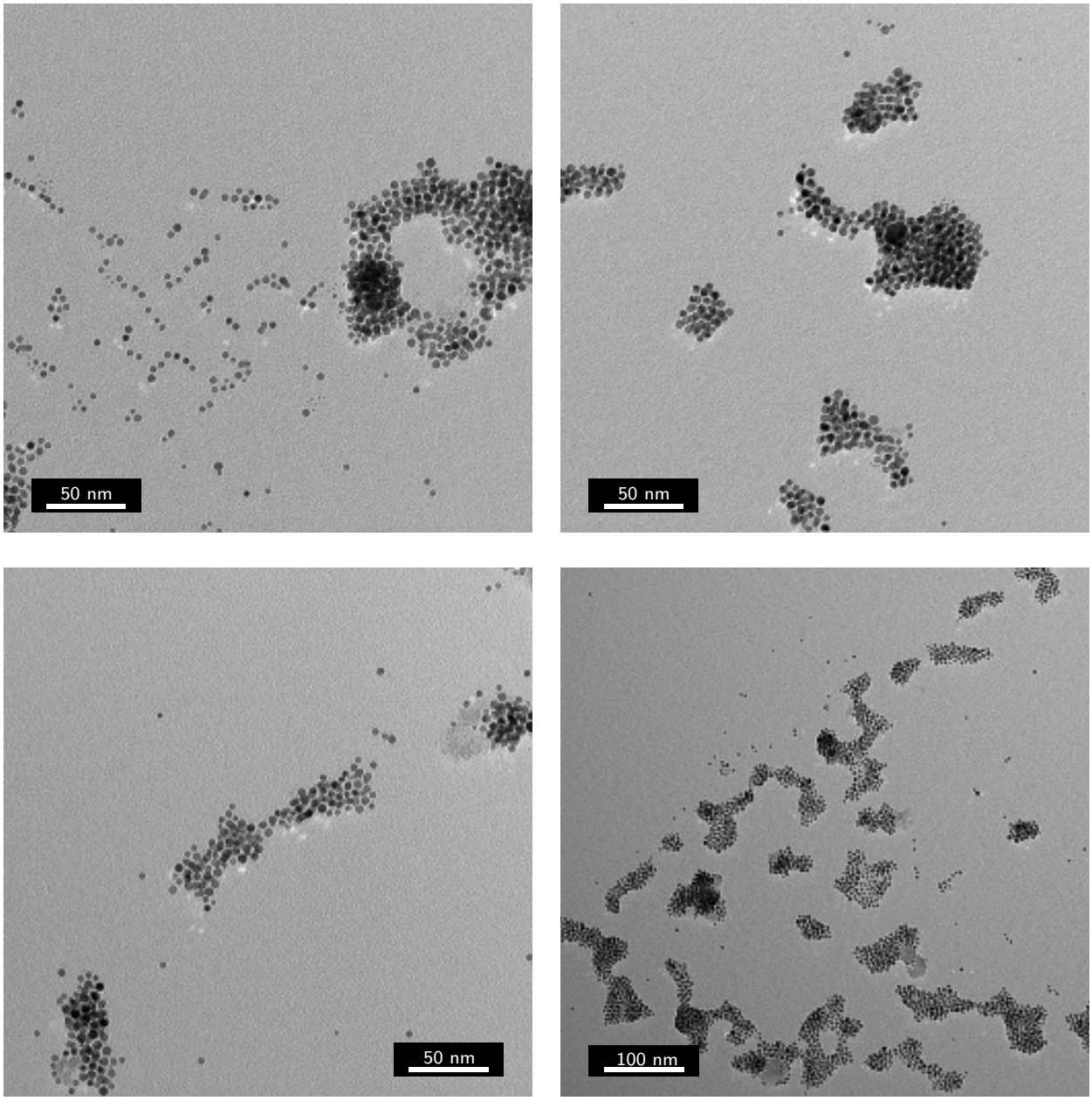

Figure 4.30: TEM images recorded after the addition of $Fe(BF_4)_2$ to the second batch of Au NPs functionalized with teryridine-terminating thiolates.

A third place exchange reaction was then performed lowering once again the molar amount of terpyridine-terminating thiols, employing 4 molar excess of functional ligand with respect to the atoms of gold. This time, the reaction was carried out on 20 mg of Au NPs protected by dodecanethiolates, so that obtaining a consistent amount of functional NPs for NMR analysis. The place exchange reaction was performed on the batch of NPs presented in Figure 4.22, characterized by an average core diameter of 4.5 nm; a representative TEM image is presented in Figure 4.31, beside a TEM image of the batch undergone place exchange reaction.

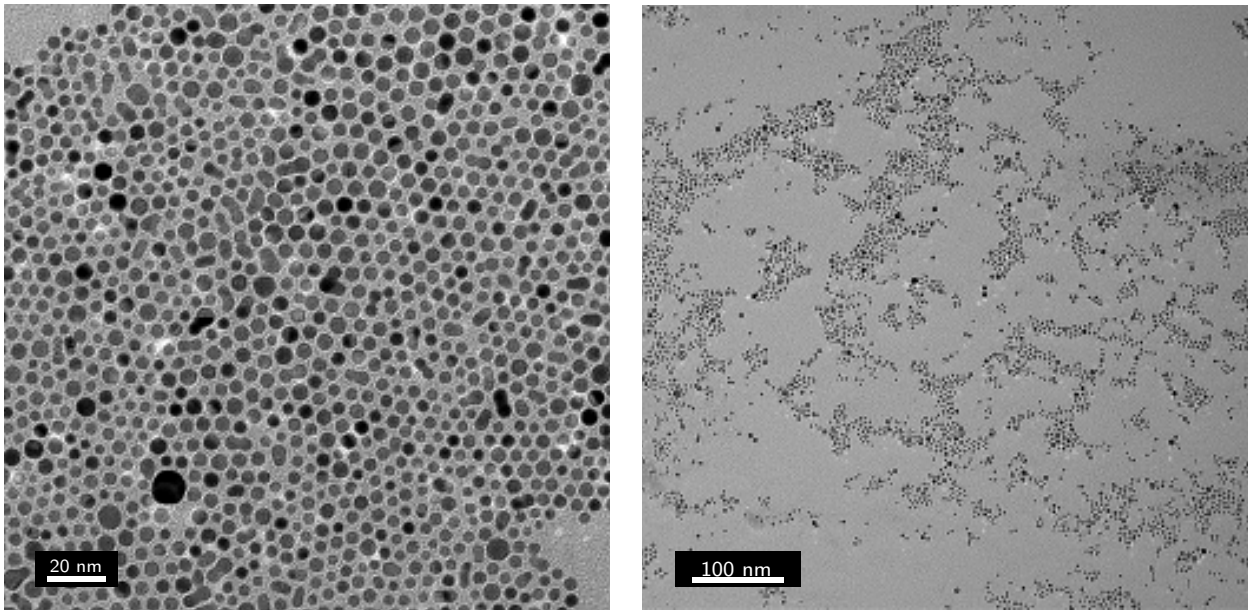

Figure 4.31: On the left, a TEM image of the batch of Au NPs having an average core diameter of 4.5 nm, before the place exchange reaction with terpy-terminating thiol in a concentration four times that of the NPs. On the right, a TEM image of the same batch after the place exchange reaction. No sensible variations in core dimensions are appreciable.

Similarly to the previous cases, a TEM analysis was performed following the same conditions already described concerning the addition of Fe(II) ions. The results from the analysis are displayed in Figure 4.32. These images depict a different situation with respect to the cases seen before. In fact, no large aggregates were observable; instead, the arrangement of the NPs resembles the typical hexagonal packing according to which NPs are used to arrange themselves on a TEM grid. This evidence could be related to the fact that no interactions arose among the NPs due to very low concentration of terpyridine bound to the gold cores; indeed, the risk of working with very low concentrations of terpyridine is the incapability of satisfying the criterion for the formation of the complexes. On the other hand, the absence of chaotic aggregates could be due to the very low degree of substitution of the dodecanethiolates by terpyridine-terminating ligands, giving rise to a situation in which only a part of the NPs of the batch are functionalized. This could be the cause of the presence of those small groups of NPs visible in two of the four TEM images presented in Figure 4.32, where the number of terpyridine units for each NP is limited and therefore the spatial extension of the aggregates formed is rather confined.

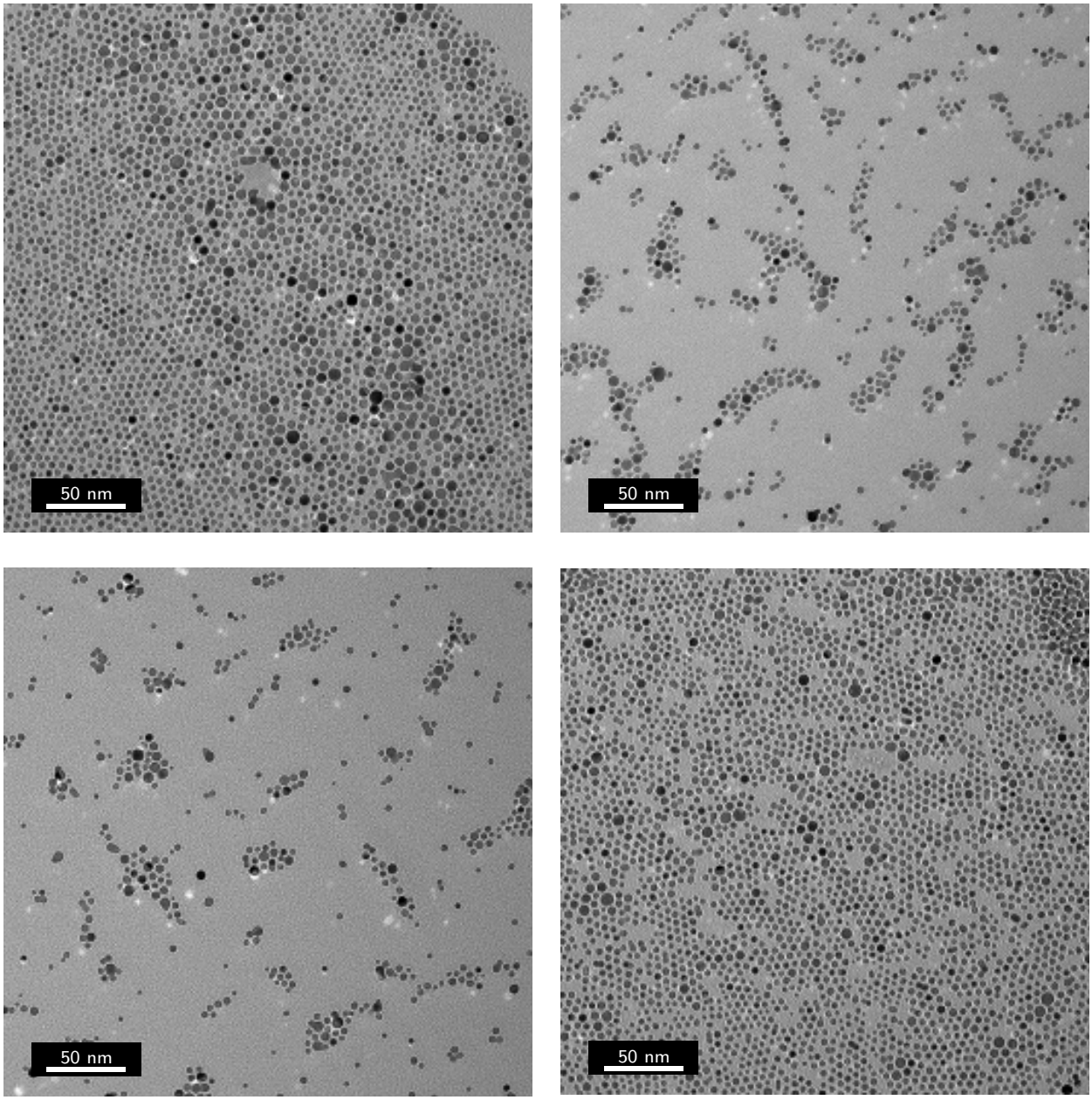

Figure 4.32: TEM images recorded after the addition of $Fe(BF_4)_2$ to the third batch of Au NPs functionalized with teryridine-terminating thiolates.

UV-Visible tests were also performed on the latter batch of functional NPs prepared. Figure 4.33 displays an UV-Vis spectrum recorded on a sample of 1 mL of a 10^{-7} M solution of functional Au NPs in chloroform treated with 15 μL of a $2.5 \cdot 10^{-3}$ M solution of $Fe(BF_4)_2$, which represents a large molar excess of Fe(II) with respect to the terpyridine moles used for the place exchange reaction. Figure 4.34 focuses the attention on the region within 380 and 300 nm, where a characteristic feature of $[Fe(terpy)_2]^{2+}$ should appear, as previously reported. However, despite the large excess of Fe(II) ions with respect to terpyridine molecules, no absorption at 319 nm could be appreciated. The reasons behind this not favourable evidence could be due to the fact that complex did form, however its concentration was so close to the limit of detection of the instrument, which is roughly 10^{-7} M, and consequently it was not possible to detect its presence. The employment of a higher concentrations of Au NPs would have hampered the registration of the

UV-Vis spectra, due to a too high absorption of Au NPs themselves, leading to the saturation of the detector.

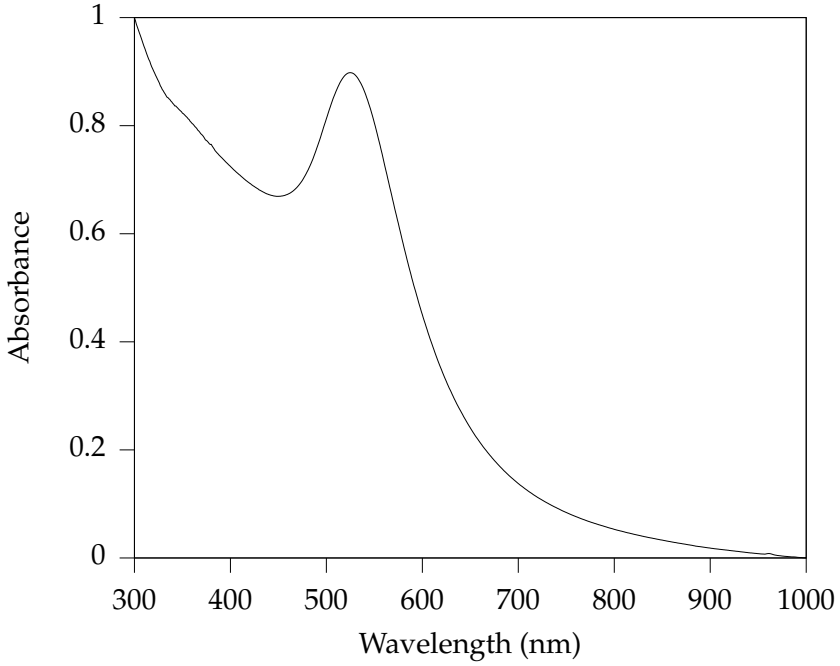

Figure 4.33: UV-Vis spectrum recorded in chloroform of the third batch of functional NPs prepared and treated with a large excess of $Fe(BF_4)_2$.

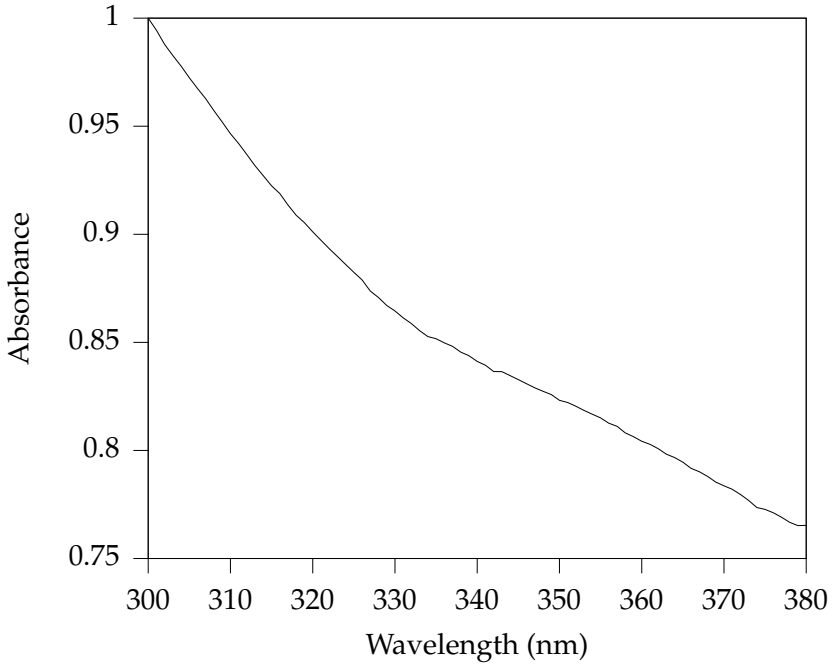

Figure 4.34: Inset of the spectrum reported in Figure 4.33 in the region within 380 and 300 nm. Notice the absence of the feature at 319 nm, characteristic of the $[Fe(terpy)_2]^{2+}$ complex.

The amount of material recovered after the place exchange reaction allowed to conduced a NMR analysis so that gathering more information concerning the amount of terpyridine molecules

effectively bound to the gold cores. Figure 4.35 reports the ^{1}H-NMR spectrum of the functional Au NPs after the place exchange reaction and their purification by means of washings of ethanol, as well as the ^{1}H-NMR spectrum obtained after the decomposition of a 5 mg of the functional NPs with an excess of iodine in chloroform and the ^{1}H-NMR spectrum of the terpyridine-terminating thiol, reported for comparison. No sharp peaks related to leftovers of unbounded thiols can be pointed out in the first spectrum, proving that the washing with ethanol were effective.

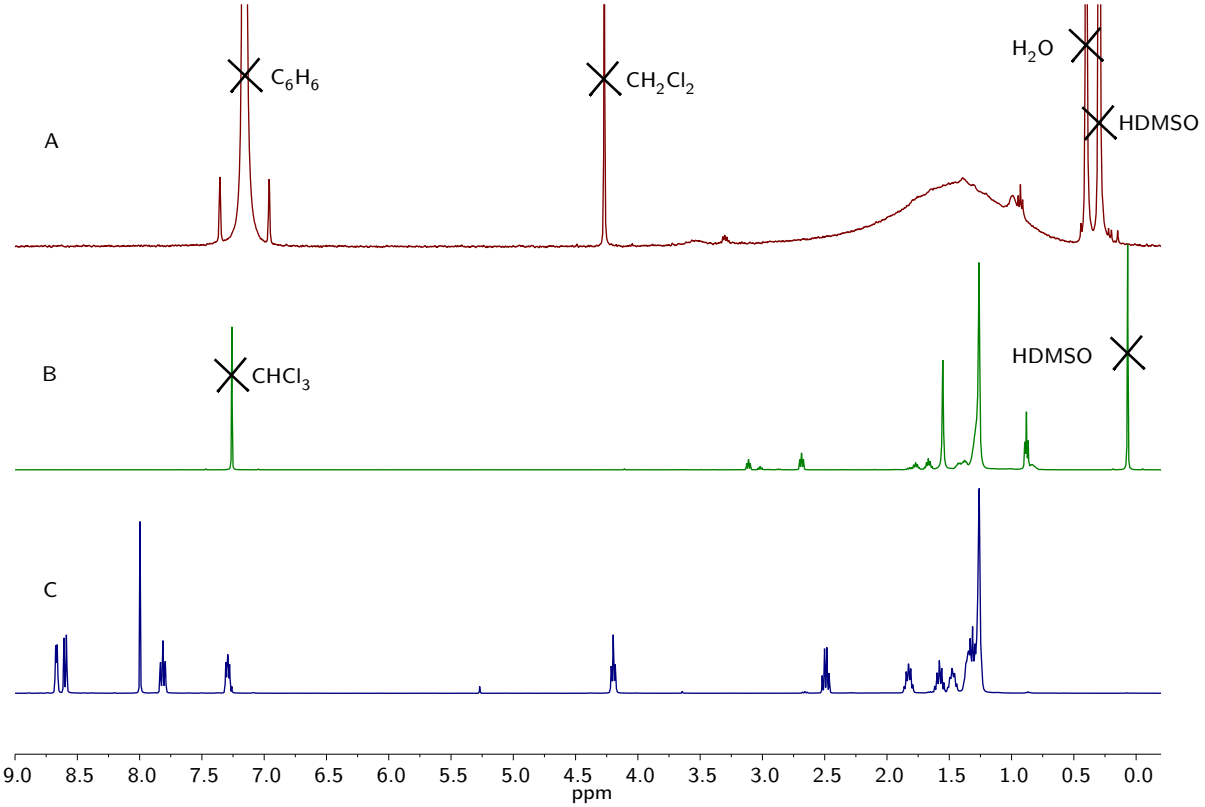

Figure 4.35: **A**: ^{1}H-NMR spectrum (400 MHz, C_6D_6) of the third batch of functional NPs. **B**: ^{1}H-NMR spectrum (500 MHz, $CDCl_3$) of decomposed Au NPs belonging to the third batch. **C**: ^{1}H-NMR spectrum (400 MHz, $CDCl_3$) of terpyridine-terminating thiol, reported for comparison.

The ^{1}H-NMR spectrum of the product of the decomposition of the functional NPs is reported also in Figure 4.36. The values of the integrals of the area of the peaks pertaining to the protons in α position of the disulphides, resonating at 2.7 ppm, and those related to the protons of the aromatic rings of terpyridine, resonating within 8.5 and 7.25 ppm, are presented. By evaluating the ratio of those integrals, previous opportune normalization, it is possible to obtain the percentage amount of the ligands bearing terpyridine units at their ends. It reasonable to think that the protons in α position of the homogeneous disulphides, composed of either two moieties of dodecanethiolate or two moieties both terminating with terpyridine molecules, and those of the heterodisulphide, composed of one moiety of dodecanethiolates and the other bearing a terpyridine unit at its end, resonates at the same frequency, since the ligands are almost identical except for the oxydation state of sulphur. Consequently, the contribution to the signal at 2.7 ppm comes from both dodecanethiolates and thiolates terminating with terpyridine units; the value of the integral of its area represents therefore the totality of the ligands. However, in

order to compare the values of the integrals for knowing the percentage amount of terpyridine-terminating ligands, it is necessary to divide the value of the integral of the peak at 2.7 ppm by 2, since the protons that resonate at such frequency are 4 for each disulphide molecule, whereas only two protons contribute to the value of the integrals of each peak in the aromatic region, visible in Figure 4.37. Therefore, by evaluating the ratio between the integrals it is possible to obtain the percentage amount of the terpyrdine-terminating ligands which is equal to 2 %. For a 4.5 nm Au NPs, the theoretical number of ligands[113] is 407; consequently, terpyrdine-terminating thiolates are 8 for each NP within the batch. Since the concentration of NPs for the UV-Vis analysis was 10^{-7} M, the concentration of terpyridine unitis within the batch is $8 \cdot 10^{-7}$ M. Supposing that all of them react forming the complexes, the concentration of complex is therefore $4 \cdot 10^{-7}$, which is indeed very close to the limit of detection of the technique, despite the high molar extinction coefficient for $[Fe(terpy)_2]^{-2}$ complexes.

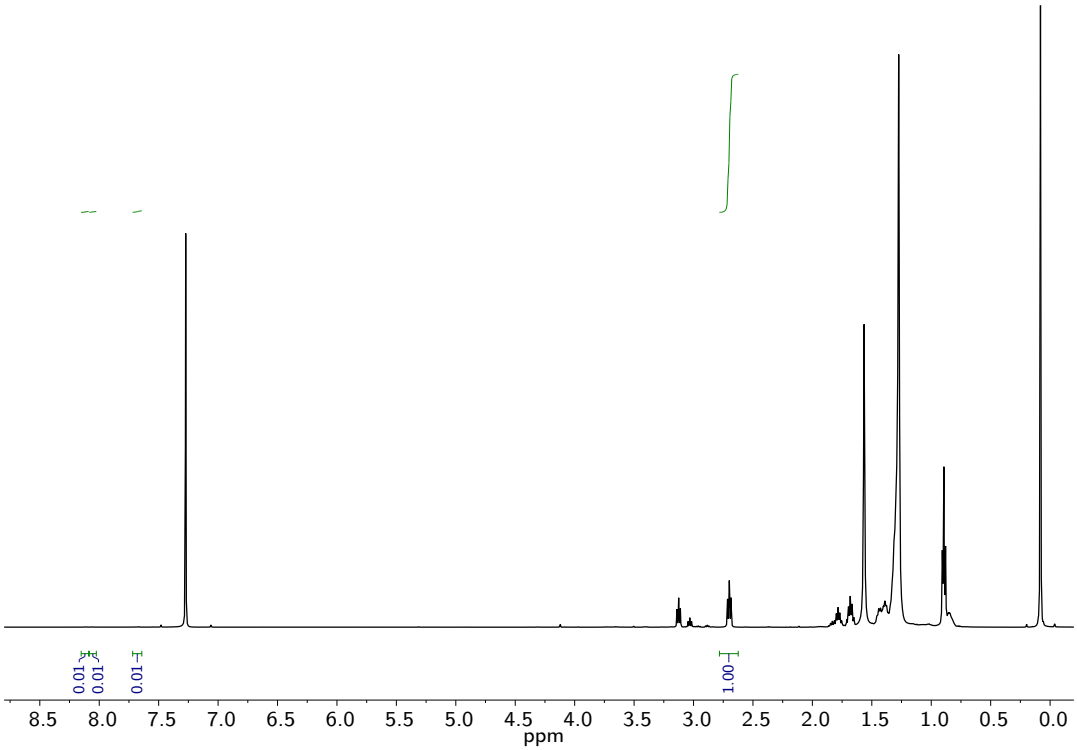

Figure 4.36: ^{1}H-NMR spectrum (500 MHz, $CDCl_3$) of the product of the decomposition of I_2 of the third batch of functional NPs, reporting also the values of the integrals of the area of the peaks pertaining to the protons of disulfides and aromatic protons or terpyridine.

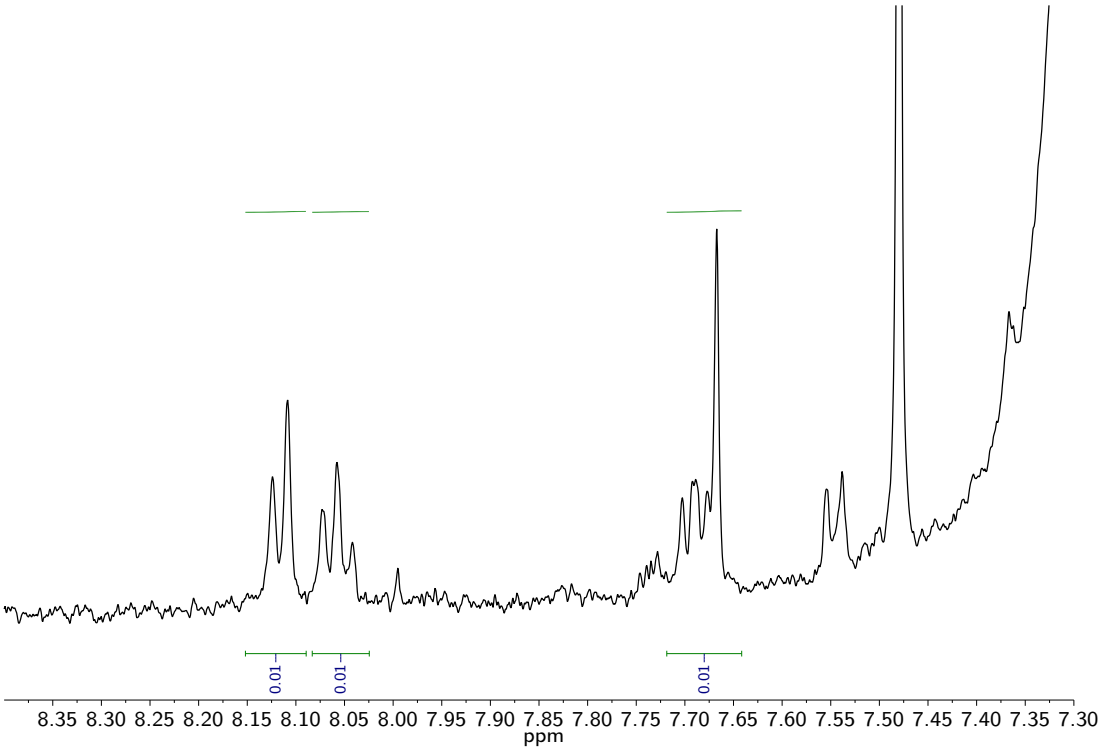

Figure 4.37: Inset of the ^{1}H-NMR spectrum reported in Figure 4.36, focusing on the aromatic region of the spectrum where the protons of the aromatic rings of terpyridine resonate.

CHAPTER 5

Study of interactions among fluorinated NPs in aqueous environment

1 Introduction

The topic of the following chapter concerns the study of the interactions among Au NPs protected by mixtures of fluorinated and hydrogenated ligands. Even though the subject of the study are once again the interactions among Au NPs, the overall approach is indeed different from that presented in the previous chapter. The systems herein analysed are built on fluorophilic interactions, which are spontaneous interactions that arise among fluorinated species, thanks to their hydrophobicity and lipophobicity. The substrate on which the whole study is based is a batch of Au NPs synthesised by Dr. Elena Pellizzoni at the University of Trieste. The NPs are protected by a mixture of hydrogenated thiolates, terminating with a sulfonate group providing them whit solubility in aqueous environments, and alkyl perfluorinated thiolates, i.e. Au NPs protected by a mixed monolayer. The employment of these ligands for synthesising the NPs gave rise to a peculiar organization of the fluorinated ligands on the surface of the gold core. The morphology of the monolayer was investigated by means of Small Angle Neutron Scattering analysis by the group of F. Stellacci and the outcomes of those studies outlined an organization of the fluorinated patches which resembles a tetrahedral arrangement of the patches themselves. Indeed, these evidences are astonishing for the fact that no similar monolayer morphology has ever been reported in literature. Therefore, the experiments discussed in the chapter were meant to confirm the peculiar organization of the fluorinated domains within the monolayer. The aim was pursued not through a direct visualization of the spatial arrangement of the ligands, since that would have been challenging and not easily feasible with the available techniques, but with an indirect one: probing the fluorinated patches making them interact with other NPs so that producing superstructures that would then have been analysed with Transmission Electron Microscopy as well as cryo-Transmission Electron Microscopy. The process of self-assembly was therefore once again exploited and studied during the work of this thesis. However, the environment where the interactions leading to the spontaneous formation of the superstructures took place was an aqueous media. The complexity of the overall system

is given by the simultaneous forces that compete together, such as the already cited fluorophilic interactions that should be the main contribute to the arising of the superstructures, hydrophobic interactions that could lead to the folding of the fluorinated ligands in order to reduce their contact with the water molecules and finally, the electrostatic repulsion that involves the NPs protected with mercaptododecanesulfonate, bringing them to repel one another and therefore facilitate the interactions with the probing NPs.
After having addressed the interest on the object of the study for a brief explanation of its chemical composition and the interesting outcomes from its study with SANS, the chapter presents the systems exploited as probing agents for the fluorinated patches. Both are batches of NPs of reduce dimensions carrying fluorinated domains or fluorinated tails able to interact with the counterparts on the monolayer of the NPs with bigger dimensions. Finally, the first experiments presented are the one performed on cryo-TEM in aqueous solution, followed by those carried out on a High Resolution TEM, where the NPs were dropcasted on a carbon-coated copper grid.

2 Object of the study

A simple representation of the NPs probed during the experiments discussed in the chapter is reported in Figure 5.1.

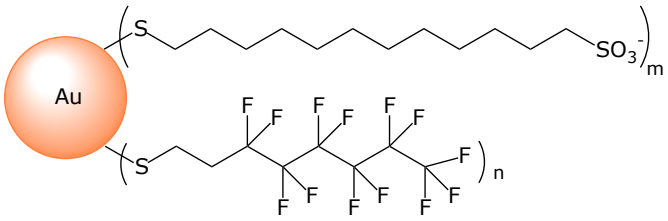

Figure 5.1: Drawing of the batch of MM Au NPs protected by MDDS and F6.

As displayed in the figure, the two kinds of thiolates that protect the gold cores are mercaptododecanesulfonate (MDDS) and 3,3,4,4,5,5,6,6,7,7,8,8,8-tridecafluoro-1-octanethiolate(F6). The first one provides the NPs with solubility in water whereas the latter was employed in the synthesis for giving phase-segregation within the monolayer itself, producing a certain morphology compatible with biological studies on cellular uptake of MM NPs. The NPs were therefore prepared by direct synthesis with the procedure[86] reported by Zheng *et al.*, widely discussed in the previous chapter and reported in detail in Chapter III. The gold precursor was mixed with a blend of MDDS and F6 ligands in a 1.5 to 1 molar ratio. The results of the synthesis is depicted in the TEM image presented in Figure 5.2, together with the histogram displaying size distribution. The TEM analysis of the batch allowed estimating an average core diameter of 3.6 nm, with a standard deviation of 0.6 nm, resulting in a variation coefficient of 0.17. The ^{1}H-NMR spectrum of the purified batch is displayed in Figure 5.3, whereas the decomposition of the NPs performed by adding an excess of iodine in chloroform is depicted in Figure 5.4. For the outcomes of the decomposition and the integration of the area pertaining to the disulphides arisen from the oxidation of the thiolates by iodine, the ratio between the two types of ligands composing the monolayer is MDDS:F6 = 2:1. As a matter of fact, since this batch of

NPs was prepared through the procedure published by the group of G.D. Stucky, the overall composition of the monolayer includes leftovers of triphenylphosphine-related species, as discussed in Chapter 4. The presence of these adventitious contaminants can be pointed out by referring to the ^{1}H-NMR spectrum reported in Figure 5.3: indeed, in the low-field region of the spectrum where aromatic protons of triphenyphosphine resonate, a broad band is clearly visible, ascribable to the presence of residual triphenylphosphine-related species within the monolayer. Their presence is also highlighted by the sharp peaks visible in the same region of the ^{1}H-NMR spectrum of Figure 5.4, after decomposition of the NPs with iodine. Their amount is considerably high and it is comparable with the amount of MDDS ligands. From the evaluation of the integrals of the area of the peaks pertaining to the different species coating the gold core, it was possible to obtained the overall ratio, which is MDDS:F6:$PPPh_3$ = 2:2:1. It is reasonable to think that the presence of the triphenylphosphine affected the arrangement of the rest of the other two types of ligands on the gold surface. This aspect was studied with SANS technique,[123,124] focusing on the spatial organization of the fluorinated ligands with respect to the others. The results of these analyses outlined the grouping of the fluorinated species into four patches directed towards the vertex of a tetrahedron. Indeed, the reconstruction of the data obtained by means of SANS displays a spatial organization of the patches that reminds a tetrahedral organization. The 3D image obtained from the process of image reconstruction is depicted in Figure 5.6. The figure actually reports the presence of the fluorinated ligands as blue spots: from the different views, it is possible to better appreciate the arrangement of the fluorinated patches on the gold surface.

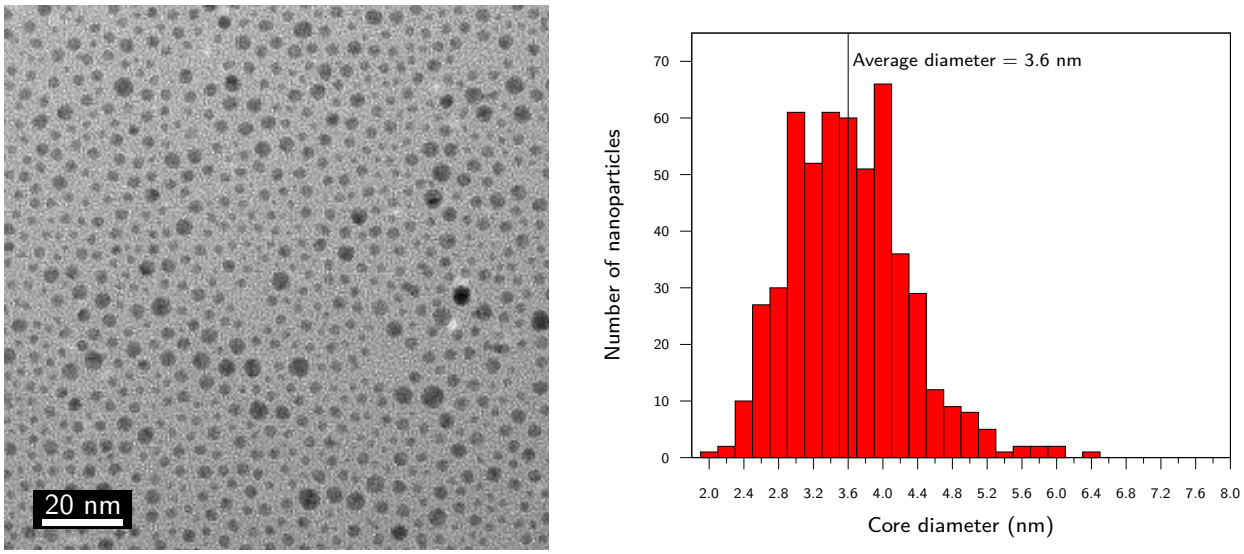

Figure 5.2: On the left, TEM image of the batch of MM Au NPs protected by MDDS and F6 ligands. On the right, histogram displaying size distribution, obtained after the analysis of core sizes over 500 NPs.

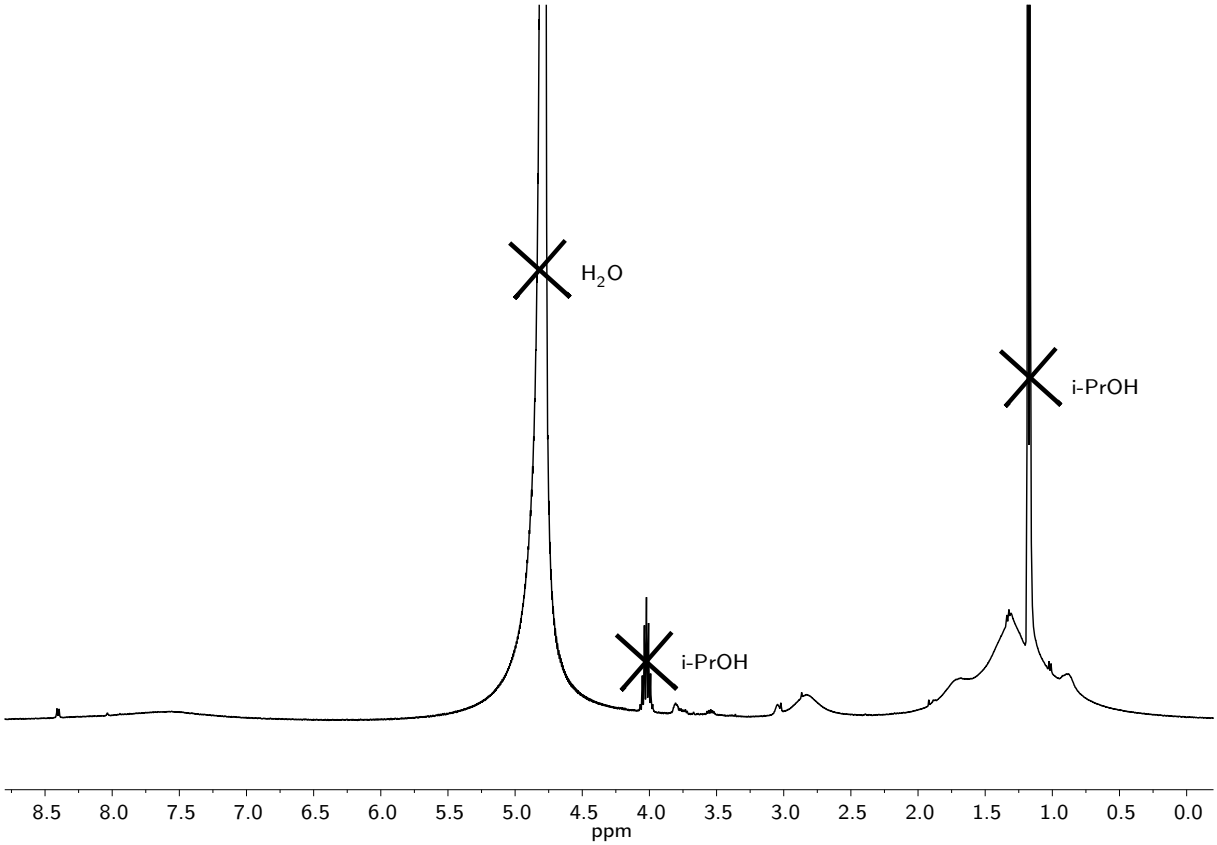

Figure 5.3: ^{1}H-NMR spectrum (400 MHz, D_2O) of the batch of MM Au NPs protected by MDDS and F6. The presence of i-PrOH peaks is due to the fact that the solvent was used to favour the dispersion of the NPs in water.

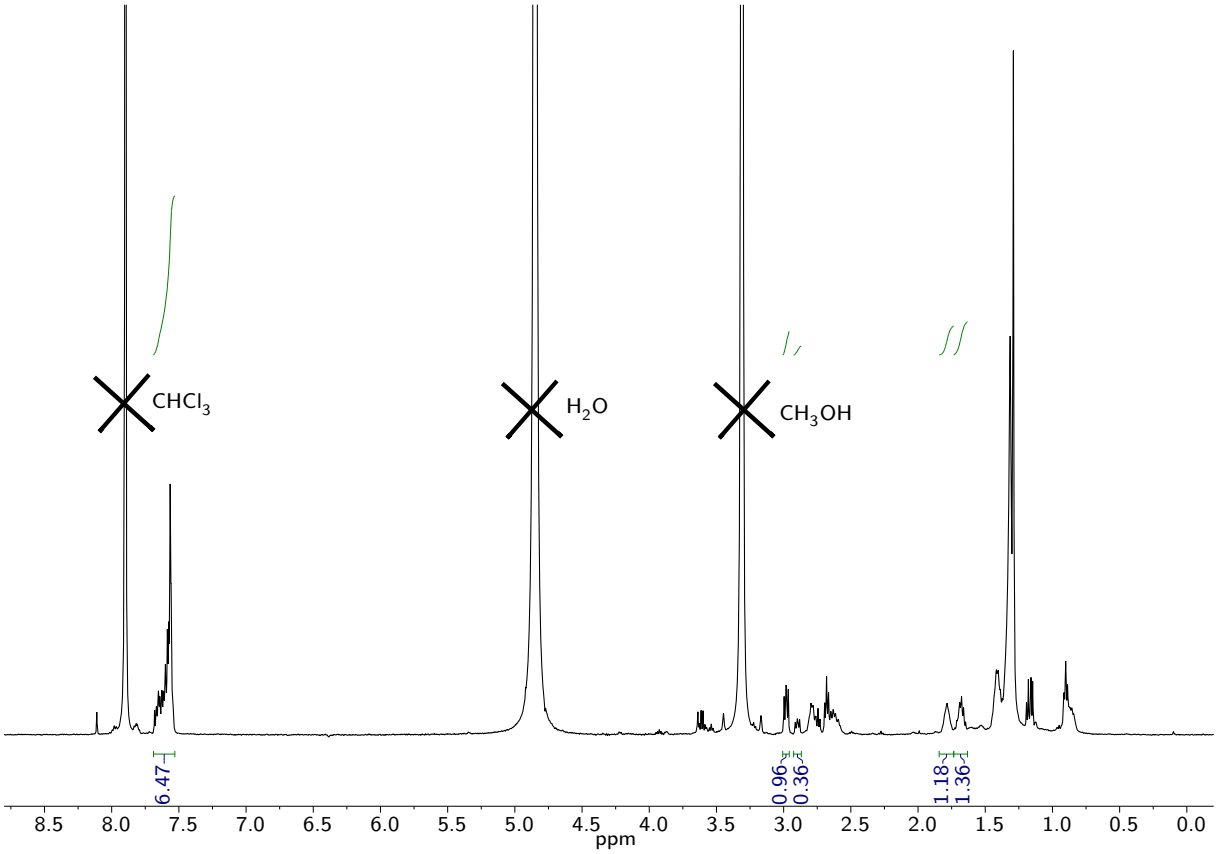

Figure 5.4: ^{1}H-NMR spectrum (400 MHz, CD_3OD) of the product from the decomposition with iodine of a small amount of MM Au NPs protected by MDDS and F6. The integrations refer to the protons in α and β positions with respect to the sulphur atom of the disulphides, as well as the protons of PPh_3.

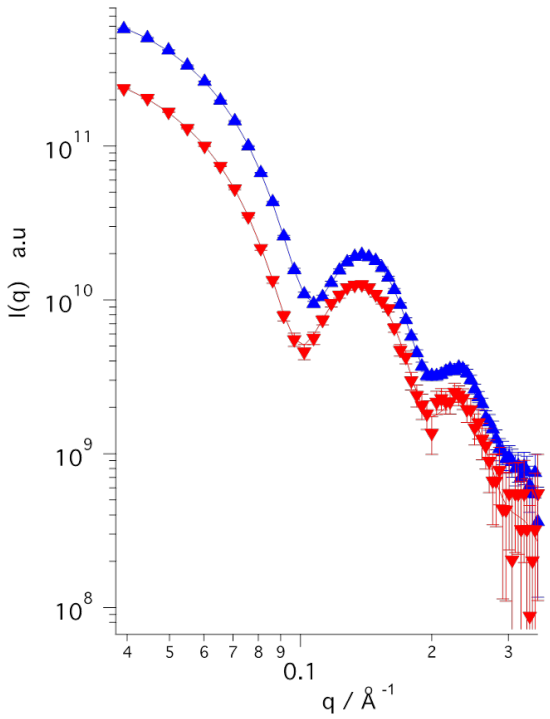

Figure 5.5: Results obtained by means of SANS technique on the batch of MM Au NPs protected by MDDS and F6 ligands.

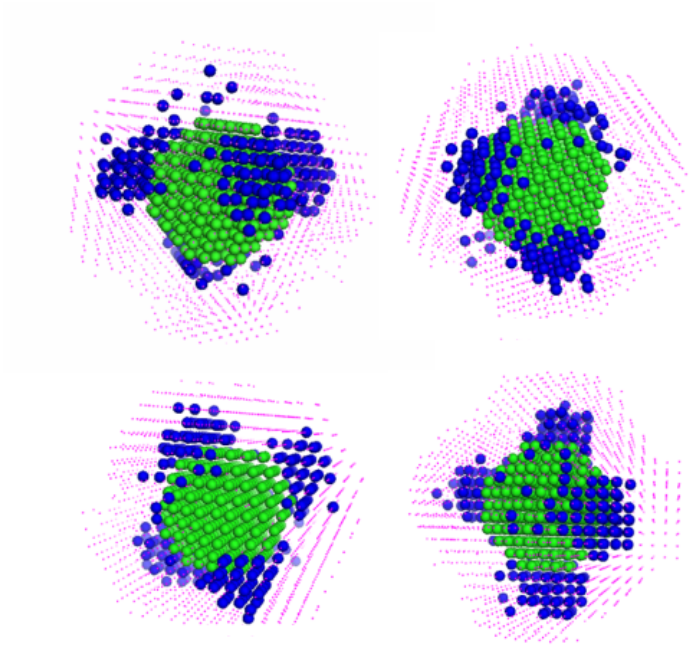

Figure 5.6: Different views of the 3D reconstruction of the SANS data reported in Figure 2.13. The green dots refer to gold atoms belonging to the core, whereas blue dots indicate the position of the fluorinated species bound to the gold surface.

As previously mentioned, the crossed self-assembly of these NPs with probing NPs was exploited in experiments carried out on cryo-TEM and HR-TEM, aiming at highlighting the arrangement of the fluorinated patches which in principle should have direct the spatial organization of the NPs acting as probing agents. The following section describes the types of Au NPs employed for the process of self-assembly and the techniques applied to study the resulting systems.

3 Self-assembly experiments on MM Au NPs with ordered fluorinated domains

The leading idea for the all the analyses presented in this section was to form tetrahedral superstructures, based on mutual fluorophilic interactions, spontaneously arising in aqueous media. The overall process is schematically represented in Figure 5.7.

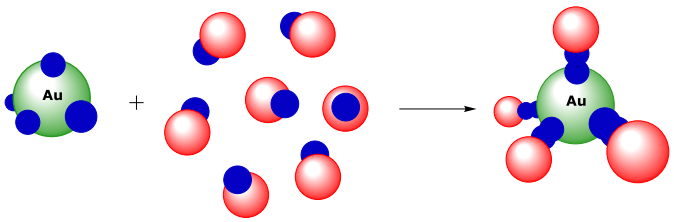

Figure 5.7: Sketch of the process of self-assembly among MM Au NPs driven by fluorophilic interactions. The blue portions are used to identify the fluorinated domains responsible for the interactions.

The formation of the superstructures is then based on the process of self-assembly between two different kinds of NPs: those composing the cores of the superstructures and depicted

in green in the figure, are the NPs studied with SANS and presented in the previous section; instead, the NPs that should interact with the previous ones and arrange themselves so that pointing towards the vertexes of the tetrahedron are the ones prepared accordingly to fulfil the prerequisite of possessing an adequate mixed monolayer, which could allow the arising of the superstructures thanks to fluorophilic interactions.

3.1 Probing NPs used for cryo-TEM analyses

For the cryo-TEM studies, the type of NPs employed were MM Au NPs protected by N−1−{2 −[2 −(2 −Methoxyethoxy)ethoxy]ethyl}−8−sulfanyloctanamide (C8TEG) and F6 thiolates. Figure 7.9 displays a graphical representation of the NPs. These Au NPs have been initially prepared following the procedure[133] reported by Pengo *et al.*: this procedure allowed to obtain NPs whose average core dimensions were 1.5 nm, with a standard deviation of 0.3, resulting in a variation coefficient of 0.2. Figure 5.9 displays a TEM image representative of the batch, together with the histogram achieved from the TEM analysis, outlining the size distribution. The monolayer of these latter NPs was composed of C8TEG thiolates which provided the NPs with high solubility in a wide range of solvents.[133] The fluorinated ligands were subsequently introduced in the monolayer by place exchange reaction with the F6 ligand; the experimental details for the preparation of these MM Au NPs are reported in Chapter III.

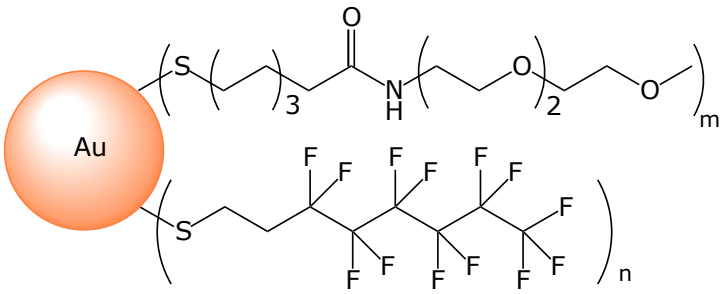

Figure 5.8: Drawing of the NPs protected by C8TEG and F6 ligands.

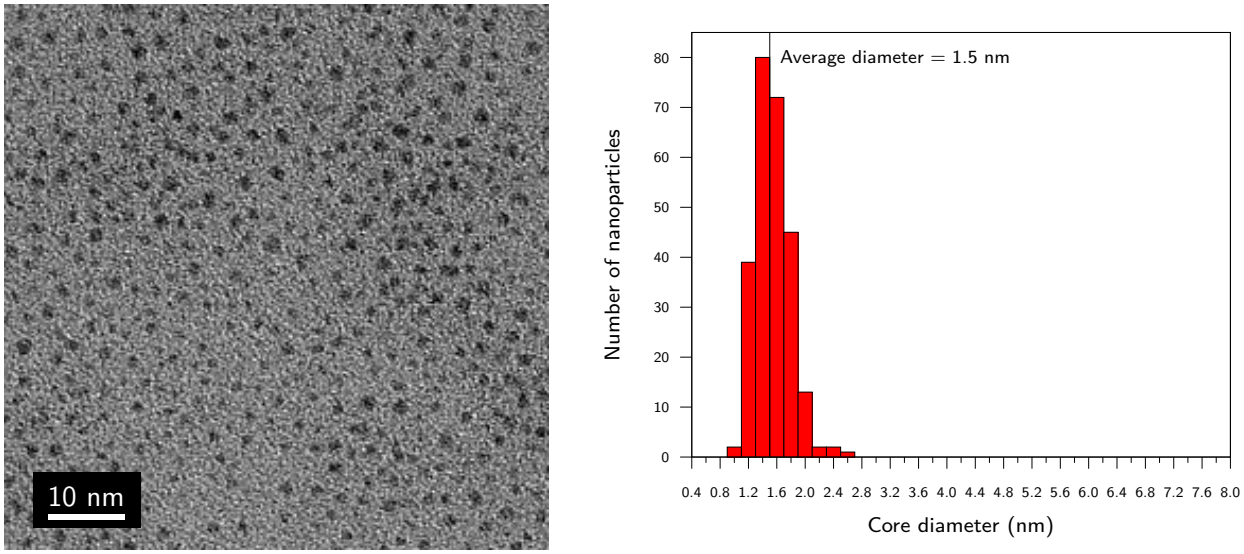

Figure 5.9: On the left, TEM image of the batch of MM Au NPs protected by C8TEG and F6 ligands. On the right, histogram displaying size distribution, obtained after the analysis of core sizes over 250 NPs.

After the insertion of the fluorinated ligands, the NPs nearly totally lost their solubility in common organic solvents. The only solvent that provided a positive test was pure trifluoroethanol or mixed with dichloromethane in a 1/4 ratio or higher. This mixture was then used for all the analyses that required their dissolution. This solubility behaviour is compatible with the insertion of a consistent number of fluorinated ligands inside the monolayer of the NPs. Indeed, this is also proved by the NMR experiments carried out on the batch to verify the absence of unbound thiols and to estimate the overall composition of the monolayer. Figure 5.10 reports the ^{1}H-NMR of the NPs after the purifications procedure: no intense sharp peaks could be outlined, therefore the batch did not contain considerable amount of unbound thiols. Figures 5.11 and 5.12 display respectively the ^{1}H-NMR and the ^{19}F-NMR spectra of the product from the decomposition of 3 mg of these MM Au NPs with a solution of iodine in chloroform. Three different types of disulphides can be produced from the decomposition of Au-C8TEG/F6: the homo TEGC8S-SC8TEG, the homo F6S-SF6 and the hetero TEGC8S-SF6. Unfortunately, the signals pertaining to methylene groups in α position with respect of the sulphur atom of these species are relatively close one another, making the attribution and the integration quite hard. However, it is possible to estimate the ratio between the two types of ligands by directly integrating the area of the peaks pertaining to the methylene groups in α position of the fluorinated portion of homo F6S-SF6 and hetero disulphides and those of the hydrogenated portion belonging to homo TEGC8S-SC8TEG and hetero disulphides. Therefore, by evaluating the ratio between the values of the integrals, it is possible to obtain the ratio between the two types of thiolates forming the monolayer. The ratio is C8TEG:F6 = 1.8:1, which corresponds to a relative amount of 64 % C8TEG thiolates and 36 % of F6 thiolates.
The ^{19}F-NMR spectrum of Figure 5.12, recorded on the product from the decomposition of this MM NPs, displays six signals related to the five CF_2 groups and the CF_3 terminal group of F6 ligands, proving their presence within the monolayer.

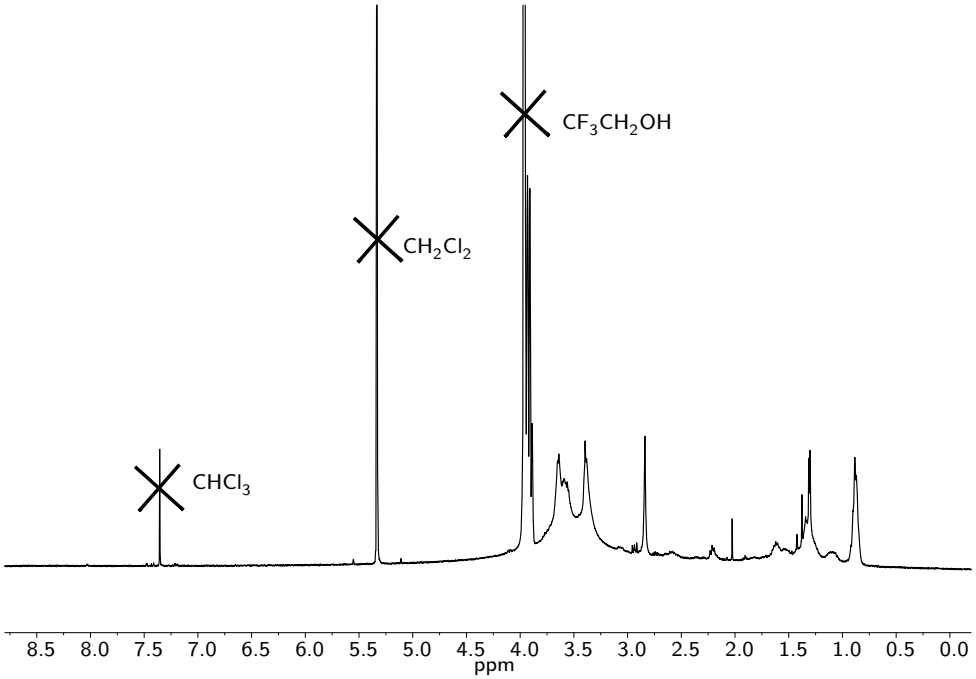

Figure 5.10: ^{1}H-NMR spectrum (400 MHz, CD_2Cl_2/CF_3CD_2OD = 4/1) of the batch of MM Au NPs protected by C8TEG and F6. The absence of sharp peaks proved the effectiveness of the purification procedure.

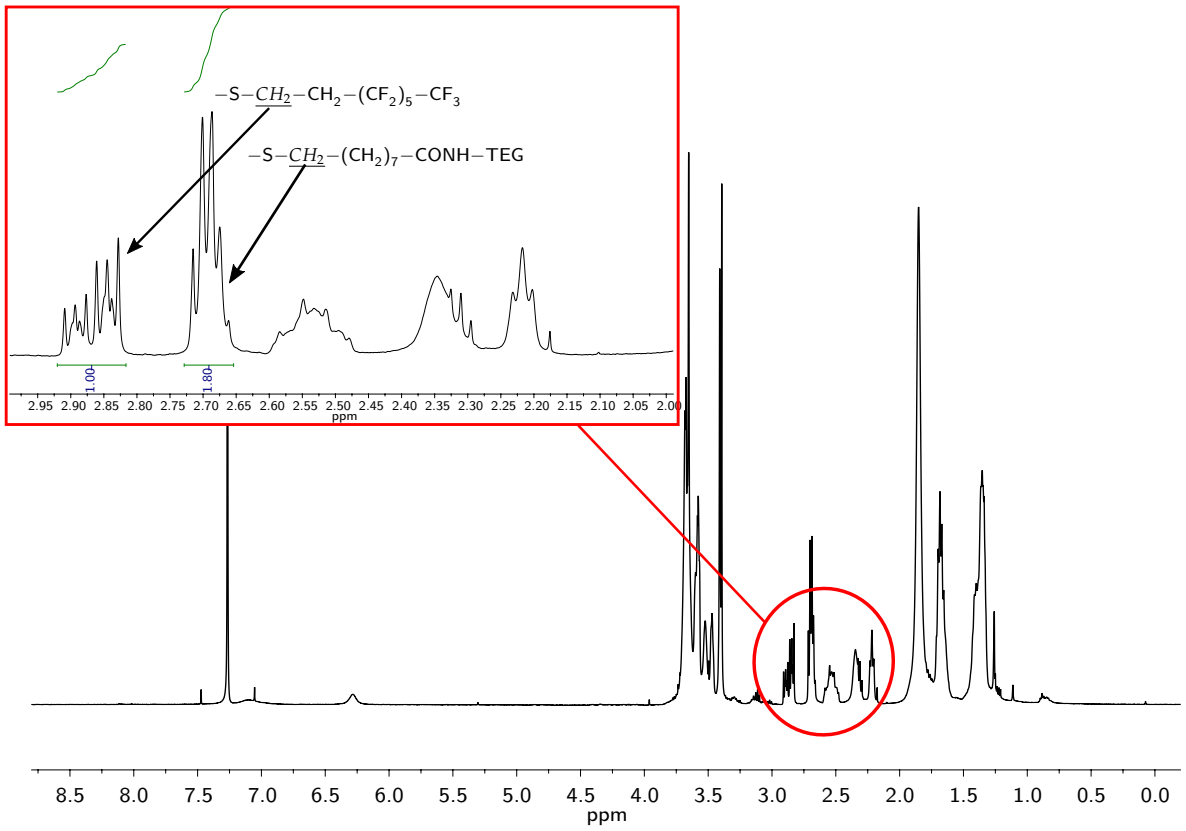

Figure 5.11: ^{1}H-NMR spectrum (400 MHz, CD_2Cl_2/CF_3CD_2OD = 4/1) of the product of the decomposition of a reduced amount of MM Au NPs protected by C8TEG and F6. In the inset, the peaks pertaining to the protons in α position with respect to the sulphur atom in the molecules of disulphide.

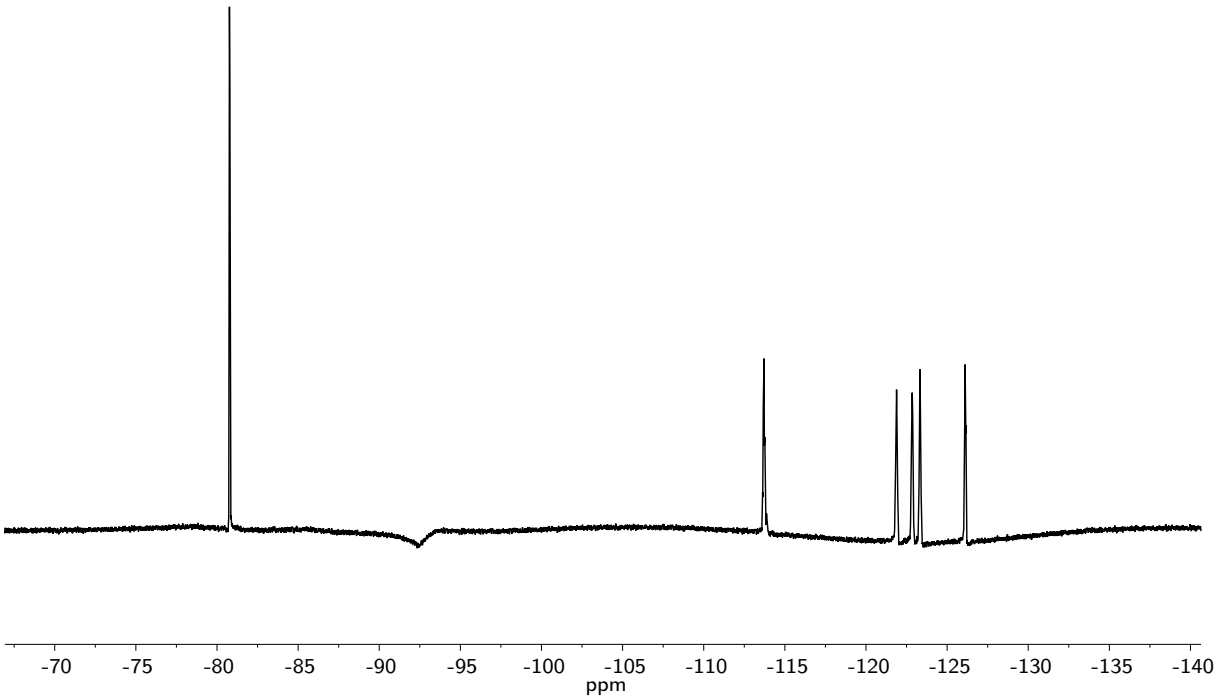

Figure 5.12: ^{19}F-NMR spectrum (470 MHz, CD_2Cl_2/CF_3CD_2OD = 4/1) of the product of the decomposition of a reduced amount of MM Au NPs protected by C8TEG and F6.

Figure 5.13 reports the UV-Vis spectrum of the NPs recorded in a mixture of CH_2Cl_2/CF_3CH_2OH = 4/1. From the spectrum, only a shoulder at 393 nm is visible. No surface plasmon band was noticeable consistent with the average size determined by TEM analysis.

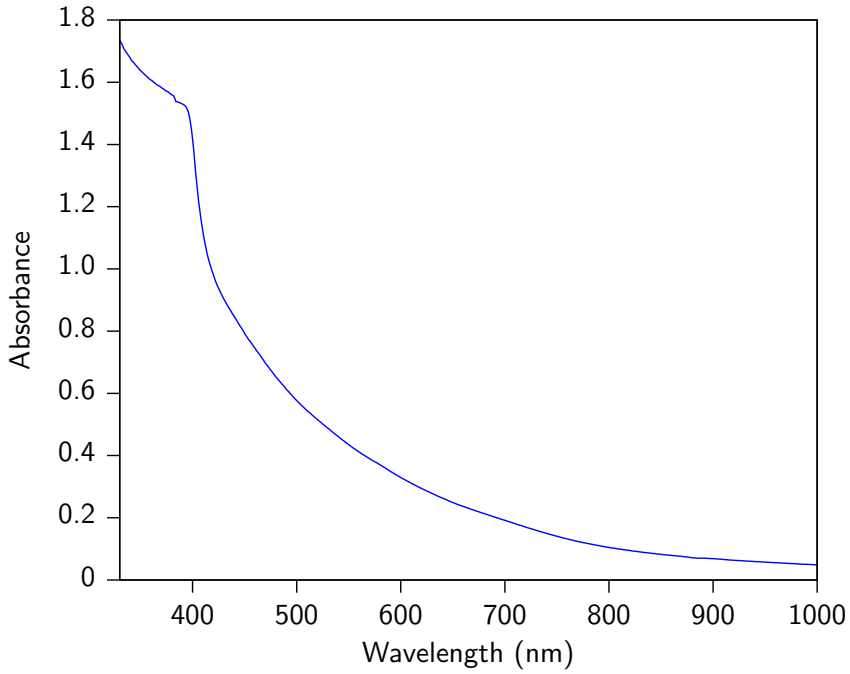

Figure 5.13: UV-Vis spectrum of the batch of MM Au NPs protected by C8TEG and F6.

Eventually, Figure 5.14 displays the outcome from a Thermogravimetric Analysis on 1.83 mg of MM NPs protected by C8TEG and F6. It can be clearly seen from the graph that the total

percent loss ascribable to the detachment of the thiols from the gold surface is 49.45 %. By considering that the theoretical average composition[113] for NPs of 1.5 nm is $Au_{116}(SR)_{53}$. Consequently, the theoretical percent amount of organic ligands can be estimated by taking into account this latter composition, the percent amount of fluorinated thiol, being 36 % as established through ^{1}H-NMR analysis, and the amount of sample analysed; therefore, the theoretical percent amount of both ligands is 45 %, which is not too far from the result achieved through TGA. Assuming the same considerations concerning the composition of the NPs, the percent weight of gold is 57 %; even though the sum of both percentages provides a result of 102 %, this little discrepancy from 100 % can be due to the error associated to the integration of the ^{1}H-NMR spectrum, leading to a percentage of fluorinated ligands into the monolayer slightly higher than the effective.

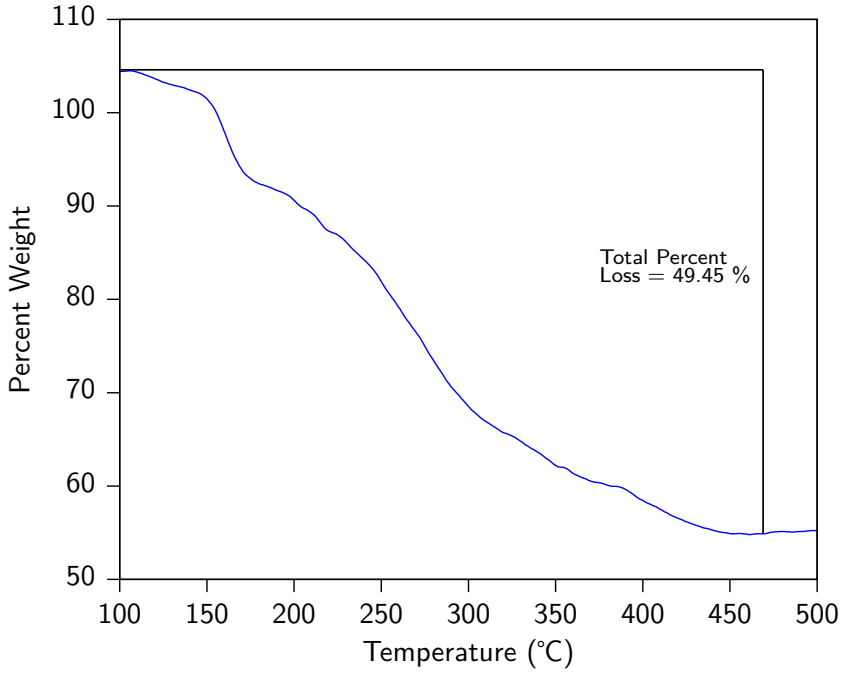

Figure 5.14: Thermogravimetric Analysis on 1.83 mg of MM Au NPs protected by C8TEG and F6 performed in air.

The outcomes from the analyses performed on this batch of NP-C8TEG/F6 related to the average core dimensions and the amount of fluorinated ligands within the monolayer, together with the considerations[59] reported in literature concerning the morphology of the monolayer of NPs with similar average dimensions and protected by blends of ligands able to self-segregate on the surface of gold, suggested that the described NPs possessed a sufficiently large domain composed of F6 ligand that should be able to interact with the patches of the NP-MDDS/F6. Therefore, the 1.5 nm MM Au NPs were firstly exploited for the cryo-TEM analyses of the outcomes from the self-assembly tests.

3.2 General considerations on cryo-TEM

Cryo-TEM was the first technique employed for the studies on the spontaneous self-assembly of MM Au NPs in water, thanks to the fact that this technique allows to gain an insight of interactions that occur in solution among NPs. Cryo-TEM is therefore a powerful technique whose usefulness spread over several fields of science. The first employments of cryo-TEM concerned structural reconstruction of biomolecules, aided by the possibility of acquiring the images at different orientations by tilting the samples, so that obtaining high-resolution three-dimensional views by reconstructing the two-dimensional images. In recent years, cryo-TEM has been exploited for many other different duties, including the study of interactions among NPs and cellular membranes and among NPs themselves as well.
As previously stated, cryo-TEM can be used to investigate the interactions among NPs arising in solution.[134] It is worth highlighting that the visualization of the outcomes from the self-assembly process employing electron microscopy is undoubtedly challenging and it could mislead to wrong conclusions, due to the artefacts that are related to a critical step during sample preparation. Indeed, the preparation of the samples for analyses performed on a conventional transmission electron microscope involves their deposition on a grid, usually coated with carbon. In the case of NPs, these latter species are dissolved and then the so-obtained solution is dropcasted on the grid and the solvent left evaporating. During the process of evaporation, the NPs could be moved on the grid, driven by removal of the solvent and brought close one another; the mutual proximity, induced by removal of the solvent, could be misinterpreted as pristine interactions. To overcome this issue, the involving of cryo-TEM could help to avoid any kind of similar artefacts due to solvent evaporation. Indeed, by trapping the NPs in frozen solution, the proximity of the NPs one to the others is a consequence of genuine interactions. Therefore, the formation of superstructures with precise hierarchical order is a consequence of interaction sites placed in specific points of the monolayer, which possesses a definite morphology. Moreover, by acquiring images at different orientations it is also possible to establish whether the NPs interact among different planes, forming complexes superstructures, *e.g.* diamond lattice.
Nevertheless, cryo-TEM requires careful sample preparation[135] and handling. Indeed, when dealing with Au NPs, the common carbon copper grids must be discharged prior to preparing the samples, so that avoiding sticking of Au NPs on the grids for electrostatic interaction, leading to a nearly impossible visualization of the NPs themselves because of the coverage of several layers of ice. Furthermore, no solvents but water can be used and the prepared grid must be kept and analysed in liquid nitrogen. This latter aspect is crucial in order to maintain the layer of amorphous ice formed during sample preparation. Indeed, amorphous ice is produced when water is very rapidly frozen, so that not giving the time to water molecules to arrange in long-range ordered lattices, typical of crystalline ice. This particular form of ice is needed because it allows the transmission of electrons; otherwise, electrons are diffracted by common crystal ice and no image is observed. The fast freezing is achieved by immersing the grid bearing the sample in liquid ethane, made condensate in a circular section of a dewar surrounded by liquid nitrogen. The use of liquid ethane is justified by the fact that its boiling temperature is higher than the temperature at which the liquid nitrogen is inside the dewar.

Therefore, the rapid plunging of the grid inside liquid ethane does not involve sudden boiling of it, preventing from the disrupt of the forming amorphous ice. The sample preparation is moreover affected by the temperature of the room in which the sample is prepared, the atmospheric pressure and the degree of humidity in the surrounding ambient, as a higher degree makes the formation of amorphous ice harder to occur. Furthermore, the analyses with cryo-TEM need a well acquired know-how and rapidity in imaging the samples: usually the focus region is close to the imaging region but the two are not the same, in order avoid melting of ice due to the electron beam. This latter is also the reason why the imaging must be carried out rapidly, otherwise the ice would start melting.

3.3 Imaging of self-assembly experiments with cryo-TEM

Figures from 5.15 to 5.18 display four cryo-TEM images recorded on a sample prepared for testing the self-assembly of 3.6 nm MM Au NPs presented in Section 2 with the 1.5 nm MM Au NPs, specifically synthesised for the purpose. The solution for studies at cryo-TEM was prepared by mixing 90 μL of a 1 mg/mL solution of NP-MDDS/F6 in water with 10 μL of a 4 mg/mL solution of 1.5 nm NP-C7TEG/F6 in trifluoroethanol. The overall mixture was sonicated for 20 minutes at 35 °C and then the most of trifluoroethanol was stripped away with an Ar flux. The carbon-coated copper grid was discharged prior to sample preparation and the latter was carried out with a Cryoplunge system.
At first look to the images, no ordered superstructures can be pointed out. Large aggregates of NP-C8TEG/F6 are noticeable, evidencing a certain preference of these NPs to segregate, without properly interacting with the NP-MDDS/F6. Indeed, these latter NPs are rarely surrounded by the small NPs, which form some sort of cloudy aggregates of different extensions. This behaviour could be partially due to residual trifluoroethanol that was not totally removed from the solution before sample preparation. The process of sonication therefore produced emulsions in the aqueous solution which included the NP-C8TEG/F6. Since these latter NPs are not soluble in pure water, the presence of residual trifluoroethanol implied a preferential dissolution of these species into the emulsion of the -C8TEG/F6 fluorinated solvent. Consequently, the permanence of NPs in the aqueous environment was apparently null, involving no interactions with the larger NPs. For this reason, the overall approach was shifted towards the employment of probing NPs not only soluble in fluorinated solvents, so that avoiding phenomena of preferential solvation that could biased the process of self-assembly based on fluorophilic interactions.
Interestingly, NP-MDDS/F6 tend to form aggregates of reduced spatial extension, despite the electrostatic repulsion due to the negatively charged SO_3^- groups. Undoubtedly, the forces responsible of the assembly are the fluorinated domains on the monolayer of these NPs. However, no information concerning the orientation of the domains can be gathered from the observation of these aggregates, whose spatial organization is hardly intelligible from the cryo-TEM images collected.

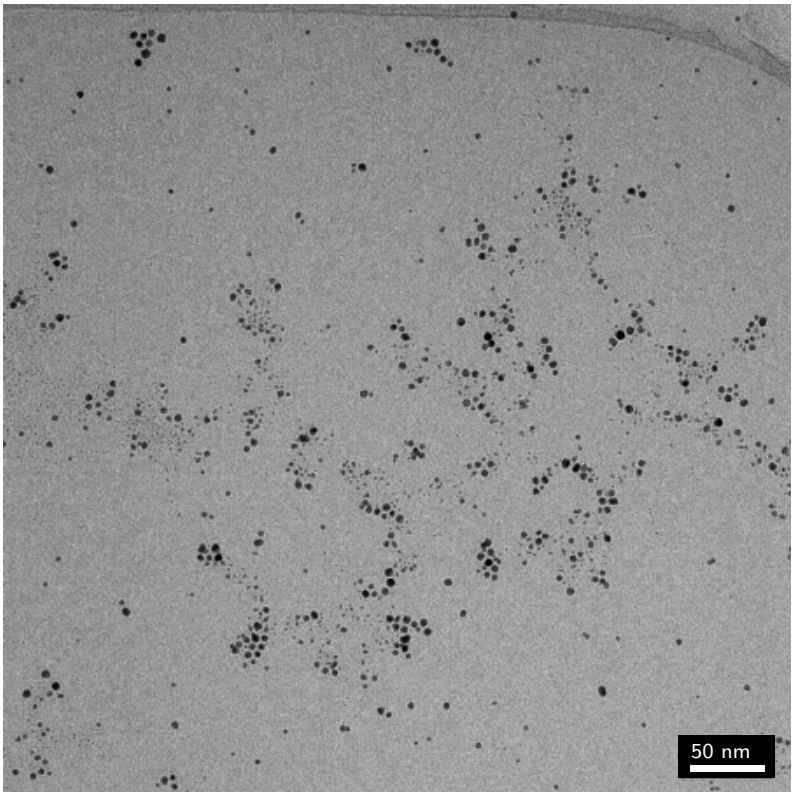

Figure 5.15: Cryo-TEM image of test for self-assembly of NP-MDDS/F6 with NP-C8TEG/F6.

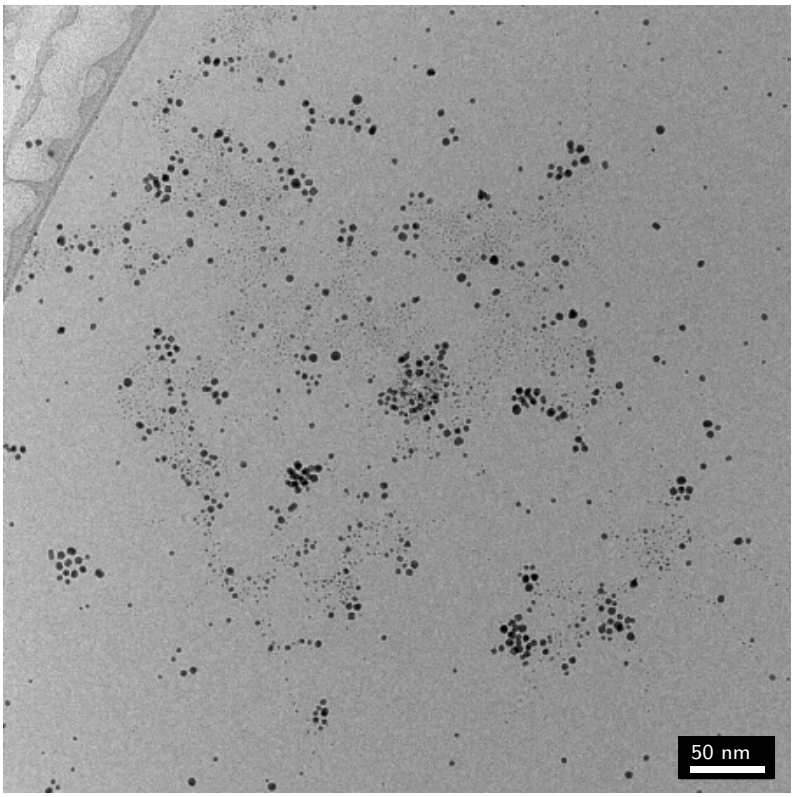

Figure 5.16: Cryo-TEM image of test for self-assembly of NP-MDDS/F6 with NP-C8TEG/F6.

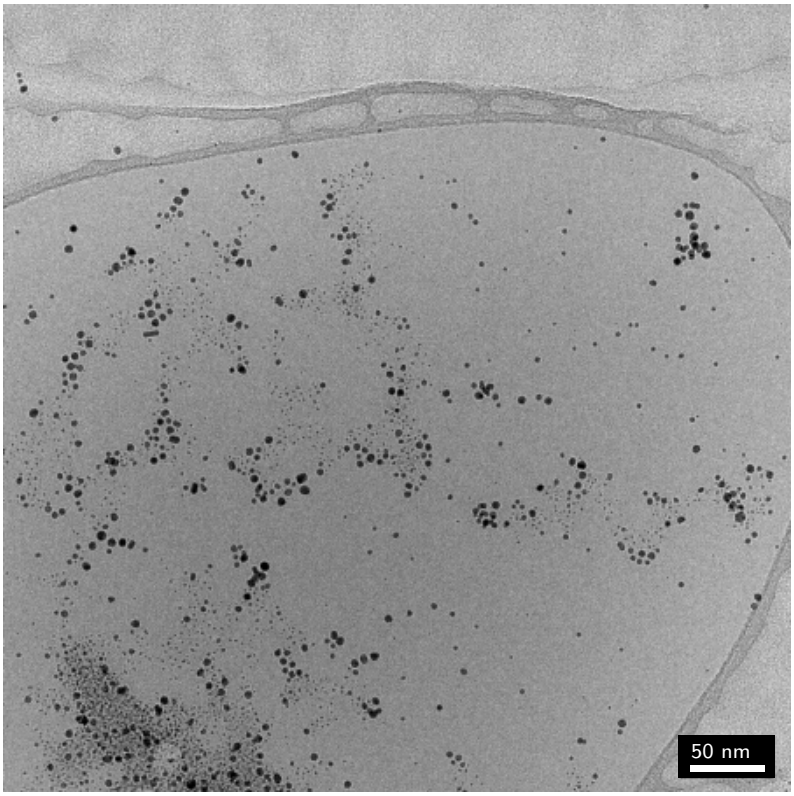

Figure 5.17: Cryo-TEM image of test for self-assembly of NP-MDDS/F6 with NP-C8TEG/F6.

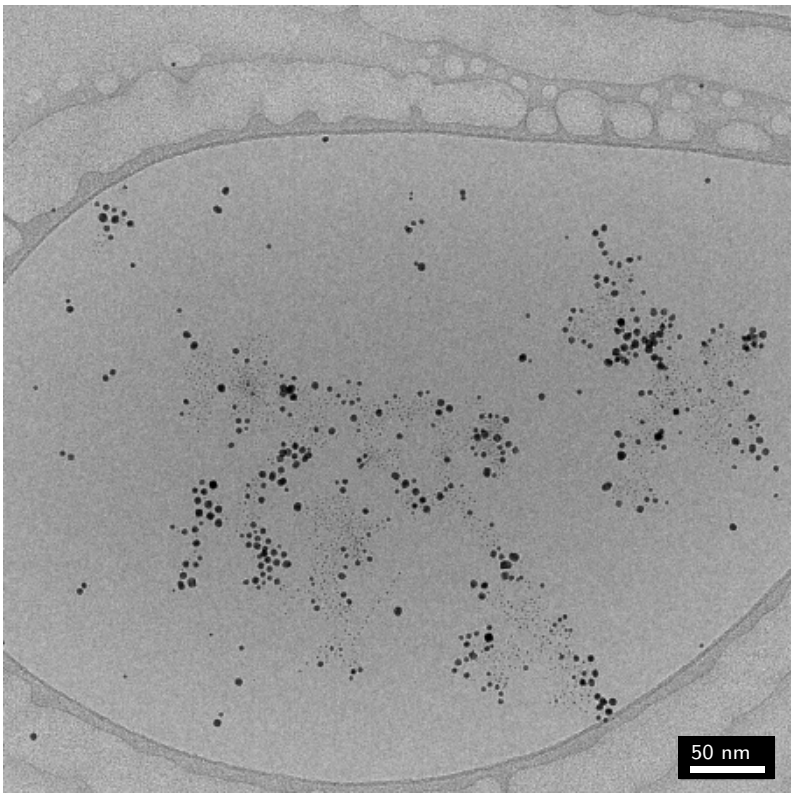

Figure 5.18: Cryo-TEM image of test for self-assembly of NP-MDDS/F6 with NP-C8TEG/F6.

4 HR-TEM Analysis

4.1 Probing NPs used for HR-TEM analyses

The batch employed for High-Resolution TEM studies involved Au NPs whose monolayer was mainly composed of C8TEG ligands. In this case, the sites of interaction were not large fluorinated domains, in order to improve the solubility in water; instead, few longer ligands bearing a fluorinated tail were the points of connection between these latter NPs and the ones exhibiting tetrahedral organization of the fluorinated domains. Figure 5.19 displays a representation of the NPs bearing the fluorinated tails.

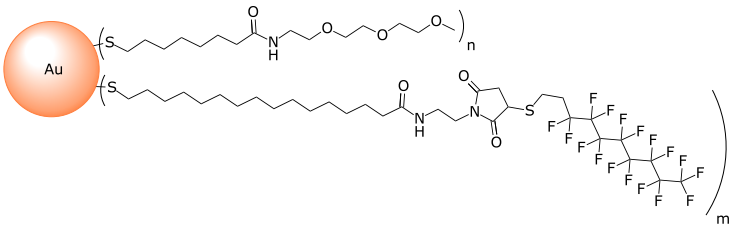

Figure 5.19: Drawing of the NPs protected by C8TEG, bearing few fluorinated tails.

The NPs were prepared by Dr. Paolo Pengo at the University of Trieste by taking advantage of place exchange reaction for introducing the fluorinated tails within the monolayer of Au NPs protected by C8TEG thiolates. The conditions employed in the place exchange reaction were so to insert a reduced number of fluorinated tails. A detailed description of the procedures followed for both the synthesis of the fluorinated tail and the preparation of MM Au NPs bearing the fluorinated tails themselves is reported in the Experimental Details part. Figure 5.20 displays the TEM analysis of the NPs bearing few fluorinated tails, together with the histogram outlining the distribution of the sizes. The outcome from the analysis evidenced an average core diameter of 2.0 nm, with a standard deviation of 0.3 nm, resulting in a variation coefficient of 0.15.

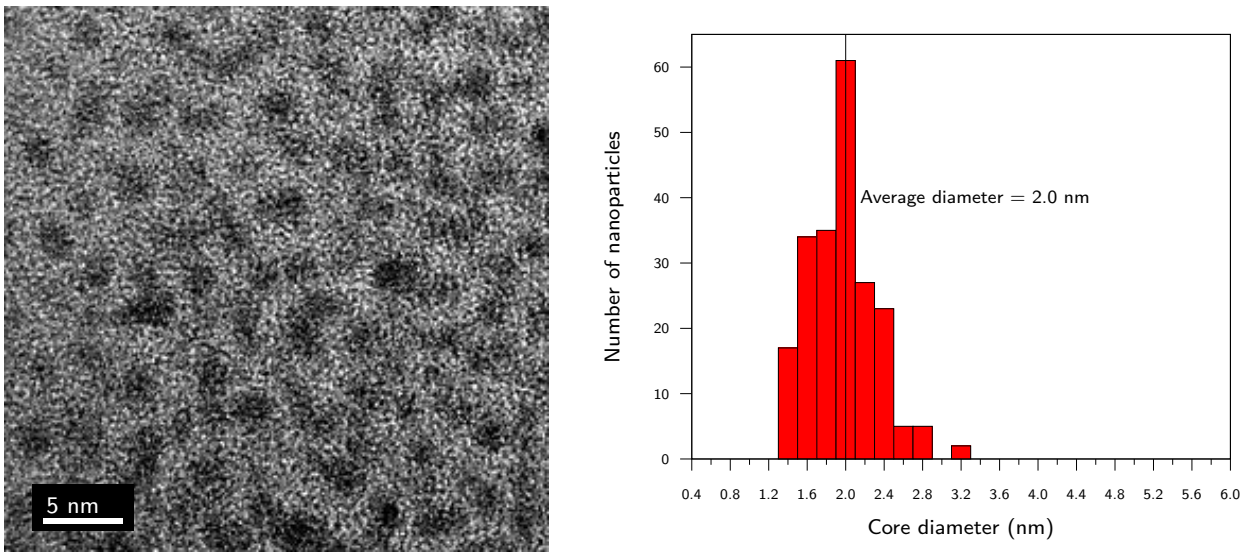

Figure 5.20: On the left, TEM image of the batch of Au NPs protected by C8TEG thiolates bearing few fluorinated tails. On the right, histogram displaying size distribution, obtained after the analysis of core sizes over 250 NPs.

In order to estimate the number of fluorinated tails per each NP composing the batch, a small amount of Au NPs was decomposed by means of iodine. The resulting mixture containing the disulphides, produced by the oxidation of the thiolates, was then analysed through ^{1}H-NMR spectroscopy and the resulting spectrum is reported in Figure 5.21. The inset in Figure 5.22 focuses on the peaks related to protons in α position with respect to sulphur atom belonging to fluorinated and hydrogenated disulphides. By calculating the ratio between the values of the integrals of the areas underneath the peaks, it is possible to obtain the relative amount of fluorinated tails with respect to the total amount of ligands, which is indeed 3.5 %.Consequently, considering the theoretical composition[113] for NPs possessing an average core diameter of 2.0 nm, corresponding to $Au_{223}(SR)_{73}$, the average number of fluorinated ligands per NP is 3, resulting in an average composition of $Au_{223}(C_8TEG)_{70}(tails)_3$.

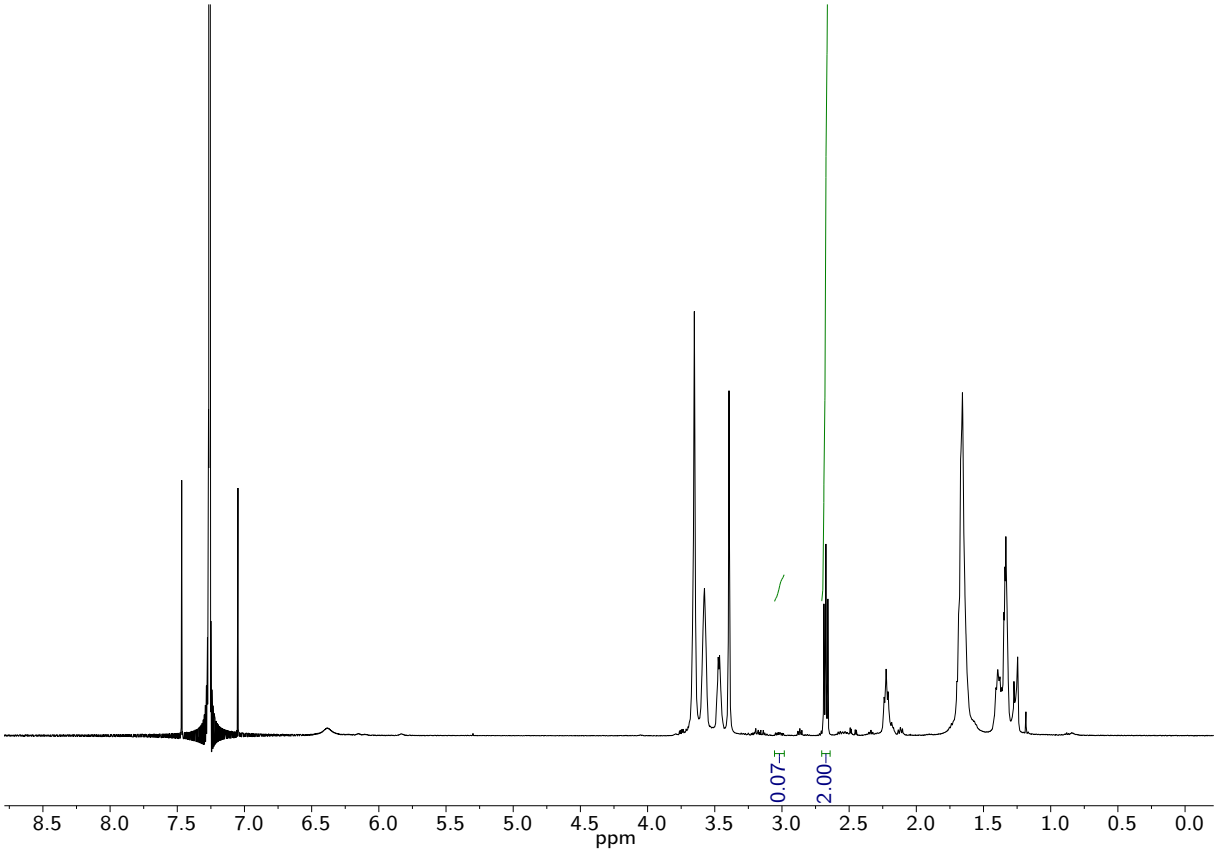

Figure 5.21: ^{1}H-NMR spectrum (500 MHz, $CDCl_3$) of the product of the decomposition of a reduced amount of Au NPs bearing few fluorinated tails.

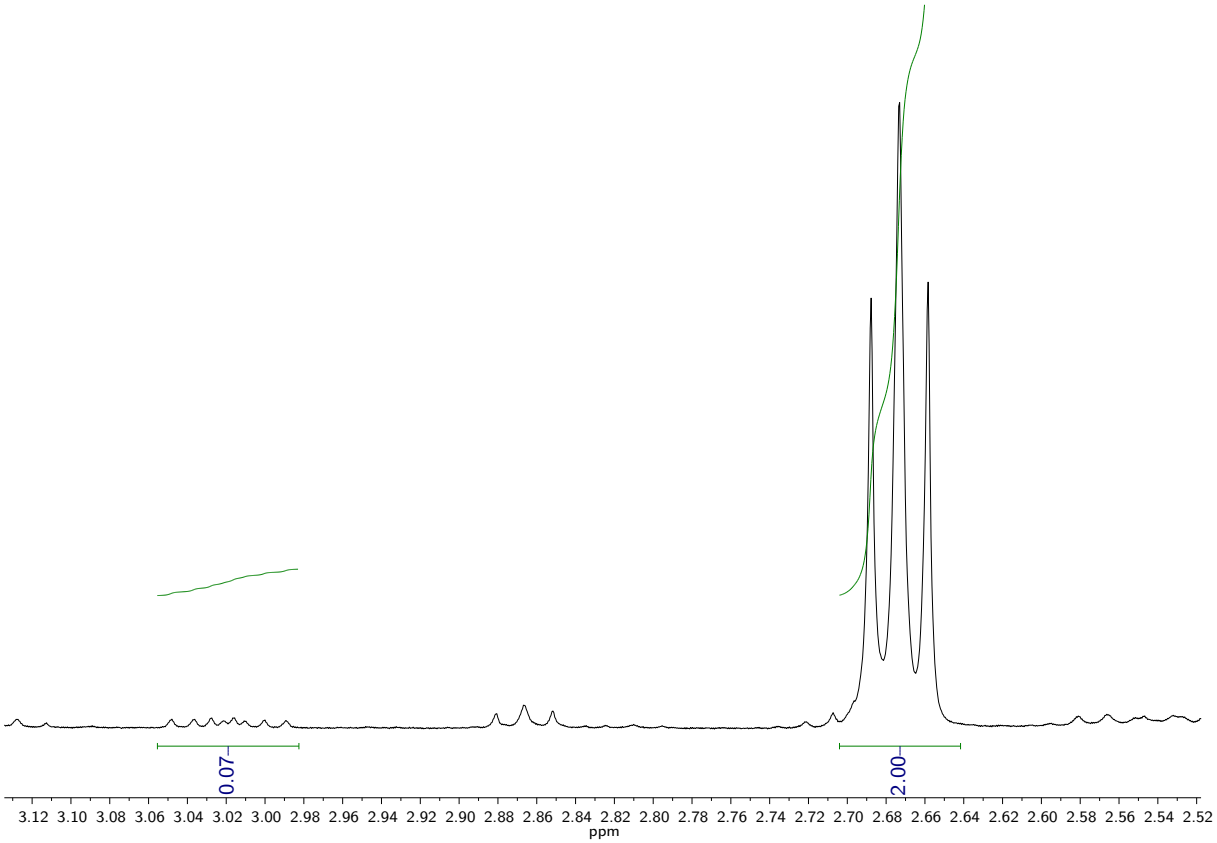

Figure 5.22: Inset of the ^{1}H-NMR spectrum reported in Figure 5.21, focusing on the signals pertaining to the protons in α position with respect to sulphur atoms of hydrogenated and fluorinated disulphides, arising form the decomposition of the NPs with iodine.

4.2 The reason behind the choice of HR-TEM

The use of HR-TEM was necessary to analyse with a high degree of precision the intermolecular distances among the NPs forming the superstructures. Indeed, as it will be discussed later on, the employment of cryo-TEM was unfortunately abandoned because of the poor solubility in water of the probing fluorinated NPs. As a matter of fact, in order to improve the solubility of these systems, mixtures of water and trifluoroethanol in a ratio of 9 to 1 were exploited. However, the presence of trifluoroethanol could bias the formation of the self-assembled structures since, being a fluorinated molecule, it could as well be interested in the fluorophilic interactions and therefore compete with the probing NPs in interacting with the NP-MDDS/F6 exhibiting tetrahedral organization of the fluorinated domains. Consequently, the overall approach was modified, moving from analyses in solution to analyses at the solid state; the probing NPs were changed as well, so that employing NPs that did not require a fluorinated solvent to be dissolved, without therefore introducing more biasing elements against the formation of the superstructures. For this reason, the NPs presented in the previous section were employed, whose low amount of fluorinated tails did not significantly alter their solubility in aqueous environments.

Even though HR-TEM allows to reach higher magnifications without risking of disrupting the specimen, as in the case of cryo-TEM for the presence of ice, the number of artefacts that could arise is considerable, due to the fact that the NPs are brought closer one another as a result of

solvent evaporation. For this reason, the criterion employed for establishing whether the interactions among the NPs could be effective consisted in focusing the attention on the distances of the probing NPs with the fluorinated tails from the NPs whit larger fluorinated domains. In order to establish an interaction distance, the lengths of the chains of the fluorinated ligands on both types of MM Au NPs were estimated, as reported in Figure 5.23.

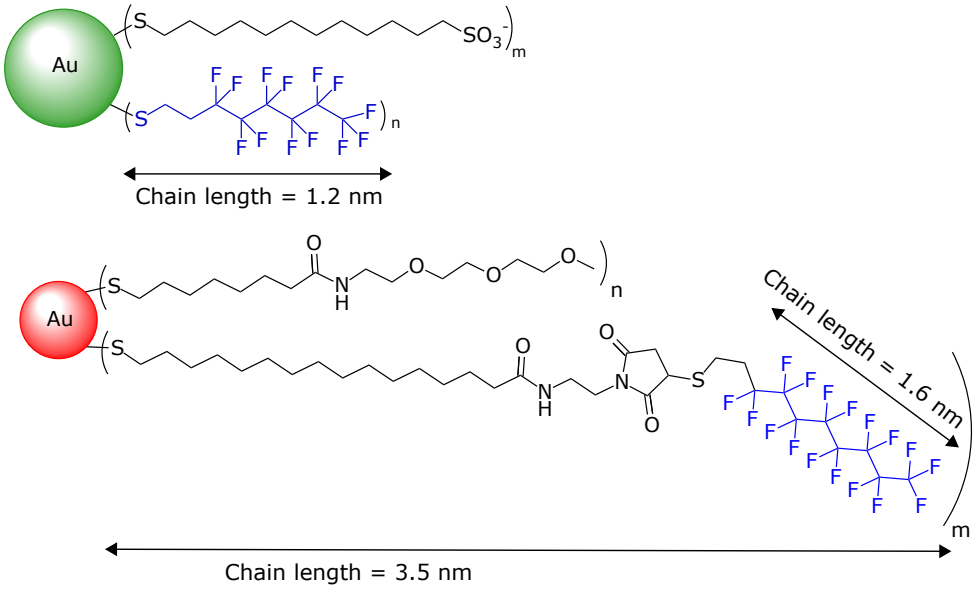

Figure 5.23: Estimated chain lengths of the ligands involved in the interactions leading to self-assembled superstructures of MM Au NPs. The length of the whole ligand bearing the fluroinated tail is actually its linear projection.

Then, the effectiveness of the interactions was evaluated as follows: if the NPs bearing the fluorinated tails were within a distance of 3.1 nm from the core of the MM Au NPs with the ordered monolayer, which is given by the sum of the chain length of the F6 thiolate (1.2 nm) and the chain length of the thiolate bearing the fluorinated tail (3.5 nm) minus the length of the fluorinated tail itself (1.6 nm), then the distances between the two cores was sufficient to give rise to a proper interaction. On the other hand, if the distance between the two cores was longer, then the two NPs were not interacting. It is worth noting that the interaction distance is not simply given by the sum of the lengths of the two thiolates because of the possible folding of the fluorinated tails; moreover, the tails could evenly interact with the fluorinated domains by placing themselves on the surfaces of the domains, whose area have been estimated to be 2 nm^2.

4.3 Imaging of self-assembly experiments with HR-TEM

Figure 5.24 reports four HR-TEM images of the result from the self-assembly test between NP-MDDS/F6 and MM NPs functionalized with fluorinated tails. The sample for the analysis was prepared by mixing 1.77 μL of a 7.9 mg/mL solution of NP-MDDS/F6 in mQ water with 0.5 μL of a 18.2 mg/mL solution of MM Au NPs bearing the fluorinated tails in a 1:1 mixture of mQ water and MeOH. 22.73 μL of mQ water were then added to the mixture so that reaching a final volume of 25 μL. Before the deposition on the carbon-coated copper grid, 10 μL of the previous mixture were diluted with 990 μL of mQ water. A drop of the so-obtained solution

was then deposited on the grid.
The red circles surrounding the NP-MDDS/F6 have been drawn to highlight the 2D projection of the spherical shell of interaction, according to the considerations concerning the values of the chain lengths of the fluorinated ligands, as previously described. As it can be seen from the images, inside this region the number of MM Au NPs bearing the fluorinated tails is variable, due to the fact that more than one NP can interact with one single fluorinated domain, due to their extension on the surface of the monolayer. The absence of the solvent however does not allow to establish whether the interactions form in solution as well.

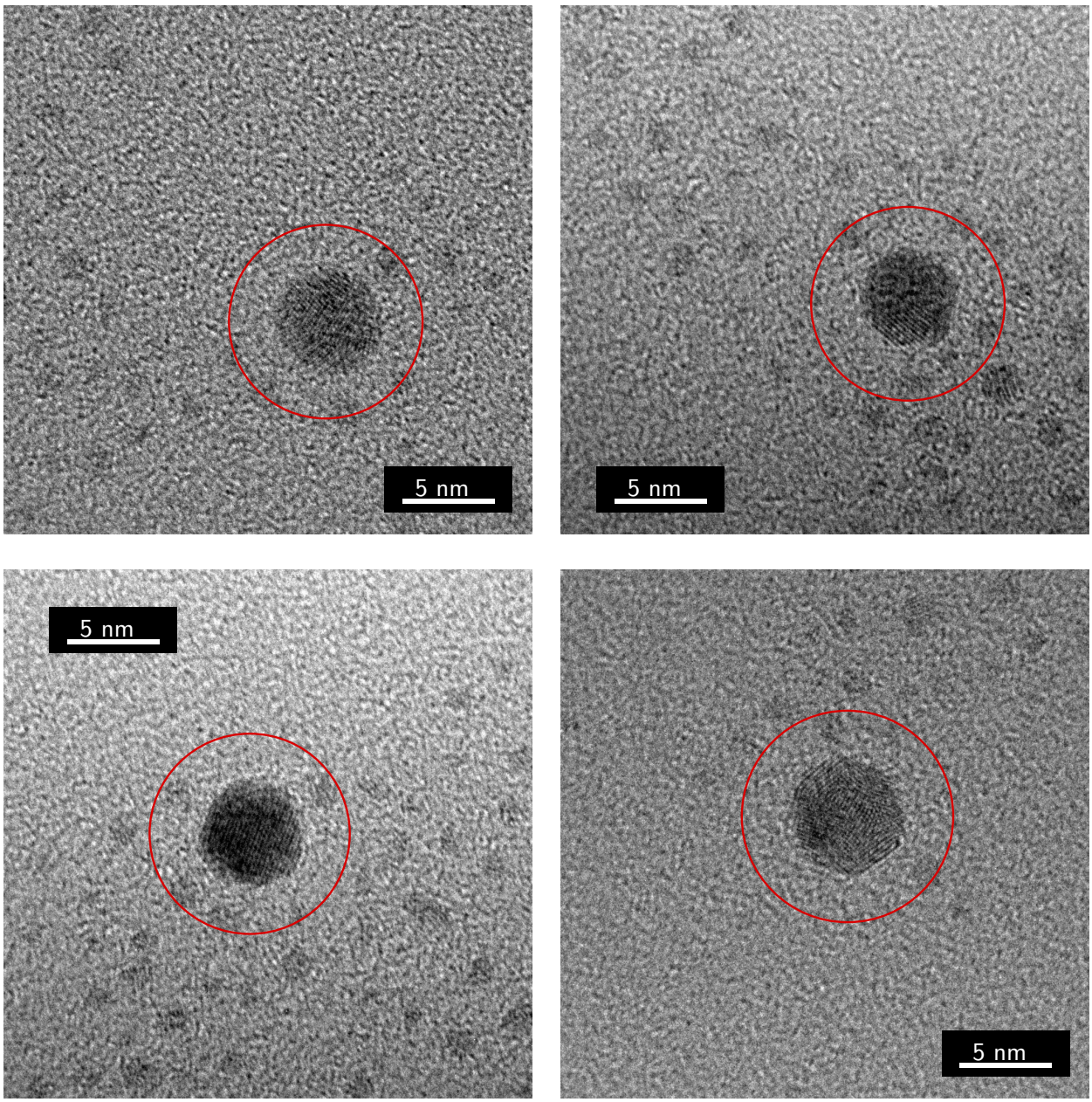

Figure 5.24: Four HR-TEM images of the product of the self-assembly experiments of NP-MDDS/F6 with MM Au NPs bearing few fluorinated chains. The red circles outline the 2D projection of spherical shell of interaction within which the NPs of reduced dimensions are considering as interacting with the 3.6 nm core.

By taking into account the NPs within the spherical shell of interaction and measuring their distances from the boundaries of the gold core of 3.6 nm MM Au NPs, it is possible to performed

an analysis on the distribution of the interacting distances and build an histogram displaying the distribution itself. The histogram is reported in Figure 5.25. All the HR-TEM images collected were analysed and only the NPs within the 2D projection of the spherical shell of interaction were considered and their distances measured. The fact that the majority of the values are far below the 3.1 nm distance previously outlined could be due to two main reasons. The first one concerns the compenetration arising among the fluorinated ligands of both types of NPs, leading to value slightly inferior to the predicted one. The latter is related to the fact that the centers of the core of the two interacting NPs could be on different planes, causing the sensible decrease of the interacting distance. Obviously, since the analysis is carried out on 2D projections of 3D systems, this situation is indeed frequent. A strategy to overcome this limitation could be represented by tomography,[136] which could improve the study of the interactions arising among the NPs by three-dimensional reconstructions of the superstructures, allowing to pinpoint any spatial extension of the various components of the superstructures themselves, the reciprocal distances and differences in planes.

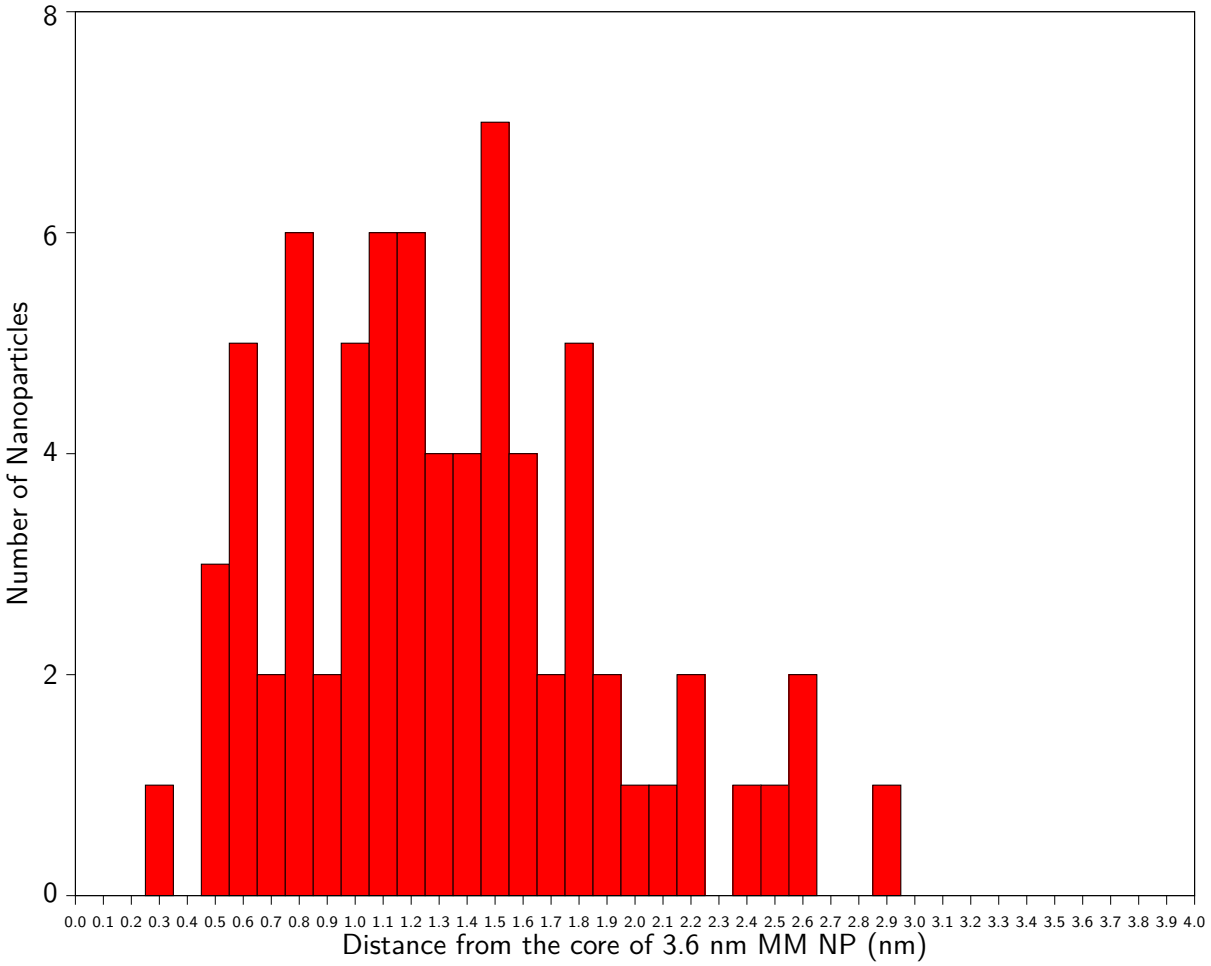

Figure 5.25: Histrogram displaying the distribution of the distances of the NPs within the 2D projection of the spherical interacting shell. No distances beyond 3.1 nm were considered for the reason previously explained.

CHAPTER 6

Matrix-Assisted Laser Desorption/Ionization-Time Of Flight Mass Spectrometry analysis on Mixed Monolayer Gold Nanoparticles

1 Introduction

This final chapter reports few attempts of characterization of MM Au NPs protected by blends of hydrogenated and fluorinated alkanethiolates by means of Matrix-Assisted Laser Desorption/Ionization-Time-Of-Flight Mass Spectrometry (MALDI-TOF MS). Indeed, the characterization of the mixed monolayers[104] is still a challenging task for scientists who deal with NPs, as the different techniques employed for this purpose generally provide average responses, coming from the whole batch undergone characterization and analysis. As a matter of fact, the average behaviour is indeed an intrinsic feature of NPs, since every synthesised batch is composed of NPs exhibiting different core sizes and therefore different monolayer morphologies may be present.

The chapter is meant to present preliminary MALDI-TOF MS studies on MM Au NPs protected by blends of ligands, which one of the two is fluorinated. The scarce interaction of fluorinated species with commonly used matrices for MALDI-TOF MS analysis gives rise to difficulties in the desorption/ionization process which lead to challenging characterization by means of the technique itself.[137–139] Furthermore, the results obtained during the MALDI-TOF analysis of MM Au NPs herein presented confirmed the different ionization tendencies of these two kinds of ligand. Hydrogenated ligands generate cations in an easier way whereas fluorinated species form preferentially anions. Unfortunately, it is not possible to simultaneously detect cations and anions. The outcomes from the MALDI-TOF MS analyses outlined therefore a biased predominance of one specie over the other, confirmed by the comparison with the NMR data concerning the average composition of the monolayer. Therefore, the usual approach fol-

lowed during MALDI-TOF MS experiments on MM Au NPs protected by polar and non-polar hydrogenated ligands does not fit for MM Au NPs covered by fluorinated and hydrogenated ligands.
Eventually, during the MALDI-TOF MS analyses on fluorinated MM Au NPs, the majority of fluorinated ligands capping the Au cores were detected either as free ligands or disulphides, rather than bound to Au atoms. The reason could be ascribed to a significant liability of the bond between Au atoms and fluorinated thiolates, which involves a high tendency of fluorinated species to desorb from the gold surface,[140] jeopardizing the possibility of determining the properties of the monolayer in terms of both ratio between ligands and morphology.

2 Batches of Au NPs analysed with MALDI-TOF MS

This section provides the information concerning the properties of the Au NPs analysed by means of MALDI-TOF MS technique. Both average core size and composition of the monolayer are expressed: the first one was analysed by means of TEM, whereas the latter was achieved by means of ^{1}H-NMR.

2.1 Au NPs protected by C8TEG thiolates

A graphic representation of this type of Au NPs is given in Figure 7.8.

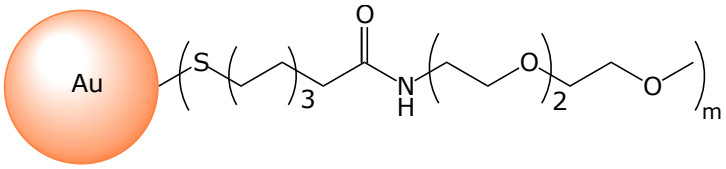

Figure 6.1: Drawing of Au NPs protected by C8TEG ligands.

A representative TEM image of the batch is reported in Figure 6.2, together with the histogram displaying the distribution of the sizes. The average core dimension that characterizes the batch is 2.0 nm, with a standard deviation of 0.3 nm, leading to a variation coefficient of 0.15.

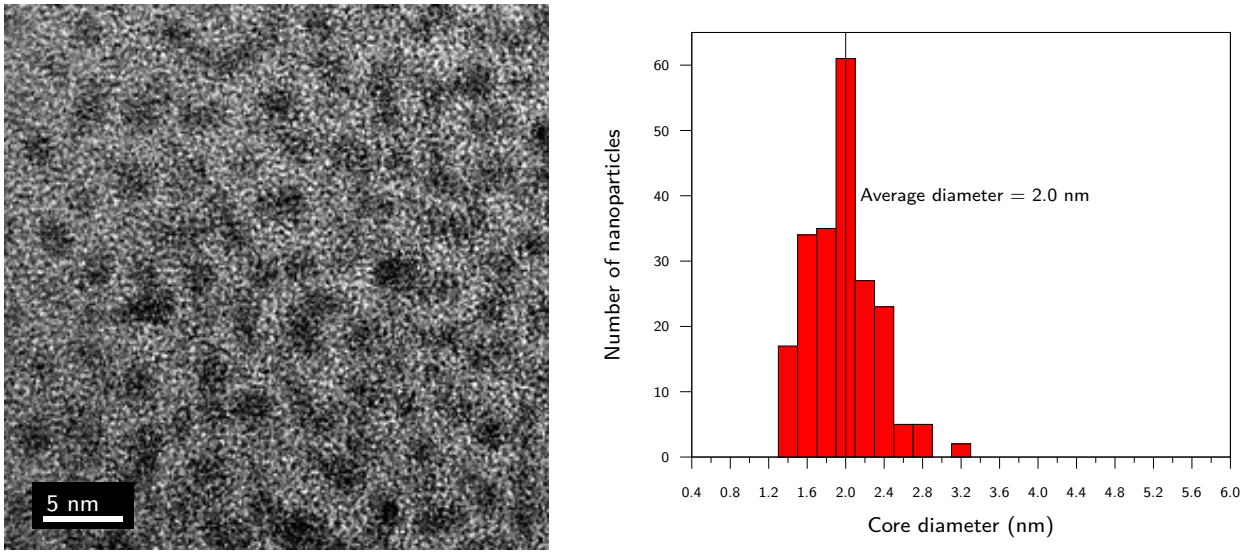

Figure 6.2: On the left, TEM image of the batch of Au NPs protected by C8TEG ligands undergone MALDI-TOF MS analysis. On the right, histogram displaying size distribution, obtained after the analysis of core sizes over 200 NPs.

The ^{1}H-NMR spectrum of the NPs is reported in Figure 6.3; no sharp peaks can be pointed out from the spectrum, denoting the absence of unbounded ligands.

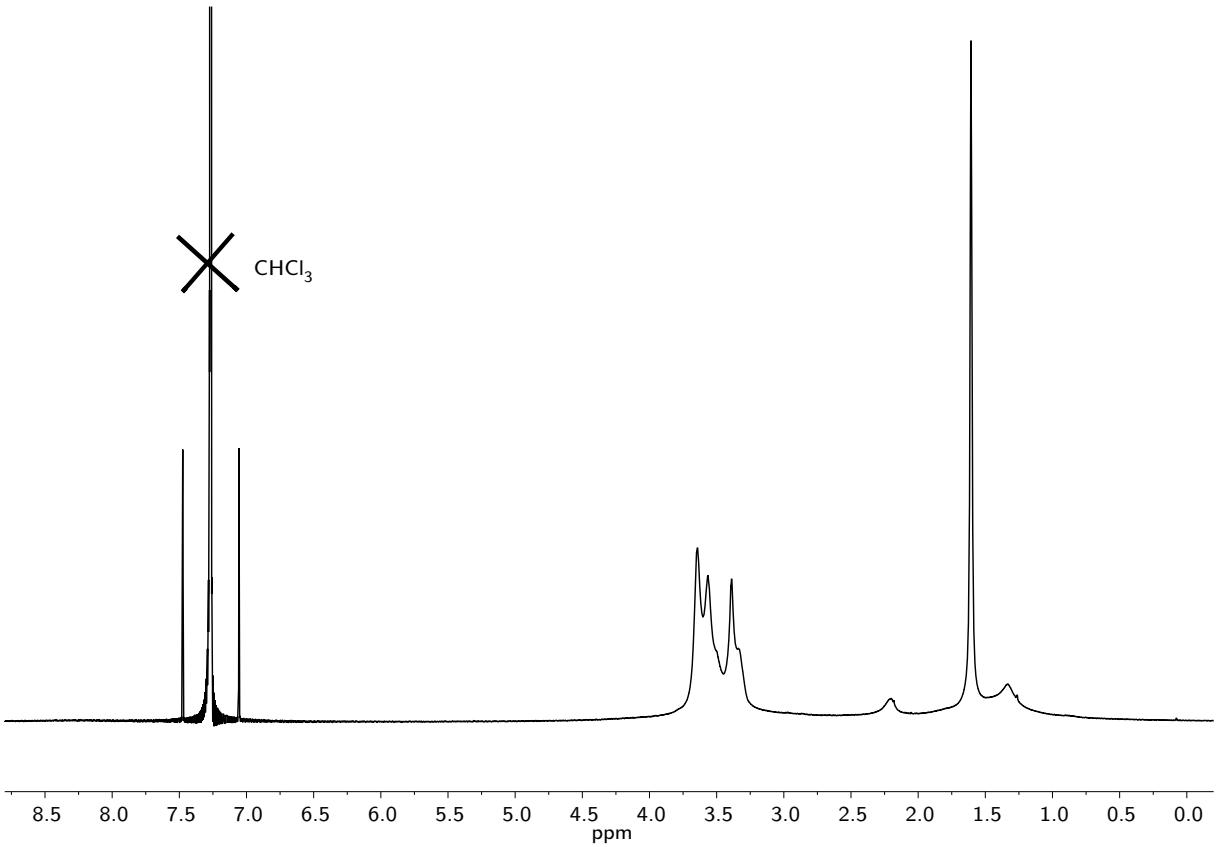

Figure 6.3: ^{1}H-NMR spectrum (400 MHz, $CDCl_3$) of the batch of Au NPs protected by C8TEG thiolates. The absence of sharp peaks confirms the absence of free thiols.

2.2 Au NPs protected by F8PEG thiolates

Figure 6.4 displays the representation of the Au NPs coated with F8PEG. As it can be seen from the picture, the ligand that covers the NPs is a fluorinated thiol bearing a PEG 550 chain at its end.

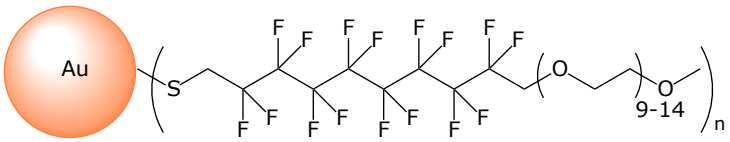

Figure 6.4: Drawing of Au NPs protected by C8TEG ligands.

The TEM analysis related to the average core dimension and the size distribution of the batch is reported in Figure 6.5. Indeed, the average core dimension for this batch of Au NPs is 2.0 nm, with a standard deviation of 0.5 nm, resulting in a variation coefficient of 0.25.

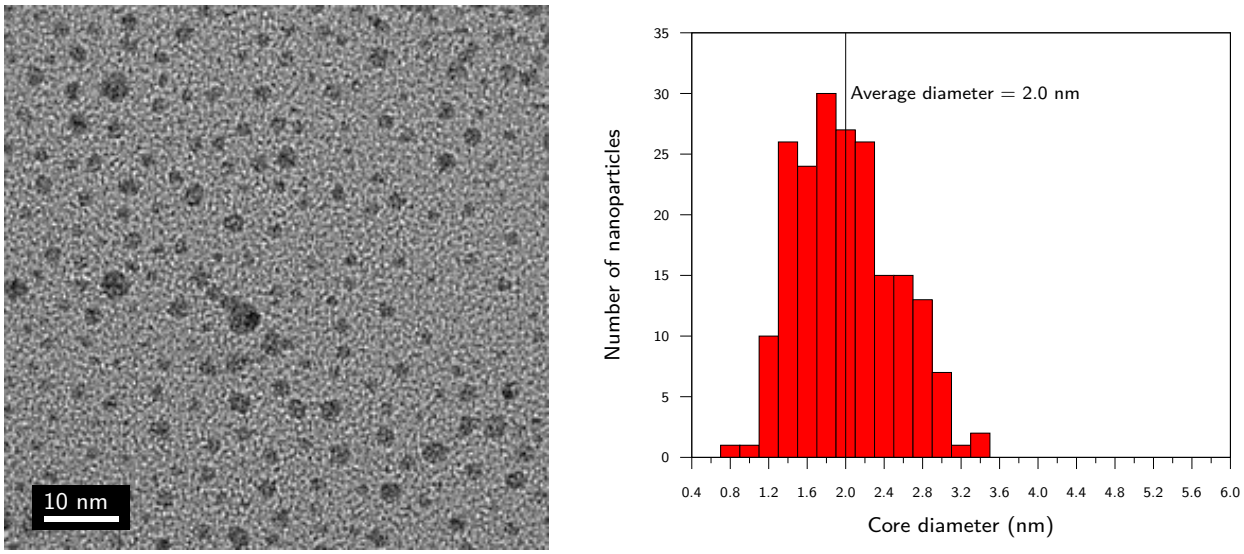

Figure 6.5: On the left, TEM image of the batch of Au NPs protected by F8PEG thiolates undergone MALDI-TOF MS analysis. On the right, histogram displaying size distribution, obtained after the analysis of core sizes over 200 NPs.

The ^{1}H-NMR spectrum of the batch of NPs is displayed in Figure 6.6. Once again, the absence of unbound ligands is proved by the absence of sharp peaks in the spectrum.

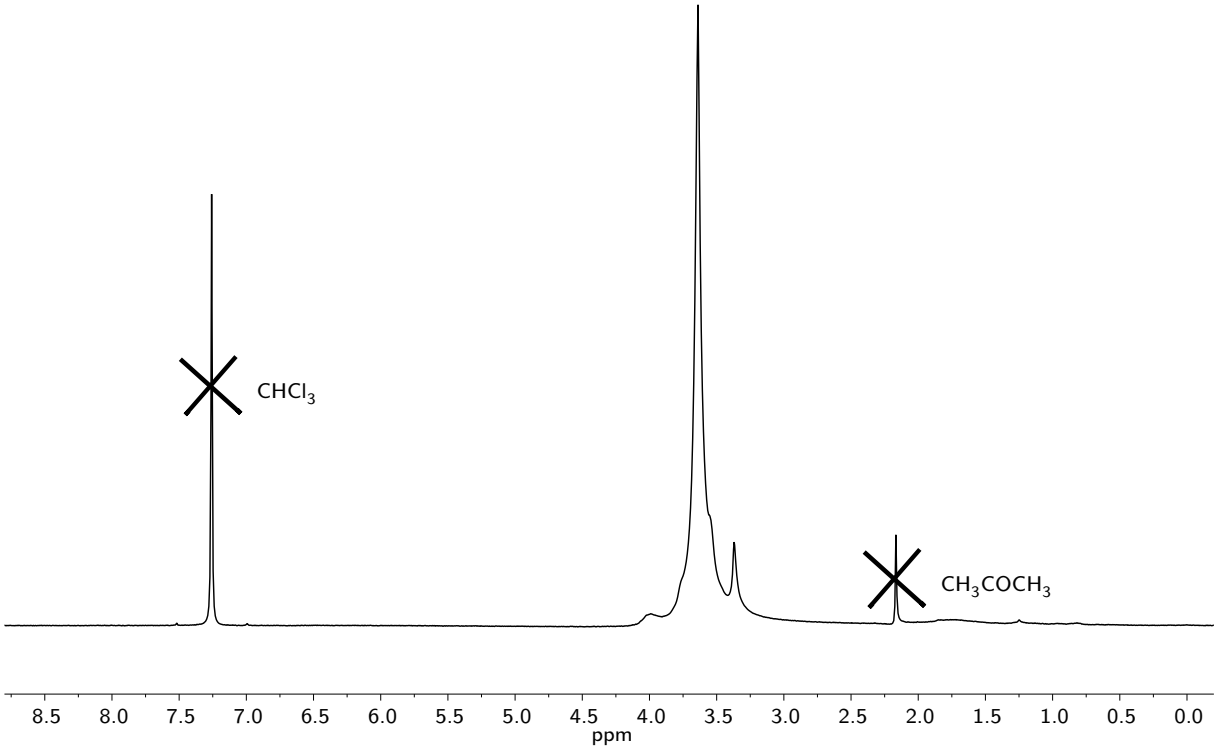

Figure 6.6: ^{1}H-NMR spectrum (400 MHz, $CDCl_3$) of the batch of MM Au NPs protected by F8PEG thiolates. The absence of sharp peaks confirms the absence of free thiols.

2.3 Au NPs protected by C8TEG and F8PEG thiolates

Figure 6.7 provides a simple sketch of the MM Au NPs. The ligands are the same of the previously presented batches, present in a blend giving rise to mixed monolayers.

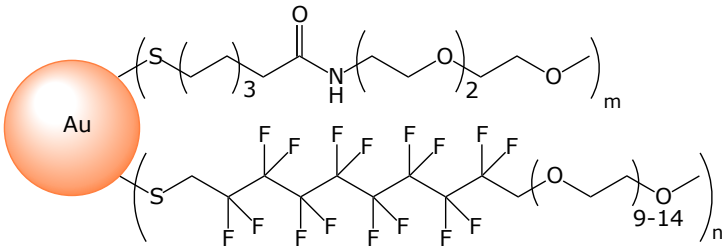

Figure 6.7: Drawing of Au NPs protected by C8TEG ligands.

Two batches prtotected by mixtures of C8TEG and F8PEG thiolates and characterized by different ratios between the two ligands were taken into account for the MALDI-TOF MS experiments. They are defined as *sample A* and *sample B*.

2.3.1 Sample A

Figure 6.8 displays the TEM analysis of the NPs forming the sample A. The average core dimension for the batch is 1.9 nm with a standard deviation of 0.7 nm, bringing to a variation coefficient of 0.37.

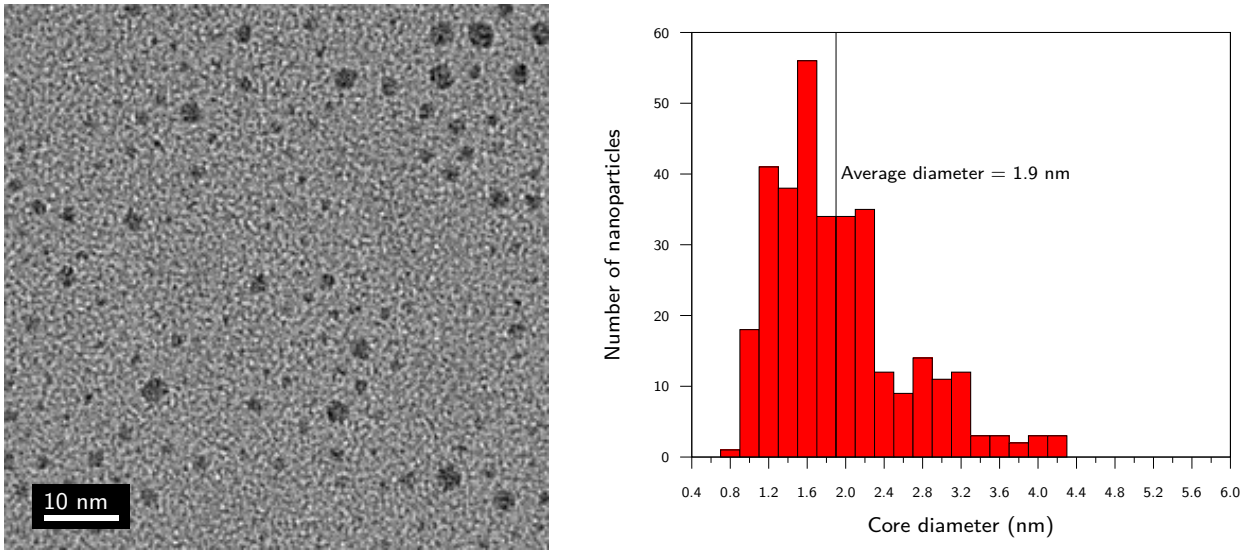

Figure 6.8: On the left, TEM image of sample A composed of Au NPs protected by C8TEG and F8PEG thiolates undergone MALDI-TOF MS analysis. On the right, histogram displaying size distribution, obtained after the analysis of core sizes over 300 NPs.

Figures 6.9 and 6.10 report respectively the ^{1}H-NMR spectrum of the pristine NPs and the ^{1}H-NMR spectrum of the product of the decomposition of a small amount of NPs with iodine. From the first spectrum it is possible to verify the absence of unbound species, whereas the latter can be employed for establishing the ratio between the two types of ligands composing the monolayer. For doing that, the signals pertaining to the protons in α position with respect to the fluorinated tail and those related to the protons in α position with respect to the carbonyl were taken into account. Therefore, the area of those peaks were integrated and the ratio between the values employed to determine the ratio between the ligands, which is C8TEG:F8PEG = 1:2.

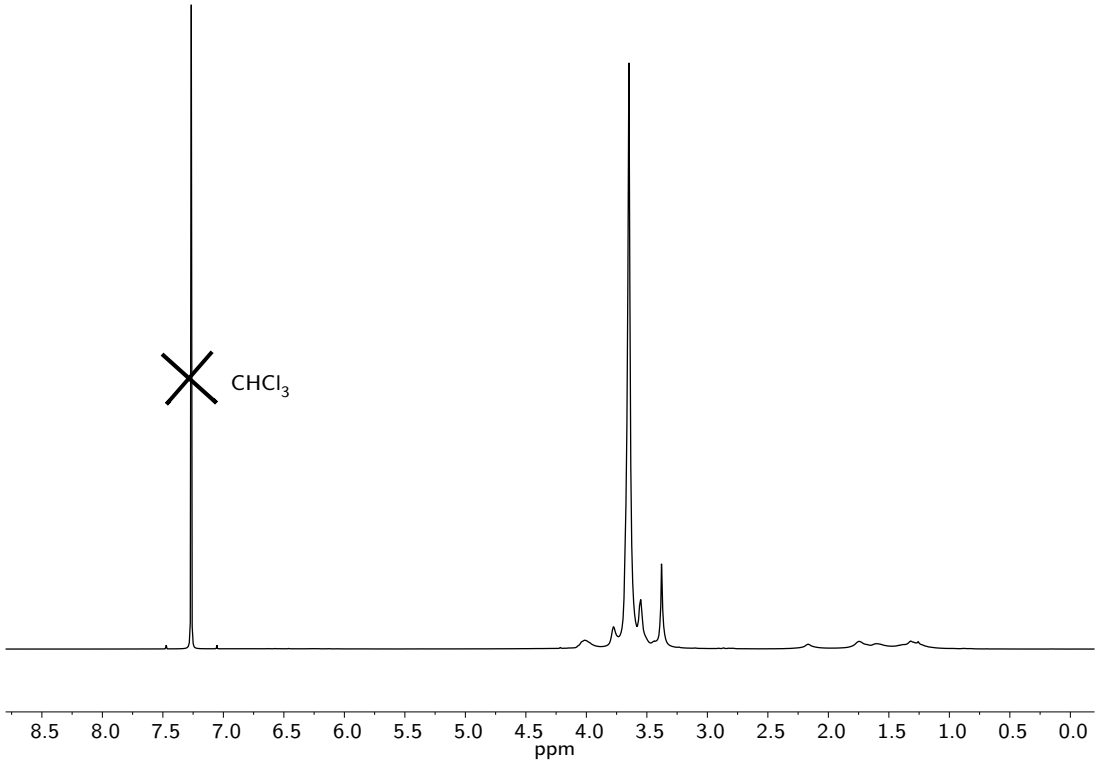

Figure 6.9: ^{1}H-NMR spectrum (400 MHz, $CDCl_3$) of sample A. No sharp peaks can be point out, confirming the absence of unbound ligands.

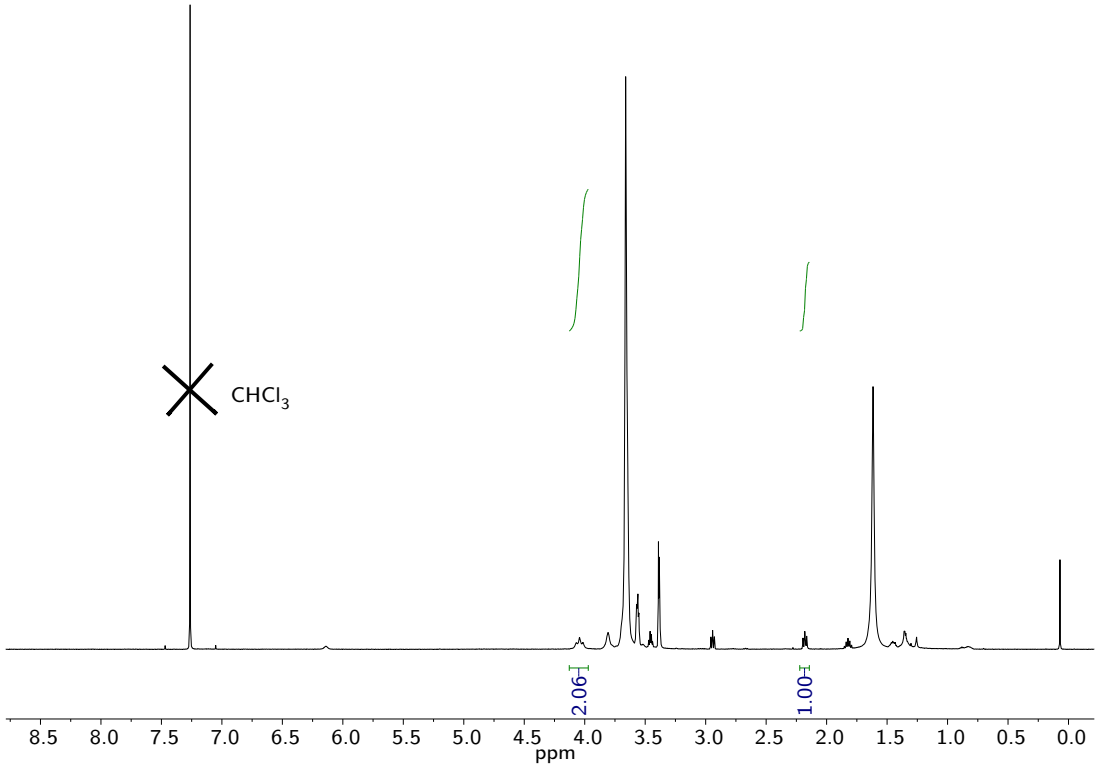

Figure 6.10: ^{1}H-NMR spectrum (400 MHz, $CDCl_3$) of the product of the decomposition of a small amount of sample A with iodine.

2.3.2 Sample B

Figure 6.11 displays the TEM analysis of the NPs forming the sample B. The average core dimension for the batch is 1.6 nm with a standard deviation of 0.4 nm, bringing to a variation coefficient of 0.25.

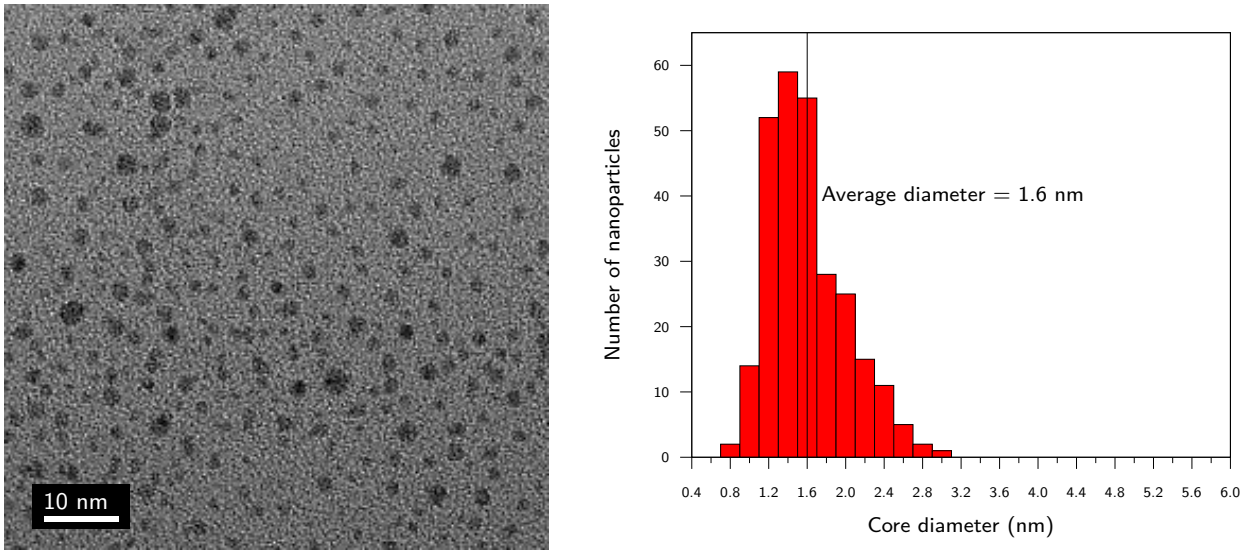

Figure 6.11: On the left, TEM image of sample B composed of Au NPs protected by C8TEG and F8PEG thiolates undergone MALDI-TOF MS analysis. On the right, histogram displaying size distribution, obtained after the analysis of core sizes over 270 NPs.

Similarly to the previous sample, Figures 6.12 and 6.13 report the ^{1}H-NMR spectrum of the pristine NPs and the ^{1}H-NMR spectrum of the product of the decomposition of a small amount of NPs with iodine. As in the cases already presented, the first spectrum is useful to check the absence of unbound species, whereas the latter can be exploited for establishing the ratio between the two type of ligands composing the monolayer. The signals taken into account are the ones considered for sample A, since the ligands are the same. The ratio between the ligands composing the monolayer of the NPs of sample B is C8TEG:F8PEG = 1:1.4.

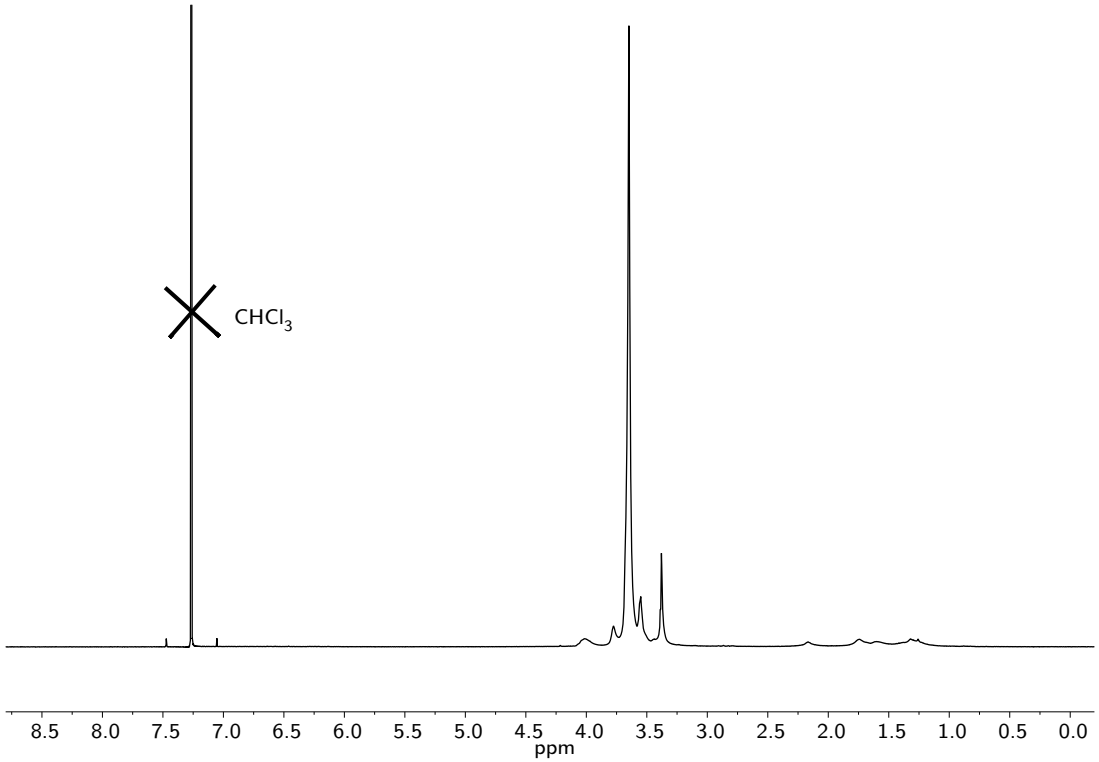

Figure 6.12: ^{1}H-NMR spectrum (400 MHz, $CDCl_3$) of sample B. The absence of sharp peaks proves the absence of unbound species.

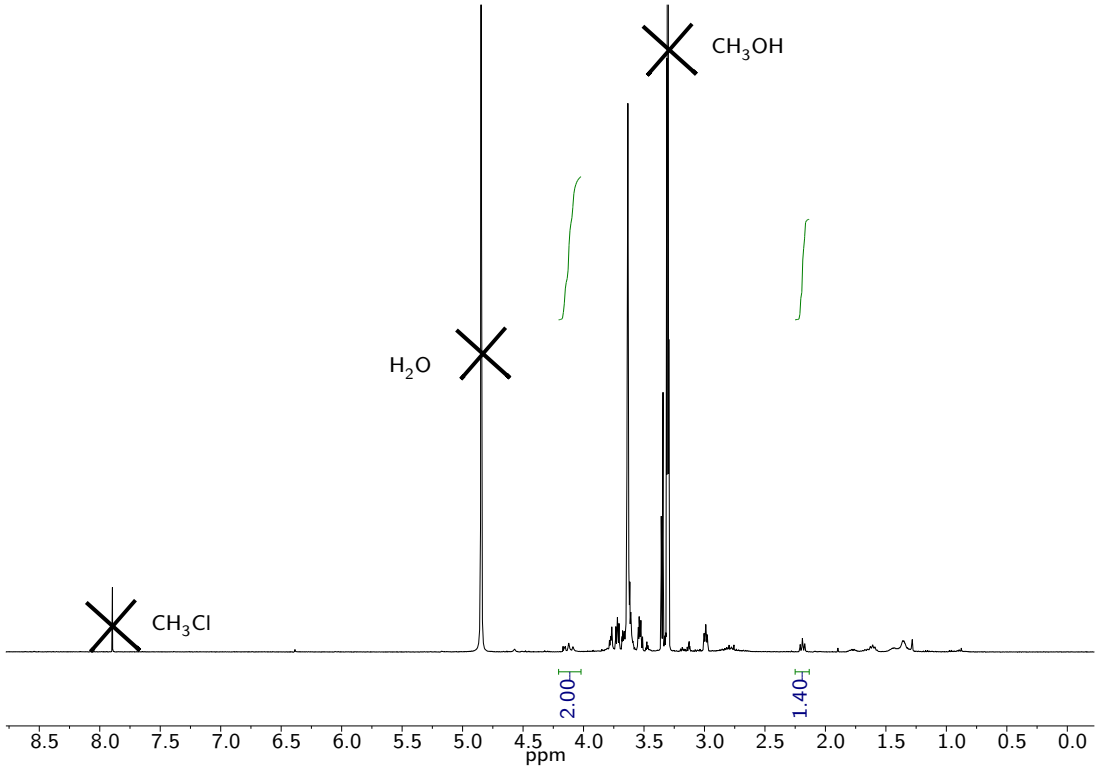

Figure 6.13: ^{1}H-NMR spectrum (400 MHz, $CDCl_3$) of the product of the decomposition of a small amount of sample B with iodine.

2.4 Au NPs protected by C16 and F6 thiolates

Figure 6.14 displays the graphic representation of the last batch of MM Au NPs analysed by means of MALDI-TOF MS.

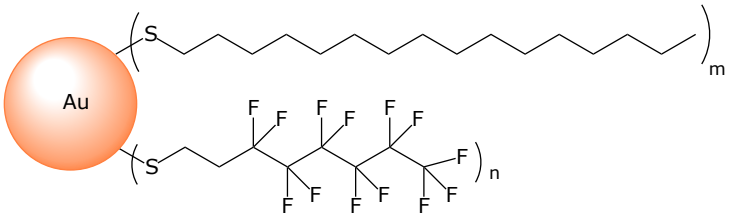

Figure 6.14: Drawing of Au NPs protected by C16/F6 ligands.

The TEM analysis of the batch is reported in Figure 6.15. The average core dimension of the batch is 2.9 nm, with a standard deviation of 0.5 nm, resulting in a variation coefficient of 0.17.

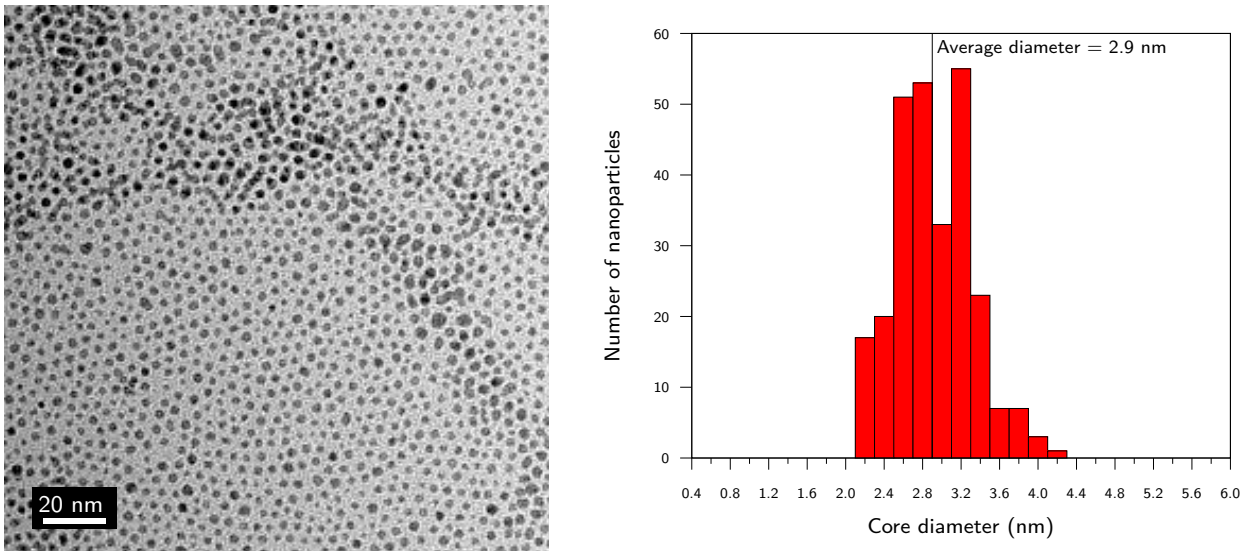

Figure 6.15: On the left, TEM image of the batch of Au NPs protected by C16/F6 thiolates undergone MALDI-TOF MS analysis. On the right, histogram displaying size distribution, obtained after the analysis of core sizes over 280 NPs.

Figure 6.16 displays the ^{1}H-NMR spectrum of the NPs protected by C16 and F6 thiolates.

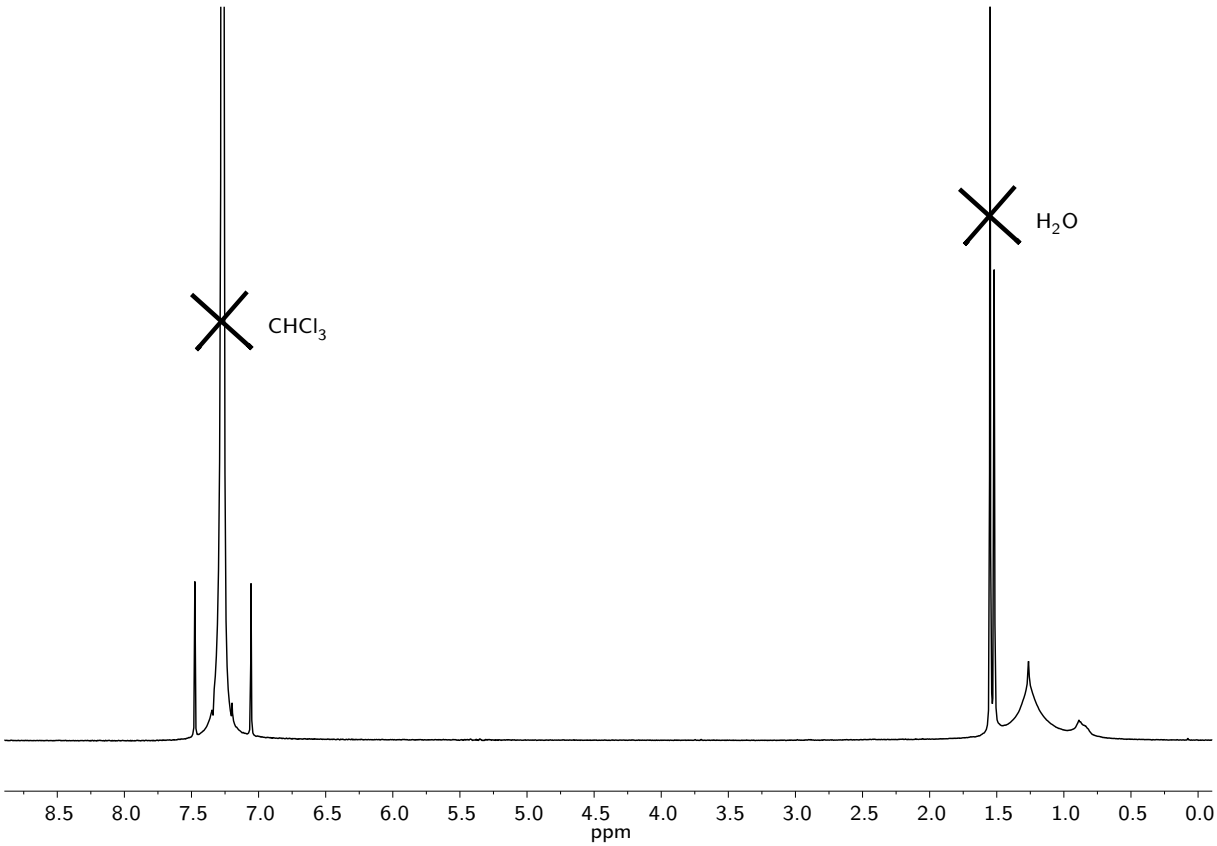

Figure 6.16: ^{1}H-NMR spectrum (400 MHz, $CDCl_3$) of the batch of MM Au NPs protected by C16 and F6.

The ratio between the ligands composing the monolayer was established by means of ^{1}H-NMR analysis of the mixture resulting from the decomposition of a small amount of MM Au NPs with iodine. The ratio is C16:F6 = 1.9:1.

3 MALDI-TOF MS Results

The batches of NPs taken into account for MALDI-TOF MS study can be divided in two main groups: those belonging to the first group are either homoligand NPs coated by a monolayer composed of solely C8TEG or F8PEG, or MM NPs coated by a mixture of the two. C8TEG is a hydrogenated ligand whose tail is formed by a very short PEG chain composed of four oxyethylene groups, whereas F8PEG is a fluorinated ligand possessing a PEG 550 tail at its end. The reason behind the use of these PEG-ylated ligands is related to the enhancement in solubility resulting from the presence of the PEG chains: indeed, these chains are meant to mask the fluorinated or the hydrogenated moieties and therefore make the overall system soluble in a wide range of solvents, such as chlorinated ones, alcohols and water. Being the PEG polymer employed polydispersed, some ligands possess longer PEG chains and some others bear shorter ones. This is clearly visible in MALDI-TOF mass spectra of this type of MM Au NPs, where the peaks pertaining to complexes containing one or more fluorinated ligands are characterized by a gaussian distribution. The second group of NPs are MM Au NPs protected by hexadecanethiolates and 1H,1H,2H,2H-perfluorooctanethiolates, soluble in chloroform only. Since these latter ligands are non-polar, trans-2-[3-(4-tert-butylphenyl)-2-methyl-

2-propenylidene]malononitrile (DCTB) was used as matrix for MALDI-TOF MS analysis on this batch of Au NPs. Indeed, the ionization process promoted by DCTB is the result of an electron transfer from the matrix to the analyte or *vice versa*; therefore, the formation of charged species will be favoured also for non-polar ligands which are not willing to be protonated. Finally, among different matrices for MALDI-TOF MS, DCTB is the one that gives the minor degree of fragmentation concerning the analysis of Au complexes and clusters.[114] On the other hand, for the NPs with PEG-ylated ligands three different matrices were tested: α-cyano-4-hydroxycinnamic acid (α-CHCA), DCTB and 2,5-dihydroxybenzoic acid (DHBA), so that establishing whether the outcomes were affected by the type of matrix employed for the experiments. Figure 6.17 reports the chemical structures the matrices used for the MALDI-TOF MS studies.

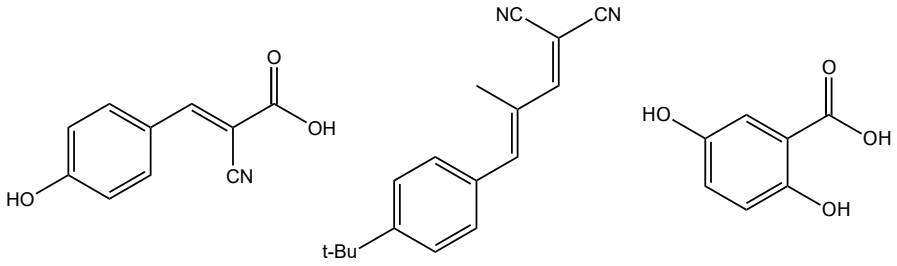

Figure 6.17: Chemical structures of the matrices used for MALDI-TOF MS analyses herein presented. From left to right: α-cyano-4-hydroxycinnamic acid (α CHCA), trans-2-[3-(4-tert-butylphenyl)-2-methyl-2-propenylidene]malononitrile (DCTB) and 2,5-dihydroxybenzoic acid (DHBA).

3.1 MALDI-TOF experiments on PEG-ylated Au NPs

As mentioned before, for the experiments on batches of MM Au NPs with PEG-ylated ligands the three different matrices previously presented were tested; the best results are reported herein and they have been obtained by employing α-CHCA, which promotes proton transfers. The spectra were recorded in linear positive mode in order to detect the cations formed after the desorption/ionization process, within the range of 1000-6000 Da. As the PEG-ylation provided the NPs with high solubility in a wide range of solvent, several solvents were used to dissolve both analyte and matrix, although similar results were obtained in all the cases. Therefore, it is reasonable to state that the solvent does not affect the outcome from a MALDI-TOF MS study on this type of MM Au NPs. The solvents tested are methanol, chloroform and trifluoroethanol. The spectra here reported are the ones achieved using methanol as solvent.

The first experiments were performed on homoligand Au NPs covered by C8TEG thiolates. Figure 6.18 displays the MALDI-TOF mass spectrum of the batch of Au NPs protected by C8TEG thiolates. The most intense peak that can be seen in the spectrum pertains to the complex $Au_4(C8TEG)_4$ charged with sodium ion, confirming that this is the most abundant specie forming during the desorption of the Au-S complexes from the surface of the NPs. Furthermore, the peaks related to $Au_5(C8TEG)_5$ complex and complexes with different stoichiometry are visible as well.

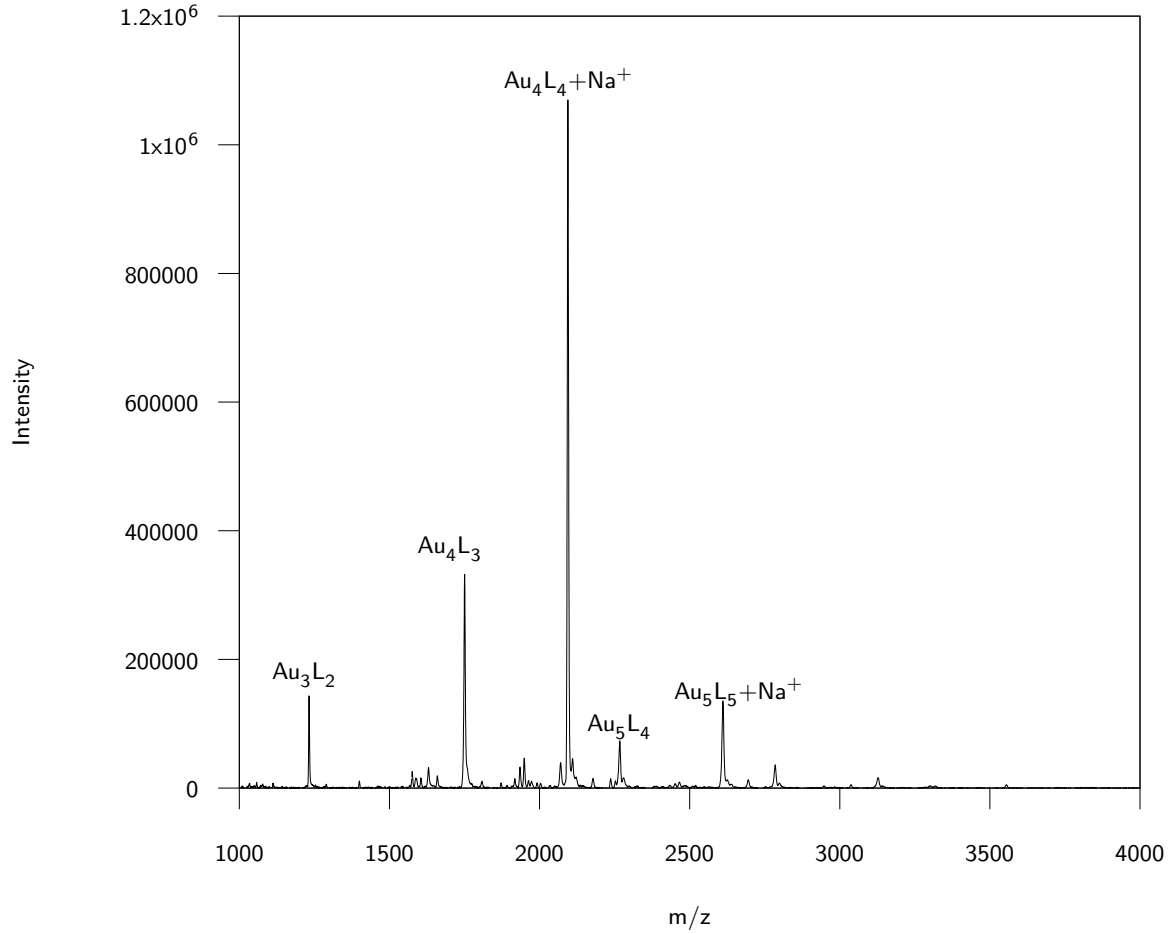

Figure 6.18: MALDI-TOF mass spectrum of Au NPs protected by C8TEG thiolates.

The analyses on MM Au NPs protected by C8TEG and F8PEG were then performed applying the same conditions followed for the experiments on the homoligand C8TEG Au NPs. Figure 6.19 displays the MALDI-TOF mass spectrum of the batch containing C8TEG/F8PEG Au NPs identified as sample A. Figure 6.20 reports an inset of the same spectrum, focusing the attention on the region where the peaks related to Au_4L_4 complexes can be pointed out. The integrals of the area of these peaks were taken into account for the determination of the ratio between the two types of ligands composing the monolayer.

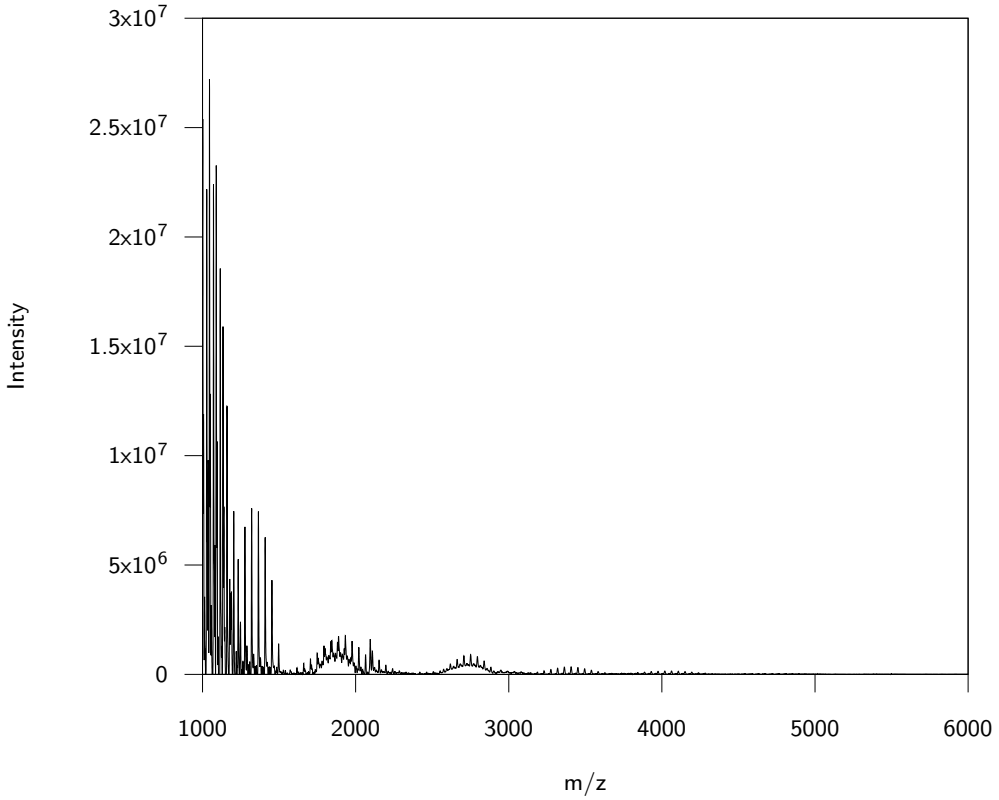

Figure 6.19: MALDI-TOF mass spectrum of sample A.

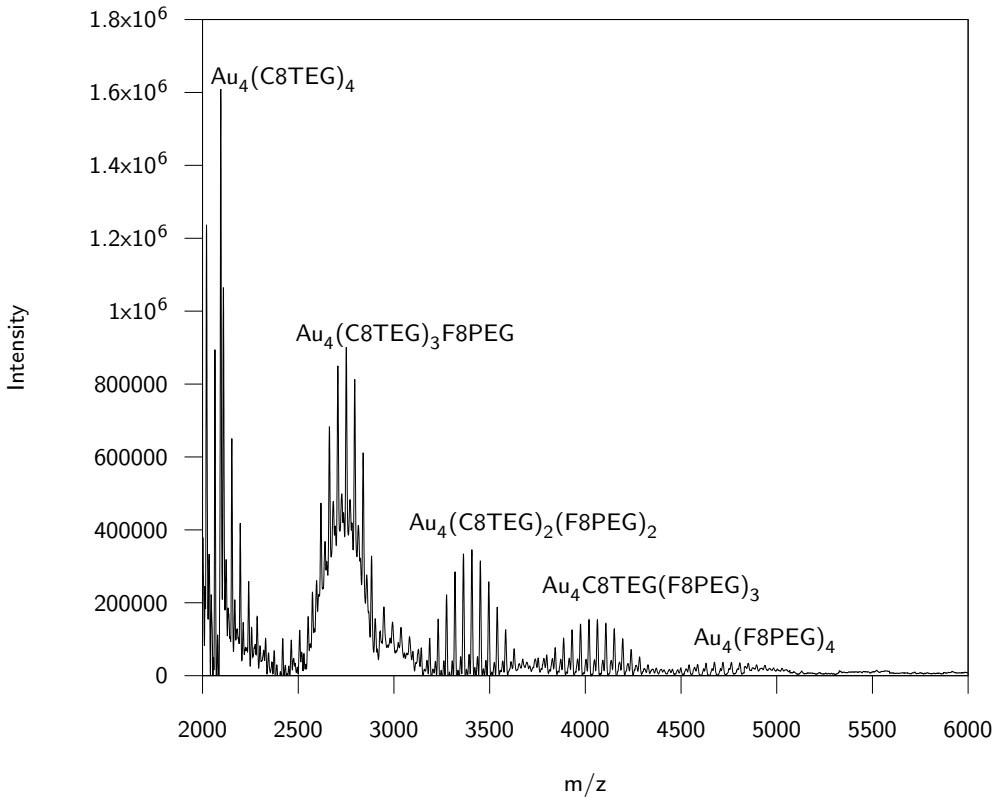

Figure 6.20: Inset of the mass spectrum reported in Figure 6.19.

The ratio between the two ligands has been evaluated by considering the integrals of the peaks pertaining to the Au_4L_4. The so-obtained ratio is C8TEG:F8PEG = 1:0.5, whereas the ratio evaluated by means of ^{1}H-NMR spectroscopy is C8TEG:F8PEG = 1:2, as reported in Figure 6.10. One possible explanation of this mismatch could be ascribed to the fact that part of the fluorinated ligand does not reach the detector bound to a gold atom forming a Au_xL_x complex. Indeed, the reason behind this hypothesis is related to the presence in the mass spectrum of peaks pertaining to both homo and hetero disulfides, which are respectively composed of two molecules of fluorinated ligand and one molecule of fluorinated ligand and one of hydrogenated ligand. The first are visible in the region of the spectrum within 1100 and 1500 m/z, whereas the latter within 1600 and 2100 m/z. Moreover, also very intense peaks related to the free fluorinated ligand can be outlined in the region within 1000 and 1300 m/z. Previous ^{1}H-NMR analyses on Au NPs did not report any sharp peak that could have been induced by an incomplete purification procedure and biased the evaluation of the ligand ratio.
Similar results were obtained after the MALDI-TOF MS analysis on sample B, whose mass spectrum is displayed in Figure 6.21.

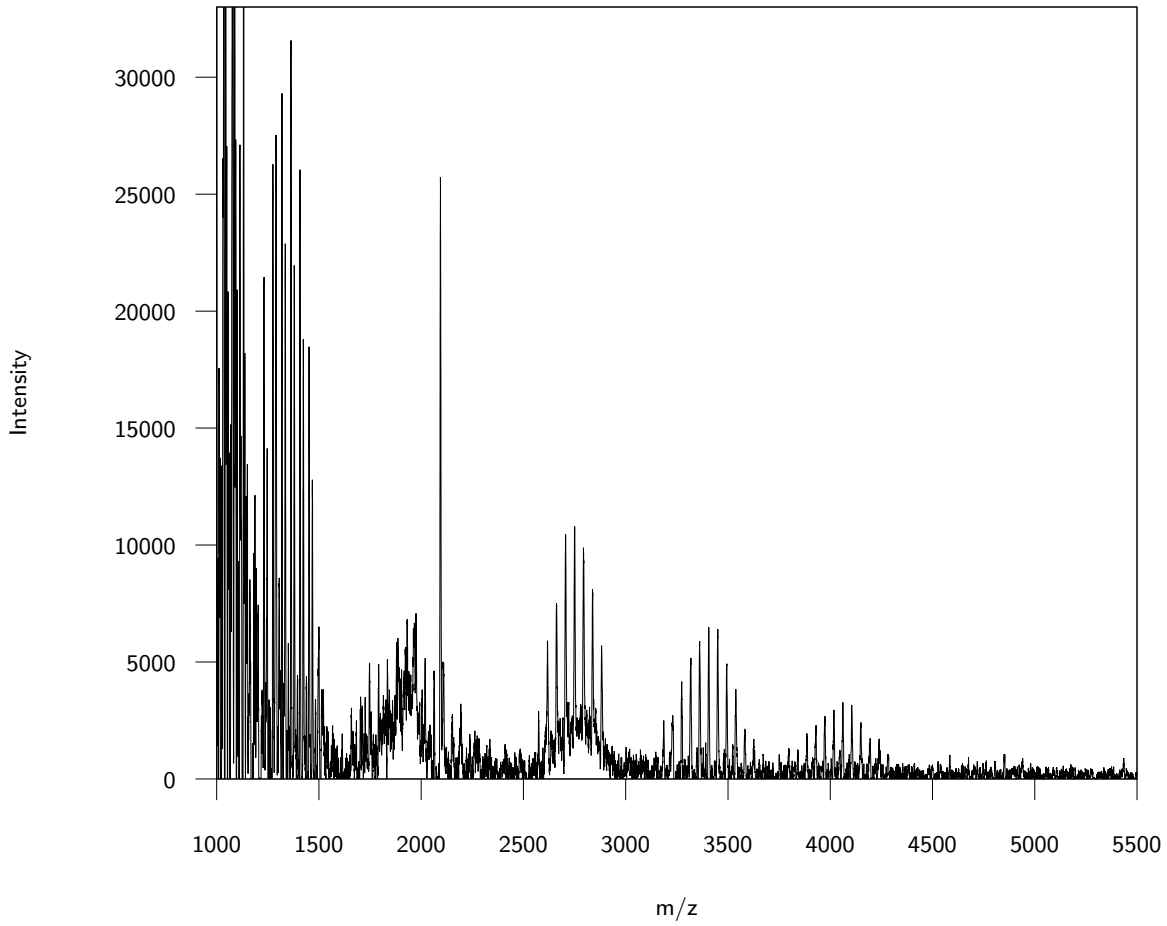

Figure 6.21: MALDI-TOF mass spectrum of sample B.

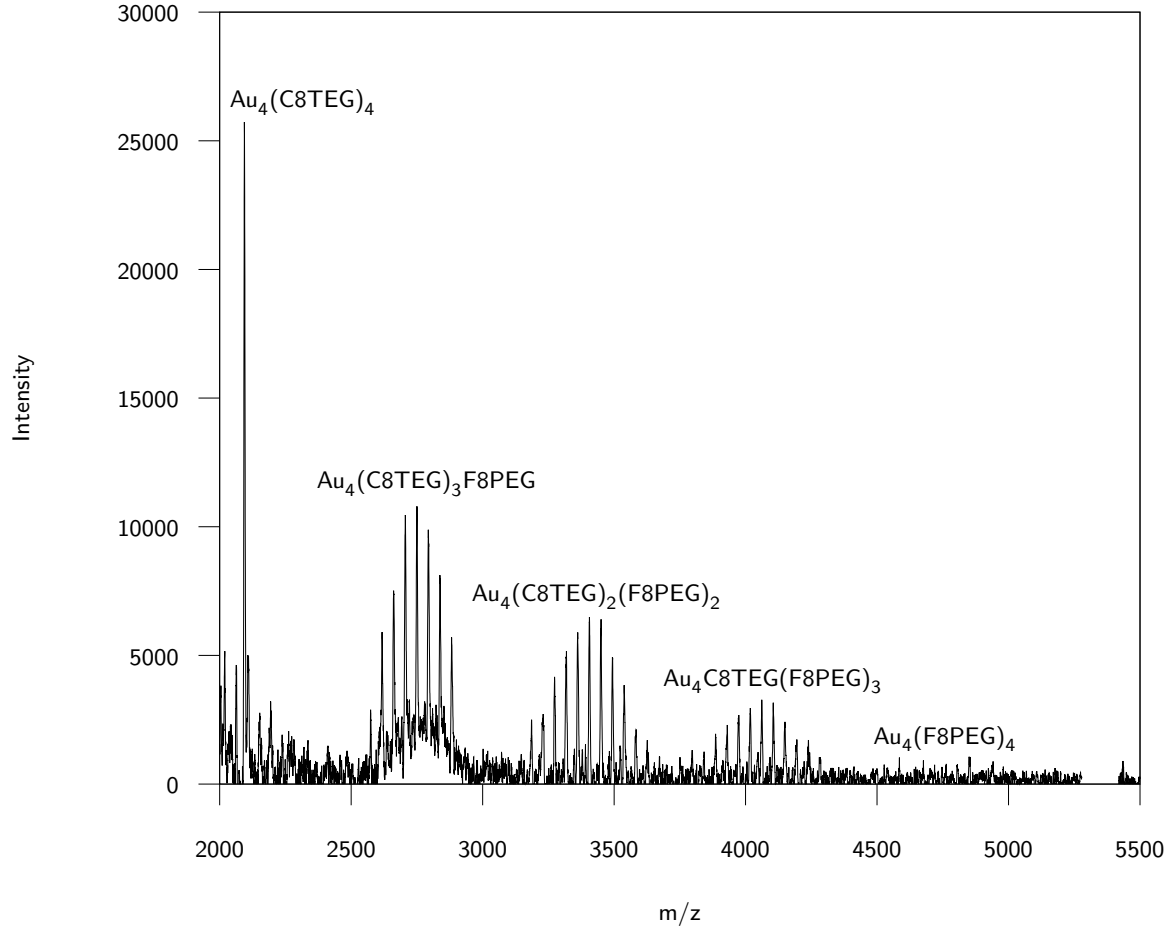

Figure 6.22: Inset of the mass spectrum presented in Figure 6.21.

Once again, the ratio between the ligands evaluated on the MALDI-TOF MS outcomes does not match that established by means of ^{1}H-NMR. Indeed, the ratio based on the signals of the Au_4L_4 complexes is C8TEG:F8PEG = 1:0.7, whereas the one evaluated from ^{1}H-NMR data is 1:1.4. Moreover, the experiments on this sample were affected by the same issues encountered during the analysis the previous sample: indeed, also in this case, besides the signals related to Au_4L_4 complexes, the presence in the spectrum of peaks pertaining to homo and hetero disulphides, as well as those belonging to the free fluorinated ligand, is remarkable. The intensities of these peaks are considerably higher than those related to the Au_4L_4 complexes. It is worth highlighting the fact that no sharp peaks related to unbound species or disulphides were visible in the ^{1}H-NMR spectra of both sample of MM Au NPs, evidencing the fact that these compounds form during the MALDI-TOF MS experiments.
For comparison, homoligand F8PEG Au NPs were also analysed through MALDI-TOF MS and the outcomes confirmed the prevalent detection of disulphides and free ligands, even though no traces of them were outlined in ^{1}H-NMR spectrum. The MALDI-TOF mass spectrum of this batch of NPs is displayed in Figure 6.23. The red dashed line in the spectrum outlines the theoretical position of the peaks pertaining to $Au_4(F8PEG)_4$ complexes.

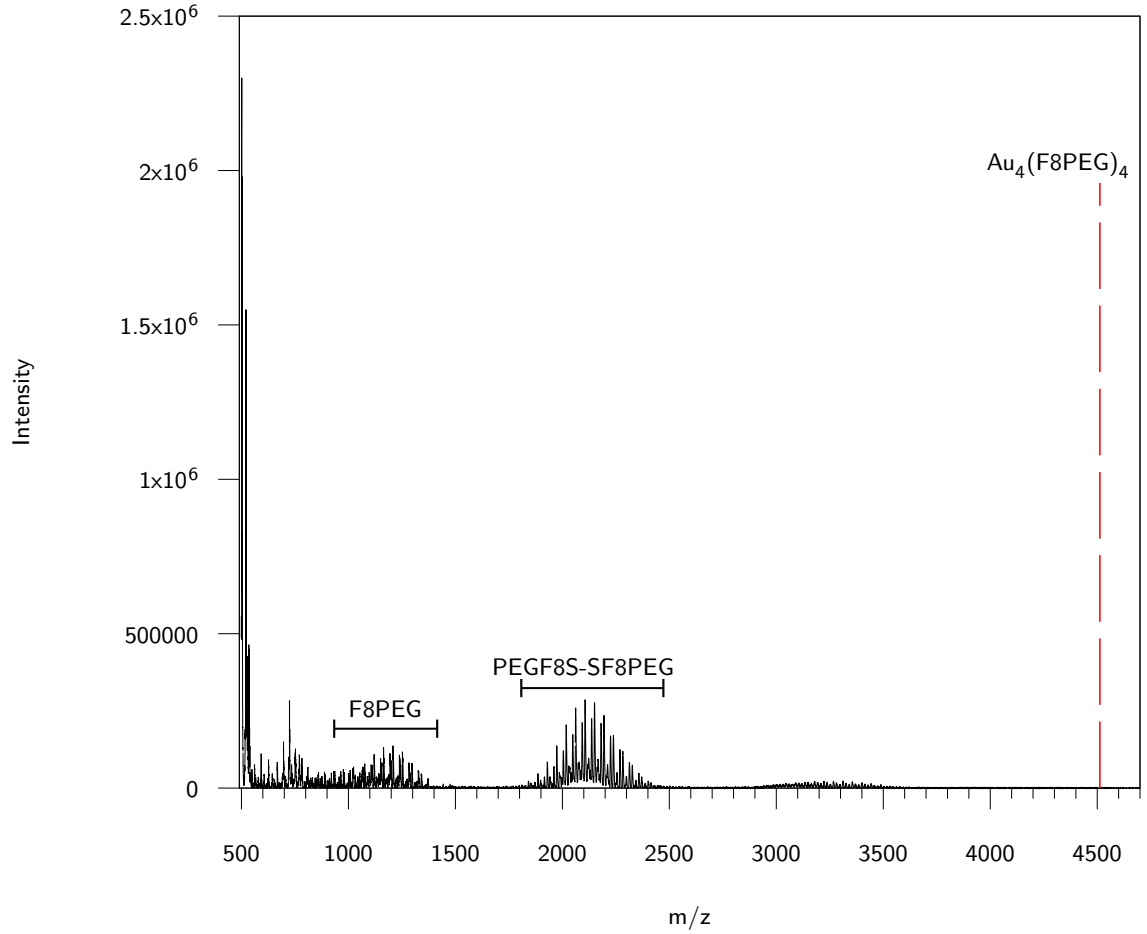

Figure 6.23: MALDI-TOF mass spectrum of F8PEG Au NPs. The red dashed line indicates where the peaks pertaining to $Au_4(F8PEG)_4$ should be found in the spectrum if their desorption was effective.

These evidences on the difficulty of detecting gold complexes containing fluorinated ligands during MALDI-TOF MS experiments agree with what[140] has been recently reported in literature by Palermo *et al.* Indeed, the authors of the paper claimed that the use of fluorinated Au NPs as agents for Nanostructure Imaging Mass Spectrometry for studying metabolites on biological tissue enhances the desorption/ionization process of the metabolites themselves, allowing their detection even at small concentration. The improvement in detecting the metabolites is indeed strictly related to the easiness in desorbing perfluoroalkyl thiols from the gold surface, which favours consequently the desorption of metabolites from living tissues. Therefore, in this case, the function of fluorinated Au NPs in NIMS is similar to that of matrices in MALDI-TOF MS. The point of strength of the technique is indeed the low energy barrier for the desorption of the fluorinated ligands from the NPs surface, which allows to employ very mild laser intensities, resulting consequently in very low degree of fragmentation of the analyte. However, this liability of the bonds involving gold atoms bounded to sulphur atoms belonging to fluorinated thiolates towards lasers employed in this type of experiments represents the major obstacle to the study of monolayer composition and morphology through MALDI-TOF MS for fluorinated MM Au NPs. Indeed, since the desorption of fluorinated ligands from the gold occurs even at the lowest laser intensities, the results are undoubtedly biased from this

adverse phenomenon, providing results that strongly deviate from the one obtained by other techniques, as the outcomes herein presented demonstrate.

3.2 MALDI-TOF MS experiments on C16/F6 Au NPs

Figure 6.24 reports the MALDI-TOF mass spectrum of a batch of MM Au NPs protected by hexadecanethiolates and 1H,1H,2H,2H-perfluorooctanethiolates. The batch is soluble only in chloroform, which was the solvent employed for preparing the sample. As previously explained, DCTB matrix was chosen since it is suitable for non-polar ligands, as hexadecanethiols and 1H,1H,2H,2H-prfluorooctanethiol are. The spectrum was recorded in linear negative mode, keeping in mind the scarce will of fluorinated species to be ionized forming positively charged species. The mass range investigated is the one from 500 Da to 6000 Da.

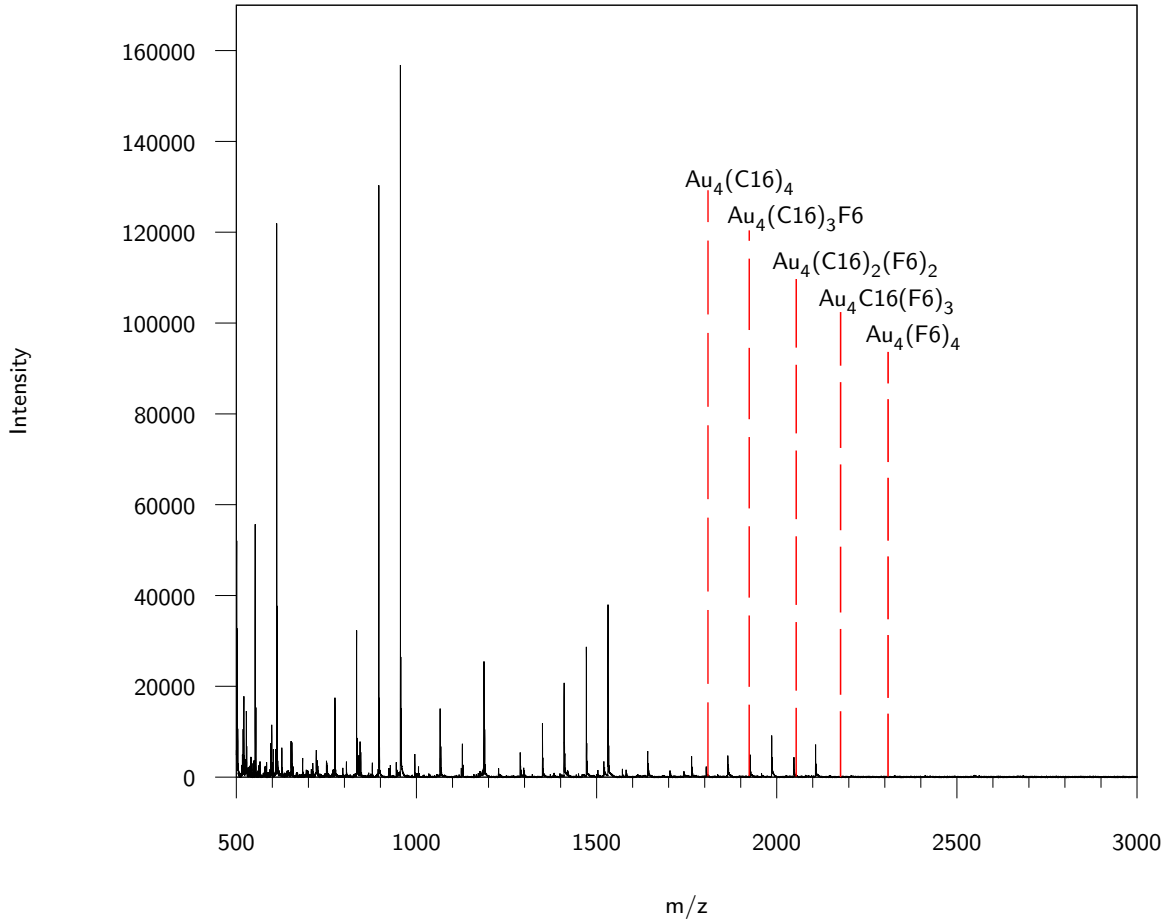

Figure 6.24: MALDI-TOF mass spectrum of C16/F6 Au NPs.

No peaks referring to Au_4L_4 complexes can be pointed out in the mass spectrum. The red dashed lines refer to the points in the spectrum where the peaks of Au_4L_4 complexes should be. Table 6.1 reports the theoretical masses for the Au_4L_4 complexes composed of C16 and F6 ligands.

Table 6.1: Theoretical masses of Au_4L_4 complexes composed of C16 and F6 thiolates.

Complex	**Mass (g/mol)**
$Au_4(C16)_4$	1817.72
$Au_4(C16)_3F6$	1939.38
$Au_4(C16)_2(F6)_2$	2061.04
$Au_4C16(F6)_3$	2182.70
$Au_4(F6)_4$	2304.36

As a matter of fact, only some of the peaks ascribable to Au_xL_{x+1} and $Au_{x+1}L_x$ complexes are visible. Therefore, no precise information concerning the ratio of the two ligands could be obtained from this analysis. Nevertheless, by considering the different patterns of molecular weights pertaining to Au_xL_{x+1} and $Au_{x+1}L_x$ complexes, the most abundant peak within each pattern pertains to wholly fluorinated complexes. On the other hand, partially hydrogenated complexes give peaks whose intensities are rather low. Once again, this result does not match with what has been established by means of ^{1}H-NMR analysis on a part of decomposed Au NPs. Indeed, the ^{1}H-NMR outcomes stated that the percent amount of fluorinated species in the monolayer of these Au NPs is 35%. Therefore, according to MALDI-TOF MS there is a predominance of fluorinated ligands that does not reflect the ratio established through ^{1}H-NMR. This evidence suggests that hydrogenated ligands scarcely tend to form negatively charged species, whereas fluorinated ligands are more willing to acquire electrons rather than losing them. This different behaviour leads to a sensible bias in MALDI-TOF MS analysis, since detecting the positively charged complexes brings to a lack of fluorinated ligands with respect to their hydrogenated counterpart; on the other hand, the results are once again hampered by detecting the anions, as a considerable part of hydrogenated ligands is not easily negatively charged and therefore detected by the instrument.

CHAPTER 7

Conclusions

The results herein presented constitute a preliminary investigation on the conditions for achieving a certain degrees of control over the process of self-assembly among functional Au NPs in organic means and Au NPs protected by hydrogenated and fluorinated mixed monolayers in aqueous environment.

For what concerns the first part, several synthetic procedures of Au NPs protected by dodecanethiolates and characterized by narrow size distribution have been tested in order to achieve a certain control both over the dimensions of the gold core and the chemical behaviour of the NPs that would eventually be functionalized for controlled self-assembly purposes. The procedure proposed by the group of G.D. Stucky[86] provided satisfying results both in terms of modulation of the core sizes according to the synthetic conditions employed and in terms of size distribution of gold cores themselves. However, in-depth ^{1}H-NMR studies on those NPs outlined the presence of triphenylphosphine-related leftovers within the monolayer of the NPs produced. Furthermore, the NPs prepared following this procedure underwent digestive ripening during place exchange reactions, evidencing a certain instability of the NPs themselves, probably due to the triphenylphosphine-based residues that alter the overall packing of the monolayer. The synthesis[87] proposed by Peng and co-workers involving the use of oleylamine as capping agent led to outcomes that fulfilled the requisite of narrow size distribution. Moreover, the possibility of tuning the dimensions of the gold core by varying the reaction temperature represents an aspect that makes the approach versatile. As a matter of fact, although the lability of the gold-nitrogen bond could be exploited for ligands exchange with the desired thiols, it introduces an intrinsic instability to the overall system that in certain case resulted in decomposition of Au NPs during place exchange reactions. Finally, the *post*-synthesis heat treatment[85] on Au NPs proposed by the group of Miyake successfully provided batches of Au NPs whose size distributions were slightly higher than those achieved with the other tested methods. Nevertheless, the batches of Au NPs prepared following the Miyake approach were the ones undergone fast place exchange reactions for controlled functionalization, since they did exhibit instability issues nor presence of adventitious contaminants.

The fast place exchange reactions were performed on Au NPs protected by dodecanethiolates prepared by means of Miyake method, meaning at introducing terpyridine-terminating thi-

ols in specific sites of the monolayer of the NPs so that producing substrates for controlled self-assembly. Different molar ratio between entering thiol and Au NPs were tested and the results analysed through UV-Visible spectroscopy and TEM after triggering complexes formation by the addition of $Fe(BF_4)_2$. Higher molar ratios brought to almost complete substitution of dodecanethiolates in favour of terpyridine-terminating thiolates, avoiding any possibilities of control over the geometry of the superstructures formed, evidenced also by TEM outcomes that displayed random and large aggregatres of Au NPs. Lower molar ratios led to a situation where the molar amount of terpyridine units was closer to the limit of detection of the techniques exploited for the analyses. Obviously, further experiments must be performed taking into account the screening of the effects of changing other reaction conditions such as temperature and time, so to reach a more complete understanding of the system. This emerged as a fundamental pre-requisite for assessing the feasibility of the overall approach, especially considering of reactive centres that may be required to attain controlled self assembly and the challenge of a precise analytical quantification of interacting points per NP.

The experiments involving the assembly of tetrahedral superstructures of fluorinated Au NPs in aqueous environment outlined the complexity of the whole system: indeed, cryo-TEM analyses of the outcomes from the attempts for the fluorophilic-interactions-driven self-assembly of 3.6 nm MDDS/F6 Au NPs with 1.5 nm C8TEG/F6 Au NPs evidenced a tendency of the latter NPs to interact among themselves rather than with the 3.6 nm ones, giving rise to chaotic and random superstructures. This behaviour could be due to the null solubility of the C8TEG/F6 Au NPs in water, leading to preferential dissolution of the NPs themselves in residues of trifluoroethanol used for their dissolution. As a matter of fact, the emulsions of this latter organic solvent could have been formed during the sonication process before sample preparation. Consequently, the addition of fluorinated species as trifluoroethanol to the aqueous environment may have interfered with the process of self-assembly. No organised superstructures were evidenced during cryo-TEM analyses, then.

By using a different MM Au NP probes consisting in NPs with a controlled number of fluorinated tails, it was possible to circumvent the problems related to the use of fluorinated solvents. HR-TEM results highlighted several superstructures composed of 3.6 nm MDDS/F6 Au NPs and the NPs bearing the fluorinated tails within 3.1 nm from the boundaries of the gold cores of the first NPs, which was the distance of interaction established on considerations related to chain lengths. Tomography experiments may help to reconstruct the three-dimensional extensions of the superstructures visualised and establish more precisely the distances between 3.6 nm MDDS/F6 Au NPs and MM Au NPs with fluorinated tails located at different planes. Furthermore, liquid-phase electron microscopy could represent the perfect technique to assess whether the interactions observed at the solid state during HR-TEM investigations arise in solution as well or not.

MALDI-TOF MS experiments on MM Au NPs protected by blends of fluorinated and hydrogenated thiolates using conventional matrices provided data that pointed out a criticality in analysing fluorinated Au NPs. Indeed, although the MALDI-TOF mass spectrum of Au NPs protected by C8TEG thiolates displayed the presence of $Au_4(C8TEG)_4$ complex as the most abundant specie, the mass spectra of MM Au NPs protected by mixtures of fluorinated and hy-

drogenated thiolates and wholly fluorinated Au NPs reported a predominant presence of free ligands or mixed and homogeneous disulphides. Consequently, neither the ratio between the two types of ligands established by means of MALDI-TOF MS matched the ratio established through ^{1}H-NMR spectroscopy nor it was possible to gather information on the morphology of MM Au NPs. A possible explanation for this behaviour could be related to the reduced energy barrier for the desorption of fluorinated ligands from the surface to the gold core, leading to preferential desorption of fluorinated ligands as such rather than bound to gold atoms, even at low laser intensities. More studies are needed to point out whether there are suitable conditions that allow to achieve reasonable outcomes from MALDI-TOF MS analyses on hydrogenated and fluorinated MM Au NPs. Those outcomes could then be used to fill the gap with the NMR results and implement a correct methodology to predict the morphology of this type of MM Au NPs.

21

Part III

Experimental Details

Experimental Details

General Information

All reagents employed were bought from Merck and Alfa Aesar and used without purification, unless where indicated. Solvents were purchased from Merck and VWR. Deuterated solvents were bought from Merck and Cambridge Isotope Laboratories. Chlorinated solvents employed for dissolving Au NPs were treated with K_2CO_3 before use. Reactions were monitored by TLC on Merck silica gel plates (0.25 mm) and visualized by UV light, $KMnO_4-H_2SO_4$ or Pancaldi solution. Flash column chromatography was performed on Normasil silica gel 60® 40-63 μm purchased from VWR. All the glassware employed for the synthesis of Au NPs and Au clusters was cleaned with aqua regia and copiously rinsed with mQ water before use.

Nuclear Magnetic Resonance spectra were recorded on a Varian 400 spectrometer and a Varian 500 spectrometer, operating respectively at 400 MHz and 500 MHz for proton. The NMR spectra have been processed by means of MestReNova software. ^{1}H-NMR spectra were referenced to the residual protons in the deuterated solvent. ^{13}C-NMR spectra were referenced to the solvent chemical shift. Chemical shifts (δ) are reported in ppm and the multiplicity of each signal is identified by the conventional abbreviations: s for singlet, d for doublet, t for triplet, q for quartet, m for multiplet, br for broad peak. Coupling constants (J) are reported in Hertz (Hz).

Mass spectrometry measurements on ligands were performed by means of electrospray ionization (ESI) technique on a Perkin Elmer APII instrument operating at 5600 eV and recorded by Dr. Fabio Hollan at the Department of Chemical and Pharmaceutical Sciences of the University of Trieste, Italy. All MALDI-TOF mass spectra on Au NPs have been recorded using a Bruker AutoFlex Speed instrument (Bremen, Germany) installed at the *Batochime* of the University of Lausanne, Switzerland. The MALDI-TOF MS spectra have been collected using flexAnalysis software and elaborated with flexControl software. The integrations of multiple peaks have been carried out by means of Origin 2016 software. The matrices employed were bought from Merck.

UV-Visible spectroscopy analyses were carried out on a Perkin Elmer Lambda 35 spectrophotometer having a scanning speed of 240 nm·min^{-1} and a slit amplitude of 2 nm, using quartz cuvettes whose optical path was 10 mm.

Transmission Electron Microscopy images were collected by means of a Philips EM 208 Electron Microscope operating at 100 kV equipped with 11 MegaPixel bottom-mounted CCD Olympus Quemesa camera with the assistance of Dr. Paolo Bertoncin at University of Trieste or through a JEOL 3010 High-Resolution Electron Microscope operating at 300 kV using a Gatan

slow-scan CCD camera by Professor Stefano Polizzi at University Ca' Foscari of Venice. Cryo-TEM experiments have been performed on a FEI Tecnai F20 Cryo at CIME (*Centre Interdisciplinaire de Microscopie Électronique*) at EPFL. Samples for Cryo-TEM were prepared employing a Cryoplunge system and carbon-coated copper grids were discharged from any residual electrostatic charge prior to use. All TEM images have been analysed through ImageJ software.
Thermogravimetric Analyses were performed on a Netzsch STA 409 instrument using alumina crucibles and a heating rate of 10 °C·min^{-1} up to 650 °C·min^{-1}.

Synthesis of Au NPs and ligands presented in Chapter 4

Synthesis of Au NPs protected by C12

The synthesis was performed following literature procedures.[86,128]
A graphical representation of these Au NPs is depicted in Figure 7.1.

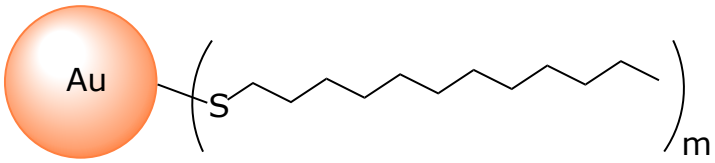

Figure 7.1: Drawing of Au NPs protected by dodecanethiolates.

Synthesis of C12-Au NPs in benzene

Procedure A In a 100 mL round-bottom flask, 0.1237 g (0.25 mmol) of $AuPPh_3Cl$ were dissolved in 20 mL of benzene at RT. 0.125 mL (0.52 mmol) of dodecanethiol were then added to the solution. After five minutes, 0.218 g (2.5 mmol) of borane tertbutylamine complex were added as a solid powder at room temperature. The colour of the solution turned to pale brown. Afterwards, the mixture was stirred for 1 hour at 55 °C and then cooled at room temperature. After few seconds of heating, the solution took a black-purple colour. The resulting solution was transferred in a 50 mL Falcon tube. The Au NPs were precipitated with EtOH and the so-obtained suspension centrifuged (4000 rpm, 10 min, 25 °C); the supernatant was removed and the Au NPs were washed twice more with MeOH (20 mL) and then twice with acetone (20 mL). After each wash, the suspension was centrifuged (4000 rpm, 10 min, 25 °C) and the supernatant discarded. The Au NPs were so dissolved in $CHCl_3$ and the solvent was subsequently evaporated by means of a gentle Ar flux. The solid residue was wash with methanol (4x20 mL). 45 mg of Au NPs were obtained as a black solid.
UV-Vis ($CHCl_3$): defined SPB at about 519 nm. ^{1}H-NMR (400 MHz, $CDCl_3$): δ: 1.27 (br, $(CH_2)_9$); 0.89 (br, CH_3). TEM: Average diameter of 6.4 nm, σ = 1.0 nm, σ^* = 0.16 count over 300 NPs.

Procedure B In a 100 mL round-bottom flask, 0.062 g (0.125 mmol) of $AuPPh_3Cl$ were dissolved in 10 mL of benzene at RT. 62.5 μL (0.26 mmol) of dodecanethiol were added to the limpid solution. Then, 10 mL of a 0.125 M solution of borane tertbutylamine complex dissolved in benzene were poured into the round-bottom flask at room temperature and the mixture was stirred for 4 h. During this period of time, the colour of the solution turned from colorless

to black-brown. EtOH was then added to the content of the round-bottom flask in order to precipitate the NPs. The mixture was stored in freezer overnight, favouring the process of precipitation. The day after, the suspension was transferred in a 50 mL Falcon tube and centrifuged (4000 rpm, 10 min, 25 °C). The supernatant was subsequently discarded and the Au NPs were washed once with EtOH (20 mL), then once with MeoH (20 mL) and finally twice with acetone (2x20 mL). After each wash, the suspension was centrifuged (4000 rpm, 5 min, 25 °C) and the supernatant discarded. The Au NPs were therefore dissolved in $CHCl_3$ and the solvent rapidly evaporated by a gentle Ar flux. The blackish-purple solid was washed again with methanol (2x20 mL) and finally acetone (2x20 mL). 13 mg of Au NPs were obtained as a black solid.
UV-Vis ($CHCl_3$): defined SPB at about 522 nm. ^{1}H-NMR (400 MHz, $CDCl_3$): δ: 1.27 (br, $(CH_2)_9$); 0.89 (br, CH_3). TEM: Average diameter = 6.6 nm, σ = 0.9 nm, σ^* = 0.14 count over 300 NPs.

Synthesis of C12-Au NPs in toluene

In a 50 mL round-bottom flask, 0.05 g (0.1 mmol) of $AuPPh_3Cl$ was dissolved in 10 mL of toluene at RT. 190 μL (0.8 mmol) of dodecanethiol were added to the solution that was therefore stirred and heated at 100 °C for 5 minutes. In the meantime, 0.087 g (1 mmol) of borane tert-buthylamine complex were dissolved in 6 mL of toluene and this second solution was stirred and heated at 100 °C as well. Then, the solution containing the reducing agent was poured into the round-bottom flask containing the first solution. The whole mixture was stirred and heated at 100 °C for 3 minutes, after which it was cooled to room temperature. The so-obtained solution was transferred in a 50 mL Falcon tube and the precipitation of the Au NPs was promoted by the addition of EtOH. The resulting suspension was centrifuged (4000 rpm, 10 min, 25 °C); the supernatant was removed and the Au NPs were washed with MeOH (2x20 mL) and acetone (2x20 mL). After each wash, the suspension was centrifuged (4000 rpm, 10 min, 25 °C) and the supernatant discarded. The Au NPs were redissolved in $CHCl_3$ and the solvent was removed by a gentle Ar flux. The resulting solid was washed again with MeOH (4x20 mL). 12 mg of Au NPs were obtained as a black solid.
UV-Vis ($CHCl_3$): defined SPB at about 518 nm. ^{1}H-NMR (400 MHz, $CDCl_3$): δ: 1.27 (br, $(CH_2)_9$); 0.89 (br, CH_3). TEM: Average diameter = 5.8 nm, σ = 0.3 nm, σ^* = 0.05, count over 300 NPs.

Synthesis of C12-Au NPs in $CHCl_3$

In a 50 mL round-bottom flask, 0.05 g (0.1 mmol) of $AuPPh_3Cl$ was dissolved in 10 mL of $CHCl_3$ at RT. 47.5 μL (0.2 mmol) of dodecanethiol were added to the solution. The mixture was then stirred and brought to reflux for 5 minutes. In the meantime, 0.087 g (2 mmol) of borane tertbuthylamine complex were dissolved in 6 mL of $CHCl_3$ and this second solution was stirred and brought to reflux as well. Then, the solution containing the reducing agent was added to the first solution. The whole mixture was stirred at reflux for 36 minutes, after which it was cooled to room temperature. The mixture was then transferred in a 50 mL Falcon tube and the precipitation of the NPs was triggered by the addition of EtOH. The precipitation was hard to trigger at RT; consequently, the mixture was placed at -18 °C for one hour. The so-obtained suspension was centrifuged (4000 rpm, 10 min, 25 °C) and the supernatant discarded.

The Au NPs were washed with MeOH (2x20 mL) and acetone (2x20 mL). After each wash, the suspension was centrifuged (4000 rpm, 5 min, 25 °C) and the supernatant discarded. The Au NPs were dissolved in $CHCl_3$ and then the solvent removed by a gentle Ar flux. The remaining solid was washed again with EtOH (4x20 mL). 26 mg of Au NPs were obtained as a black solid. UV-Vis ($CHCl_3$): defined SPB at about 508 nm. ^{1}H-NMR (400 MHz, $CDCl_3$): δ: 1.27 (br, $(CH_2)_9$); 0.89 (br, CH_3). TEM: Average diameter = 4.2 nm, σ = 0.6 nm, σ^* = 0.14, count over 300 NPs.

Synthesis of C12-Au NPs in THF

In a 100 mL round-bottom flask, 0.1 g (0.2 mmol) of $AuPPh_3Cl$ was dissolved in 20 mL of THF at RT. 96 μL (0.4 mmol) of dodecanethiol were added to the solution. The mixture was then stirred and heated at 65 °C for 5 minutes. In the meantime, 0.174 g (2 mmol) of borane tertbuthylamine complex were dissolved in 12 mL of THF and this second solution was stirred and heated at 65 °C as well. Then, the solution containing the reducing agent was added to the first solution. The whole mixture was stirred and heated at 65 °C for 36 minutes, after which it was cooled to room temperature. The mixture was then transferred in a 50 mL Falcon tube and the precipitation of the NPs was triggered by the addition of EtOH. The so-obtained suspension was centrifuged (4000 rpm, 10 min, 25 °C) and the supernatant discarded. The Au NPs were washed with MeOH (2x20 mL) and acetone (2x20 mL). After each wash, the suspension was centrifuged (4000 rpm, 5 min, 25 °C) and the supernatant discarded. The Au NPs were dissolved in $CHCl_3$ and then the solvent removed by a gentle Ar flux. The remaining solid was washed again with EtOH (4x20 mL). 26 mg of Au NPs were obtained as a black solid. UV-Vis ($CHCl_3$): defined SPB at about 515 nm. ^{1}H-NMR (400 MHz, $CDCl_3$): δ: 1.27 (br, $(CH_2)_9$); 0.89 (br, CH_3). TEM: Average diameter = 4.1 nm, σ = 0.3 nm, σ^* = 0.07, count over 300 NPs.

Synthesis of Au NPs protected by OLAM

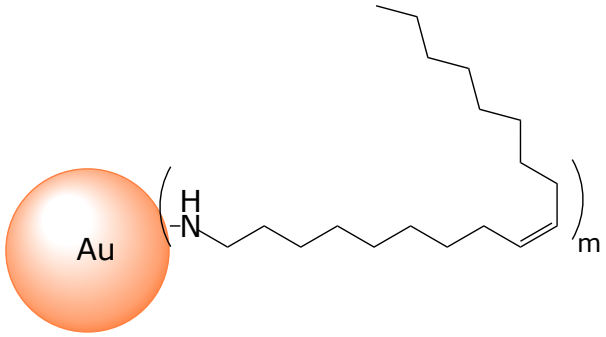

Figure 7.2: Drawing of Au NPs protected by oleylamine.

The references for the synthesis are Peng *et al.*, 2008[87], Wu *et al.*, 2013[90] and Wrasman *et al.*, 2018[92]. Slight modifications to the already reported procedures were made and they are herein specified. The following is a general procedure that has been performed several times for obtaining different batches of Au NPs protected by OLAM. For synthetic details, such as temperature and solvent, and their effects on the outcome of the synthesis refer to Chapter 4.
0.098 g (0.25 mmol) of $HAuCl_4 \cdot 3\,H_2O$ were dissolved in 10 mL of OLAM (technical grade, 70%

or higher) and 1-octadecene (technical grade, 90% or higher) at the desired temperature under an Ar flow. A reducing solution of 0.043 g (0.5 mmol) of borane *tert*-butylamine complex has been prepared in 1 mL of oleylamine and 1 mL of 1-octadecene. The resulting mixture was sonicated for few minutes, so that completely dissolving TBAB. As soon as $HAuCl_4 \cdot 3\,H_2O$ dissolved in the OLAM:1-octadecene mixture, the reducing solution was rapidly injected into the reactor. The colour of the solution slowly moved from orange to dark purple or dark red, according to the dimensions of the gold core. The so-obtained solution was stirred for 1 hour at the desired temperature. Thereupon, the Au NPs were transferred in a 50 mL Falcon tube and precipitated by adding a 5:1 ethanol:isopropanol mixture; the suspension was therefore centrifuged (4500 rpm, 10 minutes, 25 °C) and the NPs were redispersed in hexane. The precipitation procedure was repeated once more. The NPs were finally redissolved in hexane and stored in solution at 4 °C. The overall procedure allows to obtained rather monodisperse batch of Au NPs protected by oleylamine; the size of the gold core can be tuned by adjusting the reaction temperature. The modifications related to the synthesis concern the grade of purity of oleylamine, since Wu and coworkers[90] used oleylamine at 80-90% grade, and the solvent, as Wrasman and coworkers[92] used 1,2,3,4-tetrahydronaftalene instead of 1-octadecene. The synthesis can also be performed in hexane, with similar result.
For TEM characterization of the batches of Au NPs prepared following this procedure see Chapter 4, Section 2.1.4.

Place Exchange Reaction on Au NPs protected by OLAM

The place exchange was performed by considering the work of Kluenker and coworkers[131] as starting point. 20 mL of a 2 mg/mL solution of (3.4 ± 0.4) nm OLAM capped Au NPs in deoxygenated toluene was treated with 600 molar excess (approximately 6.8 g) of C12 thiols. The reaction was carried on for three and a half days, at 25 °C, covered from light. Passed the desired amount of time, the NPs were precipitated by adding MeOH. The suspension was therefore centrifuged (4500 rpm, 10 minutes, 20 °C); the NPs were redissolved in hexane and reprecipitated by adding EtOH. The suspension was once more centrifuged (4500 rpm, 5 minutes, 20 °C) and the supernatant discarded. The solid NPs were washed several times with EtOH; however, ^{1}H-NMR spectrum exhibited the presence of residual thiol. A LH-20 Sephadex colomun has been performed in order to remove the excess of thiol, without appreciable success.

Synthesis of Au NPs protected by C12 and their growth by heat treatment

The reference for the synthesis is Shimizu *et al.*, 2003.[85] 0.153 g (0.388 mmol) of $HAuCl_4 \cdot 3\,H_2O$ were dissolved in 38.6 mL of mQ water. This latter solution was added to 103.3 mL of a solution containing 0.425 g (0.781 mmol) of tetraoctylammonium bromide in toluene. The resulting mixture was vigorously stirred. The yellow aqueous solution became colorless while the toluene phase turned red. The two-phases mixture was then transferred in a separating funnel and the organic layer was separated from the aqueous one. A solution containing 0.157 g (0.776 mmol) of dodecanthiol in 11.5 mL of toluene was added to the organic solution and stirred at RT for 10 minutes. A freshly prepared aqueous solution of 0.147 g (3.88 mmol) of $NaBH_4$ in 38.6 mL of mQ water was rapidly added under vigorous stirring and the resulting mixture was stirred for

18 h at RT. After the separation of the two layers, the organic phase was removed at reduced pressure. The crude solid was heat-treated at 154 °C at the heating rate of 2 °C·min^{-1} and held for 30 minutes at this temperature. The heat-treated product was subsequently dissolved in 45 mL of toluene and 0.121 g (0.6 mmol) of dodecanethiol were added. The so-obtained solution was stirred overnight at RT. Most of the solvent was removed by rotary evaporator; the concentrated raw product was transferred in a 50 mL Falcon tube and MeOH was added to precipitate the NPs. The suspension was centrifuged (4000 rpm, 10 minutes, 25°C) and the supernatant discarded. The solid was washed five more times with MeOH and twice more with acetone. After each washing, the suspension was centrifuged (4000 rpm, 10 minutes, 25 °C) and the supernatant was discarded. The total amount of product obtained was 80 mg.
^{1}H-NMR (400 MHz, $CDCl_3$): δ: 1.27 (br, $(CH_2)_9$); 0.89 (br, CH_3). TEM: Average diameter = 4.2 nm, σ = 0.8 nm, σ^* = 0.19, count over 1000 NPs.

Synthesis of *S*-(12-bromododecyl)ethanethioate

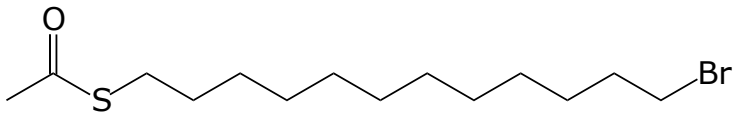

Figure 7.3: Chemical structure of *S*-(12-bromododecyl)ethanethioate.

2.87 g (8.76 mmol) of 1,12-dibromododecane and 0.25 g (2.19 mmol) of potassium thioacetate were transferred in a 100 mL round-bottom flask. 28 mL of freshly distilled dry acetone were poured inside the round-bottom flask *via* canula transfer. The resulting mixture was then heated at reflux and stirred overnight under an Ar atmosphere, covered from light. The mixture was filtered on filter paper and the raw product was purified through flash column chromatography (silica gel, eluent: gradient of petrolium ether/DCM, from 100/0 to 80/20). 0.493 g of pure product were recovered. Yield: 69.4 %.
^{1}H-NMR (400 MHz, $CDCl_3$): δ: 3.35 (t, 2H, J = 6.9, $C\underline{H}_2-Br$); 2.81 (t, 2H, J = 7.3, $C\underline{H}_2-S$); 2.27 (s, 3H, $S-CO-C\underline{H}_3$); 1.86-1.71 (m, 2H, $C\underline{H}_2-CH_2S$); 1.56-1.46 (m, 2H, $C\underline{H}_2-CH_2Br$); 1.42-1.17 (m, 16H, $-(C\underline{H}_2)_8-$).

Synthesis of *S*-(12-([2,2′:6′,2″-terpyridin]-4′-yloxy)dodecyl) ethanethioate

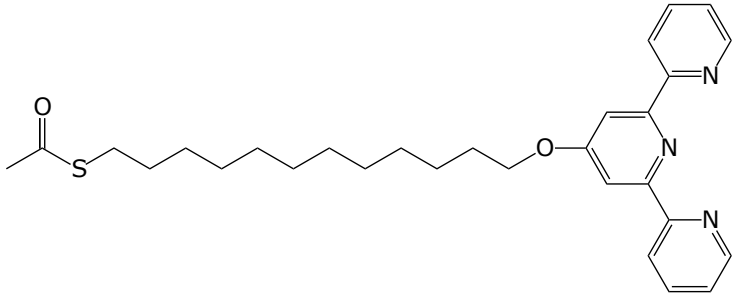

Figure 7.4: Chemical structure of *S*-(12-([2,2′:6′,2″-terpyridin]-4′-yloxy)dodecyl) ethanethioate.

0.473 g (1.46 mmol) of *S*-(12-bromododecyl)ethanethioate, 0.401 g (1.61 mmol) of [2,2′:6′,2″-terpyridin]-4′(1′*H*)-one , 0.445 g (3.22 mmol) of potassium carbonate and 0.01 g (0.06 mmol) of potassium iodide were transferred in a 250 mL three-neck round-bottom flask. 63 mL of freshly distilled dry acetone were poured inside the round-bottom flask *via* canula transfer. The so-obtained mixture was heated at reflux and stirred for 23 hours under an Ar atmosphere, protected from light. Afterwards, the mixture was filtered on filter paper and the raw product was recrystallized from hexane. 0.545 g of pure product were obtained. Yield: 76 %.
^{1}H-NMR (500 MHz, $CDCl_3$): δ: 8.86 (d, 2H, J = 4.0, Terpy); 8.59 (d, 2H, J = 8.0, Terpy); 7.99 (s, 2H, Terpy); 7.81 (m, 2H, Terpy); 7.29 (m, 2H, Terpy); 4.19 (t, 2H, J = 6.4, $C\underline{H}_2-$OTerpy); 2.81 (t, 2H, J = 7.3, $C\underline{H}_2-$S); 2.27 (s, 3H, S$-$CO$-C\underline{H}_3$); 1.86-1.71 (m, 2H, $C\underline{H}_2-CH_2$S); 1.63-1.25 (m, 2H, $C\underline{H}_2-CH_2-$OTerpy); 1.52-1.21 (m, 16H, $-(C\underline{H}_2)_8-$). ^{13}C-NMR (125 MHz, $CDCl_3$): δ: 196.04, 167.36, 157.01, 156.21, 149.01, 136.75, 123.75, 121.32, 107.40, 77.26, 68.21, 30.64, 29.54, 29.53, 29.49, 29.46, 29.30, 29.17, 29.11, 29.03, 28.82, 25.94.

Synthesis of 12-([2,2′:6′,2″-terpyridin]-4′-yloxy)dodecane-1-thiol

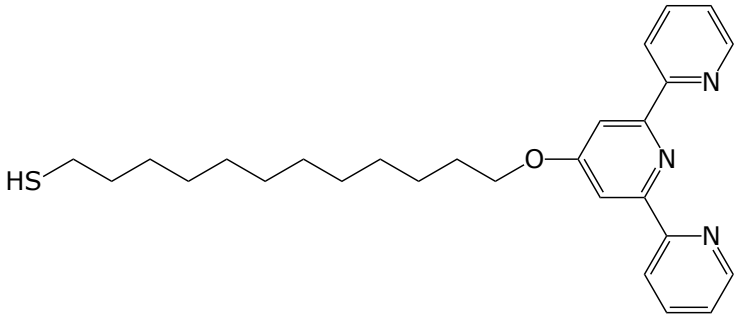

Figure 7.5: Chemical structure of 12-([2,2′:6′,2″-terpyridin]-4′-yloxy)dodecane-1-thiol.

The synthesis has been taken from Norsten *et al.*, 2002.[51]
0.123 g (0.25 mmol) of *S*-(12-([2,2′:6′,2″-terpyridin]-4′-yloxy)dodecyl) ethanethioate were dissolved in 6.5 mL of a solution obtained by mixing 3.75 mL of THF which was previously distilled over Na and benzophenone and 2.75 mL of deoxygenated MeOH. 1 mL of a 0.57 M solution of MeONa in MeOH were subsequently added to the mixture, which was therefore stirred for two hours at RT, under an Ar atmosphere and protected from light. The reaction was then quenched by adding 15 mL of a saturated aqueous solution of NH_4Cl. The organic layer was removed by rotary evaporator and the aqueous residues containing the product were transferred in a separating funnel. Six extractions with CH_2Cl_2 were performed and the reunited organic fractions were dried over Na_2SO_4 and filtered on filter paper. The solvent was removed under vacuum and the product dried in vacuum pump. The product required no further purifications, as from NMR analysis. Final amount of product obtained: 102 mg. Yield: 91 %.
^{1}H-NMR (400 MHz, $CDCl_3$): δ: 8.86 (d, 2H, J = 4.0, Terpy); 8.59 (d, 2H, J = 8.0, Terpy); 7.99 (s, 2H, Terpy); 7.81 (m, 2H, Terpy); 7.29 (m, 2H, Terpy); 4.19 (t, 2H, J = 6.4, $C\underline{H}_2-$OTerpy); 2.49 (m, 2H, $C\underline{H}_2-$SH); 1.86-1.76 (m, 2H, $C\underline{H}_2-CH_2$SH); 1.63-1.25 (m, 2H, $C\underline{H}_2-CH_2-$OTerpy); 1.52-1.21 (m, 16H, $-(C\underline{H}_2)_8-$). MS-ESI (CH_3OH) M/Z: 450.3 [M^+].

Place exchange reaction on Au NPs protected by C12 with Terpy-terminating ligands

First batch 100 μL of a 16.4 mg/mL (36 mM) solution of 12-([2,2':6',2''-terpyridin]-4'-yloxy)dodecane-1-thiol in DCM were added to 300 μL of a 20 mg/mL solution of (4.2$\pm$0.8) nm Au NPs protected by C12 in DCM. The final concentration of Au NPs in solution was then 15 mg/mL. The reaction was carried out inside a 2 mL glass vial for 15 minutes at 25 °C. The reaction was then stopped, the solvent removed by means of an Ar flux and the solid residue copiously washed with EtOH.

Second batch 40 μL of a 2.1 mg/mL (4.5 mM) solution of 12-([2,2':6',2''-terpyridin]-4'-yloxy)dodecane-1-thiol in DCM were added to 125 μL of a 20 mg/mL solution of (4.2$\pm$0.8) nm Au NPs protected by C12 in DCM. The reaction was carried out inside a 2 mL glass vial for 15 minutes at 25 °C. The reaction was then stopped, the solvent removed by means of an Ar flux and the solid residue copiously washed with EtOH.

Third batch 22 μL of a 16.4 mg/mL (0.036 M) solution of 12-([2,2':6',2''-terpyridin]-4'-yloxy)dodecane-1-thiol in DCM were added to 750 μL of a 20 mg/mL solution of (4.5$\pm$1) nm Au NPs protected by C12 in DCM. 228 μL of DCM were then added to reach a final concentration of NPs of 15 mg/mL. The reaction was carried out inside a 2 mL glass vial for 15 minutes at 25 °C. The reaction was then stopped, the solvent removed by means of an Ar flux and the solid residue copiously washed with EtOH.

Synthesis of Au NPs and ligands presented in Chapter 5

Synthesis of MDDS/F6 Au NPs

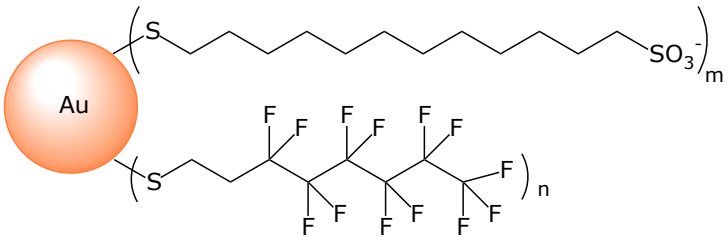

Figure 7.6: Drawing of Au NPs protected by MDDS and F6 thiolates.

The preparation of this batch of Au NPs was performed by Dr. Elena Pellizzoni at the Department of Chemical and Farmaceutical Sciences of the University of Trieste.
In a 50 mL round-bottom flask, 0.1 g (0.2 mmol) of $AuPPh_3Cl$ was added to 15.8 mL of a 1:1 deoxygenated mixture of toluene and EtOH at RT. 15.8 mL of a solution containing 18 mg of MDDS (0.06 mmol) and 15 mg of F6 (0.04 mmol) thiols dissolved in a 1:1 deoxygenated mixture toluene and EtOH were then poured into the same round-bottom flask. The so-obtained suspension was stirred and heated to reflux for 7 minutes under an Ar atmosphere. In the meantime, 0.174 g (2 mmol) of borane tertbuthylamine complex were added to 7.8 mL of the

same 1:1 tolune:EtOH mixture, which was subsequently heated to reflux under an Ar atmosphere. The refluxing reducing solution was then rapidly added to the mixture containing the gold salt and the blends of thiols; the mixture rapidly moved to a black-reddish colour and the reaction was carried on for 3 minutes under an Ar atmosphere. Passed this amount of time, the resulting suspension was cooled to RT and the NPs started to precipitate from the reaction mixture. The suspension was transferred in a 50 mL Falcon tube and centrifuged (4500 rpm, 10 min, 25 °C). The supernatant was discarded and the NPs washed again with a 1:1 mixture of toluene and EtOH, then hot MeOH and finally with the hot 1:1 mixture of toluene and EtOH. After each washing, the suspension was centrifuged (4500 rpm, 5 min, 25 °C). The final amount of NPs obtained was 42.8 mg
^{1}H-NMR (400 MHz, D_2O): δ: 3.1-2.7 (br); 1.7-0.9 (br). TGA: Total percent loss = 18.3 %. TEM: Average diameter = 3.6 nm, σ = 0.6 nm, σ^* = 0.17, count over 300 NPs.

Synthesis of N-1-{2-[2-(2-Methoxyethoxy)ethoxy]ethyl}-8-sulfanyloctanamide (HSC8TEG)

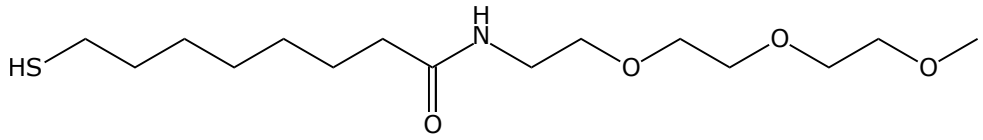

Figure 7.7: Chemical structure of HSC8TEG

In a 50 mL round bottom flask, 0.144 g (0.396 mmol) of AcSC8TEG have been dissolved in 17.2 mL of dry deoxygenated MeOH. This solution has been cooled at 0 °Cand 34.7 mL of a solution of dry HCl in dry deoxygenated MeOH has been added through canula transfer. This latter solution has been prepared by drop-wise addition of 4.3 mL of distilled AcCl in 34.7 mL of dry deoxygenated MeOH at 0 °C. The reaction mixture has been heated to reflux and stirred for 90 minutes. Then, the solvent was removed under reduced pressure. 0.125 g of thiol were obtained in quantitative yield.
^{1}H-NMR: (500 MHz, $CDCl_3$): δ: 6.14 (br, 1H N$\underline{H}$); 3.60-3.50 (m, 10H, (O−C$\underline{H}_2$); 3.50 (m, 2H, C$\underline{H}_2$−NH); 3.33 (s, 3H, O−C$\underline{H}_3$); 2.45 (m, 2H, C$\underline{H}_2$S); 2.12 (t, 2H, J = 8.0, C$\underline{H}_2$−CO; 1.62-1.50 (m, 4H, C$\underline{H}_2$); 1.36-1.22 (m, 6H, C$\underline{H}_2$). ^{13}C-NMR (125 MHz, $CDCl_3$): δ: 173.12, 71.87, 70.40, 70.31, 70.10, 69.94, 69.81, 58.95, 39.07, 36.49, 33.88, 29.10, 28.74, 28.12, 25.57.

Synthesis of C8TEG Au NPs

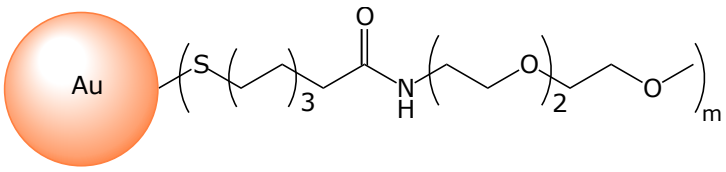

Figure 7.8: Drawing of Au NPs protected by C8TEG thiolates.

The reference for the synthesis is Pengo *et al.* 2003.[133]
0.051 g (0.129 mmol) of $HAuCl_4 \cdot 3\,H_2O$ were weighed under an Ar atmosphere and then transferred into a 250 mL round-bottom flask. The gold salt was then dissolved in 9 mL of deoxygenated mQ water. 0.125 g (0.389 mmol) of HSC8TEG were dissolved in 14.7 mL of dry deoxygenated MeOH; the resulting solution was added to the aqueous solution. The overall solution was stirred at RT for 10 minutes. After the addition of the thiol, the colour of the solution moved from yellow to brown and it progressively lightened. Subsequently, the round-bottom flask was placed inside an ice bath and stirred at 0 °Cfor 15 minutes. 0.055 g (1.47 mmol) of $NaBH_4$ were dissolved in 6.9 mL of deoxygenated mQ water and the so-obtained solution was cooled to 0 °C. This latter solution was added to the first in 10 seconds. The colour of the solution rapidly turned to brown. The solution was stirred at 0 °Cfor 10 minutes and then for 3 hours at RT. Passed this amount of time, the reaction was stopped and MeOH was removed under reduced pressure and the residual aqueous solution has been poured into a separating funnel and treated with a saturated aqueous solution of NaCl. Extractions with CH_2Cl_2 were performed until the aqueous solution was almost colourless. Thereupon, most of CH_2Cl_2 was removed under reduced pressure but the raw product was not brought to dryness. The few remaining drops of water were pipetted-off and the solution was transferred into a 50 mL falcon tube and concentrated by evaporating part of the solvent by means of a gentle Ar flux. The Au NPs were precipitated through the addition of 35 mL of diethyl ether. The so-obtained suspension was centrifuged (4500 rpm, 5 minutes, 20 °C) and then the supernatant discarded. More washing with diethyl ether were performed (8 x 20 mL); after each addition of diethyl ether, the suspension was sonicated, centrifuged (4500 rpm, 5 minutes, 20 °C) and then the supernatant discarded. 44 mg of Au NPs were obtained.
UV-Vis (DCM): small feature at 410 nm, absence of SPB. ^{1}H-NMR (400 MHz, $CDCl_3$): δ: 3.75-3.25 (br), 2.25-2.05 (br), 1.90-1.25 (br). TEM: Average diameter = 1.5 nm, σ = 0.3 nm, σ^* = 0.2, count over 250 NPs.

Synthesis of C8TEG/F6 Au NPs

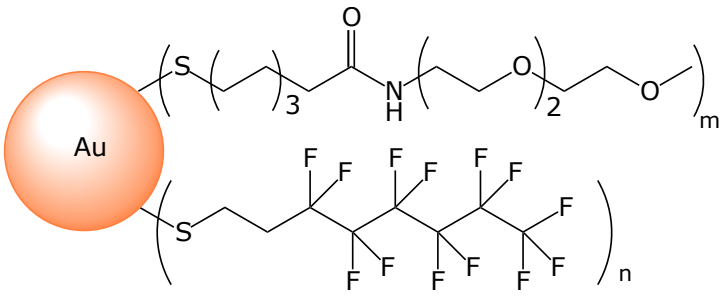

Figure 7.9: Drawing of Au NPs protected by C8TEG and F6 thiolates.

44 mg of Au NPs protected by C8TEG were dissolved in 33.6 mL of deoxygenated iPrOH and transferred into a 100 mL vial. 0.022 g (58 μmol) of 3,3,4,4,5,5,6,6,7,7,8,8,8-tridecafluoro-1-octanethiol (F6) were then added to the solution. The vial was stoppered and the reaction mixture was heated to 40 °C and stirred for two whole days. Once the place exchange reaction was

stopped, the mixture was transferred into a 100 mL round-bottom flask and concentrated, removing most of the solvent under reduced pressure. Afterwards, the solution was transferred into a 50 mL Falcon tube. A large amount of diethyl ether was added so that the precipitation of the Au NPs occurred. The suspension was centrifuged (4500 rpm, 5 minutes, 20 °C). More washings with diethyl ether were performed (8 x 20 mL); after each addition of diethyl ether, the suspension was sonicated, centrifuged (4500 rpm, 5 minutes, 20 °C) and the supernatant discarded. 33 mg of purified Au NPs were obtained.
Solubility behaviour: the so-obtained NPs were only soluble in 3,3,3-trifluoroethanol, the other solubility tests performed in alcohols (MeOH, EtOH, iPrOH), hexane, toluene and chlorinated solvents (chloroform and DCM) provided all negative results. UV-Vis (DCM/TFE=4/1): small feature at 410 nm, absence of SPB. ^{1}H-NMR (400 MHz, CD_2Cl_2/CF_3CD_2OD=4/1): δ: 3.75-3.25 (br), 2.8 (br) 2.25-2.05 (br), 1.90-1.25 (br). ^{19}F-NMR (375 MHz, CD_2Cl_2/CF_3CD_2OD=4/1): δ: -82 (br), from -113.8 to -115.2 (br), from -122.1 to -124.4 (br), -126.8(br). Molar ratio between C8TEG/F6 thiols within the monolayer = 1.8/1 from ^{1}H-NMR NMR analysis on decomposed NPs.

Synthesis of 16-(tritylthio)hexadecanoic acid

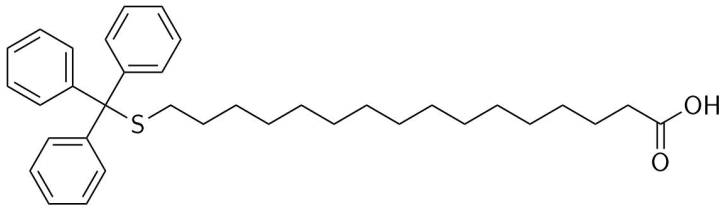

Figure 7.10: Chemical structure of 16-(tritylthio)hexadecanoic acid.

In a 50 mL round bottom flask were introduced 0.307 g (1.06 mmol) of 16-mercaptohexadecanoic acid and 0.297 g (1.06 mmol) of trityl chloride taken-up with 4.0 mL of dry DMF obtaining a white suspension. The mixture was left stirring at room temperature overnight. The heterogeneous mixture was then diluted with 10 mL of distilled water and extracted with ethyl acetate (2 x 50 mL). The organic solution was brought to dryness and 550 mg of thick oil were obtained. The crude material was purified by flash chromatography using a gradient of AcOEt/EP 1/3 to AcOEt/EP 2/3. 373 mg of the product as a white solid were obtained. Yield: 73.6 %.
^{1}H-NMR (400 MHz, $CDCl_3$): δ: 7.40 (d, 6H, J = 7.5), 7.27 (t, 6H, J = 7.0), 7.20 (t, 3H, J = 7.5), 2.34 (t, 2H, J = 7.5), 2.13 (t, 2H, J = 7.5), 1.63 (qt, 2H, J = 7.0), 1.38 (q, 2H, J = 7.5), 1.10-1.37 (m, 22H).

Synthesis of N-[2-(2,5-dioxo-2,5-dihydro-1H-pyrrol-1-yl)ethyl]-16-(tritylthio)hexadecanamide

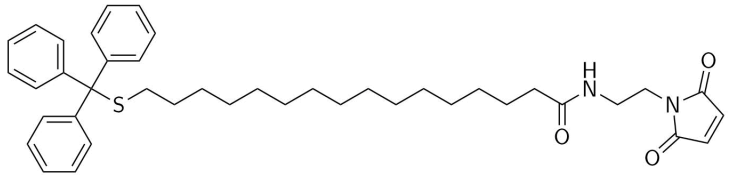

Figure 7.11: Structure of N-[2-(2,5-dioxo-2,5-dihydro-1H-pyrrol-1-yl)ethyl]-16-(tritylthio)hexadecanamide.

In a 50 mL round bottom flask 373 mg (0.70 mmol) of the trityl protected thiol and 114 mg (0.844 mmol) of hydroxybenzotriazole were introduced as solid materials; these were taken-up with 10 mL of dry dichloromethane obtaining a white suspension. To the heterogeneous mixture, 150 mg (0.78 mmol) of EDC were added, obtaining a clear solution. The reaction mixture was left stirring at room temperature for 30 minutes. The maleimide was added as a solid and thereupon 0.29 mL (1.68 mmol) of DIEA were added to the mixture which was left stirring overnight at room temperature. After this time, the mixture was faintly red. The solvent was removed in vacuo and the crude was diluted with 30 mL of AcOEt. The organic solution was extracted with an aqueous solution $KHSO_4$ at 5% (2 x 15 mL), brine (1 x 15 mL), and water (1 x 20 mL). The solution was dried over Na_2SO_4 and the solvent removed obtaining 575 mg of crude product. The crude material was purified by flash chromatography under isocratic conditions obtaining 250 mg of purified product. Yield: 55 %.
^{1}H-NMR (400 MHz, $CDCl_3$): δ: 7.40 (d, 6H, J = 7.5), 7.27 (t, 6H, J = 7.0), 7.20 (t, 3H, J = 7.5), 6.70 (s, 2H), 5.88 (br, 1H), 3.86 (t, 2H, J = 7.5), 3.46 (q, 2H, J = 7.5), 2.14 (m, 4H), 1.55 (m, 2H), 1.38 (q, 2H, J = 7.5), 1.10-1.37 (m, 22H). MS-ESI(CH_3OH) M/Z: 675.4 $(M^+Na)^+$

Synthesis of N-(2-{3-[(3,3,4,4,5,5,6,6,7,7,8,8,9,9,10,10,10-heptadecafluorodecyl)thio]-2,5-dioxopyrrolidin-1-yl}ethyl)-16-(tritylthio)hexadecanamide

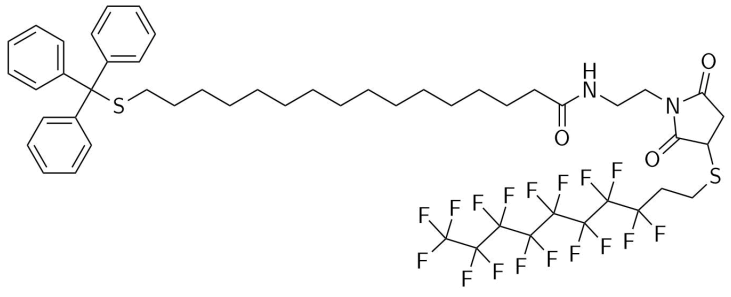

Figure 7.12: Chemical structure of N-(2-{3-[(3,3,4,4,5,5,6,6,7,7,8,8,9,9,10,10,10-heptadecafluorodecyl)thio]-2,5-dioxopyrrolidin-1-yl}ethyl)-16-(tritylthio)hexadecanamide.

In a 25 mL round bottom flask and working under an argon atmosphere, 184 mg (0.28 mmol) of compound protected thiol0and 10 mL of anhydrous DCM were introduced. After the complete dissolution, 30 μL of DIEA were added to the mixture followed by the addition of 85 μL (0.33 mmol) of fluotinated thiol. The mixture was left stirring for 20 minutes. The solvent was

removed and the volatile species were removed under vacuum, obtaining 320 mg of crude material. The crude was purified by flash chromatography under isocratic condition using AcOEt/EP 2/3 as eluent, obtaining 260 mg of product as a white foaming solid. Yield: 80%. ^{1}H-NMR (500 MHz, $CDCl_3$): δ: 7.40 (d, 6H, J = 7.5), 7.27 (t, 6H, J = 7.0), 7.20 (t, 3H, J = 7.5), 5.71 (br, 1H), 3.72-3.63 (m, 3H), 3.49 (m, 2H), 3.23-3.12 (m, 2H), 3.01 (m, 1H), 2.53 (m, 3H), 2.11 (m, 4H), 1.55 (m, 2H), 1.38 (q, 2H, J = 7.5), 1.10-1.37 (m, 22H). MS-ESI (CH_3OH) M/Z: 1155.3 $(M^+Na)^+$

Synthesis of N-(2-{ 3-[(3,3,4,4,5,5,6,6,7,7,8,8,9,9,10,10,10-heptadecafluorodecyl)thio]-2,5-dioxopyrrolidin-1-yl}ethyl)-16-mercaptohexadecanamide

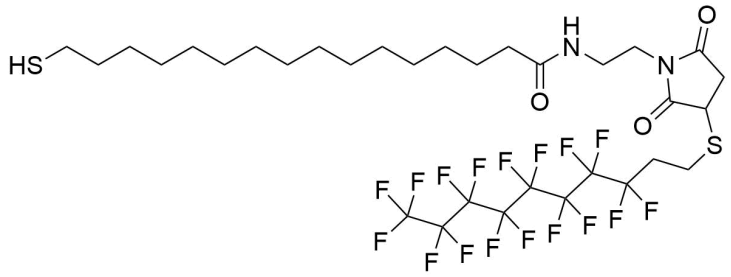

Figure 7.13: Chemica structure of N-(2-{3-[(3,3,4,4,5,5,6,6,7,7,8,8,9,9,10,10,10-heptadecafluorodecyl)thio]-2,5-dioxopyrrolidin-1-yl}ethyl)-16-mercaptohexadecanamide.

In a 5 mL round bottom flask, 24.1 mg (0.021 mmol) of protected thiol were introduce, dissolved in 1.5 mL of anhydrous deoxygenated DCM. To the so-obtained solution, an excess of triisopropylsilane was added (60 μL, 0.3 mmol). The mixture was treated with TFA until no further yellow colour developed, this required the use of 5 μL of TFA corresponding to an amount of 0.065 mmol (3 equivalents respect to the protected thiol) of acid. The solvent was removed in vacuo and the high melting point compounds were stripped under high vacuum. The white residue was treated with deoxygenated hexane (10 x 1.5 mL) to remove triphenylmethane. The material was dried under high vacuum obtaining 16.8 mg of deprotected thiol. Yield: 89 %. ^{1}H-NMR (500 MHz, $CDCl_3$): δ: 5.71 (br, 1H), 3.72-3.63 (m, 3H), 3.49 (m, 2H), 3.23-3.12 (m, 2H), 3.01 (m, 1H), 2.60-2.44 (m, 5H), 2.11 (t, 2H, J = 7.5), 1.55 (m, 2H), 1.38 (q, 2H, J = 7.5), 1.32 (t, 1H, J = 7.5) 1.10-1.37 (m, 22H).

Synthesis of C8TEG Au NPs with fluorinated tails

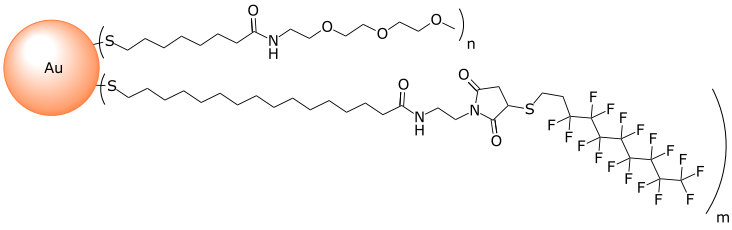

Figure 7.14: Drawing of Au NPs protected by C8TEG and bearing fluorinated tails.

In a screw capped pyrex vial, 10.6 mg ($1.57 \cdot 10^{-7}$ mol) of C8TEG NPs with composition $Au_{223}(C8\,TEG)_{73}$ were introduced, dissolved in 1.8 mL of deoxygenated DCM. To this solution, 180 μL of a 12 mg/mL (13.5 mM) solution of thiol, corresponding to $2.43 \cdot 10^{-6}$ mol, were added. The solution was kept at 40 °C for three days. The solvent was then removed after transferring the reaction mixture in a 15 mL screw capped tube. The residue was washed with diethyl ether (5 x 5 mL) and centrifuged (4000 rpm, 10 min, 25 °C). The residue was dissolved with few drops of DCM, which was afterwards evaporated under argon. The residue therefore was washed with diethyl ether (5 x 5 mL). The process was repeated three times overall. The product was further purified by size exclusion chromatography on Sephadex LH-20 using DCM as eluent. 10.3 mg of NPS were obtained.
^{1}H-NMR (400 MHz, $CDCl_3$): δ: 4.0-3.25 (br), 2.11 (br), 2.0-1.0 (br).

Synthesis of Au NPs presented in Chapter 2.12

The following syntheses were performed by Dr. Maria Şologan at the Department of Chemical and Farmaceutical Sciences of the University of Trieste.

Synthesis of C8TEG Au NPs

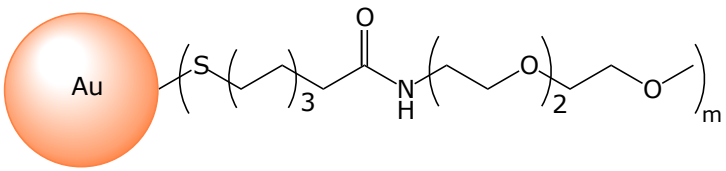

Figure 7.15: Drawing of Au NPs protected by C8TEG thiolates.

0.077 g (0.195 mmol) of $HAuCl_4 \cdot 3\,H_2O$ were weighed under an Ar atmosphere and then transferred into a 250 mL round-bottom flask. The gold salt was then dissolved in 41.3 mL of deoxygenated mQ water. 0.126 g (0.391 mmol) of HSC8TEG were dissolved in 41.3 mL of dry deoxygenated MeOH; the resulting solution was added to the aqueous solution. The overall solution was stirred at RT for 30 minutes. After the addition of the thiol, the colour of the solution moved from yellow to brown and it progressively lightened. Subsequently, the round-bottom flask was placed inside an ice bath and stirred at 0 °Cfor 30 minutes. 0.084 g (2.22 mmol) of $NaBH_4$ were dissolved in 20.6 mL of deoxygenated mQ water and the so-obtained solution was cooled to 0 °C. This latter solution was added to the first in 12 seconds. The colour of the solution rapidly turned to brown. The solution was stirred at 0 °Cfor 30 minutes and then for 2 hours at RT. Passed this amount of time, the reaction was stopped and the solvent was removed under reduced pressure. The residue was dissolved in CH_2Cl_2 and transferred into a 50 mL Falcon tube and concentrated by evaporating part of the solvent by means of a gentle Ar flux. The Au NPs were precipitated through the addition of diethyl ether. The so-obtained suspension was centrifuged (4500 rpm, 5 minutes, 20 °C) and then the supernatant discarded. Four More washing with diethyl ether were performed and then the NPs were purified by gel permeation chromatography (Sephadex LH-20, MeOH). 66 mg of Au NPs were obtained.

^{1}H-NMR (400 MHz, $CDCl_3$): δ: 3.75-3.25 (br), 2.25-2.05 (br), 1.90-1.25 (br). TGA: Total percent loss = 34.8 % TEM: Average diameter = 2.0 nm, σ = 0.3 nm, σ^* = 0.15, count over 300 NPs.

Synthesis of F8PEG Au NPs

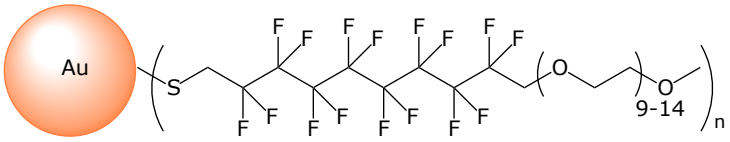

Figure 7.16: Drawing of Au NPs protected by F8PEG thiolates.

In a 50 mL round-bottom flask, 0.092 g (0.088 mmol) of F8PEG were dissolved in 13.9 mL of deoxygenated MeOH. 0.5 mL of a 0.5 M solution of NaOMe in MeOH were added to the solution containing the thiol. The so-obtained mixture was left stirring for 50 minutes, protected from light. In the meantime, in a 250 mL three-neck round-bottom flask 0.069 g (0.178 mmol) of $HAuCl_4 \cdot 3\,H_2O$ were dissolved in 31.4 mL of mQ water. The mixture containing the resulting thiolate was poured into the three-neck round-bottom flask through canula transfer. The so-achieved mixture was stirred for one hour at RT protected from light. During this period of time, a reducing solution containing 0.076 g (2 mmol) of $NaBH_4$ in 5 mL of mQ water was prepared. This latter solution was then added to the previously prepared mixture in 14 minutes at RT. The so-obtained reaction mixture was stirred at RT for 4 hours after which the reaction was stopped and the solvent removed in vacuum. The raw product was then recovered with CH_2Cl_2 and transferred in a 50 mL Falcon tube. The NPs were precipitated by adding diethyl ether and centrifuged (4500 rpm, 10 minutes, 25 °C). The supernatant was discarded and six more washings were performed, each of them followed by centrifugation (4500 rpm, 5 minutes, 25 °C) and supernatant removal. The NPs were finally purified by means of gel permeation chromatography (Sephadex LH-20, MeOH). 33.9 mg of NPs were obtained.
UV-Vis ($CHCl_3$): no appreciable features. ^{1}H-NMR (400 MHz, $CDCl_3$): δ: 4.10-3.20 (br), 1.80-1.50 (br). TGA: Total percent loss = 39.3 %. TEM: Averqage diameter = 2.0 nm, σ = 0.5 nm, σ^* = 0.25, count over 300 NPs.

Synthesis of C8TEG/F8PEG Au NPs

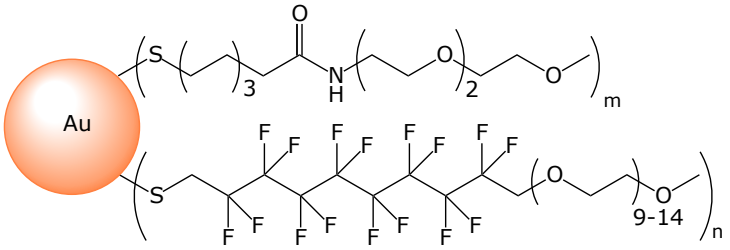

Figure 7.17: Drawing of Au NPs protected by C8TEG and F8PEG thiolates.

Sample A In a 10 mL round-bottom flask, 0.022 g (0.07 mmol) of C8TEG were dissolved in 3 mL of dry deoxygenated MeOH under an Ar atmosphere. 0.6 mL of a 0.5 M solution of NaOMe

in MeOH were added to the previously prepared solution. The overall mixture was stirred for 30 minutes, protected from light. Similarly, 0.29 g (0.278 mmol) of F8PEG were dissolved in 3 mL of dry deoxygenated MeOH under an Ar atmosphere. 0.8 mL of a 0.5 M solution of NaOMe in MeOH were added to the solution containing F8PEG and the resulting mixture was stirred for 30 minutes, protected from light. The two solutions were then reunited by means of canula transfer and 7.6 mL of dry deoxygenated MeOH were added to the resulting mixture. This latter solution was then added to a solution containing 0.068 g (0.174 mmol) of $HAuCl_4 \cdot 3\,H_2O$ dissolved in 34 mL of mQ water inside a 250 mL round-bottom flask. The so-obtained mixture was stirred for one hour at RT. During this period of time, a reducing solution containing 0.075 g (1.98 mmol) of $NaBH_4$ in 4.8 mL of mQ water was prepared. This latter solution was then added to the previously prepared mixture in 10 minutes at RT. The reaction was stopped after 3 hours and 30 minutes and the solvent was removed under vacuum. The raw product was then dissolved in CH_2Cl_2 and transferred in a 50 mL Falcon tube. The solvent was therefore removed and the solid residue was washed eight times with 15 mL of diethyl ether. The NPs were finally purified through gel permeation chromatography (Sephadex LH-20, MeOH). 54 mg of NPs were obtained.
^{1}H-NMR (400 MHz, $CDCl_3$): δ: 4.10-3.20 (br), 2.25-2.05 (br), 1.90-1.20 (br). TGA: Total percent loss = 45.8 %. TEM: Averqage diameter = 1.9 nm, σ = 0.7 nm, σ^* = 0.37, count over 300 NPs. Molar ratio between C8TEG/F8PEG thiols within the monolayer = 1/2 from ^{1}H-NMR analysis on decomposed NPs.

Sample B In a 10 mL round-bottom flask, 0.026 g (0.08 mmol) of C8TEG were dissolved in 3.4 mL of dry deoxygenated MeOH under an Ar atmosphere. 0.65 mL of a 0.5 M solution of NaOMe in MeOH were added to the previously prepared solution. The overall mixture was stirred for 30 minutes, protected from light. Similarly, 0.24 g (0.23 mmol) of F8PEG were dissolved in 2.6 mL of dry deoxygenated MeOH under an Ar atmosphere. 0.65 mL of a 0.5 M solution of NaOMe in MeOH were added to the solution containing F8PEG and the resulting mixture was stirred for 30 minutes, protected from light. The two solutions were then reunited by means of canula transfer and 6.8 mL of dry deoxygenated MeOH were added to the resulting mixture. This latter solution was then added to a solution containing 0.061 g (0.156 mmol) of $HAuCl_4 \cdot 3\,H_2O$ dissolved in 32.4 mL of mQ water inside a 250 mL round-bottom flask. The so-obtained mixture was stirred for one hour at RT. During this period of time, a reducing solution containing 0.067 g (1.78 mmol) of $NaBH_4$ in 4.6 mL of mQ water was prepared. This latter solution was then added to the previously prepared mixture in 10 seconds at RT. The reaction was stopped after 3 hours and 30 minutes and the solvent was removed under vacuum. The raw product was then dissolved in CH_2Cl_2 and transferred in a 50 mL Falcon tube. The solvent was therefore removed and the solid residue was washed twelve times with 15 mL of diethyl ether. The NPs were finally purified through gel permeation chromatography (Sephadex LH-20, MeOH). 60 mg of NPs were obtained.
^{1}H-NMR (400 MHz, $CDCl_3$): δ: 4.10-3.20 (br), 2.25-2.05 (br), 1.90-1.20 (br). TGA: Total percent loss = 58 %. TEM: Averqage diameter = 1.6 nm, σ = 0.4 nm, σ^* = 0.25, count over 300 NPs. Molar ratio between C8TEG/F8PEG thiols within the monolayer = 1/1.3 from analysis of the ^{1}H-NMR spectrum of decomposed NPs.

Synthesis of C16/F6 Au NPs

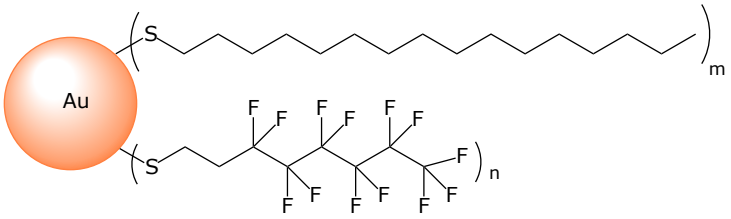

Figure 7.18: Drawing of Au NPs protected by C16 and F6 thiolates.

In a 100 mL round-bottom flask, 0.336 g (0.615 mol) of tetraoctylammonium bromide were dissolved in 16.7 mL of CH_2Cl_2. To this latter solution, another solution prepared dissolving 0.098 g (0.248 mmol) of $HAuCl_4 \cdot 3\,H_2O$ in 7.3 mL of mQ water was added. The mixture was vigorously stirred at RT, observing fading of the aqueous phase while the organic phase turned orange. After the phase transfer was completed, a freshly prepared solution containing 10.7 mg (0.041 mmol) of C16 and 15.6 mg (0.041 mmol) of F6 thiols in DCM was added to the reaction mixture. The resulting mixture was left stirring at RT for 10 minutes and afterwards, a freshly prepared aqueous solution containing 0.094 g (2.48 mmol) of $NaBH_4$ was added in 4 minutes and 30 seconds at RT under vigorous stirring. The reaction mixture was left stirring for 18 hours at RT. The organic and the aqueous layers were separated and the organic layer was washed with brine (1 x 20 mL). The NPs were then precipitated by addition of MeOH. The suspension was transferred in a 50 mL Falcon tubes and centrifuged (4500 rpm 3 minutes, 15 °C). The supernatant was discarded and the precipitate was washed with MeOH and the suspension centrifuged (4500 rpm 3 minutes, 15 °C). The NPs were dissolved with $CHCl_3$ and the solvent was subsequently removed by means of an Ar flux. The residue was washed with MeOH (7 x 15 mL). The purified NPs were finally subjected to selective extractions with $CHCl_3$ and afterwards with hexane. 59 mg of NPs were obtained.
^{1}H-NMR (500 MHz, $CDCl_3$): δ: 1.27 (br, $(CH_2)_9$); 0.89 (br, CH_3); ^{19}F-NMR (470 MHz, $CDCl_3$): δ: -81.40 (br, CF_3), from -120.8 to -125.2 (br, $(CF_2)_3$), -126.70 (br, $C\underline{F}_2-CF_3$). TEM: Average diameter = 2.9 nm, σ = 0.5 nm, σ^* = 0.17, count over 300 NPs. Molar ratio between C16/F6 thiols within the monolayer = 1.8/1 from analysis of ^{1}H-NMR spectrum on decomposed NPs.

Preparation of MALDI-TOF MS samples

The general procedure for setting up samples for MALDI-TOF MS analysis on Au NPs consists in preparing a 5 mg/mL solution of Au NPs in the desired solvent and a 10 mg/mL solution of the chosen matrix in the same solvent of the previous solution. If the ratio between analyte and matrix must have been varied, only the amount of matrix was changed accordingly to the desired ratio. 10 μL of Au NPs solution were mixed with 10 μL of the matrix solution into a 2.5 mL Eppendorf tube. The resulting mixture was dropcasted on a polished steel plate for MALDI-TOF analysis and the solvent was left evaporating.

Bibliography

(1) Sheregii, E.; A.Derengowska; Depciuch, J.; Wojnarowska-Nowak, R.; Polit, J.; Broda, D.; Nechaj, N.; Gonchar, M. Study of Optical Properties of a Glutathione Capped Gold Nanoparticles using Linker (MHDA) by Fourier Transform Infra Red Spectroscopy and Surface Enhanced Raman Scattering. *World Academy of Science, Engineering and Technology* **2013**, *73*, 611–614.

(2) Jiang, H.-L.; Akita, T.; Ishida, T.; Haruta, M.; Xu, Q. Synergistic Catalysis of Au@Ag CoreShell Nanoparticles Stabilized on MetalOrganic Framework. *Journal of the American Chemical Society* **2011**, *133*, 1304–1306.

(3) Love, J. C.; Estroff, L. A.; Kriebel, J. K.; Nuzzo, R. G.; Whitesides, G. M. Self-Assembled Monolayers of Thiolates on Metals as a Form of Nanotechnology. *Chemical Reviews* **2005**, *105*, 1103–1170.

(4) Cure, J. et al. High stability of ultra-small and isolated gold nanoparticles in metalorganic framework materials. *J. Mater. Chem. A* **2019**, *7*, 17536–17546.

(5) Gallud, A.; Klöditz, K.; Ytterberg, J.; Östberg, N.; Katayama, S.; Skoog, T.; Gogvadze, V.; Chen, Y.-Z.; Xue, D.; Moya, S.; Ruiz, J.; Astruc, D.; Zubarev, R.; Kere, J.; Fadeel, B. Cationic gold nanoparticles elicit mitochondrial dysfunction: a multi-omics study. *Scientific Reports* **2019**, *9*, 4366.

(6) Huang, X.; El-Sayed, M. A. Gold nanoparticles: Optical properties and implementations in cancer diagnosis and photothermal therapy. *Journal of Advanced Research* **2010**, *1*, 13–28.

(7) Klinkova, A.; Choueiri, R. M.; Kumacheva, E. Self-assembled plasmonic nanostructures. *Chemical Society reviews* **2014**, *43*, 3976–91.

(8) Gong, J.; Li, G.; Tang, Z. Self-assembly of noble metal nanocrystals: Fabrication, optical property, and application. *Nano Today* **2012**, *7*, 564–585.

(9) Zabet-Khosousi, A.; Dhirani, A.-A. Charge Transport in Nanoparticle Assemblies. *Chem. Rev.* **2008**, *108*, 4072–4124.

(10) Anker, J. N.; Hall, W. P.; Lyandres, O.; Shah, N. C.; Zhao, J.; Van Duyne, R. P. Biosensing with plasmonic nanosensors. *Nature Materials* **2008**, *7*, 442–453.

(11) Lee, A.; Ahmed, A.; dos Santos, D. P.; Coombs, N.; Park, J. I.; Gordon, R.; Brolo, A. G.; Kumacheva, E. Side-by-Side Assembly of Gold Nanorods Reduces Ensemble-Averaged SERS Intensity. *J. Phys. Chem. C* **2012**, *116*, 5538–5545.

(12) Dykman, L.; Khlebtsov, N. Gold nanoparticles in biomedical applications: recent advances and perspectives. *Chem. Soc. Rev.* **2012**, *41*, 2256–2282.

(13) Xia, Y.; Song, L.; Zhu, C. Turn-On and Near-Infrared Fluorescent Sensing for 2,4,6-Trinitrotoluene Based on Hybrid (Gold Nanorod)(Quantum Dots) Assembly. *Anal. Chem.* **2011**, *83*, 1401–1407.

(14) Choi, I.; Song, H. D.; Lee, S.; Yang, Y. I.; Kang, T.; Yi, J. Core-Satellites Assembly of Silver Nanoparticles on a Single Gold Nanoparticle via Metal Ion-Mediated Complex. *Journal of the American Chemical Society* **2012**, *134*, 12083–12090.

(15) Huang, X.; Jain, P. K.; El-Sayed, I. H.; El-Sayed, M. A. Plasmonic photothermal therapy (PPTT) using gold nanoparticles. *Lasers in Medical Science* **2007**, *23*, 217.

(16) Govorov, A. O.; Richardson, H. H. Generating heat with metal nanoparticles. *Nano Today* **2007**, *2*, 30–38.

(17) Kim, J.-W.; Deaton, R. Molecular Self-Assembly of Multifunctional Nanoparticle Composites with Arbitrary Shapes and Functions: Challenges and Strategies. *Particle & Particle Systems Characterization* **2013**, *30*, 117–132.

(18) Wei, Y.; Han, S.; Kim, J.; Soh, S.; Grzybowski, B. A. Photoswitchable Catalysis Mediated by Dynamic Aggregation of Nanoparticles. *Journal of the American Chemical Society* **2010**, *132*, 11018–11020.

(19) Kitching, H.; Shiers, M. J.; Kenyon, A. J.; Parkin, I. P. Self-assembly of metallic nanoparticles into one dimensional arrays. *Journal of Materials Chemistry A* **2013**, *1*, 6985.

(20) Bhuvana, T.; Kulkarni, G. U. Highly conducting patterned Pd nanowires by direct-write electron beam lithography. *ACS Nano* **2008**, *2*, 457–462.

(21) Brust, M.; Schiffrin, D. J.; Bethell, D.; Kiely, C. J. Novel gold-dithiol nano-networks with non-metallic electronic properties. *Advanced Materials* **1995**, *7*, 795–797.

(22) Vries, G. A. D.; Brunnbauer, M.; Ying Hu, A. M. J.; Long, B.; Neltner, B. T.; Uzun, O.; Wunsch, B. H.; Stellacci, F. Divalent Metal Nanoparticles. *Science* **2007**, *315*, 358–361.

(23) Gao, B.; Alvi, Y.; Rosen, D.; Lav, M.; Tao, A. R. Designer nanojunctions: orienting shaped nanoparticles within polymer thin-film nanocomposites. *Chemical Communications* **2013**, *49*, 4382–4.

(24) Sangeetha, N. M.; Blanck, C.; Nguyen, T. T. T.; Contal, C.; Mésini, P. J. Size-selective 2D ordering of gold nanoparticles using surface topography of self-assembled diamide template. *ACS Nano* **2012**, *6*, 8498–8507.

(25) Fu, X.; Wang, Y.; Huang, L.; Sha, Y.; Gui, L.; Lai, L.; Tang, Y. Assemblies of metal nanoparticles and self-assembled peptide fibrils - Formation of double helical and single-chain arrays of metal nanoparticles. *Advanced Materials* **2003**, *15*, 902–906.

(26) Fullam, S.; Cottell, D.; Rensmo, H.; Fitzmaurice, D. Carbon nanotube templated self-assembly and thermal processing of gold nanowires. *Advanced Materials* **2000**, *12*, 1430–1432.

(27) Zhao, Y.; Xu, L.; Liz-Marzán, L. M.; Kuang, H.; Ma, W.; Asenjo-García, A.; García De Abajo, F. J.; Kotov, N. A.; Wang, L.; Xu, C. Alternating plasmonic nanoparticle heterochains made by polymerase chain reaction and their optical properties. *Journal of Physical Chemistry Letters* **2013**, *4*, 641–647.

(28) Polavarapu, L.; Xu, Q.-H. A single-step synthesis of gold nanochains using an amino acid as a capping agent and characterization of their optical properties. *Nanotechnology* **2008**, *19*, 075601.

(29) Rapino, S.; Zerbetto, F. Dynamics of thiolate chains on a gold nanoparticle. *Small* **2007**, *3*, 386–388.

(30) Si, K. J.; Chen, Y.; Shi, Q.; Cheng, W. Nanoparticle Superlattices: The Roles of Soft Ligands. *Advanced Science* **2018**, *5*, 1700179.

(31) Kiely, C. J.; Fink, J.; Brust, M.; Bethell, D.; Schiffrin, D. J. Spontaneous ordering of bimodal ensembles of nanoscopic gold clusters. *Nature* **1998**, *396*, 444–446.

(32) Kanehara, M.; Kodzuka, E.; Teranishi, T. Self-Assembly of Small Gold Nanoparticles through Interligand Interaction. *Journal of the American Chemical Society* **2006**, *128*, 13084–13094.

(33) Brousseau III, L. C.; Novak, J. P.; Marinakos, S. M.; Feldheim, D. L. Assembly of Phenylacetylene-Bridged Gold Nanocluster Dimers and Trimers. *Advanced Materials* **1999**, *11*, 447–449.

(34) Yao, H.; Kojima, H.; Sato, S.; Kimura, K. Interparticle Spacing Control in the Superlattices of Carboxylic Acid-Capped Gold Nanoparticles by Hydrogen-Bonding Mediation. *Langmuir* **2004**, *20*, 10317–10323.

(35) Lin, G.; Chee, S. W.; Raj, S.; Král, P.; Mirsaidov, U. Linker-Mediated Self-Assembly Dynamics of Charged Nanoparticles. *ACS Nano* **2016**, *10*, 7443–7450.

(36) Zhou, H.; Yan, H.; Zhang, A.; Zheng, L.; Jia, H. $\pi\pi$ stacking interaction induced the assembly of gold nanorods. *Materials Chemistry and Physics* **2014**, *148*, 503–506.

(37) Hobara, D.; Kondo, S.; Choi, M. S.; Ishioka, Y.; Hirata, S.; Murata, M.; Azuma, K.; Kasahara, J. Construction of a two-dimensional molecule-nanoparticle network using iron(II) bis(terpyridine) complex formation for molecular-device applications. *Physica Status Solidi (A) Applications and Materials Science* **2007**, *204*, 1706–1711.

(38) Ohno, K.; Koh, K.; Tsujii, Y.; Fukuda, T. Fabrication of Ordered Arrays of Gold Nanoparticles Coated with High-Density Polymer Brushes. *Angewandte Chemie International Edition* **2003**, *42*, 2751–2754.

(39) Cheng, L.; Liu, A.; Peng, S.; Duan, H. Responsive Plasmonic Assemblies of Amphiphilic Nanocrystals at OilWater Interfaces. *ACS Nano* **2010**, *4*, 6098–6104.

(40) Huang, H.-Y.; Chen, W.-F.; Kuo, P.-L. Self-Assembly of Gold Nanoparticles Induced by Poly(oxypropylene)diamines. *J. Phys. Chem. B* **2005**, *109*, 24288–24294.

(41) Pinto, Y. Y.; Le, J. D.; Seeman, N. C.; Musier-Forsyth, K.; Taton, T. A.; Kiehl, R. A. Sequence-Encoded Self-Assembly of Multiple-Nanocomponent Arrays by 2D DNA Scaffolding. *Nano Lett.* **2005**, *5*, 2399–2402.

(42) Stanca, S. E.; Eritjab, R.; Fitzmaurice, D. DNA-templated assembly of nanoscale architectures for next-generation electronic devices. *Faraday Discussions* **2006**, *131*, 155–165, 155–165.

(43) Zhou, Y.; Zeng, H. C. Simultaneous synthesis and assembly of noble metal nanoclusters with variable micellar templates. *Journal of the American Chemical Society* **2014**, *136*, 13805–13817.

(44) Mirkin, C. A.; Letsinger, R. L.; Mucic, R. C.; Storhoff, J. J. A DNA-based method for rationally assembling nanoparticles into macroscopic materials. *Nature* **1996**, *382*, 607–609.

(45) Alivisatos, A. P.; Johnsson, K. P.; Peng, X.; Wilson, T. E.; Loweth, C. J.; Bruchez, M. P.; Schultz, P. G. Organization of 'nanocrystal molecules' using DNA. *Nature* **1996**, *382*, 609–11.

(46) Kim, Y.; Macfarlane, R. J.; Jones, M. R.; Mirkin, C. A. Transmutable nanoparticles with reconfigurable surface ligands. *Science* **2016**, *351*, 579–582.

(47) Liu, W.; Tagawa, M.; Xin, H. L.; Wang, T.; Emamy, H.; Li, H.; Yager, K. G.; Starr, F. W.; Tkachenko, A. V.; Gang, O. Diamond family of nanoparticle superlattices. *Science* **2016**, *351*, 582–586.

(48) Guarise, C.; Pasquato, L.; Scrimin, P. Reversible aggregation/deaggregation of gold nanoparticles induced by a cleavable dithiol linker. *Langmuir* **2005**, *21*, 5537–5541.

(49) Templeton, A. C.; Zamborini, F. P.; Wuelfing, W. P.; Murray, R. W. Controlled and reversible formation of nanoparticle aggregates and films using Cu(II)-carboxylate chemistry. *Langmuir* **2000**, *16*, 6682–6688.

(50) De la Fuente, J. M.; Barrientos, A. G.; Rojas, T. C.; Rojo, J.; Cañada, J.; Fernández, A.; Penadés, S. Gold Glyconanoparticles as Water-Soluble Polyvalent Models To Study Carbohydrate Interactions. *Angewandte Chemie International Edition* **2001**, *40*, 2257–2261.

(51) Norsten, T. B.; Frankamp, B. L.; Rotello, V. M. Metal Directed Assembly of Terpyridine-Functionalized Gold Nanoparticles. *Nano Letters* **2002**, *2*, 1345–1348.

(52) Zhu, L.; Xue, D.; Wang, Z. Metallic Cation Induced One-Dimensional Assembly of Poly (acrylic acid) -1-Dodecanethiol-Stabilized Gold Nanoparticles. *Langmuir* **2008**, *24*, 11385–11389.

(53) Chan, Y. T.; Li, S.; Moorefield, C. N.; Wang, P.; Shreiner, C. D.; Newkome, G. R. Self-assembly, disassembly, and reassembly of gold nanorods mediated by bis(terpyridine)-metal connectivity. *Chemistry - A European Journal* **2010**, *16*, 4164–4168.

(54) Holyer, R. H.; Hubbard, C. D.; Kettle, S. F.; Wilkins, R. G. The Kinetics of Replacement Reactions of Complexes of the Transition Metals with 1,10-Phenanthroline and 2,2'-Bipyridine. *Inorganic Chemistry* **1965**, *4*, 929–935.

(55) Goze, C.; Ulrich, G.; Charbonnière, L.; Cesario, M.; Prangé, T.; Ziessel, R. Cation Sensors Based on Terpyridine-Functionalized Boradiazaindacene. *Chemistry - A European Journal* **2003**, *9*, 3748–3755.

(56) Jackson, A. M.; Myerson, J. W.; Stellacci, F. Spontaneous assembly of subnanometre-ordered domains in the ligand shell of monolayer-protected nanoparticles. *Nature Materials* **2004**, *3*, 330–336.

(57) Jackson, A. M.; Hu, Y.; Silva, P. J.; Stellacci, F. From homoligand-to mixed-ligand-monolayer-protected metal nanoparticles: a scanning tunneling microscopy investigation. *Journal of the American Chemical Society* **2006**, *128*, 11135–49.

(58) Liu, X.; Yu, M.; Kim, H.; Mameli, M.; Stellacci, F. Determination of monolayer-protected gold nanoparticle ligand-shell morphology using NMR. *Nature Communications* **2012**, *3*, 1–9.

(59) Singh, C.; Ghorai, P. K.; Horsch, M. A.; Jackson, A. M.; Larson, R. G.; Stellacci, F.; Glotzer, S. C. Entropy-mediated patterning of surfactant-coated nanoparticles and surfaces. *Physical Review Letters* **2007**, *99*, 1–4.

(60) Ong, Q. K.; Reguera, J.; Silva, P. J.; Moglianetti, M.; Harkness, K.; Longobardi, M.; Mali, K. S.; Renner, C.; De Feyter, S.; Stellacci, F. High-resolution scanning tunneling microscopy characterization of mixed monolayer protected gold nanoparticles. *ACS Nano* **2013**, *7*, 8529–8539.

(61) Şologan, M.; Marson, D.; Polizzi, S.; Pengo, P.; Boccardo, S.; Pricl, S.; Posocco, P.; Pasquato, L. Patchy and Janus Nanoparticles by Self-Organization of Mixtures of Fluorinated and Hydrogenated Alkanethiolates on the Surface of a Gold Core. *ACS Nano* **2016**, *10*, 9317–9325.

(62) Gentilini, C.; Franchi, P.; Mileo, E.; Polizzi, S.; Lucarini, M.; Pasquato, L. Formation of Patches on 3D SAMs Driven by Thiols with Immiscible Chains Observed by ESR Spectroscopy. *Angewandte Chemie* **2009**, *121*, 3106–3110.

(63) Posocco, P.; Gentilini, C.; Bidoggia, S.; Pace, A.; Franchi, P.; Lucarini, M.; Fermeglia, M.; Pricl, S.; Pasquato, L. Self-Organization of Mixtures of Fluorocarbon and Hydrocarbon Amphiphilic Thiolates on the Surface of Gold Nanoparticles. *ACS Nano* **2012**, *6*, 7243–7253.

(64) Şologan, M.; Cantarutti, C.; Bidoggia, S.; Polizzi, S.; Pengo, P.; Pasquato, L. Routes to the preparation of mixed monolayers of fluorinated and hydrogenated alkanethiolates grafted on the surface of gold nanoparticles. *Faraday Discussions* **2016**, *191*, 527–543.

(65) Li, J.; Hu, X. K.; Lipson, R. H. On-chip enrichment and analysis of peptide subsets using a maleimide-functionalized fluorous affinity biochip and nanostructure initiator mass spectrometry. *Analytical Chemistry* **2013**, *85*, 5499–5505.

(66) Li, J.; Lipson, R. H. Assays using a NIMS chip: Loosely bound but highly selective. *Analytical Chemistry* **2013**, *85*, 6860–6865.

(67) Rapp, H. M.; Bacher, S.; Ahrens, A.; Rapp, W.; Kammerer, B.; Nienhaus, G. U.; Bannwarth, W. Attachment of proteins to surfaces by fluorous-fluorous interactions restoring their structure and activity. *ChemPlusChem* **2012**, *77*, 1066–1070.

(68) Xu, Z.; Oleschuk, R. D. A fluorous porous polymer monolith photo-patterned chromatographic column for the separation of a flourous/fluorescently labeled peptide within a microchip. *Electrophoresis* **2014**, *35*, 441–449.

(69) Zhang, J.; Chaker, M.; Ma, D. Pulsed laser ablation based synthesis of colloidal metal nanoparticles for catalytic applications. *Journal of Colloid and Interface Science* **2017**, *489*, 138–149.

(70) Masitas, R. A.; Allen, S. L.; Zamborini, F. P. Size-Dependent Electrophoretic Deposition of Catalytic Gold Nanoparticles. *Journal of the American Chemical Society* **2016**, *138*, 15295–15298.

(71) Ishida, Y.; Sumi, T.; Yonezawa, T. Sputtering synthesis and optical investigation of octadecanethiol-protected fluorescent Au nanoparticles. *New J. Chem.* **2015**, *39*, 5895–5897.

(72) Kong, C.; Ma, B.; Liu, K.; Zhang, W.; Yang, Z. Continuous UV irradiation synthesis of ultra-small Au nanoparticles decorated Cu_2O with enhanced photocatalytic activity. *Composites Communications* **2018**, *9*, 27–32.

(73) Arcoleo, V.; Liveri, V. AFM investigation of gold nanoparticles synthesized in water/AOT/n-heptane microemulsions. *Chemical Physics Letters* **1996**, *258*, 223–227.

(74) Ong, Q. K.; Zhao, S.; Reguera, J.; Biscarini, F.; Stellacci, F. Comparative STM studies of mixed ligand monolayers on gold nanoparticles in air and in 1-phenyloctane. *Chem. Commun.* **2014**, *50*, 10456–10459.

(75) Marbella, L. E.; Millstone, J. E. NMR techniques for noble metal nanoparticles. *Chemistry of Materials* **2015**, *27*, 2721–2739.

(76) Harkness, K. M.; Balinski, A.; McLean, J. A.; Cliffel, D. E. Nanoscale phase segregation of mixed thiolates on gold nanoparticles. *Angewandte Chemie - International Edition* **2011**, *50*, 10554–10559.

(77) Fields-Zinna, C. A.; Parker, J. F.; Murray, R. W. Mass Spectrometry of Ligand Exchange Chelation of the Nanoparticle $Au_{25}(SCH_2CH_2C_6H_5)_{18}^{1-}$ by $CH_3C_6H_3(SH)_2$. *Journal of the American Chemical Society* **2010**, *132*, 17193–17198.

(78) Faraday, M. The Bakerian Lecture: Experimental Relations of Gold (and Other Metals) to Light. *Philosophical Transactions of the Royal Society of London* **1857**, *147*, 145–181.

(79) Turkevich, J.; Stevenson, P. C.; Hillier, J. A study of the nucleation and growth processes in the synthesis of colloidal gold. *Discuss. Faraday Soc.* **1951**, *11*, 55–75.

(80) Frens, G. Controlled Nucleation for the Regulation of the Particle Size in Monodisperse Gold Suspensions. *Nature Physical Science* **1973**, *241*, 20–22.

(81) Giersig, M.; Mulvaney, P. Preparation of ordered colloid monolayers by electrophoretic deposition. *Langmuir* **1993**, *9*, 3408–3413.

(82) Brust, M.; Walker, M.; Bethell, D.; Schiffrin, D. J.; Whyman, R. Synthesis of Thiol-derivatised Gold Nanoparticles in a Two-phase Liquid-Liquid System. *Chemical Communications* **1994**, 801–802.

(83) Sardar, R.; Funston, A. M.; Mulvaney, P.; Murray, R. W. Gold Nanoparticles: Past, Present, and Future. *Langmuir* **2009**, *25*, 13840–13851.

(84) Goulet, P. J. G.; Lennox, R. B. New Insights into BrustSchiffrin Metal Nanoparticle Synthesis. *Journal of the American Chemical Society* **2010**, *132*, 9582–9584.

(85) Shimizu, T.; Teranishi, T.; Hasegawa, S.; Miyake, M. Size Evolution of Alkanethiol-Protected Gold Nanoparticles by Heat Treatment in the Solid State. *Journal of Physical Chemistry B* **2003**, *107*, 2719–2724.

(86) Zheng, N.; Fan, J.; Stucky, G. D. One-step one-phase synthesis of monodisperse noblemetallic nanoparticles and their colloidal crystals. *Journal of the American Chemical Society* **2006**, *128*, 6550–6551.

(87) Peng, S.; Lee, Y.; Wang, C.; Yin, H.; Dai, S.; Sun, S. A facile synthesis of monodisperse Au nanoparticles and their catalysis of CO oxidation. *Nano Research* **2008**, *1*, 229–234.

(88) Song, J.; Kim, D.; Lee, D. Size control in the synthesis of 1-6 nm gold nanoparticles via solvent-controlled nucleation. *Langmuir* **2011**, *27*, 13854–13860.

(89) Jiang, Y.; Huang, Y.; Cheng, H.; Liu, Q.; Xie, Z.; Yao, T.; Jiang, Z.; Huang, Y.; Bian, Q.; Pan, G.; Sun, Z.; Wei, S. Solvent influence on the role of thiols in growth of thiols-capped Au nanocrystals. *Journal of Physical Chemistry C* **2014**, *118*, 714–719.

(90) Wu, B.-H.; Yang, H.-Y.; Huang, H.-Q.; Chen, G.-X.; Zheng, N.-F. Solvent effect on the synthesis of monodisperse amine-capped Au nanoparticles. *Chinese Chemical Letters* **2013**, *24*, 457–462.

(91) Elbert, K. C.; Jishkariani, D.; Wu, Y.; Lee, J. D.; Donnio, B.; Murray, C. B. Design, Self-Assembly, and Switchable Wettability in Hydrophobic, Hydrophilic, and Janus Dendritic Ligand-Gold Nanoparticle Hybrid Materials. *Chemistry of Materials* **2017**, *29*, 8737–8746.

(92) Wrasman, C. J.; Boubnov, A.; Riscoe, A. R.; Hoffman, A. S.; Bare, S. R.; Cargnello, M. Synthesis of Colloidal Pd/Au Dilute Alloy Nanocrystals and Their Potential for Selective Catalytic Oxidations. *Journal of the American Chemical Society* **2018**, *140*, 12930–12939.

(93) Elbert, K. C.; Lee, J. D.; Wu, Y.; Murray, C. B. Improved Chemical and Colloidal Stability of Gold Nanoparticles Through Dendron Capping. *Langmuir* **2018**, *34*, 13333–13338.

(94) Hostetler, M. J.; Templeton, A. C.; Murray, R. W. Dynamics of place-exchange reactions on monolayer-protected gold cluster molecules. *Langmuir* **1999**, *15*, 3782–3789.

(95) Donkers, R. L.; Song, Y.; Murray, R. W. Substituent effects on the exchange dynamics of ligands on 1.6 nm diameter gold nanoparticles. *Langmuir* **2004**, *20*, 4703–4707.

(96) Ingram, R. S.; Hostetler, M. J.; Murray, R. W. Poly-hetero--functionalized Alkanethiolate-Stabilized Gold Cluster Compounds. *Journal of the American Chemical Society* **1997**, *119*, 9175–9178.

(97) Banerjee, A.; Berezhkovskii, A.; Nossal, R. On the Size Dependence of Cellular Uptake of Nanoparticle via Clathrin-Mediated Endocytosis. *Biophysical Journal* **2013**, *104*, 622a.

(98) Neshatian, M.; Chung, S.; Yohan, D.; Yang, C.; Chithrani, D. B. Determining the Size Dependence of Colloidal Gold Nanoparticle Uptake in a Tumor-like Interface (Hypoxic). *Colloids and Interface Science Communications* **2014**, *1*, 57–61.

(99) Cargnello, M.; Gentilini, C.; Montini, T.; Fonda, E.; Mehraeen, S.; Chi, M.; Herrera-Collado, M.; Browning, N. D.; Polizzi, S.; Pasquato, L.; Fornasiero, P. Active and Stable Embedded Au@CeO2 Catalysts for Preferential Oxidation of CO. *Chemistry of Materials* **2010**, *22*, 4335–4345.

(100) Ding, Y.; Fan, F.; Tian, Z.; Lin Wang, Z. Atomic Structure of Au-Pd Bimetallic Alloyed Nanoparticles. *Journal of American Chemical Society* **2010**, *132*, 12480–12486.

(101) Jadzinsky, P. D.; Calero, G.; Ackerson, C. J.; Bushnell, D. A.; Kornberg, R. D. Structure of a Thiol Monolayer-Protected Gold Nanoparticle at 1.1 Å Resolution. *Science* **2007**, *318*, 430–433.

(102) Liu, X.; Atwater, M.; Wang, J.; Huo, Q. Extinction coefficient of gold nanoparticles with different sizes and different capping ligands. *Colloids and Surfaces B: Biointerfaces* **2007**, *58*, 3–7.

(103) Rahme, K.; Nolan, M.; Doody, T.; McGlacken, e.; Morris, M.; O'Driscoll, C.; Holmes, J. Highly stable PEGylated gold nanoparticles in water: Applications in biology and catalysis. *RSC Advances* **2013**, *3*, 21016–21024.

(104) Ong, Q.; Luo, Z.; Stellacci, F. Characterization of Ligand Shell for Mixed-Ligand Coated Gold Nanoparticles. *Accounts of Chemical Research* **2017**, *50*, 1911–1919.

(105) Hu, Y.; Wunsch, B. H.; Sahni, S.; Stellacci, F. Statistical Analysis of Scanning Tunneling Microscopy Images of 'Striped' Mixed Monolayer Protected Gold Nanoparticles. *Journal of Scanning Probe Microscopy* **2009**, *4*, 24–35.

(106) Biscarini, F.; Ong, Q. K.; Albonetti, C.; Liscio, F.; Longobardi, M.; Mali, K. S.; Ciesielski, A.; Reguera, J.; Renner, C.; De Feyter, S.; Samorì, P.; Stellacci, F. Quantitative Analysis of Scanning Tunneling Microscopy Images of Mixed-Ligand-Functionalized Nanoparticles. *Langmuir* **2013**, *29*, 13723–13734.

(107) Kuna, J. J.; Voïtchovsky, K.; Singh, C.; Jiang, H.; Mwenifumbo, S.; Ghorai, P. K.; Stevens, M. M.; Glotzer, S. C.; Stellacci, F. The effect of nanometre-scale structure on interfacial energy. *Nature Materials* **2009**, *8*, 837–842.

(108) Lee, Z.; Jeon, K.-J.; Dato, A.; Erni, R.; Richardson, T. J.; Frenklach, M.; Radmilovic, V. Direct Imaging of SoftHard Interfaces Enabled by Graphene. *Nano Letters* **2009**, *9*, 3365–3369.

(109) Yang, J. A.; Murphy, C. J. Evidence for Patchy Lipid Layers on Gold Nanoparticle Surfaces. *Langmuir* **2012**, *28*, 5404–5416.

(110) Milne, J. L. S.; Borgnia, M. J.; Bartesaghi, A.; Tran, E. E. H.; Earl, L. A.; Schauder, D. M.; Lengyel, J.; Pierson, J.; Patwardhan, A.; Subramaniam, S. Cryo-electron microscopy a primer for the non-microscopist. *The FEBS Journal* **2013**, *280*, 28–45.

(111) Atukorale, P. U.; Guven, Z. P.; Bekdemir, A.; Carney, R. P.; Van Lehn, R. C.; Yun, D. S.; Jacob Silva, P. H.; Demurtas, D.; Yang, Y.-S.; Alexander-Katz, A.; Stellacci, F.; Irvine, D. J. StructureProperty Relationships of Amphiphilic Nanoparticles That Penetrate or Fuse Lipid Membranes. *Bioconjugate Chemistry* **2018**, *29*, 1131–1140.

(112) Cagno, V. et al. Broad-spectrum non-toxic antiviral nanoparticles with a virucidal inhibition mechanism. *Nature Materials* **2018**, *17*, 195–203.

(113) Hostetler, M. J.; Wingate, J. E.; Zhong, C.-J.; Harris, J. E.; Vachet, R. W.; Clark, M. R.; Londono, J. D.; Green, S. J.; Stokes, J. J.; Wignall, G. D.; Glish, G. L.; Porter, M. D.; Evans, N. D.; Murray, R. W. Alkanethiolate Gold Cluster Molecules with Core Diameters from 1.5 to 5.2 nm: Core and Monolayer Properties as a Function of Core Size. *Langmuir* **1998**, *14*, 17–30.

(114) Dass, A.; Stevenson, A.; Dubay, G. R.; Tracy, J. B.; Murray, R. W. Nanoparticle MALDI-TOF Mass Spectrometry without Fragmentation: $Au_{25}(SCH_2CH_2Ph)_{18}$ and Mixed Monolayer $Au_{25}(SCH_2CH_2Ph)_{18\text{-}x}(L)_x$. *Journal of the American Chemical Society* **2008**, *130*, 5940–5946.

(115) Harkness, K. M.; Cliffel, D. E.; McLean, J. A. Characterization of thiolate-protected gold nanoparticles by mass spectrometry. *Analyst* **2010**, *135*, 868–874.

(116) Yan, B.; Zhu, Z.-J.; Miranda, O. R.; Chompoosor, A.; Rotello, V. M.; Vachet, R. W. Laser desorption/ionization mass spectrometry analysis of monolayer-protected gold nanoparticles. *Analytical and Bioanalytical Chemistry* **2010**, *396*, 1025–1035.

(117) Luo, Z.; Huo, J.; Menin, L.; Ong, Q. K.; Stellacci, F. Evolution of the Ligand Shell Morphology during Ligand Exchange Reactions on Gold Nanoparticles. *Angewandte Chemie International Edition* **2017**.

(118) Luo, Z.; Zhao, Y.; Darwish, T.; Wang, Y.; Hou, J.; Stellacci, F. Mass spectrometry and Monte Carlo method mapping of nanoparticle ligand shell morphology. *Nature Communications* **2018**, *9*, 4478.

(119) Chu, B.; Liu, T. Characterization of Nanoparticles by Scattering Techniques. *Journal of Nanoparticle Research* **2000**, *2*, 29–41.

(120) Von White, G.; Mohammed, F. S.; Kitchens, C. L. Small-Angle Neutron Scattering Investigation of Gold Nanoparticle Clustering and Ligand Structure Under Antisolvent Conditions. *The Journal of Physical Chemistry C* **2011**, *115*, 18397–18405.

(121) Hore, M. J. A.; Ye, X.; Ford, J.; Gao, Y.; Fei, J.; Wu, Q.; Rowan, S. J.; Composto, R. J.; Murray, C. B.; Hammouda, B. Probing the Structure, Composition, and Spatial Distribution of Ligands on Gold Nanorods. *Nano Letters* **2015**, *15*, 5730–5738.

(122) Diroll, B. T.; Weigandt, K. M.; Jishkariani, D.; Cargnello, M.; Murphy, R. J.; Hough, L. A.; Murray, C. B.; Donnio, B. Quantifying Softness of Organic Coatings on Gold Nanoparticles Using Correlated Small-Angle X-ray and Neutron Scattering. *Nano Letters* **2015**, *15*, 8008–8012.

(123) Moglianetti, M.; Ong, Q. K.; Reguera, J.; Harkness, K. M.; Mameli, M.; Radulescu, A.; Kohlbrecher, J.; Jud, C.; Svergun, D. I.; Stellacci, F. Scanning tunneling microscopy and small angle neutron scattering study of mixed monolayer protected gold nanoparticles in organic solvents. *Chemical Science* **2014**, *5*, 1232–1240.

(124) Luo, Z.; Marson, D.; Ong, Q. K.; Loiudice, A.; Kohlbrecher, J.; Radulescu, A.; Krause-Heuer, A.; Darwish, T.; Balog, S.; Buonsanti, R.; Svergun, D. I.; Posocco, P.; Stellacci, F. Quantitative 3D determination of self-assembled structures on nanoparticles using small angle neutron scattering. *Nature Communications* **2018**, *9*, 1343.

(125) Luo, Z.; Yang, Y.; Radulescu, A.; Kohlbrecher, J.; Darwish, T. A.; Ong, Q. K.; Guldin, S.; Stellacci, F. Multidimensional Characterization of Mixed Ligand Nanoparticles Using Small Angle Neutron Scattering. *Chemistry of Materials* **2019**, *31*, 6750–6758.

(126) Ge, X.; Ke, P. C.; Davis, T. P.; Ding, F. A Thermodynamics Model for the Emergence of a Stripe-like Binary SAM on a Nanoparticle Surface. *Small* **2015**, *11*, 4894–4899.

(127) Fetisov, E. O.; Siepmann, J. I. Structure and Phase Behavior of Mixed Self-Assembled Alkanethiolate Monolayers on Gold Nanoparticles: A Monte Carlo Study. *The Journal of Physical Chemistry B* **2016**, *120*, 1972–1978.

(128) Goldmann, C.; Ribot, F.; Peiretti, L. F.; Quaino, P.; Tielens, F.; Sanchez, C.; Chanéac, C.; Portehault, D. Quantified Binding Scale of Competing Ligands at the Surface of Gold Nanoparticles: The Role of Entropy and Intermolecular Forces. *Small* **2017**, *13*, 1604028.

(129) Atkins, P.; Overton, T.; Rourke, J.; Weller, M.; Armstrong, F., *Shriver and Atkins' Inorganic Chemistry*, 5th; Oxford University Press: 2010.

(130) Tarazona-Vasquez, F.; Balbuena, P. B. Ab Initio Study of the Lowest Energy Conformers and IR Spectra of Poly(amidoamine)-G0 Dendrimers. *The Journal of Physical Chemistry B* **2004**, *108*, 15982–15991.

(131) Kluenker, M.; Mondeshki, M.; Nawaz Tahir, M.; Tremel, W. Monitoring Thiol-Ligand Exchange on Au Nanoparticle Surfaces. *Langmuir* **2018**, *34*, 1700–1710.

(132) DeVries, G. A.; Brunnbauer, M.; Hu, Y.; Jackson, A. M.; Long, B.; Neltner, B. T.; Uzun, O.; Wunsch, B. H.; Stellacci, F. Divalent metal nanoparticles. *Science* **2007**, *315*, 358–361.

(133) Pengo, P.; Polizzi, S.; Battagliarin, M.; Pasquato, L.; Scrimin, P. Synthesis, characterization and properties of water-soluble gold nanoparticles with tunable core size. *Journal of Materials Chemistry* **2003**, *13*, 2471–2478.

(134) G. Egan, J.; Drossis, N.; Ebralidze, I.; Fruehwald, H.; Laschuk, N.; Poisson, J.; W. de Haan, H.; Zenkina, O. Hemoglobin-driven iron-directed assembly of gold nanoparticles. *RSC Advances* **2018**, *8*, 15675–15686.

(135) Thompson, R. F.; Walker, M.; Siebert, C. A.; Muench, S. P.; Ranson, N. A. An introduction to sample preparation and imaging by cryo-electron microscopy for structural biology. *Methods* **2016**, *100*, 3–15.

(136) Stewart, P. L. Cryo-electron microscopy and cryo-electron tomography of nanoparticles. *Wiley Interdisciplinary Reviews: Nanomedicine and Nanobiotechnology* **2017**, *9*, e1417.

(137) Latourte, L.; Blais, J. C.; Tabet, J. C.; Cole, R. B. Desorption Behavior and Distributions of Fluorinated Polymers in MALDI and Electrospray Ionization Mass Spectrometry. *Analytical Chemistry* **1997**, *69*, 2742–2750.

(138) Marie, A.; Alves, S.; Fournier, F.; Tabet, J. C. Fluorinated matrix approach for the characterization of hydrophobic perfluoropolyethers by matrix-assisted laser desorption/ionization time-of-flight MS. *Analytical Chemistry* **2003**, *75*, 1294–1299.

(139) Gaiffe, G.; Cole, R. B.; Lacpatia, S.; Bridoux, M. C. Characterization of Fluorinated Polymers by Atmospheric-Solid-Analysis-Probe High-Resolution Mass Spectrometry (ASAP/HRMS) Combined with Kendrick-Mass-Defect Analysis. *Analytical Chemistry* **2018**, *90*, 6035–6042.

(140) Palermo, A.; Forsberg, E. M.; Warth, B.; Aisporna, A. E.; Billings, E.; Kuang, E.; Benton, H. P.; Berry, D.; Siuzdak, G. Fluorinated Gold Nanoparticles for Nanostructure Imaging Mass Spectrometry. *ACS Nano* **2018**, *12*, 6938–6948.